

Inflammation Modulation, Growth Factor Reservoir and Chronic
Wound Healing Potential:
From Nanoscale Coatings to a Free-Standing Layer-by-Layer
Platform

Dissertation zur Erlangung des
Doktorgrades der Naturwissenschaften (Dr. rer. nat.)

der

Naturwissenschaftlichen Fakultät I – Biowissenschaften –
der Martin-Luther-Universität Halle-Wittenberg,

vorgelegt von

Herrn Apotheker, M.Eng. Adrian Hautmann

Gutachter:

Prof. Dr. rer. nat. habil. Thomas Groth

Prof. Dr. med. habil. Faramarz Dehghani

Dr. rer. nat. habil. Christian Wölk

Verteidigt am 16.05.2024

Table of Contents

Table of Contents	2
Abbreviations	4
Graphical Abstract	8
Abstract	9
Zusammenfassung	11
Preamble	13
Chapter 1 - Introduction	14
1.1 Skin Wounds – the Clinical Setting	14
Physiology of Skin Wound Healing	14
Chronic Wounds - Key Players and Deficiencies	20
1.2 Biopolymers - Building Blocks for Bioactive Surface Coatings & Wound Dressings..	28
Hyaluronic Acid	29
Heparin	31
Chitosan	32
Alginate	33
Gelatin	34
1.3 Wound Dressings – State of the Art and Recent Trends	35
Recent Trends in Wound Dressings Design – Use of Growth Factors, Biopolymers and Nanostructured Materials	38
1.4 The Layer-by-Layer Technology - from Surface Modification to 3d-Applications	41
Technological Developments - Dipping, Spinning, Spraying	42
Layer-by-Layer Based Free-Standing Films	44
Research Aim	45
Chapter 2 - Study on the potential mechanism of anti-inflammatory activity of covalently immobilized hyaluronan and heparin	46
Chapter 3 - Studies on the Mechanisms of Anti-Inflammatory Activity of Heparin- and Hyaluronan- Containing Multilayer Coatings—Targeting NF-κB Signalling Pathway	60

Chapter 4 - Free-standing multilayer films as growth factor reservoirs for future wound dressing applications	79
Chapter 5 - Design of a composite wound dressing: Combining an electrospun fleece with a free-standing multilayer film	92
Chapter 6 - Conclusion and Outlook	124
References	129
List of Illustrations.....	145
Acknowledgement	146
Publication List	147
Oral Presentations.....	149
Posters.....	149
Curriculum Vitae	150
Selbstständigkeitserklärung	151

Abbreviations

Abbreviation	Definition
AFM	Atomic Force Microscopy
AKT	PI3K/AKT/mTOR pathway
ALG	Alginate
AP1	Activator Protein 1
ATIII	Antithrombin III
AWMF	Arbeitsgemeinschaft der Wissenschaftlichen Medizinischen Fachgesellschaften
BCR	B Cell Receptor
BMBF	Bundesministerium für Bildung und Forschung
BMP-2	Bone Morphogenetic Protein-2
CAD	Computer-Aided Design
CCR	C-C Chemokine Receptor
CD44	CD44 Molecule
CDP	Dendritic Cell Precursor
CHI	Chitosan
CLSM	Confocal Laser Scanning Microscopy
CXC	CXC-chemokines
DAMPS	Damage-Associated Molecular Pattern
DNA	Deoxyribonucleic Acid
ECM	Extracellular Matrix
EDA	Ectodysplasin A
EDC	1-Ethyl-3-(3-Dimethylaminopropyl)carbodiimide
EGF	Epidermal Growth Factor
ELISA	Enzyme-Linked Immunosorbent Assay
ESEM	Environmental Scanning Electron Microscope
EU	European Union
FBGC	Foreign Body Giant Cell
FDA	Food and Drug Administration
FGF2	Fibroblast Growth Factor 2
FITC	Fluorescein Isothiocyanate
FSF	Free-Standing Film
GAG	Glycosaminoglycan
GF	Growth Factor
GM-CSF	Granulocyte Macrophage Colony-Stimulating Factor
HA	Hyaluronic Acid

Hep	Heparin
HIF-1	Hypoxia-Induced Factor 1
HMW	High Molecular Weight
HYAL	Hyaluronidase
ICAM	Intercellular Adhesion Molecule
IF	Immunofluorescence
IFN	Interferon-N
IKK	IκB Kinase
IL	Interleukin
IRAK	Interleukin-1 Receptor-Associated Kinase
LL-37	Cathelicidin LL-37
LMW	Low Molecular Weight
LPS	Lipopolysaccharide
LYVE-1	Lymphatic Vessel Endothelial Hyaluronic Acid Receptor-1
MCP-1	Monocyte Chemoattractant Protein (CCL2)
MDP	Monocyte-Dendritic Progenitor
MIP-1	Macrophage Inflammatory Protein-1
MMP	Matrix Metalloproteinase
NF-κB	Nuclear Transcription Factor-κB
NHS	N-Hydroxysuccinimide
NO	Nitric Oxide
NOS	Nitric Oxide Synthase
PAMPS	Pathogen-Associated Molecular Patterns
PCL	Polycaprolactone
PDGF	Platelet-Derived Growth Factor
PEI	Polyethyleneimine
PEM	Polyelectrolyte Multilayer
PG	Proteoglycans
PI3K	PI3K/AKT/mTOR pathway
PP	Polypropylene
PRR	Pattern Recognition Receptor
PS	Polystyrene
PTFE	Polytetrafluoroethylene
PVC	Poly(vinyl chloride)
PVP	Polyvinylpyrrolidone
RHAMM	Receptor for Hyaluronan-Mediated Motility
RNA	Ribonucleic Acid

ROS	Reactive Oxygen Species
SAM	Self-Assembled Monolayer
SELE	Selectin E
SEM	Scanning Electron Microscope
STAT	Signal Transducer and Activator of Transcription
TCR	T-Cell Receptor
TF_{II}D	Transcription Factor IID
TGF	Transforming Growth Factor
THP-1	THP-1 cell line
TLR	Toll-Like Receptor
TNF	Tumor Necrosis Factor
TSG-6	Tumor necrosis factor-inducible gene 6 protein
VCAM1	Vascular Cell Adhesion Molecule 1
VEGF	Vascular Endothelial Growth Factor
WCA	Water Contact Angle
ZP	Zeta Potential

Graphical Abstract

Inflammation Modulation, Growth Factor Reservoir and Chronic Wound Healing Potential: From Nanoscale Coatings to a Free-Standing Layer-by-Layer Platform

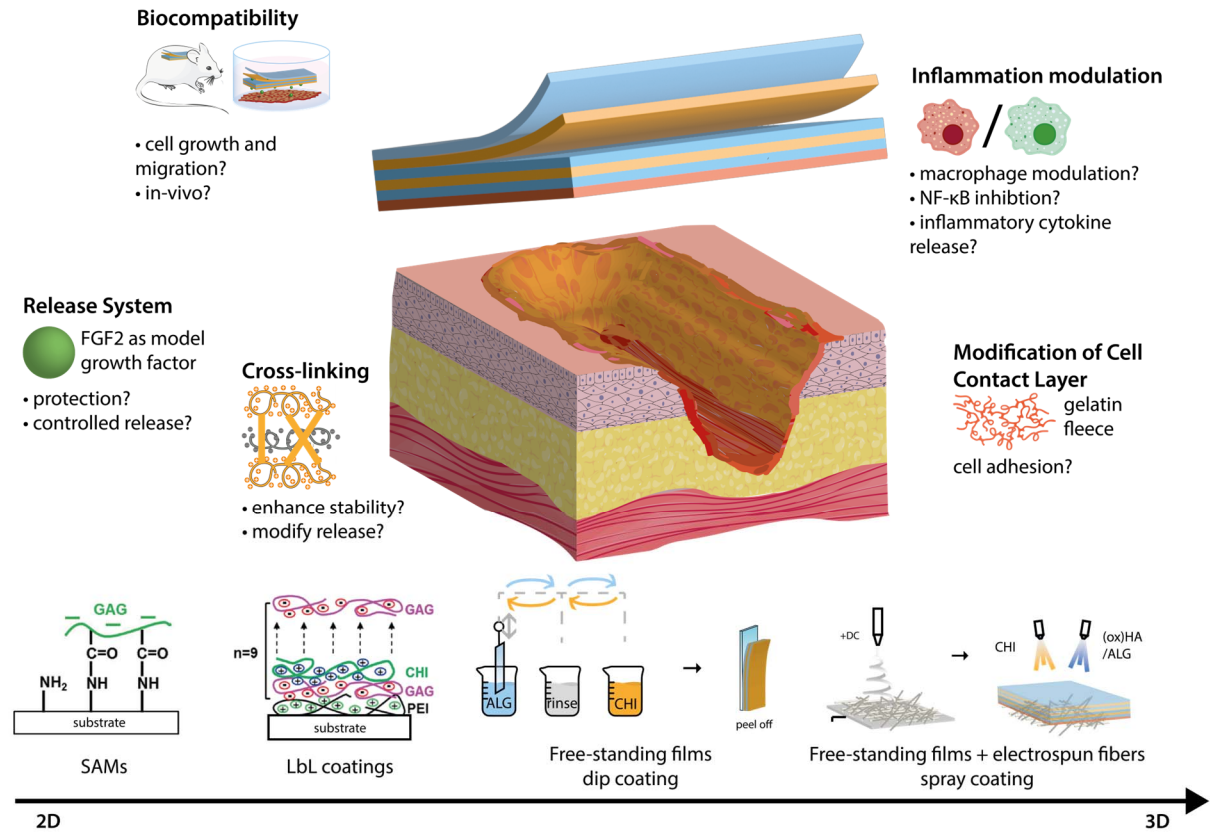


Figure 1 - Graphical Abstract

Abstract

Chronic skin wounds are a pressing concern in aging societies, suffering from high prevalences of metabolic disorders and reduced mobility. The perpetuated chronic inflammation associated with these wounds leads to extended healing periods and complex clinical treatments. By mitigating inflammation and supporting regeneration, faster healing with less scarring becomes possible.

In this thesis, various techniques for surface modification, preparation of free-standing films, and composites are investigated with the common goal of modulating the inflammatory response and promoting wound healing. To explore the anti-inflammatory potential and pathway of action of glycosaminoglycans (GAGs) acting on macrophages, hyaluronic acid (HA) and heparin (Hep), were immobilized either covalently as a monolayer or adsorptively as multilayers using the layer-by-layer (LbL) technique on model materials. In addition, to the physical characterization, confirming the successful immobilization, the successful uptake of the GAGs, a reduction in pro-inflammatory cytokine release, and the signal transduction of the nuclear transcription factor- κ B (NF- κ B), a central player in inflammatory modulation of macrophages, was measured. The results revealed that Hep and HA inhibit the activation and translocation of the p65 subunit of NF- κ B into the nucleus, modulating the inflammatory response of macrophages. Building upon these findings, novel LbL based biomaterials were developed, to push the existing boundaries of LbL assemblies. These include a multilayer free-standing film (FSF) composed of chitosan/alginate (CHI/ALG) with incorporated fibroblast growth factor 2 (FGF2) and a composite consisting of electrospun nanofibers combined with a CHI/HA/ALG FSF. Characterizations demonstrated that these FSFs possess ideal swelling properties for wound exudate uptake, excellent oxygen permeability, and robust anti-bacterial effects. To further enhance their stability against degradation and to tune the FGF2 release, two crosslinking methods, 1-ethyl-3-(3-dimethylaminopropyl)carbodiimide (EDC)/N-hydroxysuccinimide (NHS) and genipin, were compared to non-crosslinked FSFs. *In vitro* tests indicated their ability to boost cell growth and fibroblast migration, which supports granulation tissue formation and accelerated wound closure. However, *in vivo* studies in mice revealed the limited stability of non-crosslinked FSF and a slight pro-inflammatory reaction against EDC/NHS crosslinked FSF. Genipin crosslinked FSF, on the other hand, demonstrate high biocompatibility and remarkable regenerative effects. Given that CHI/ALG FSF alone do not promote direct cell adhesion due to their low stiffness and high hydrophilicity, a novel spray coating method was developed, to modify the cell contact layer with an electrospun gelatin fleece in a final study. The resulting composite retains the nanotopography of the fleece side as confirmed by various topography and structural analyses. The

bioactive properties of HA/ALG and CHI in connection with the electrospun scaffold greatly improves cell adhesion and growth of fibroblasts *in vitro* while it reduces the release of pro-inflammatory cytokines in macrophages. Moreover, genipin was tested as a post-crosslinking technique, further enhancing the composite's stability and bioactive properties without changes in its anti-inflammatory potential.

In conclusion this thesis underscores the high potential of free-standing LbL based wound dressings. The anti-inflammatory properties of GAGs, when combined with the modularity of LbL assemblies, allowing controlled growth factor delivery, antibacterial properties, and the introduction of nanostructures, hold the promise of significantly improving human health.

Zusammenfassung

Chronische Wunden sind ein drängendes Problem in modernen alternden Gesellschaften, die unter einer hohen Prävalenz von Stoffwechselstörungen und eingeschränkter Mobilität leiden. Die anhaltende chronische Entzündung, die mit diesen Wunden einhergeht, führt zu langen Heilungszeiten und komplexen klinischen Behandlungen. Durch die Eindämmung der Entzündung und die Unterstützung der Regeneration wird eine schnellere Heilung mit weniger Narbenbildung möglich.

In dieser Arbeit wurden verschiedene Techniken zur Oberflächenmodifizierung, zur Herstellung von freistehenden Filmen und Kompositen mit dem gemeinsamen Ziel untersucht, die Wundheilung zu fördern und die Entzündungsreaktion zu modulieren. Zur Untersuchung des entzündungshemmenden Potenzials und der Wirkungsweise von Glykosaminoglykanen (GAGs), die auf Makrophagen wirken, wurden die GAGs Hyaluronsäure (HA) und Heparin entweder kovalent als Monoschicht oder adsorptiv als Multischicht mit der Layer-by-Layer-Technik (LbL) auf Modellmaterialien immobilisiert. Darüber hinaus wurden die physikalische Charakterisierung, die die erfolgreiche Immobilisierung bestätigt, die Aufnahme der GAGs, die Freisetzung proinflammatorischer Zytokine und die Signaltransduktion des nuklearen Transkriptionsfaktors- κ B (NF- κ B), eines zentralen Akteurs bei der entzündlichen Modulation von Makrophagen, gemessen. Die Ergebnisse zeigten, dass Heparin und Hyaluronsäure die Aktivierung und Verlagerung der p65-Untereinheit von NF- κ B in den Zellkern hemmen. Aufbauend auf diesen Erkenntnissen wurden neuartige Biomaterialien auf LbL-Basis entwickelt. Dazu gehören ein freistehender Mehrschichtfilm (FSF) aus Chitosan/Alginat (CHI/ALG) mit Fibroblasten-Wachstumsfaktor 2 (FGF2) als mitogenen Wachstumsfaktor und ein Komposit aus elektrogesponnenen Nanofasern in Kombination mit einem CHI/HA/ALG-FSF, welche die Möglichkeiten der LbL-technik ausreizen. Charakterisierungen zeigten, dass diese FSFs ideale Quelleigenschaften für die Aufnahme von Wundexsudat, eine ausgezeichnete Sauerstoffdurchlässigkeit und eine robuste antibakterielle Wirkung besitzen. Um ihre Stabilität gegenüber dem Abbau weiter zu erhöhen und die FGF2-Freisetzung zu steuern, wurden zwei Vernetzungsmethoden, 1-Ethyl-3-(3-Dimethylaminopropyl)carbodiimide (EDC)/ N-Hydroxysuccinimide (NHS) und Genipin, mit nicht vernetzten FSF verglichen. *In vitro*-Tests zeigten, dass sie das Zellwachstum und die Fibroblastenmigration fördern, die Bildung von Granulationsgewebe unterstützen und den Wundverschluss beschleunigen können. *In vivo*-Studien an Mäusen zeigten jedoch die begrenzte Stabilität von unvernetztem FSF und eine leichte entzündungsfördernde Reaktion von EDC/NHS-vernetztem FSF. Die mit Genipin vernetzten FSF zeigten dagegen eine hohe Biokompatibilität und bemerkenswerte regenerative Wirkungen. Da

CHI/ALG-FSF allein aufgrund ihrer geringen Steifigkeit und hohen Hydrophilie keine direkte Zelladhäsion fördern, wurde eine neuartige Sprühbeschichtungsmethode entwickelt, um die Zellkontaktschicht mit einem elektrogenesponnenen Gelatinevlies zu modifizieren. Das resultierende Komposit behielt die Nanotopographie der Vliesseite bei, was durch verschiedene Topographie- und Strukturanalysen bestätigt wurde. Die bioaktiven Eigenschaften von HA/ALG und CHI in Verbindung mit dem elektrogenesponnenen Scaffold verbessern die Zelladhäsion und das Wachstum von Fibroblasten *in vitro* erheblich, während die Freisetzung von proinflammatorischen Zytokinen in Makrophagen reduziert wurde. Darüber hinaus wurde Genipin als Nachvernetzungstechnik getestet, wodurch sich die Stabilität und die bioaktiven Eigenschaften des Komposits weiter verbesserten, ohne dass sich sein entzündungshemmendes Potenzial veränderte.

Zusammenfassend unterstreicht diese Arbeit das große Potenzial von freistehenden LbL-basierten Wundauflagen. Die entzündungshemmenden Eigenschaften von GAGs in Kombination mit der Anpassungsfähigkeit von schichtweise aufgebauten Verbänden für die kontrollierte Abgabe von Wachstumsfaktoren, antibakteriellen Eigenschaften und der Einführung von Nanostrukturen versprechen eine deutliche Verbesserung der menschlichen Gesundheit.

Preamble

The scope of this thesis is the development and analysis of anti-inflammatory and wound healing biomaterials. To explore this topic in greater depth the introduction (chapter 1) will focus on the common points between all publications; skin wound healing and inflammation, the biopolymers used in the studies, as well as the LbL technique. The following two chapters (chapter 2 and 3) will provide an insight into the anti-inflammatory effects of GAGs such as HA and Hep applied as surface coatings either based on self-assembling monolayers (SAMs) or LbL technique. Afterwards, the use of free-standing multilayer films based on CHI and ALG and loaded with FGF2 as wound dressings are tested for biocompatibility *in vitro* and *in vivo*, their ability to facilitate wound closure and to exert antibacterial properties (chapter 4). Finally, in chapter 5 a combination of an electrospun fleece and a free-standing film with (HA/ALG)/CHI is presented as a novel composite and its capabilities to modulate inflammation and facilitate wound regeneration assayed.

Chapter 1 - Introduction

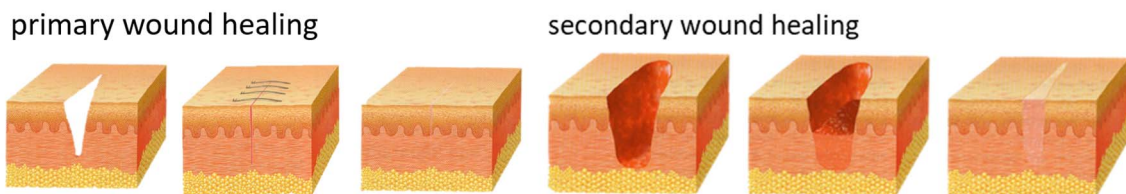
1.1 Skin Wounds – the Clinical Setting

Wound-related issues have become a growing burden on both healthcare systems and individuals (1). The aging population in Germany and other parts of the world is associated with a significant increase in higher rates of hospitalization, posing a growing challenge for health care. In nursing homes in Germany about 7.8 % of all residents have chronic wounds (2). Chronic wounds are also gaining importance due to secondary factors such as metabolic disorders (e.g. diabetes) and reduced mobility causing pressure ulcers (3). These factors have a significant impact on the inflammatory processes in wounds, causing them to deviate from the physiological and controlled healing pathway and leading to chronic conditions. As a result, the urgency and significance of wound treatment research has significantly grown in recent years. Great progress has been made in the management of wounds (4). However, in the current German treatment guide for chronic wounds “*S3-Leitlinie Lokalthherapie chronischer Wunden bei Patienten mit den Risiken periphere arterielle Verschlusskrankheit, Diabetes mellitus, chronisch venöse Insuffizienz*” (5) there is no mentioning of active wound dressings except for anti-bacterial silver, iodine and polyhexanide soaked gauzes as well as HA and collagen based wound dressings. Skin grafting or the use of growth factors, except the (in the EU) discontinued and not available platelet-derived growth factor (PDGF)-based Regranex® gel, is not represented. Nonetheless, it becomes evident that innovation in the use of modern wound dressing stalled and there is a mismatch between the developments in regenerative medicine and the adopted and available treatment options in practice. This illuminates the need for innovative and easy to produce multifunctional biomaterials that form the basis of new treatment options.

Physiology of Skin Wound Healing

A wound is defined as the disruption or impairment of the biological integrity of the skin. Wounds can arise from various sources, such as trauma, injuries (e.g. burns or accidents), surgical procedures, aging, and secondary complications associated with different conditions like diabetes mellitus (6). Numerous local and systemic factors influence wound healing. Local factors directly affect wound properties, including oxygen supply, infections, and foreign bodies (4). Systemic factors encompass an individual's overall health status, influencing wound healing capacity. These factors range from age, stress, obesity, alcohol consumption, smoking, and immune-compromised conditions to diseases like diabetes and fibrosis (7). Superficial, small, and clean wounds typically experience a brief hemostatic and inflammatory phase, blood clot

formation is limited to sealing the wound and clearing minor cell debris (8). Partial thickness wounds that involve the epidermis and partially the dermis generally heal through primary intention, resulting in the restoration of intact skin appendages including hair, nails, and sebaceous and sweat glands (9). In contrast, full-thickness wounds encompass complete destruction of both the epidermis and dermis, along with deeper structures necessitate a longer healing period due to extended hemostasis and removal of cell debris and necrotic tissue (10). Tissue repair in such cases begins with the formation of granulation tissue, which fills the defect before epithelial coverage can occur. This form of wound healing is termed healing by secondary intention (8). Differences are illustrated in **Fehler! Verweisquelle konnte nicht gefunden werden..**



Healing mechanism	Healing type		
	Epithelial wound healing	Primary wound healing	Secondary wound healing
Granulation tissue	-	+	++
Contraction	-	+	+++
Epithelisation	+++	+	+

Figure 2 - Primary wound healing; a minimal tissue defect with smooth, closely spaced wound edges, and a well perfused wound area are the prerequisites for primary wound healing. Examples include surgically placed wounds and some lacerations and cuts. They can be closed with sutures, staples or suture strips. The wound edges grow firmly together within eight days. Secondary wound healing: The processes of secondary wound healing are more complex, more prone to failure and take longer. The tissue defect is gradually filled with granulation tissue, which is then remodeled into scar tissue. Based on (11)

Depending on the duration required for healing, wounds are categorized into acute wounds (which typically heal within 8-12 weeks) and chronic wounds (requiring more than 12 weeks for healing) (4). Acute wounds heal by a well-coordinated process of hemostasis (coagulation), inflammation, proliferation, and remodeling that sequentially restores the damaged skin's integrity (8)

Hemostasis

Hemostasis serves as the initial phase of wound healing. This process unfolds in three pivotal steps: vasoconstriction, primary hemostasis, and secondary hemostasis (10). After injury, blood vessels promptly undergo constriction to reduce bleeding from the microvasculature. This constriction is orchestrated through the automatic tightening of vascular smooth muscle, prompted by vasoconstrictors like endothelin (8). Moreover, vasoconstriction is stimulated by

circulating catecholamines and prostaglandins, released by injured cells (10). Following the brief 5- to 10-minute period of vasoconstriction, blood vessels undergo dilation. Through ruptured vessels thrombocytes (platelets) populate the provisional matrix. In Figure 3 the distribution of cell populations over time is shown. In the primary hemostasis, exposed collagen and von Willebrand factor starts the clotting cascades (12). Secondary hemostasis refers to the activation of the coagulation cascade, in which soluble fibrinogen converts to insoluble strands that constitute the fibrin mesh. Platelet degranulation leads to formation of a blood clot that fills the wound cavity, doubling as a provisional fibrin matrix, which functions as a scaffold for the migration of diverse cells (10). Furthermore, an array of cytokines and growth factors are released into the wound milieu by platelets. These attract inflammatory cells (neutrophils and monocytes) and fibroblasts to the wound area. The complex signal interplay for hemostasis are systematically summarized elsewhere in more detail; Versteeg et al. (13).

Inflammation Phase

The inflammation phase, which overlaps with the hemostasis phase, sets the stage for subsequent repair processes. In this phase pathogens should be eliminated, and tissue repair initiated. This phase is characterized by the rapid migration of immune cells into the wound area, where they collaborate to remove debris, fight infections, and create an environment favorable to subsequent healing stages (6). It is characterized by a complex interplay of cytokines, chemokines, and growth factors, which collectively shape the milieu at the wound site (10). This wound milieu consisting of various proteinases, pH gradients, and pO₂ gradients which all have a major impact on cellular functions of macrophages, fibroblasts, and keratinocytes (6). As the injury occurs, danger signals emerge, arising from both the damaged tissues themselves and potential invading pathogens. These signals encompass damage-associated molecular patterns (DAMPs) released by stressed or necrotic cells and pathogen-associated molecular patterns (PAMPs) specific to foreign invaders. DAMPs are molecules from the host like shock proteins and free DNA or RNA while PAMPs are components of bacteria, fungi, or damaged epithelial cells (14). Wound healing in the initial stages is driven by tissue-resident macrophages and neutrophils as key players which possess receptors for DAMPs and PAMPs (10, 15). Neutrophils are attracted by these breakdown products and travel to the wound site. Endothelial cells express adhesion molecules, including intercellular adhesion molecule 1 (ICAM1), vascular cell adhesion molecule 1 (VCAM1), and e-selectin (SELE) which mediate the adherence of neutrophils to the wall of blood vessels (12). The neutrophils bind to endothelial cells and alter their cytoskeletal structure that initiate their extravasation from the bloodstream (16). Upon leaving the blood vessels, neutrophils react to a chemokine gradient within the skin, inducing their migration towards areas

of higher chemokine concentration: specifically, the wound site where these signaling molecules are released (6). In the absence of infection, neutrophils usually remain at the wound site for a duration of 2 to 5 days (17). During that time neutrophils engage in phagocytosis, engulfing pathogens, and cellular debris, while also releasing a spectrum of antimicrobial substances, such as cationic peptides and proteinases as well as tumor necrosis factor (TNF)- α , interleukin (IL)-1 β , and IL-6 as pro-inflammatory stimuli (14). Beyond the innate immune arm, the adaptive immune system, predominantly represented by B and T lymphocytes, also assumes a role in the healing process. Regulatory T cells can regulate tissue inflammation via the attenuation of the interferon- γ (IFN- γ) production and the accumulation of pro-inflammatory macrophages (15). This role of the adaptive immune system is covered in detail in: *Rodrigues et al.* (10).

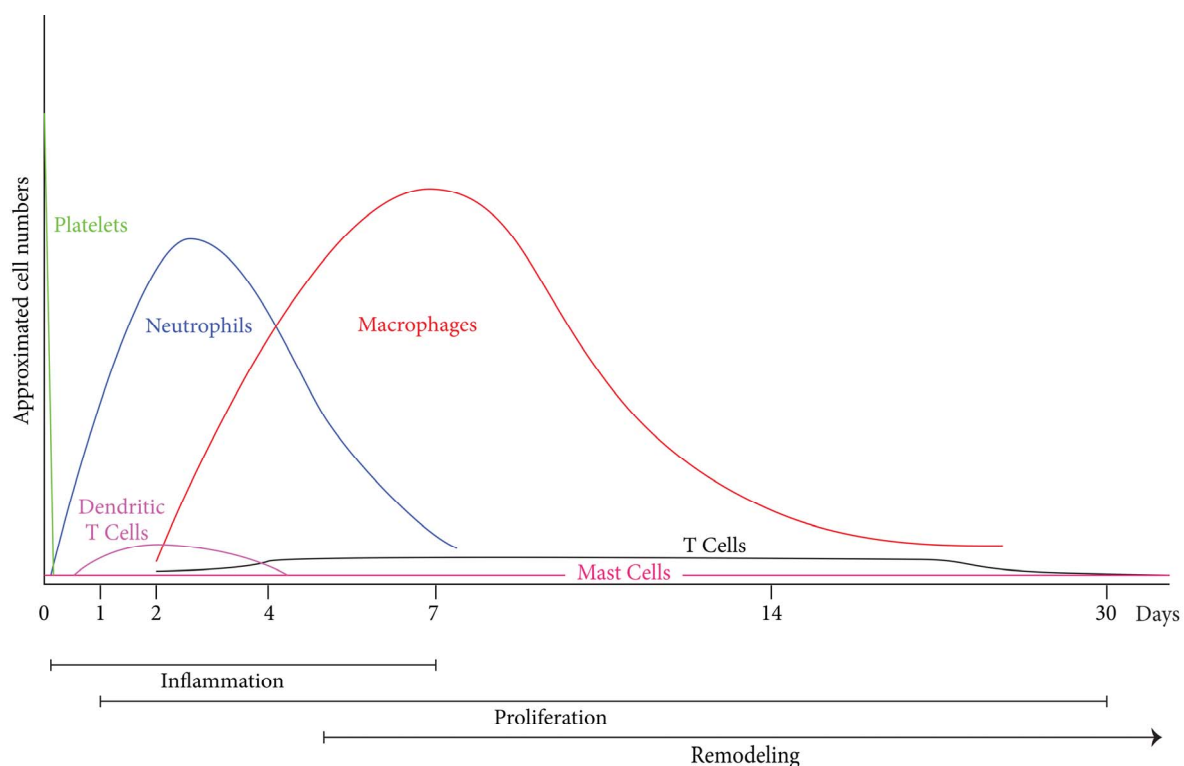


Figure 3 - The individual duration of healing phases is found in the bars at the bottom of the graphic. The cell number is represented in the diagram. After the peak of platelets during hemostasis, neutrophil accumulation in the wound increases during the initial inflammatory phase and starts declining 4 days later until the end of the week. Macrophages are the most abundant cell in all phases of wound repair. Their number increases during the inflammation phase and reach maximum during the proliferation phase and decline progressively during the remodeling phase. Lymphocytes start increasing their number after injury and reach a plateau at day 4 that continues to be present until the last phase. Based on (15)

Approximately 2 days post-injury, monocyte numbers increase, recruited by platelet and mast cell degranulation (10). Circulating human monocytes are derived from a monocyte-dendritic progenitor (MDP) in the bone marrow which generates both monocytes and a dendritic cell precursor (CDP) (15). Stimulated by neutrophils and T-reg cells, these monocytes mature into macrophages. Macrophages show great plasticity, which is reflected in the M1/M2 dichotomy (18). For example, macrophages can recognize PAMPs and DAMPs through their pattern

recognition receptors (PRRs). Additionally, IL-1 β , IFN γ and TNF- α by neutrophils and T cells stimulate macrophages to adopt an inflammatory phenotype (M1) (18). M1 macrophages are associated with phagocytosis and scavenging pathogens, along with producing pro-inflammatory mediators. After a while, M1 macrophages can undergo a transition into the M2 subset, which demonstrates a reparative macrophage phenotype. M2 macrophages play a role in generating anti-inflammatory mediators, promoting the constructing of extracellular matrix (ECM), initiating fibroblast growth, and promoting angiogenesis (19). Additionally, they terminate the inflammation phase by phagocytosis of neutrophils and cell debris, removing pro-inflammatory stimuli from the wound. Failure to undergo the M1-M2 transition can lead to the development of non-healing or chronic wounds (19). The impact of macrophages on the healing process is substantial, as they are responsible for shifting the phase from inflammation to proliferation. Therefore, this process will be explored in detail in a dedicated section (subchapter Macrophages, p.24).

Proliferation: Neoangiogenesis, Granulation Tissue Formation and Epithelialization

The proliferative phase includes neoangiogenesis, granulation tissue formation and re-epithelialization (15). During the proliferative phase, nutrients and oxygen are limiting factors due to the high metabolic activities of the regenerative processes. Therefore, neoangiogenesis is essential for proper wound healing. The reduced blood supply coupled with the increased metabolism of cells working to repair injury leads to hypoxia, a key stimulus to angiogenesis (8). Hypoxic conditions stimulate the synthesis of hypoxia-induced factor-1 (HIF-1) in macrophages, fibroblasts, vascular endothelial cells and keratinocytes. The release of proangiogenic factors such as vascular endothelial growth factor (VEGF), FGF2, PDGF, transforming growth factor- β 1 (TGF- β 1) and the metabolic switch of endothelial cells induce neovascularization (15). Soon after, activated by VEGF, lymph angiogenesis starts by lymphatic endothelial cell (20). In full thickness wounds the exposed connective tissues requires granulation tissue formation for epithelial migration to take place (21). Granulation tissue consists of fibroblasts, granulocytes, macrophages, blood vessels, in complex with type I collagen bundles and ECM components, which partially recovers the structure of the skin tissue (16). During the proliferative phase, the anti-inflammatory phenotype (M2) of macrophages becomes the dominant cell population and orchestrates the interaction with endothelial cells, fibroblasts, keratinocytes, ECM and peripheral nerves (10). Additionally, wound-healing macrophages are involved in collagen production as up-regulated arginase activity in this subtype allows for the conversion of arginine to ornithine, which is an essential precursor in collagen production (15). Fibroblasts have a key role in creating granulation tissue. They migrate into the wound mainly from the nearby dermis in

response to cytokines such as PDGF, TGF- β and FGF2 produced by platelets and macrophages in the wound (12). If the wound takes a long time to heal, the fibroblasts in the wound may also come from fibrocytes. These are mesenchymal precursor cells that either reside in vessels and glands or travel through the blood stream from the bone marrow (22). Fibrocytes move to areas of skin damage and help the healing process by becoming a type of fibroblast in the wound (12). Fibrocytes also secrete cytokines, chemokines, and growth factors, as well as improve angiogenesis and present antigens. Once fibroblasts migrate into the wound provisional matrix they generate proteinases, such as matrix metalloproteinases (MMPs), which break down the provisional fibrin matrix. They also deposit collagen and other ECM components, such as proteoglycans and HA (21).

Cutaneous wounds need to undergo closure, while rodents primarily heal through contraction, in humans, reepithelialization contributes to about 80 % of wound closure (8). The mode of reepithelialization in humans depends on numerous factors such as wound location, depth, size and microbial contamination. In partial thickness wounds, cells need to cover around 500 μm and achieve complete epithelialization typically within 8–10 days (9). The resurfacing of epidermal wounds happens by migrating of an epidermal tongue formed by the leading row of keratinocytes adjacent to the wound, where activated keratinocytes reorganize their cytoskeleton over the fibrin, fibronectin, and vitronectin derived from the blood clot (23). Upon reaching the middle of the wound, contact inhibition halts keratinocyte migration, completing wound coverage (10).

Remodeling

Wound closure and replacement of the original tissue with a collagenous scar is the best outcome of secondary wound repair in children and adults. It marks the end of the last wound healing phase, e.g., the remodeling phase. Cutaneous scars have no epidermal appendages (hair follicles and sebaceous glands) and a densely packed collagen fiber pattern that is distinctly different from unwounded skin where a reticular collagen pattern is found (24, 25). These new collagen fibers are secreted by fibroblasts which are present as early as 3 days. Activated by growth factors like TGF- β , Ectodysplasin A (EDA)-fibronectin and mechanical tension, dermal fibroblasts transform into stress fiber-expressing proto-myofibroblasts (21). Myofibroblasts, which appear around 4 days post-injury, play a significant role in wound contraction fiber deposition. The disordered deposition of these contraction fibers can lead to fibrosis, which manifests itself as hypertrophic scarring (26). Initially scars appear red due to capillary growth, which recedes as the scar matures, revealing its true pigmentation as full mature scars usually appear hypopigmented, due to the absence of melanocytes (10). With the wound closure the

healing is complete after around 12 weeks. However, scar remodeling takes months to years.

Scarless Healing

Opposed to the conventional way of skin wound healing following the above-mentioned timeline, there also exists the possibility of scarless healing. Fetuses until the second trimester can heal injuries with complete restoration, where the epidermis, dermis with hair follicle and sweat glands are restored to a normal architecture and the collagen dermal matrix pattern is unchanged from unwounded dermis (8, 24). This might be due to the specific response of fetal fibroblasts to the pro-fibrotic mediator TGF- β (27). Meanwhile in adults some cases of excessive scarring can be found. These wounds missing "stop" cues which halt the repair process once the dermis is closed, and epithelialization completed (8). The exact molecular mechanisms responsible for this process remain unknown (27). Overexpression of pro-fibrotic cytokines and reduced collagenase activity in the skin tissue have been found in patients (8). There is a deficiency in programmed cell death, known as apoptosis, at the end of the healing process with the persistent activity of fibroblasts and myofibroblasts that secrete ECM components (8). The most common nonsurgical therapy for the treatment of keloids and hypertrophic scars is the topical application or intralesional injections of corticosteroids, but with limited benefits and downsides like delaying wound closure and (27). The anti-scarring impact of several anti-TGF- β treatments were investigated, but was insufficient to prevent scarring (28, 29). Reduction through TGF- β alone is unlikely due to the redundancy of action among growth factors (27). Tissue mechanics, duration of wound closure and intensity of the inflammatory response have become crucial factors in addressing excessive scarring (27). Novel strategies are developed which to limit inflammation, the use of scaffolds to allow migration and the supplementation of mitogenic growth factors like FGF2 (30–32). Another option might be the inhibition of post-translational modification of collagen (33).

Chronic Wounds - Key Players and Deficiencies

Chronic wounds in comparison to normal healing wounds fail to resolve the inflammation phase and are clinically defined as wounds, not healed beyond 12 weeks (8). Chronic wounds, such as non-healing ulcers, exhibit a disruption in the epidermal stem cell niche due to ongoing inflammation resulting from infection, hypoxia, ischemia, and excessive exudates, limiting the cell pool as a result (10). As shown in Figure 4, compared to the trajectory physiological wound healing the resolution of chronic wounds is nonlinear and complex, potentially involving varying metabolic states in different wound areas (7).

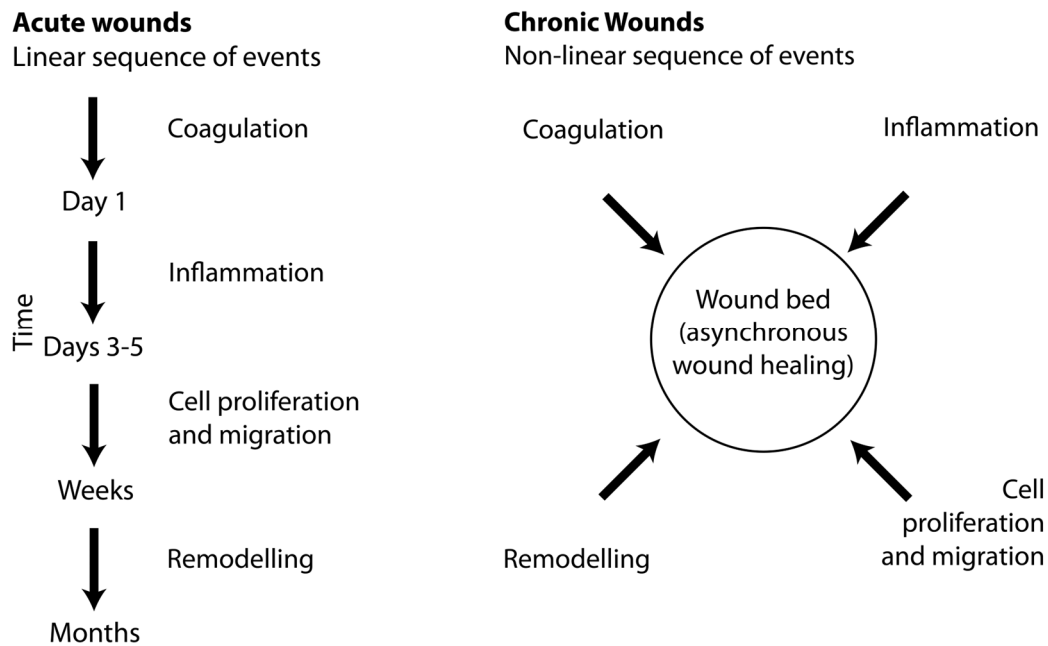


Figure 4 - Wound healing processes in acute and chronic wounds. In acute wounds the individual phases of normal healing are follow a linear sequence, while chronic wounds (right) are characterized by a process in which the distinct phases occur randomly and without a defined time frame. Additionally, parts of chronic wounds can be at different phases of healing. Surgical debridement tries to synchronize the different areas of the chronic wound's bed for a more unified therapeutic approach. Based on: (7)

The inflammation phase is considered to be a critical period for clearing bacteria and providing a favorable environment for regeneration of the tissue (7). Disturbances in the immune response during wound healing, such as an increase in necrotic tissue, poor perfusion, elevated levels of pro-inflammatory cytokines, proteases, and ROS, as well as infections, lead to abnormalities in immune cell recruitment, altered proteolytic balance, and impaired blood vessel formation (34). As discussed in the chapter before, the resolution of inflammation and the initiation of the regenerative phases depends on an intricate interplay of signaling proteins within the wound environment (15). To date there is no singular focal point in the signaling cascade or master regulator known, which might be the origin of the myriad of dysregulated processes in chronic wounds. Nevertheless, several well-established hallmarks of chronic wounds emerge from this complex scenario.

Macrophages assume a vital role in eliminating apoptotic neutrophils and in regulating inflammation, depending on their activation state (18). However, in chronic wounds, these macrophages have a limited ability to clear apoptotic neutrophils and their switch from the pro-inflammatory M1 state to the M2 state is disrupted (7). As depicted in Figure 5, M1 macrophages are most prevalent in chronic wounds, failing to establish a regenerative wound milieu. Excessive neutrophil infiltration is another pivotal factor contributing to chronic inflammation (10). An abundance of neutrophils results in the overproduction of ROS, which directly increases ECM degradation (34). This further impairs cell migration, reduces fibroblast proliferation, and hinders

collagen synthesis. Moreover, ECM degradation products further promote ongoing inflammation, perpetuating a self-sustaining process. MMPs are another factor that can delay wound healing (35). Both neutrophils and activated macrophages produce pro-inflammatory cytokines such as IL-1 β and TNF- α , which not only increase MMP production, but also reduce the amounts of tissue inhibitors of MMPs (TIMPs) (35). In normal wound healing MMPs are required in lesser amounts to stimulate the proliferation of keratinocytes (23). However, their dysregulation leads to impaired epithelialization and is strongly associated with hard-to-heal wounds. Beside the activity of neutrophils and macrophages, T cell activity, the ratios of CD4 and CD8 T cells, was identified to differ from normal healing wounds (10). However, depletion of CD4 and CD8 T cells in mice does not appear to affect wound closure rates (36).

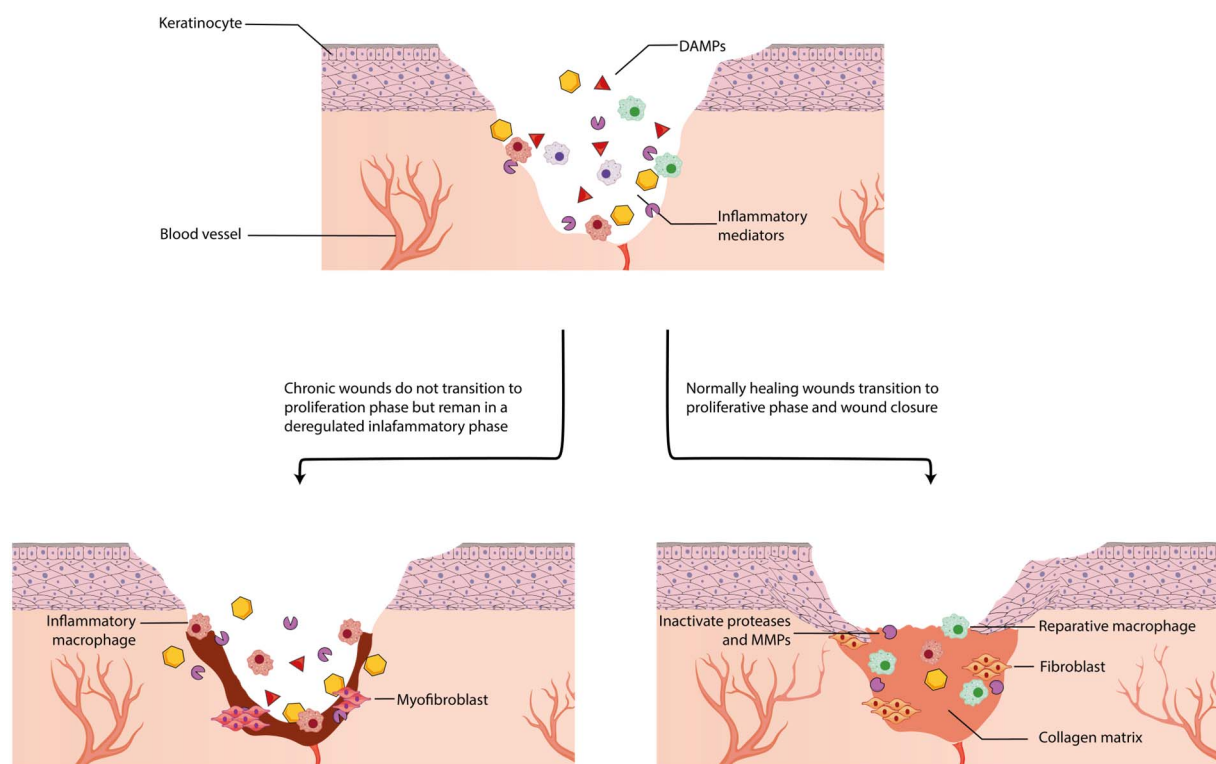


Figure 5 - Following the inflammation phase, normal healing wounds undergo a transition into the proliferative phase of wound healing. A key feature of this phase is the shift of immune cells towards anti-inflammatory and proliferative responses, facilitating tissue repair (bottom right). In contrast, chronic wounds exhibit an inability to overcome local inflammatory responses. This leads to a stagnant and irregular inflammation phase, preventing the progression toward tissue repair (bottom left). Based on (7)

In addition to immune disturbances, wound infections are another prominent factor contributing to chronic inflammation (4). If the infection is not adequately controlled in a timely manner, it can result in the formation of a biofilm. The formation of a biofilm leads to the secretion of an exopolysaccharide matrix, which acts as a protective shield for bacteria against antibiotic treatment and the host's immune response (34). Consequently, the presence of bacteria and endotoxins triggers an abnormal increase in pro-inflammatory factors, further perpetuating the state of inflammation (12). Another factor in chronic wounds is inadequate tissue oxygenation.

Oxygen is a crucial element in the wound healing process, playing a role in protecting wounds from infection, improving the proliferation and migration of fibroblasts, inducing angiogenesis, enhancing the differentiation of keratinocytes, promoting re-epithelialization, increasing collagen synthesis, and facilitating wound contraction (34). When all these factors come together, they contribute to the persistence of inflammation, tissue destruction, and the ineffective removal of pathogenic bacteria.

Growth Factors - Deficiencies in Chronic Wounds

Growth factors in wound healing have received significant attention as important promoters of the repair process (37, 6, 38). Beside GFs a number of other signaling molecules have been identified and utilized as targets for wound healing modulation; CXC-chemokines and CC-chemokines (e.g. MCP-1) (39), matrix metalloproteinases (35), interleukins (e.g. IL-4, IL-1 β) (40), interferons (e.g. IFN γ) (41), the TNF family (e.g. TNF- α) (42), keratins (43), and LL-37 as well as cathelicidin (44). To describe the high number of different signal molecules, their intricate interplay, and dependencies during the wound healing processes would go beyond the scope of this thesis. Refer to this review: Schreml *et al.* (6).

GFs are polypeptides that are released by a variety of activated cells at the wound site (16). Figure 6 provides an overview of GFs and their target cell types.

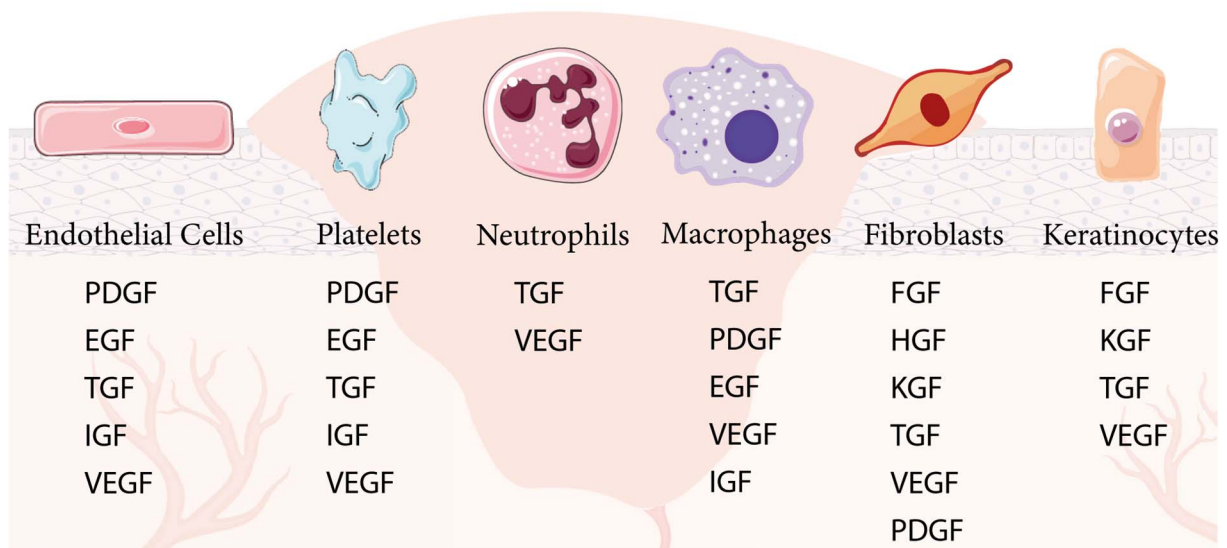


Figure 6 - Major GFs involved in wound healing and their targeted cell types. Based on (45)

In chronic wounds, there is a notable decline in the levels of key growth factors, including epidermal growth factor (EGF), FGFs, TGF- β , PDGF, and VEGF. (37). PDGF attracts neutrophils, macrophages, and fibroblasts to the wound site. It promotes cell proliferation, migration, and the production of ECM components of fibroblasts and smooth muscle cells, thereby contributing

significantly to tissue repair but also scar formation (12). PDGF also plays a critical role in angiogenesis, stimulating endothelial cell migration and the formation of new blood vessels, increasing nutrient and oxygen delivery to the wound site (15). EGF is influencing predominantly epidermal cells, particularly keratinocytes. EGF stimulates keratinocyte proliferation, migration, and differentiation, facilitating the process of re-epithelialization, which is fundamental for wound closure (9). Additionally, EGF promotes angiogenesis by inducing endothelial cell proliferation (16). The FGF family, which includes various isoforms such as FGF2 (basic FGF) and FGF7 (keratinocyte growth factor), plays a critical role in activating fibroblasts. FGFs are instrumental in collagen synthesis, ECM remodeling. Notably, FGFs are also promoting angiogenesis by attracting endothelial cells to the wound site (15). TGF- β 1, with its distinct isoforms, including TGF- β 1, TGF- β 2, and TGF- β 3b predominates in adult wound healing, demonstrating its pro-migratory and pro-fibrotic attributes (21, 8). This growth factor directly engages fibroblasts, to synthesize collagen and reducing ECM degradation. TGF- β 1 is a versatile signaling molecule, originating from various cell types at the wound site, including platelets, macrophages, fibroblasts, and keratinocytes. When experimentally applied to wounds with no inherent repair deficiency, TGF- β 1 accelerates the wound healing process, though this acceleration often comes at the expense of heightened fibrosis, which may lead to excessive scarring in the context of normal skin healing (8).

Macrophages

While GFs are mediators, which stimulate mostly reparative functions, macrophages are a focal point of cell signal processes during the inflammation phase. The function of other immunomodulating cells present in chronic wounds are T cells, mast cells, neutrophils and dendritic cells are covered in a review by *Rodrigues et al.* (10).

Macrophages are a crucial component of the host innate immune system, exhibiting diverse functions essential for tissue homeostasis and defense against foreign invasion (46). These cells specialize in phagocytosis, clearing damaged cells and foreign molecules, making them valuable scavenger cells during infections and transplantation. They hold a well-established role in the intricate process of wound healing, a function that is owed to their plasticity (47). Most macrophages originate from differentiated monocytes, a subgroup of the white blood cells. Monocytes are derived from precursors in the bone marrow, which circulate through the blood vessels. Responding to inflammation signals, like chemokines (e.g. CCR2) and adhesion molecules (e.g. ICAMs, integrins), the monocytes transmigrate through capillary walls into the appropriate tissue and differentiate to macrophages or dendritic cells (48). Certain tissue-resident macrophages, such as those in the brain, liver, skin and heart, represent exceptions to

this differentiation process (49). Upon infiltration into affected tissues, macrophages actively contribute to degradation, tissue regeneration and angiogenesis (50). Beyond their role in the innate immune system, macrophages also play a significant part in the adaptive immune response. As antigen-presenting cells, they engulf, digest, and present antigens to T helper cells, leading to antibody production against the antigen (51). Additionally, macrophages can influence the activation states of granulocytes, lymphocytes, fibroblasts, and endothelial cells through cytokine release (52).

In the 1960s, it became clear that macrophages could enter an activated state in which their microbicidal activity was enhanced (53). Since then, similar to the T helper cell classification a classical (M1 state) and an alternative activated phenotype (M2 state) has been introduced (47). However, this separation cannot be described as two distinct subcategories, but is now known as a continuum with M1 and M2 as cornerstones (49). Macrophage polarization is orchestrated by a variety of stimuli present in the tissue microenvironment, encompassing cytokines, growth factors, and PAMPs (52) (Figure 7). Stimuli frequently associated with the M1 phenotype are IFN- γ , TNF- α , lipopolysaccharides (LPS), and Granulocyte macrophage colony-stimulating factor (GM-CSF) (47). M1 macrophages produce pro-inflammatory cytokines and chemokines such as IL-1, IL-6, IL-8, IL-12, TNF- α , and macrophage inflammatory protein-1 (MIP-1) through the mediation of diverse nuclear transcription factors, including signal transducer and activator of transcription (STAT)1, STAT5, and NF- κ B (52, 51). These cytokines may intensify inflammation by (self-)stimulating macrophages and recruiting leukocytes. Furthermore, upon classical activation, macrophages produce elevated levels of inducible nitric oxide synthase (iNOS) and reactive oxygen species (ROS) and increase their capacity to eliminate microbes through the creation of cytotoxic nitric oxide (NO) (51). However, this heightened oxidative response can also lead to inadvertent damage to the surrounding tissue due to the generation of radicals (54). In contrast, the M2 phenotype exhibits a regulatory and wound healing nature, presenting a vital role in tissue repair processes (47). Th2-cells, basophiles, and granulocytes are responsible for producing IL-4, which serves as the primary stimulus for M2-macrophages (47). Moreover, IL-13, IL-10, and GM-CSF have also been identified as significant stimuli for M2-macrophage activation. These cytokines exert their influence through nuclear transcription factors, such as STAT6 and STAT3, leading to the downregulation of pro-inflammatory cytokines like IL-12 and TNF- α (52). At the same time, they up-regulate anti-inflammatory cytokines, including IL-10, as well as various growth factors such as VEGF, TGF- β , and PDGF (47).

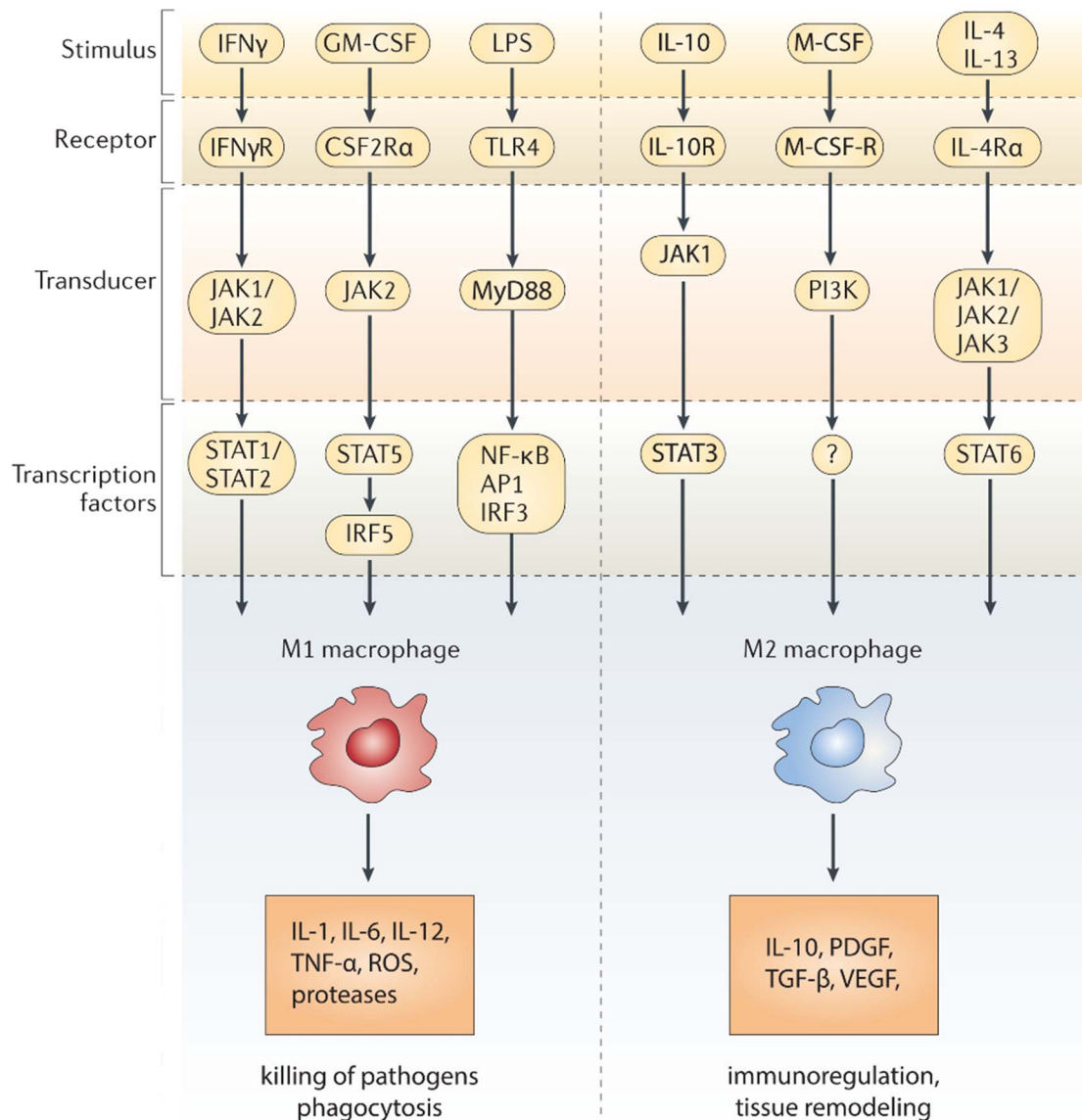


Figure 7 – Transcriptional Regulation of macrophage activation. Adapted from (52) with data from (47) and (55).

Consequently, this intricate network of regulatory elements acts to attenuate inflammation while promoting wound healing through the modulation of fibroblasts (56). During the immune responses, all macrophage phenotypes are present, dependent on the phase of the host response (18). It is still debated whether the polarized macrophages are recruited to the inflammation site, or the macrophages can change their phenotype (49). However, recent findings implicate that macrophages keep their functional adaptivity (57). This plasticity of macrophages underlines that macrophages, as immunomodulating cells, have an enormous impact on the resolution of the inflammation phase (18). This makes them a valuable target for anti-inflammatory therapies.

NF- κ B Signaling Pathway – Key Signal Transducer of Macrophage Modulation

The NF- κ B pathway is a pivotal orchestrator of many physiological processes, such as the development and regulation of the immune system, cell proliferation, and programmed cell death (58). Since its discovery in 1986 by Sen & Baltimore it was identified to play a significant clinical role in inflammation, autoimmune diseases, atherosclerosis, neurodegeneration and cancer (59). During inflammation, the NF- κ B pathway regulates the activation, differentiation and effector function of inflammatory T cells and macrophages (60). In chronic inflammatory diseases, like chronic skin wounds, a deregulated NF- κ B activation is typical (60). Therefore, the mechanism of NF- κ B activation and pro-inflammatory function is of great significance for therapeutic strategies in the treatment of chronic inflammation (60). The NF- κ B consists of five subunits p65/RelA, c-Rel, RelB, p50, and p52. Under normal circumstances, the NF- κ B subunits are sequestered by the inhibitory I κ Bs protein family (61). During activation of the NF- κ B pathway, the inhibitor proteins get degraded via the I κ B Kinase (IKK α , IKK β and IKK γ), leaving NF- κ B phosphorylated and ready to translocate to the nucleus (60, 62). This makes the NF- κ B a rapid acting transcription factor, due to the high amount of NF- κ B are always available to act. On the other hand, the genes controlled by NF- κ B are numerous (about 500), making it a part in bigger transformation processes of cells (63). After translation of the promoted DNA-sequences NF- κ B activation gets terminated, by a high number of autoregulatory proteins, which repress NF- κ B in various ways (64). Among them are also the I κ Bs, which elevated synthesis rate, blocks the DNA-binding of NF- κ B subunits. Finally, the already bound NF- κ B gets degraded by the proteasome (64).

NF- κ B gets activated by a diverse range of mediators, such as Toll-like receptors and antigen receptors, to cytokine and growth factor receptors, as well as physical, oxidative and genotoxic stress as illustrated in Figure 8 (61). The most studied pathways are the TNF-receptor-, the toll-like receptor (TLR)-, the TCR- and the B cell receptor (BCR)-pathway. These receptors are activated by endogenous and exogenous proteins associated with inflammation. The TLR-receptor, for example, react to PAMPs (65). These PAMPs encompass proteins or structural motifs which are distinctive across a broad spectrum of microbes (7). For macrophages, induction of the NF- κ B pathway, orchestrates a shift towards a pro-inflammatory M1 phenotype. PAMPs mediated by TLRs initiate the NF- κ B pathway and the subsequent production of pro-inflammatory M1-associated cytokines, chemokines and growth factors, such as IL-1, IL-6, IL-8, TNF- α and GM-CSF (61, 58).

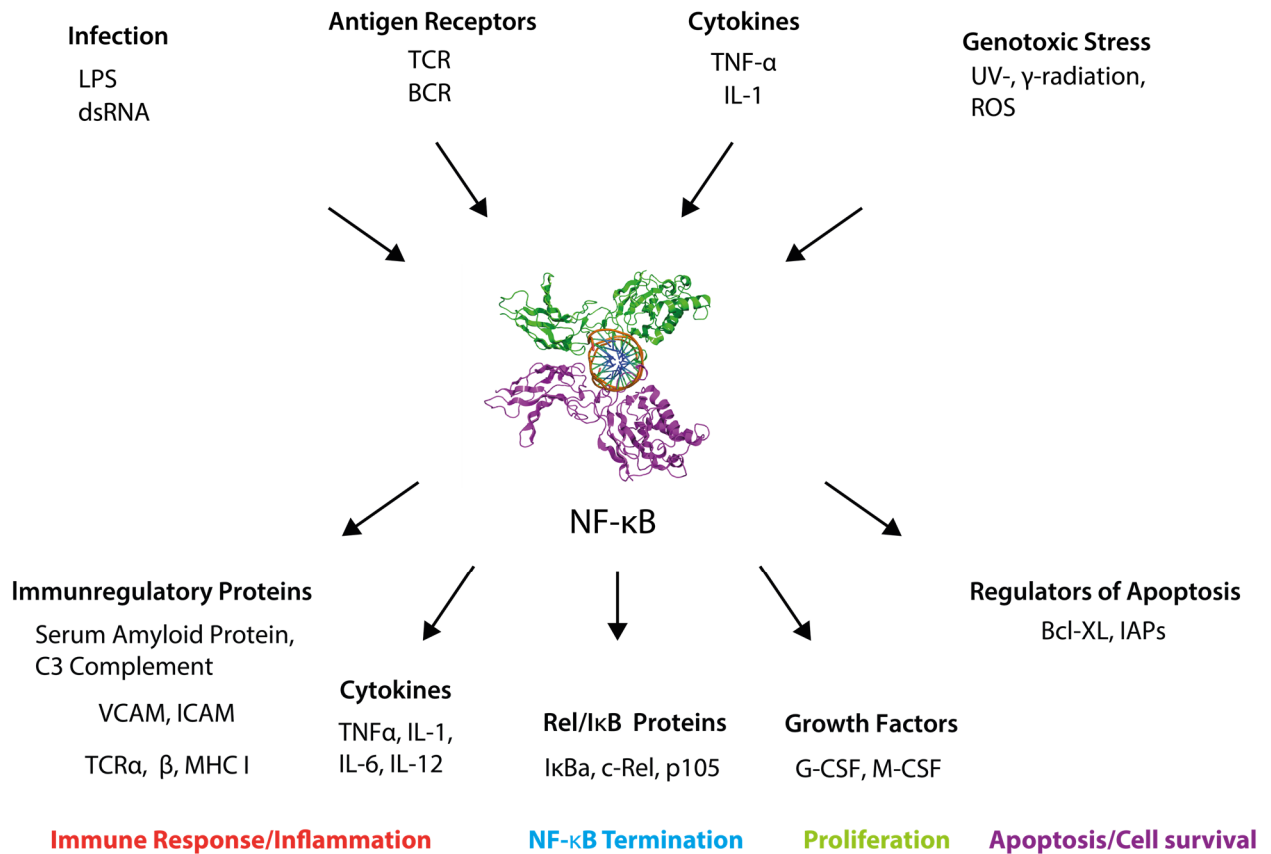


Figure 8 - Representative examples of NF-κB stimuli and target genes. Based on (61).

This stimulates macrophages in a paracrine and autocrine manner. Moreover, the iNOS synthesis is stimulated, which increases the microbicidal activity (66). Since the shift and accumulation of M1-macrophages during inflammation relates to a poor outcome, the suppression of the NF-κB-pathway is a valuable target for anti-inflammatory designs.

1.2 Biopolymers - Building Blocks for Bioactive Surface Coatings and Wound Dressings

Biopolymers and specifically polysaccharides possess high popularity in biomaterial design. In particular HA, Chi and ALG are frequently used in wound dressings application, where they have been used before, although not in this combination (67–69). Hep is a popular building block in surface coatings (70). All are known for their polyionic nature and possess a backbone of repeating disaccharide units and changing amounts of amine, carboxyl groups or sulfonate groups, making them easily available for chemical modification. At the same time, they allow the easy covalent coupling to SAMs, for example by the EDC/NHS crosslinking chemistry. As a result, they are useful in layer-by-layer based approaches or covalent binding on self-assembling monolayers. Meanwhile gelatin is a protein-based biopolymer frequently used in tissue engineering (71).

Hyaluronic Acid

HA is a non-sulphated GAG found abundantly in animals (72). It has a linear polysaccharide structure consisting of repeating disaccharide units of D-glucuronic acid and N-acetyl-D-glucosamine linked by $\beta(1\rightarrow4)$ and $\beta(1\rightarrow3)$ glycosidic linkages (73) (Figure 9).

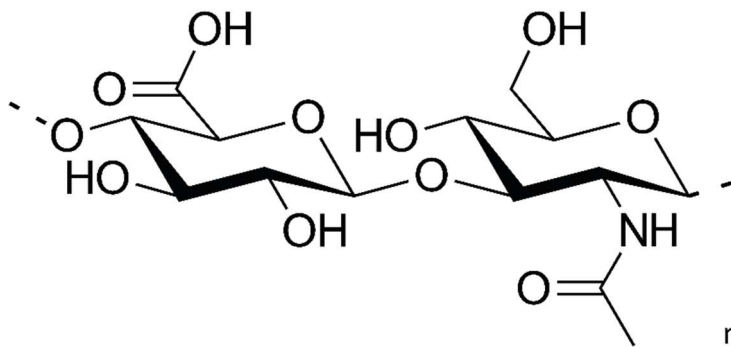


Figure 9 - Skeletal formula of HA. Consisting of D-glucuronic acid and N-acetyl-D-glucosamine linked via alternating $\beta(1\rightarrow4)$ and $\beta(1\rightarrow3)$ glycosidic bonds. Modified, used under CC BY 4.0

It is highly distributed in synovial fluid, vitreous humor, and connective, epithelial, and neural tissues of mammals (72). HA is anionic due to the presence of carboxyl groups in its backbone structure (pKa of about 3.2 to 3.5) and has a molecular mass of up to 10^7 kDa (72). HA mainly interacts with proteoglycans (PG), such as versican and aggrecan (74). By forming extensive networks, these hyaladherins contribute to the structural integrity of tissues, particularly in cartilage and skin. Other hyaluronan-binding proteins, also known as hyaladherins, are known to be involved in immune homeostasis as signaling receptors include tumor necrosis factor-inducible gene 6 protein (TSG-6), CD44, TLR-2/4 and RHAMM. Consequently, HA serves as a natural biosensor providing insight into tissue integrity (75). Over the past the importance of HA became evident in a number of fields; e.g. tumor progression (76), inflammation (75) and wound healing (77). In all these fields the dichotomy between low molecular weight (LMW < 1000 kDa) and high molecular weight HA (HMW) is evident. Under physiological conditions there is a balanced turnover of HA production by HA synthases and cellular uptake and degradation by hyaluronidases (HYAL1 and 2) in the lysosome (74). In inflamed tissues or tumors, HMW-HA is degraded to low molecular weight forms by ROS secreted by neutrophils, hyaluronidases, which have been released from microbes or the lysosome of dying cells (75). Cells of the immune system, such as leukocytes and macrophages, can detect changes in the molecular weight of HA and respond accordingly as shown in Figure 10.

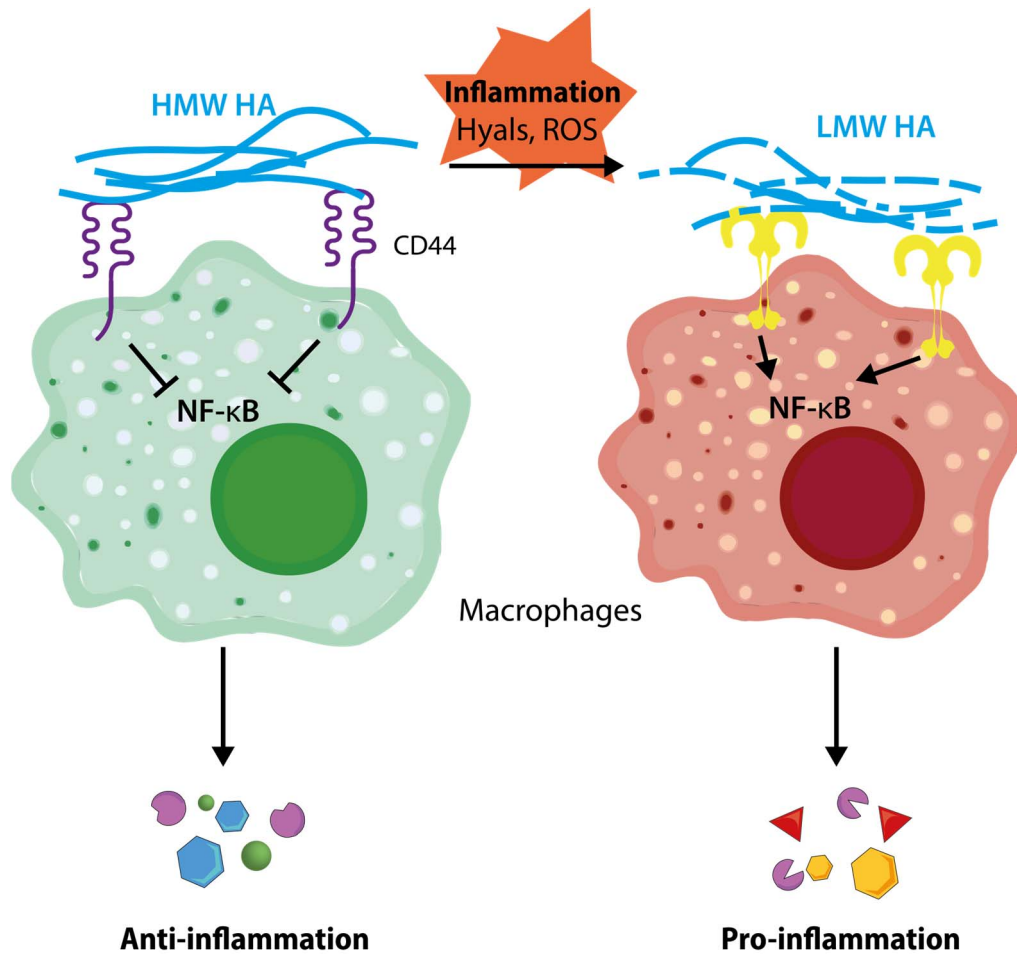


Figure 10 - Representation of the pathway of action of different molecular weight HA. HMW-HA shows anti-inflammatory effects, mediated by the CD44 crosslinking and subsequent attenuating of NF- κ B-signaling. LMW-HA shows proinflammatory effects since the activation of the TLR-receptors is promoting NF- κ B signaling. Based on (78)

Leukocyte production and proliferation increase, while macrophage polarization shifts in response to HA's molecular weight. As a result, LMW-HA is known to have pro-inflammatory characteristics (79). Additionally, LMW-HA has been found to promote angiogenesis and lymphangiogenesis, mediated by the lymphatic vessel endothelial hyaluronan receptor-1 (LYVE-1)-signaling pathway, contributing to the formation of new blood and lymphatic vessels, which are crucial for wound healing (80). The pro-inflammatory effects of HA are mediated by the activation of TLRs. LMW-HA fragments have been shown to signal via TLR4 and TLR2. TLR4 is also known to be activated by PAMPs such as LPS (81). TLR activation leads to increased translocation of NF- κ B to the nucleus, resulting in the production of proinflammatory cytokines associated with proinflammatory macrophages (58). CD44 is another cell surface receptor that is known to be activated by HA. It is widely expressed on various cell types and plays a significant role in cell adhesion and metastasis. The binding of HA to CD44 receptors affects cell growth, activation, survival, differentiation, and immune homeostasis (82). On macrophages the expression of CD44 is particularly high and it is further induced by pro-inflammatory stimuli such as TNF- α and LPS (83). LMW-HA is internalized by CD44 via endocytosis and delivered to lysosomes where both

LMW-HA and CD44 are degraded, resulting in a reduction in active CD44 levels (82). Similar to the TLR receptors, when the molecular weight of HA exceeds a certain threshold the internalization of HA by CD44 is sterically inhibited (82). Instead, HMW-HA can crosslink CD44 (84), which has a suppressing effect on the pro-inflammatory TLR signaling pathway (75). The exact underlying pathway underlying the suppression of TLR signaling by CD44 remains unclear; Either crosslinking of CD44 results in elevated expression of tumor necrosis factor alpha-induced protein 3 (A20) and Interleukin-1 Receptor-Associated Kinase (IRAK-M), which are negative regulators of TLR signaling or protein kinase B (Akt) in the PI3K/Akt pathway gets inhibited, which is downstream of TLR activation (85, 86). However, it has been verified that this suppression ultimately leads to a decrease in the production of proinflammatory cytokines and a shift to an alternatively activated macrophage state (M2). Another noteworthy anti-inflammatory property of HA is its function as an antioxidant. HA has the ability to scavenge oxidative stress, thereby potentially preventing cell damage (73).

Heparin

Heparin, a sulfated GAG, is composed of alternating saccharide units of N-acetylated or N-sulfated D-glucosamine, that are $\alpha(1-4)$ - or $\beta(1-4)$ -linked to uronic acids (L-iduronic or D-glucuronic acid) as shown in Figure 11 (78). At physiological pH, both the carboxyl and the sulfate groups are ionized, making Hep a highly charged polyanion having typical polyelectrolyte behavior (87).

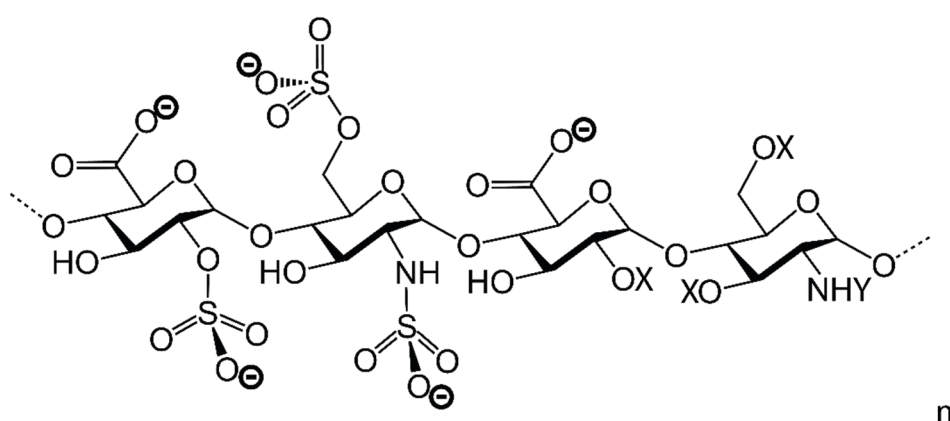


Figure 11 – Skeletal structure of heparin. Heparin consists of variable sulfated repeating disaccharide unit consisting of N-acetylated or N-sulfated D-glucosamine, which are $\alpha(1-4)$ - or $\beta(1-4)$ -linked to uronic acids (L-iduronic or D-glucuronic acid). (X = -OH or -OSO₃⁻; Y = - Ac or -OSO₃⁻) Modified, used under CC BY 4.0

Within the ECM, GAGs and PGs function as binding and crosslinking agents, providing mechanical stability and forming a dense interlocking network. This network regulates substance transport, acts as a reservoir for growth factors and cytokines, and serves as an anchor point for adhesive proteins, thereby influencing cell proliferation, adhesion, migration, regulation, and differentiation (88). Hep and its derivatives are widely used for their anticoagulant properties in

medical application. Its effect on cancer, neurodegenerative diseases, respiratory diseases and as an anti-microbicidal agent is under investigation (89). It is primarily synthesized in connective-tissue mast cells and basophil granulocytes. Once synthesized, it is annealed to a core protein (serglycin). The resulting Hep chains are subsequently cleaved, forming Hep macromolecules with a size range of 5 to 25kDa, which are stored in mast cell granules. Upon contact with antigens, mediated by surface bound immunoglobulin E (IgE) antibodies, Hep is released from mast cells and regulates various cellular activities, such as binding to histamine and modulating proteases within the granules (90). Hep in the bloodstream acts as an anti-coagulant, impeding blood clotting by binding to antithrombin III (ATIII) and enhancing ATIII's affinity for thrombin, factor Xa, and other proteases, ultimately inhibiting their enzymatic activity (90). With its capacity to bind numerous chemokines, cytokines, and complement factors, it effectively prevents their pro-inflammatory interactions with receptors (91). Additionally, Hep exhibits anti-inflammatory properties by influencing selectin-mediated neutrophil adhesion, a crucial interaction between endothelial cells and neutrophils that serves as an immune system integrity signal (92). By binding to L- and P-selectin, Hep effectively masks activated endothelial cells, leading to reduced leukocyte activation and infiltration, thus mitigating inflammation (91). Another anti-inflammatory effect is the inhibition of NF- κ B. Hep treated cells show decreased levels of NF- κ B mediated pro-inflammatory cytokines, especially after stimulation with LPS (93). Hep molecules are taken up by endocytosis. Inside the cell Hep can bind to numerous proteins, due to its high negative charge. The NF- κ B complex is positively charged, therefore it is assumed that Hep prevents NF- κ B translocation (92, 93). However, recent studies propose a direct interaction of Hep and NF- κ B in the nucleus, by blocking the ability of NF- κ B to bind to the DNA (94). Subsequently, inhibiting the translation of the NF- κ B mediated pro-inflammatory cytokines. This hypothesis is supported by the discovery of the role of the structurally similar heparansulfate in the nucleus, as shuttling molecules for growth factors and cytokines, as an inhibitor of topoisomerase-I activity and its inhibition of binding oligo-DNA to transcription factors, like activator protein 1 (AP1), protein C-ets-1 (Ets1), Sp1 transcription factor (Sp1), transcription factor II D (TF_{II}D) and NF- κ B (95).

Chitosan

Chitosan, derived from chitin via partial deacetylation under alkaline conditions, consists of β -(1-4)-linked D-glucosamine (deacetylated unit) and N-acetyl-D-glucosamine (acetylated unit) (Figure 12) (96). Chitin, a structural polysaccharide, ranks as the second most prevalent natural polymer after cellulose. It mainly originates from arthropod exoskeletons like shrimps and crabs, but fungal cell walls also contain it and are the main commercial source of chitin (96). The

chemical and properties depend on the deacetylation degree of CHI which ranges typically between 50 % to 95 %. Additionally, different molecular weights are available ranging from 100 kDa to 1000 kDa affecting the viscosity of CHI (97). The glucosamine residue's amino group in CHI protonates under acidic conditions ($\text{pH} < 6.5$), forming a polycationic structure (98).

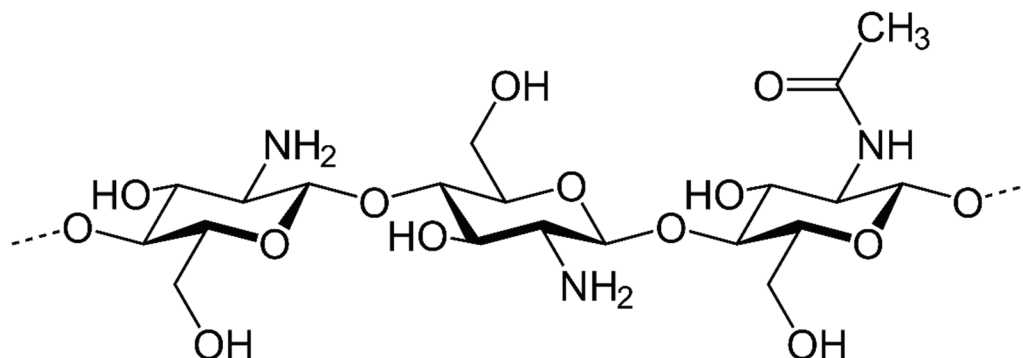


Figure 12 -Skeletal structure of the chitosan repeating unit; β -(1 \rightarrow 4)-linked D-glucosamine (deacetylated unit) and N-acetyl-D-glucosamine (acetylated unit). Used under CC BY 4.0

Shared structural traits between CHI and glycosaminoglycans, including N-acetyl-D-glucosamine, facilitate specific interactions with receptors, growth factors, and adhesion molecules, resulting in bioactive capabilities. Chitosan is biocompatible, biodegradable, and has anti-microbial activity, making it popular in wound healing research (99–101, 97). It acts as a hemostat, promoting blood clotting (102, 97). Research also suggests CHI's role in activating fibroblasts during the inflammatory phase of wound healing. The gradual release of N-acetyl-D-glucosamine, resulting from CHI's slow depolymerization, initiates fibroblast proliferation (103).

Alginate

Alginate is a linear acidic polysaccharide which can be extracted from brown seaweeds and several bacterial strains (104). Since alginic acid is insoluble in water, monovalent salts with sodium are common. Comprised of β -(1–4)-linked D-mannuronate (M) and α -(1–4)-linked L-gulonate (G) uronate sugars, ALG features M, G, and MG blocks, forming a characteristic arrangement as depicted in Figure 13 (105).

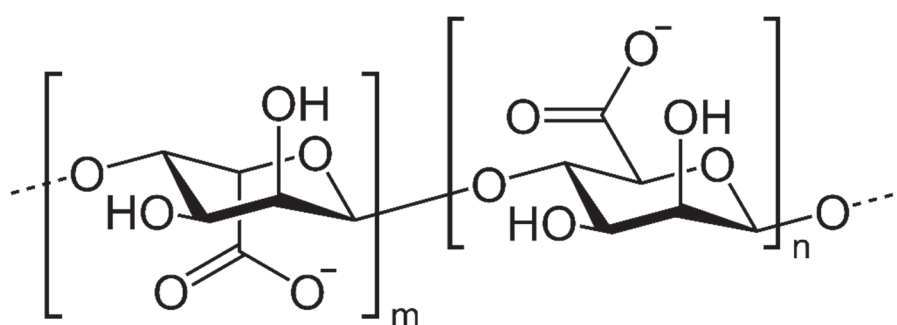


Figure 13- Skeletal structure of alginate; (1 \rightarrow 4)-linked β -D-mannuronate (M) and α -L-gulonate (G). Used under CC BY 4.0

The arrangement of these blocks varies from their source and influence viscosity and swelling ability (104). ALG is a popular raw material for hydrogel-based biomaterials, due to its gelation properties. Most common is the gelation of ALG by divalent cations, particularly calcium, which create ionic crosslinks by binding to adjacent guluronate residues, adopting an "egg-box" pattern (104). Due to its biocompatibility, biodegradability, non-toxicity, cost-effectiveness, and widespread availability, ALG is used in diverse wound healing applications (67, 68, 106). ALG hydrogels enable sustained of heparin binding growth factors like FGF2 and VEGF due to a reversible binding with ALG (105). Possessing anionic polyelectrolyte properties at pH 4 ALG has been explored in combination with CHI as drug carrier or membrane (100, 104). ALG-based wound dressings rely on the establishment of a moist wound environment (67). Additionally, ALG possess hemostatic properties (107). However, ALGs high in mannuronic acid (M-blocks) have been found to have stimulating potential on *in vitro* monocytes to produce pro-inflammatory cytokines (108).

Gelatin

Gelatin, a naturally occurring biopolymer derived from collagen, is the result of partial acid hydrolysis (known as gelatin type A) or alkaline hydrolysis (gelatin type B) of native collagen, which can be derived from animal collagen found in the hides, cartilage, bones, and tendons of various animals (71). In its molecular structure, out of 18 amino acids glycine is one of the primary modulators of cell adhesion (71). Gelatin carries a negative charge at higher pH levels (around pH 9) and a positive charge at lower pH levels (around pH 5). The isoelectric point for type A gelatin is typically near pH 9, while type B gelatin is around pH 5. As a protein-based biomaterial, gelatin offers several advantages, including excellent biocompatibility, water solubility, low immunogenicity, flexibility, adhesiveness, promotion of cell adhesion and growth, cost effectiveness, and the ability to form transparent gels under certain conditions (109). As a result, it has received considerable attention for use in pharmaceutical and medical applications (110). However, gelatin's rapid dissolution in aqueous environments limits its biomedical applications. To improve its stability against enzymatic degradation, researchers have applied physical or chemical cross-linking treatments (111). In the field of tissue engineering, submicron and nanometer gelatin fiber mats are widely used to mimic the ECM of human tissues and organs (71). In addition, electrospun gelatin and gelatin-based scaffolds have found applications in various biomedical fields, including bone regeneration, skin tissue engineering, nerve tissue engineering, cardiac tissue engineering, tubular scaffold fabrication, and drug delivery (110, 112–114).

1.3 Wound Dressings – State of the Art and Recent Trends

Wound treatment aims to accelerate wound healing, minimize scarring, relieve pain and restore normal skin function (17). Historically, wounds were cleansed and treated with astringents or antimicrobial substances such as honey and resin and covered with plasters soaked in oil, grease, wine and vinegar (115). Until the mid-1900s, it was believed that wounds should be left uncovered to dry to promote faster healing, but this perspective shifted in the 1980s with the clinical acceptance of new dressings that supported a moist wound environment (116). Current treatments for impaired wound healing focus mainly on optimizing controllable healing factors such as clearing of infections, mechanical protection, and nutritional support. Only a few targeted approaches have been developed. These include the topical application of growth factor gel, which unfortunately have limited clinical efficacy (12). Nonetheless there exists a definition for a potential ideal wound dressing (Figure 14). It incorporates several requirements: a) be sterile, non-toxic and non-allergenic, b) the facilitation of gas exchange between the wound site and the surrounding environment, c) provide protection against bacterial infection, d) the ability to establish and maintain a moist wound environment, e) the ability to adsorb exudate f) not adhere to the wound surface to ensure easy removal after healing (117)

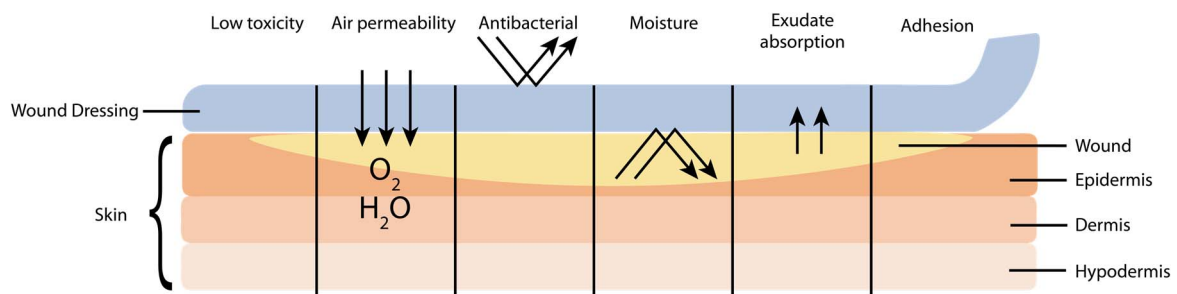


Figure 14 - Schematic representation of the various functions of the ideal wound dressing. Based on (69)

However, this definition is simplified as it does not account for all types of wound dressings, which can target different wound phases. For example, a wound dressing for debridement purposes in an early treatment stage needs to adhere firmly to the wound bed. This subchapter tries to list the treatment options available today and their respective advantages and disadvantages compared to new wound dressings design approaches.

Semi-Permeable Film Dressings

At first, dressings made from nylon derivatives with adhesive polyethylene frames were occlusive and unsuitable for wounds with exudate as they had limited absorption capacity and caused tissue maceration (118). The introduction of semi-permeable film dressings, composed of transparent polyurethane, enables water vapor and gas permeation, while at the same time

they effectively prevent bacterial penetration (119). As such, these dressings are suitable for low to mildly exuding wounds (4). These dressings are easy to use due to their elastic nature and allow wound inspection without needing to be removed (117). Another proposed benefit of semi-permeable film dressings is the accumulation of healing mediators in wound fluid as it could be demonstrating that retained fluid from acute wounds covered by film dressings can stimulate keratinocyte proliferation *in vitro* (120). Examples of these dressings on the market include Opsite™, Tegaderm™, and Bioocclusive™.

Semi-Permeable Foam Dressings

Semi-permeable foam dressings consist of a hydrophobic foam inner core and hydroconductive outer layers commonly made of polyurethane with blends of polyvinyl alcohol and silicone to adjust the surface hydrophilicity (121). The wound contacting hydrophilic layer allows wound fluid passage. The inner hydrophobic core is a highly absorbent porous structure which draws wound exudate into the pores while permitting gas exchange and water vapor transmission (118). In a clinical setting it is often combined with a semi-permeable film dressing to defend against bacterial infections and control the evaporation. As such they are suitable to treat moderate to highly exuding wounds (4). Foam dressings provide added cushioning owing to their soft physical nature and can be easily removed. Additionally, they are very economical in production. Disadvantages of using a foam dressing are that it requires frequent replacement, due to the limited capacity for wound exudate and it is not suitable for low-exudate wounds and dry wounds. Examples include Lyofoam™, Allevyn™, and Tielle™.

Hydrogel Dressings

Wound healing commercially available hydrogels are made from synthetic polymers like poly(methacrylate) and polyvinylpyrrolidone (PVP). They are hydrophilic and insoluble with a water content of 70-90 % and create a moist environment aiding granulation and reepithelization (118). Hydrogel dressings consist of both sheets and amorphous gels, which may share a polymer composition but differ significantly in their physical properties due to the higher crosslinking degree of sheets (122). Furthermore, the high hydration of hydrogel dressings limits the amount of exudate absorption. Nevertheless, autolytic debridement is closely related to moist surroundings, enabling spontaneous enzymatic reactions. Consequently, hydrogel dressings are established as the standard treatment for dry, necrotic and sloughy chronic wounds. Hydrogels also lower cutaneous wound temperature, offering a soothing effect, making them very suitable for burns (123). The softness of the material enables effortless application and safe removal once the wound has healed. Drawbacks include exudate accumulation causing maceration, bacterial proliferation and their low mechanical strength poses handling challenges (122). Notable

hydrogel examples include Intrasite™, Nu-gel™, Aquaform™

Hydrocolloid Dressings

Hydrocolloid dressings consist of two layers: an inner hydrocolloidal layer and an outer water-impermeable layer as a flexible occlusive film and/or foam. These dressings combine gel-forming agents (like polyvinyl alcohol, carboxymethylcellulose, gelatin, and pectin) with elastomers and adhesives (118). Hydrocolloids are capable of providing moisture to the wound since they form a gel after contact with the wound fluid (124). Hydrocolloids allow water vapor diffusion but block bacteria, debride, and absorb wound exudates. They suit lightly to moderately exuding wounds (117). Hydrocolloid dressings are notably occlusive, leading to a highly hypoxic wound environment. (125). Hypoxia in wounds is a critical factor driving chronic wound progression, but it is also linked to positive effects such as enhanced epithelialization and angiogenesis (120). Short changing intervals are mandatory. They are available as sheets or thin films, examples are Granuflex™, Comfeel™, and Tegaserb™.

Alginate Dressings

ALG dressings sometimes are counted among the hydrogel dressings. They consist of sodium and calcium salts, usually in an 80:20 ratio or solely calcium alginate salt, derived from brown seaweed (67). Upon contact with the wound, an ion exchange occurs between the calcium ions in the dressing and the sodium ions in the fluid. This leads to a gradual transformation of the calcium alginate to water-soluble sodium alginate leads to the formation of a gel (68). With an absorption capacity of 15 to 20 times their weight, they suit highly exuding wounds but can cause discomfort and tissue damage upon removal in wounds with minimal exudate due to their adhesive nature (124). Several research papers indicate diverse biological activity of ALG dressings, acting as hemostatic agents and pro-inflammatory factor. These effects are reviewed in the next subchapter of this thesis. ALG dressings are suitable for low to moderate drainage wounds, they are not recommended for dry wounds, due to painful removal (117). Secondary dressings are required to prevent wound dehydration delaying healing (67). Commercial options include Sorbsan™, Kaltostat™, and Algisite™.

Xenografts, Allografts, Acellular Matrices

Most common is still the treatment with non-active wound dressings, mostly films, foams and ALG based wound dressings. However, xeno and allografts are gaining interest in practice, this procedure is limited by the availability of donor skin, may be painful, time-consuming, and expensive (17). A review can be found here: *Salloum et al.* (126)

Another emerging interesting choice are acellular matrices, which can be derived from natural sources like animal tissues (porcine, equine) or human skin (cadaver), where the cells are removed, and pathogens are deactivated. Artificial matrices, consist of various animal-derived components such as collagen (types I, III, and V), elastin, and glycosaminoglycans. Most of these membranes and films have a monolithic structure of collagen. However, they do not mimic native dermis in its entirety and despite their known excellent biocompatibility, they have the major disadvantage that they degrade rapidly *in vivo* and do not supply the structural integrity necessary for the overall process of tissue regeneration. Covered in the review by *Hussey et al.* (127)

Recent Trends in Wound Dressings Design – Use of Growth Factors, Biopolymers and Nanostructured Materials

As discussed in chapter 1.1 GF levels dramatically affect the inflammatory, proliferative and epithelization phase of wound healing. Therefore, various topical formulations have been researched to deliver derivates of PDGF, FGF2 and EGF (128). PDGF was the first topically applied growth factor available; Regranex (becaplermin gel - a recombinant PDGF derivate) entered the market in 1997 for the treatment of pressure ulcers. However, a 20-month follow-up study showed an increased malignancy risk associated with becaplermin use (37). Although, there was no association with a particular type of malignancy, and all cancers were remote from the treatment site, it led to an announcement by the FDA in 2008, warning about the malignancy risk associated with Becaplermin. As a result, the product was withdrawn from the market in the EU. The same topical formulation of PDGF has been applied to venous ulcers although with minimal efficacy (129). Reasons for failed efficacy were attributed due to poor growth factor penetration into the wound (129). This is further complicated by the fact that growth factor application often requires daily treatment, which makes frequent dressing changes mandatory (37). Building on these efforts the use of TGF- β was researched as it was a promising therapy at that time, but notably failed to produce results such as shown with PDGF in clinical tests (130, 131). Additionally, excessive scarring was found to be a problem, since TGF- β guides differentiation of fibroblasts to myofibroblasts, which develop a contractile activity and secrete excessively ECM proteins, like collagen, but in a disordered manner (131, 37). Levels of FGF2 are decreased in chronic wounds as discussed in the subchapter Growth Factors. It has been shown that FGF2 regulates the synthesis and deposition of various ECM components by fibroblasts, increases keratinocyte and fibroblast migration, and stimulates them to produce collagen (132). On the other hand, FGF2 may downregulate myofibroblast presence, reduces wound contraction and hence scarring (32). Therefore, FGF2 plays a role in granulation tissue formation, reepithelialization, and tissue remodeling (132). In addition, FGF2 is not only a mitogen for many

types of cells, but also a potent factor in angiogenesis, which may have a positive impact on revascularization of chronic wounds (31). Since 2001 a FGF2 spray (Fiblast® Spray) is available and showed wholly positive outcomes in (rather small) clinical studies (133, 134). This formulation was recently further developed into FGF2 impregnated gelatin sheets, to prolong the efficacy (133, 135). This is following the general trend in wound dressing research to incorporate the growth factors directly in the wound dressing to control the release and mitigate wound dressing changes (Figure 15). Several studies exist of FGF2 releasing dressings (136–139). However, to date none of these developments entered clinical testing for approval.

A notable development in wound dressing design is the application of hydrogels, which through the changes in crosslinking and/or porosity can easily be tuned to deliver growth factors to the wound (140). An extensive review on bioactive hydrogel dressings on the basis of natural and synthetic polymers can be found here: *Yuan et al.* (69). Similarly, ALG wound dressings are extensively researched to harness the biocompatible nature of biopolymers and their derivatives, based on the positive results of ALG dressings achieve in the clinical world. The main advantage of natural polymers over synthetic polymers is that they more closely mimic the original cellular environment and ECM. Increasingly popular is the development of CHI-based wound dressings, often in combination with ALG, to exploit their anti-bacterial effect (96, 141–145). From its use in cosmetics as a filler and moisturizing agent, HA is also slowly acknowledged as a wound-healing polymer and used in combination with ALG (68, 146). A review about HA applications in wound healing can be found here: *Fakhari et al.* (147). Other popular biopolymers for wound dressing applications are fibrin (148), cellulose (149) and collagen/gelatin (137). Although, several drawbacks may limit their wider application; most of these natural polymers are subject to degradation processes in conjunction with poor stability and mechanical performance (150). However, various chemical synthesis and/or processing modifications may be performed in order to overcome some of these disadvantages (150). Gaining popularity are also wound dressing designs based on nano-structured fibers prepared by electrospinning (151). These nanofibers can control and guide the wound healing process by integrating controlled release strategies within scaffold materials. nanostructured drug delivery systems (152). The fiber diameter and/or porosity of a scaffold can be optimized for fibroblast and keratinocyte adhesion, growth and migration since they are mimicking topographical features of the ECM (153, 113). Through various electrospinning techniques, such as blending, specific or nonspecific surface modifications, coaxial electrospinning, emulsion electrospinning, and combination of electrospinning with other conventional techniques, GFs, like VEGF, FGF2 and PDGF can be loaded (154, 138). A detailed review on the developments of this field can be found here: *Liu et al.* (114). Electrospun based dressings try to combine the advantages found in foam dressings and acellular matrices,

most importantly a large surface area, nanofibrous structure and adjustable porosity. However, they also possess some of their drawbacks, e.g. susceptibility to bacterial colonization and degradation, due their large surface area (155).

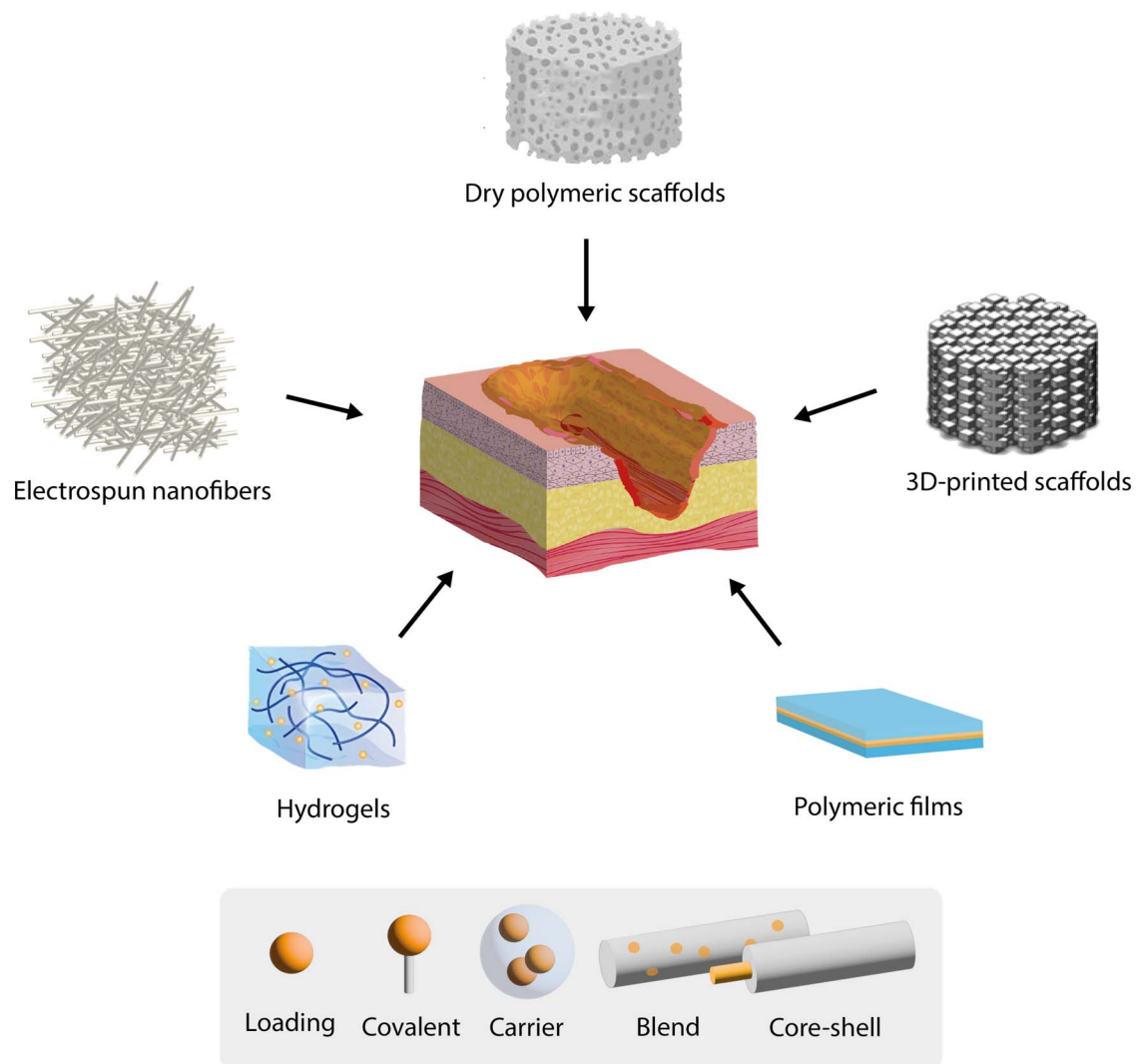


Figure 15 -Various technologies have recently been proposed for the controlled release of GFs from advanced wound dressings. Single or multiple GFs can be loaded into different polymeric matrix structures using suitable methods. (panel below). These methods include direct blending into the entire polymeric matrix, creating core-shell structures, covalently conjugating them to the scaffold's surface, entrapping them within drug carriers within the scaffolds, and combining these techniques. The ultimate objective is to mimic the essential wound microenvironment necessary for effective tissue regeneration by achieving the precise spatiotemporal release of bioactive molecules. Based on (156)

Wound treatment using exogenous GFs can have significant beneficial effects, although topically administered growth factors show somewhat limited efficacy (7). Exogenous GFs for the treatment of wounds rapidly diffuse and are readily digested or deactivated by proteases in the hostile, often microbially colonized environment of chronic wounds (37). Additionally, GFs show low permeation through the outermost skin layer surrounding the lesion and rapid elimination by exudation from the wound bed (129). Most GFs used in wound therapy act on cells producing ECM, these cells need to be present and susceptible to growth stimuli, hence the inflammation phase needs to be resolved. Therefore, exogenous added GFs are strictly dependent on their

correct distribution within the wound in time and place dimension (156). Consequently, high doses and/or repeated administration over an extended period are required to support and sustain tissue regeneration, leading to supra-physiological exposure to GFs which can lead to side effects (157). In particular, care needs to be taken when using pro-angiogenic factors as they can perpetuate oncogenesis (156). Finally, in an environment where so many factors are deficient and dysregulated, simply treating one growth factor deficiency is unable to heal chronic wounds, however regulatory complexities hinder synergistic application of growth factors. Alternatively, it is also likely that a “master regulator” of wound healing has yet to be identified (17, 156).

1.4 The Layer-by-Layer Technology - from Surface Modification to 3d-Applications

The layer-by-layer (LbL) technique is a method of building up films by alternating between layers of positively and negatively charged materials. It was rediscovered by *Decher et al.* in 1992 (158), although the origins of the LbL technique can be traced back to 1966 by *Iler et al.* (159), which unfortunately, did not receive much attention at the time. The LbL technique allows the incorporation of an extensive range of building blocks such as polyelectrolyte polymers, peptides, carbon nanotubes, clays, dyes, metal oxides and components including particles, proteins, enzymes, viruses and nucleic acids into the multilayer films to add new functionalities and capabilities (160, 161). Nowadays, the LbL technology has emerged as an exponential growing innovation field, offering a multitude of unique properties. It facilitates the precise deposition of uniform films with controlled thickness (162). The LbL technique possesses exceptional loading capabilities, enabling the controlled release of biomolecules and drugs of diverse compositions (163, 164). These coatings exhibit remarkable stability when subjected to physiological conditions (165). As a result of these attributes, the LbL approach has rapidly ascended to become an important method for crafting film coatings on a variety of biomedical substrates (166). This encompasses (patterned) surfaces, medical devices and implants (161). At the same time, the concept of constructing multilayer capsules has emerged, holding great promise as nano- and micro-carriers geared towards innovative drug delivery applications (163). The underlying mechanisms to form polyelectrolyte multilayers (PEMs) involve several types of interactions, including electrostatic and non-electrostatic forces. These interactions include short-range effects such as hydrophobicity, hydrogen bonding, van der Waals forces. Therefore, the composition of PEM is dependent on the properties of the polyelectrolytes themselves (e.g. structure, charge density and chain stiffness) (167). However, they can be further fine-tuned by manipulating factors such as pH and salt concentration to modulate protonation states and the availability of charged groups as well as adjusting temperature to enhance molecular mobility of

the surrounding medium (168). For some PEMs charge transfer halogen interactions and potentially covalent bonds formed by click chemistry are also observable (169). In addition, the multilayer formation is not only driven by electrostatic forces, but also by the increase in entropy resulting from the release of counterions (169).

Technological Developments - Dipping, Spinning, Spraying

Layer by layer assembly has gone through several developments. Initially, LbL assemblies were produced by manual dipping or immersion. For coatings on small surfaces in lab scale the manual change of the polyelectrolytes and washing in between can be done in well plates, by pipetting back and forth the different solutions. Similarly, particulate material, even cells, can be coated (170). Although, there is the need of skimming or centrifugation after each deposition or washing step. The typical immersion time for each deposition step varies from 1 min to about 15 min (160). This incubation time depends on the mobility of the polyelectrolytes used, as for particles or colloids very short times can be used while for polymers a time of at least 12 min is recommended (171). One of the benefits of this method is the ability to coat substrates that have more complex geometries (167). Nevertheless, the automation of dipping was developed to ease the preparation which enable the construction of new LbL based designs like FSFs in 2005 (172). Although there are several attempts to lower assembly time; by agitation, which increases the probability of aligning a polymer on the last layer and therefore reducing the incubation time or by using alternating polar and nonpolar solvents to accelerate dewetting, removing the need for rinsing in between the deposition steps (173). The incubation time for each immersion step is what stands in the way of a high-throughput/large scale application of the dipping technique (173). Additionally, the high volumes of polyelectrolytes which are necessary in dip coating renders the use of complex polyelectrolytes (e.g. nanoparticles, liposomes etc.) commercially unviable (160).

In 2001, Schlenoff and colleagues described the production of PEMs by using spray deposition onto a substrate for the first time (174). The study showed that these sprayed films had comparable composition and thickness to a film produced by traditional immersion deposition. Unfortunately, this initial technique was not explored further for larger areas. Izquierdo and colleagues in 2005 discovered that even with spraying times as brief as 3 seconds, the resulting films exhibit remarkable uniformity (173). When considering equivalent contact durations between the polyelectrolyte solutions and the surfaces, spraying consistently generates thinner and smoother films than the dipping method (173). By eliminating the washing step, it was also discovered that the film thickness increases without affecting the film quality (175). Furthermore, Spray coating enables the construction of merged or granule systems by the simultaneous

spraying (176). However, the layered nature gets lost (177). The automatization of the spray coating process leads to higher bilayer numbers and is more economical compared to dip coating regarding the needed volumes.

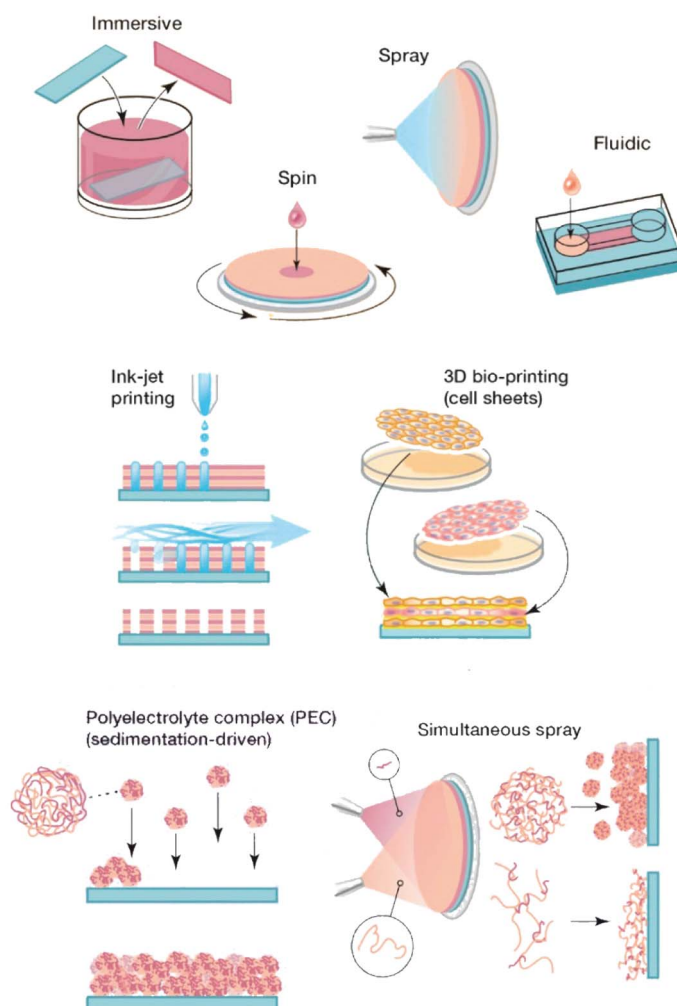


Figure 16 - Most common used layer-by-layer techniques. Modified, original by (160)

Besides dipping and spraying deposition there exists several other unconventional or quasi LbL assembly techniques. Importance gained the micro-fluidic based approach, which enabled the production of coatings with biochemical or physical gradients (178, 179). Another solution to introduce gradients or mixed assemblies is the inkjet assembly which works by a piezo induced vaporization of small liquid droplets (180). Due to the movement of the print head and the targeted deposition, small grids with varying deposition in the μm -range can be achieved (181). There is an excellent review by *Richardson et al.* (160) covering all unconventional LbL assembly techniques.

Layer-by-Layer Based Free-Standing Films

As a result of its modularity, a multitude of application of the LbL technique has seen the light. One of the more recent is the research of FSFs. First developed by *Lavalle et al.* in 2005 it is based on the automatization of layer-by-layer preparation to achieve a significant number of bilayers. FSF were produced with at least of 15 bilayers, as a minimum of stability is needed for the handling of the films. The simplest approach to removing the deposited PEM stack from the underlying substrate is direct peeling (182). However, it is known that is difficult to control the peelability of the film using this method, which might result in structural imperfections and compromised mechanical strength, making it unsuitable for large scale manufacturing requirements. This method is only possible with the right choice of substrate which enables initial deposition, but also allow the easy removal of the films. For example, for CHI/ALG films polystyrene (PS), polypropylene (PP), polyvinylchlorid (PVC) and polytetrafluoroethylene (PTFE) surfaces were successfully used (183, 184, 98, 185). Additionally, it is advisable to remove mechanically robust films in polar solvents, which induces film swelling and therefore reduces strain disparities (186). As an advancement, sacrificial layers, which allow the release of a build-up film from the substrate were developed based on switches like pH changes (187, 188), enzymatic cleavage (189), light-induced disassembly (190) ion exchange (191), temperature responsive (192) and the dissolution of CaCo₃ (193).

Although the research field covering LbL-based FSF is to date a rather small part of general LbL-research several interesting applications and modifications for FSF have been developed in recent years due to their modular construction. A key focus is the use of FSFs in tissue engineering applications. However, the use of common biopolymers leads to quite hydrophilic and soft surface, which limits cell adhesions (194, 192). This was in part addressed using adhesive polymers in the final layers (195). In a further development micro-patterning was used to influence cell adhesion and differentiation (196–198). FSF were also characterized as drug delivery system, for cancer or anti-bacterial drugs (199, 200). Loading of GFs into polyelectrolyte multilayers made of polysaccharides has been shown for EGF (201). It was also found that such multilayer systems are not only preserving but also enhancing activity of GFs due to juxtacrine presentation to their corresponding cell receptors (202). Off the medical uses there is also research on FSFs as nanofiltration (203) or gas separation membranes (204). Additionally, FSFs were developed with ultra hydrophobic surfaces for anti-fouling use (205), shape memory for mechanical actuators (184, 206) and the incorporation of sensing capabilities (207).

Research Aim

While it is widely recognized that chronic wounds are associated with persistent inflammation, there is a lack of emphasis on addressing inflammation and providing a regenerative environment, while fighting bacterial colonization in traditional wound dressing design. Therefore, this thesis focusses on advancing the understanding of the anti-inflammatory potential of GAGs and their utilization to construct and evaluate innovative wound dressings based on free-standing multilayer films and composites with the common goal of promoting wound healing and modulating the inflammatory response.

The research investigates the inflammatory response of macrophages growing on surfaces modified with HA and heparin. A primary focus is on whether macrophages can uptake the GAGs and, consequently, how these uptaken or associated GAGs modulate the NF- κ B-pathway and pro-inflammatory cytokine release of macrophages. The next phase evaluates the regenerative potential of CHI/ALG FSF loaded with FGF2, emphasizing on wound dressing related physical properties, antibacterial effects, and their ability to enhance fibroblast growth and migration. Special attention is given to the *in-vivo* reaction towards these novel FSF in mice. In the ultimate step the study explores how FSFs can be further modified to combine the regenerative and inflammatory potential. Here a novel composite consisting of an electrospun gelatin fleece and a CHI/HA/ALG FSF is tested, to determine whether it can improve adhesion and growth of fibroblasts, while reducing the inflammatory cytokine release of macrophages. The findings are presented herein.

Chapter 2 - Study on the potential mechanism of anti-inflammatory activity of covalently immobilized hyaluronan and heparin

Here the anti-inflammatory mechanisms of GAGs, focusing on the NF- κ B signaling pathway is explored. Two GAGs, heparin and HA were selected for this study which were known to modulate inflammation prior (92, 76, 81). However, the direct interaction of macrophages with surface attached GAGs was not tested before. Using EDC/NHS cross-linking chemistry, we covalently immobilized HA and Hep onto amino-terminated surfaces, to produce SAMs. Physico-chemical evaluations, such as atomic force microscopy (AFM), water contact angle (WCA), and zeta potential (ZP) measurements, confirm the successful GAG immobilization onto to the amino-terminated control surfaces. Both surfaces are more hydrophilic compared to the control. Moreover, the high content of sulfate monoesters and sulfamido groups in Hep results in the highest in wettability and negative surface charge. Biological studies were conducted with THP-1 derived macrophages. LPS was used as stimulator to induce an M1-like state of the macrophages and simulate the recognition of PAMPs. The number of adhered macrophages, their spreading and fusion to form multi-nucleated giant cells were of interest, as a marker of inflammatory potential of material surfaces. HA-modified surfaces with their hydrophilicity and steric repulsive effects of HA express a slightly higher reduction of initial macrophage adhesion and spreading compared to Hep-modified surfaces but there is no difference in the macrophage fusion between both. Additionally, we measured the release of the pro-inflammatory IL-1 β cytokine under stimulation with LPS, which is reduced in macrophages on both GAG-modified surfaces. To reveal the underlying anti-inflammatory mechanism of GAGs acting on macrophages, we measured the uptake of fluorescein isothiocyanate (FITC)-labelled GAGs and their effect on the NF- κ B signaling pathway. Both GAGs demonstrate the ability to either associate with or internalize GAGs labelled with FITC as verified by confocal laser scanning microscopy (CLSM) and flow cytometry. As a result, we found decreased NF- κ B levels in whole cell lysates of macrophages by immunoblotting of activated (phosphorylated) p65. Additionally, immunofluorescence (IF) staining of the p65 subunit exposed the translocation of p65 from the cytoplasm to the nucleus. Results show that Hep has a stronger inhibiting effect on p65 translocation to the nucleus compared to HA. In conclusion, our findings suggest that the potential anti-inflammatory effect of GAGs is not solely attributed to their cell repulsive hydrophilic and anionic nature but also involves their inhibition of the NF- κ B signaling pathway. These insights contribute to a better understanding of the interactions between GAGs and inflammatory responses and laid the basis for the investigations of multilayer films in the following chapters.

Received: 22 August 2019 | Revised: 7 January 2020 | Accepted: 10 January 2020

DOI: 10.1002/jbm.a.36885

ORIGINAL ARTICLE



Study on the potential mechanism of anti-inflammatory activity of covalently immobilized hyaluronan and heparin

Hala AlKhoury^{1,2} | Adrian Hautmann¹ | Frank Erdmann³ | Guoying Zhou¹ |
Sanja Stojanovic^{4,5} | Stevo Najman^{4,5} | Thomas Groth^{1,2,6} 

¹Department of Biomedical Materials, Institute of Pharmacy, Martin Luther University Halle-Wittenberg, Halle (Saale), Germany

²Interdisciplinary Center of Materials Science, Martin Luther University Halle-Wittenberg, Halle (Saale), Germany

³Pharmaceutical Biology and Pharmacology Department, Institute of Pharmacy, Martin Luther University Halle Wittenberg, Halle (Saale), Germany

⁴Department of Biology and Human Genetics, Faculty of Medicine, University of Niš, Niš, Serbia

⁵Department for Cell and Tissue Engineering, Scientific Research Center for Biomedicine, Faculty of Medicine, University of Niš, Niš, Serbia

⁶Laboratory of Biomedical Nanotechnologies, Institute of Bionic Technologies and Engineering, I.M. Sechenov First Moscow State University, Moscow, Russian Federation

Correspondence

Thomas Groth, Department of Biomedical Materials, Institute of Pharmacy, Martin Luther University Halle Wittenberg, Heinrich Damerow Strasse 4, D 06120 Halle (Saale), Germany.
Email: thomas.groth@pharmazie.uni-halle.de

Funding information

Ministry of Education, Science and Technological Development of the Republic of Serbia; German Academic Exchange Service

Abstract

Inflammation and subsequent fibrotic encapsulation that occur after implantation of biomaterials are issues that fostered efforts in designing novel biocompatible materials to modulate the immune response. In this study, glycosaminoglycans (GAG) like hyaluronic acid (HA) and heparin (Hep) that possess anti-inflammatory activity were covalently bound to NH₂-modified surfaces using EDC/NHS cross-linking chemistry. Immobilization and physical surface properties were characterized by atomic forces microscopy, water contact angle studies and streaming potential measurements demonstrating the presence of GAG on the surfaces that became more hydrophilic and negatively charged compared to NH₂-modified. THP-1 derived macrophages were used here to study the mechanism of action of GAG to affect the inflammatory responses illuminated by studying macrophage adhesion, the formation of multinucleated giant cells (MNGCs) and IL-1 β release that were reduced on GAG-modified surfaces. Detailed investigation of the signal transduction processes related to macrophage activation was performed by immunofluorescence staining of NF- κ B (p65 subunit) together with immunoblotting. We studied also association and translocation of FITC-labeled GAG. The results show a significant decrease in NF- κ B level as well as the ability of macrophages to associate with and take up HA and Hep. These results illustrate that the anti-inflammatory activity of GAG is not only related to making surfaces more hydrophilic, but also their active involvement in signal transduction processes related to inflammatory reactions, which may pave the way to design new anti-inflammatory surface coatings for implantable biomedical devices.

KEYWORDS

cell adhesion and multinucleated giant cells formation, covalent immobilization, endocytosis immunoblotting, glycosaminoglycans, inflammation, macrophages, NF- κ B

1 | INTRODUCTION

Biomaterials are widely used to support and replace partially or completely tissues and organs to improve, augment, or restore biological functions (Brovold et al., 2018). However, implantation of biomaterials is followed by blood-material interaction, which leads to protein adsorption that can initiate an inflammatory cascade comprising injury, followed

by acute and chronic inflammation, formation of granulation tissue, foreign body response, and eventually fibrous encapsulation. This represents in the majority of cases an undesired event and is largely influenced by the characteristics of the implanted biomaterials, such as surface properties and compliance and shape (Vasconcelos, Águas, Barbosa, Pelegrín, & Barbosa, 2019; Velnar, Bunc, Klobucar, & Gradisnik, 2016). Macrophages play a significant role in the inflammation process and are

considered as key effector and dominant cells secreting pro-inflammatory cytokines such as IL-1 β and tumour necrosis factor- α (TNF α), chemokines and growth factors, such as monocyte chemoattracting protein 1 (MCP-1), transforming growth factor- β , and platelet-derived growth factor (Oishi & Manabe, 2018; Wynn & Vannella, 2016). In addition, macrophages may fuse on the biomaterial in an attempt to phagocytose the implant larger in size than themselves, forming foreign body giant cells, which represents also a sign of chronic inflammation (Kastellorizios, Tipnis, & Burgess, 2015; Moore & Kyriakides, 2015).

There is a multitude of attempts to dampen inflammatory response after biomaterial implantation. One capitalizes on passive mechanisms, based on hydrophilicity of materials and steric repulsion that shall reduce opsonization of the implant material. Hence, adsorption of proteins, like complement factors, immunoglobulins, coagulation factors, and others is reduced, which leads to decreased activation of leukocytes. However, it is difficult to have a long-term inhibition of protein adsorption. Therefore, the success of this approach is limited (Franz, Rammelt, Scharnweber, & Simon, 2011; Vroman, Adams, Fischer, & Munoz, 1980). Others are based on presence and release of anti-inflammatory drugs like nonsteroidal anti-inflammatory drugs (e.g., naproxen) that may reduce acute and chronic inflammation (Al-Khoury et al., 2019; Suarez et al., 2013). Quite recently, it was also discovered that biomaterial-induced inflammatory response can be attenuated by the use of glycosaminoglycans (GAG) like hyaluronic acid (HA) or heparin (Hep) that possess anti-inflammatory properties (Wu et al., 2015; Zhang et al., 2018). For instance, the presence of intact GAG like hyaluronan (HA) is considered as a tissue integrity signal that reduces inflammation through its binding to CD44, a cell-surface glycoprotein, which promotes the production of anti-inflammatory cytokines (IL-2 and IL-10; Altman et al., 2019; Chen et al., 2019). In addition, this interaction causes a negative regulation of the pro-inflammatory toll-like-receptor (TLR) signaling in which TLR is considered as an immunoreceptor mediator for NF- κ B activation (Avenoso et al., 2018). Furthermore, high molecular weight HA regulates T-cell populations by increasing the levels of transcription factor Foxp3 in regulatory T-cells (Tregs), a specialized sub-population of CD4+ T cells, thus promoting their function through enhanced anti-inflammatory cytokine production (Ruppert et al., 2014). On the other hand, the highly sulphated GAG heparin (Hep) has demonstrated many benefits in the prevention and treatment of venous thrombosis, pulmonary diseases, burns, but recently also in the control of inflammation (Paschoa, 2016; Shastri, Peterson, & Patel, 2017). Heparin can suppress the classical pathway of the complement system by regulating the complement factors C activity (Rent et al., 1975; Weiler, Edens, Linhardt, & Kapelanski, 1992), potentiating the C1 esterase inhibitor action (Caughman, Boackle, & Vesely, 1982), interfering with the binding of C1q to immune complexes (Golan, Burger, & Loos, 1982) and inhibiting the interaction of C1s with C4 and C2 (Loos, Volanakis, & Stroud, 1976). Heparin and Hep-related compounds like heparin sulphate also inactivate chemokines through its binding to Hep-binding proteins which eventually prevent the activation and recruitment of inflammatory cells into tissue (Poterucha, Libby, & Goldhaber, 2017; Young, 2008). It has been shown also to possess an inhibitory effect on the nuclear transcription factor- κ B (NF- κ B), which in

turn suppresses leukocyte activation as well as pro-inflammatory cytokine production (Qi, Zhang, & Wang, 2016). The NF- κ B signaling pathway is inhibited by two different mechanisms with Hep; first one is by inhibiting the translocation of the transcription factor into the nucleus, while the second one is that Hep interferes nonspecifically to DNA binding of NF- κ B in the nucleus (Lee, Lee, Seo, Kim, & Ahn, 2007).

It has been shown previously that the NF- κ B pathway is essential in a variety of physiological processes like control of the immune response, cell proliferation, and death (Hayden & Ghosh, 2004). It has been also identified as key factor in inflammation having a direct influence on downregulating cytokine release (Lawrence, 2009). In other words, the inhibition of NF- κ B can potentially reduce inflammatory-related gene activation and regulate the gene expression and production of pro-inflammatory cytokines, chemokines, and adhesion molecules (Thourani et al., 2000). The NF- κ B transcription factor family consists of a wide variety of subunits, which share the same Rel homology domain (RHD, a protein domain), responsible for dimerization, inhibitor binding, nuclear translocation, and DNA binding (Hayden & Ghosh, 2008; Wan & Lenardo, 2009). Therefore, during activation, the inhibitory protein family (I κ Bs) gets degraded, leaving the NF- κ B, which can then translocate to the nucleus (Hayden & Ghosh, 2004).

In previous studies, we have shown that both covalent monolayer and adsorptive multilayer immobilization of GAG on model surfaces led to a reduction of inflammatory response of macrophages (Zhou, Al-Khoury, & Groth, 2016; Zhou, Niepel, Saretia, & Groth, 2016). Here, we extend these finding focusing on the effect of covalently immobilized HA and Hep toward the inhibition of p65 subunit translocation to the nuclear area and of phosphorylation of NF- κ B protein family, which is related to activation of THP-1 monocyte-derived macrophages (Chanput, Mes, & Wichers, 2014) in terms of NF- κ B pathway suppression by these covalently immobilized GAGs.

2 | MATERIALS AND METHODS

2.1 | Chemicals for surface modification

Glass cover slips were obtained from Menzel GmbH (Bielefeld, Germany) of (\varnothing 12 and 15 mm) surfaces. Silicon wafers were provided from LG Siltron Inc. (Gumi, Korea) of (10 \times 10) mm² surface. In addition, 3-Aminopropyltriethoxysilane 98% (APTES) were delivered from ABCR GmbH & CO. KG (Karlsruhe, Germany). HA was provided as a kind gift from M. Schnabelrauch, Innovent e.V. (Jena, Germany), while heparin (Hep) was obtained from Serva (Heidelberg, Germany). 1-(3-Dimethylaminopropyl)-3-ethylcarbodiimide hydrochloride, 98 + % (EDC) was purchased from Thermo Fischer Kandel GmbH (Karlsruhe, Germany) while N-Hydroxy-succinimide 98% (NHS) was obtained from Sigma-Aldrich (Taufkirchen, Germany). Acetone \geq 99.5% was provided from Roth (Karlsruhe, Germany) and Ethylene diamine from Sigma-Aldrich (Taufkirchen, Germany). 2-(N-Morpholino) ethaneulphonic acid monohydrate (MES) was purchased from VWR International Ltd. (Hunter Boulevard, England). Ammonia and hydrogen peroxide were delivered from Th. Geyer GmbH & Co. KG 25% and Roth 30%

(Renningen, Karlsruhe, Germany), respectively. AFM tips were obtained from AppNano (Applied Nanostructures Inc., Santa Clara, CA).

2.1.1 | Preparation of amino-terminated surfaces

Silicon wafers and glass cover slips were used for modification with APTES to generate amino groups for subsequent immobilization of GAG. The substrates were cleaned using the Radio Corporation of America cleaning protocol which is based on mixing a solution of ammonia, hydrogen peroxide, and water (1:1:5, v/v/v) at 75°C for 10 min, respectively. Then, ultrapure water (6 × 5 min) was used to wash the substrates with a further drying step by a stream of nitrogen (Macek, 1993). Furthermore, 2% (v/v) solution of APTES in 99.8% acetone was prepared to immerse the substrates for 1 hr at room temperature (RT). The resulted NH₂-modified surfaces were rinsed extensively with acetone, ethanol and washed with double-distilled water (8 × 5 min) then dried with a stream of nitrogen.

2.1.2 | Immobilization of GAG onto amino-terminated surfaces

MES buffer at a concentration of 50 mM at pH 4.70 was prepared. GAG solutions of HA ($M_w \approx 1.3$ MDa) and heparin (Hep, $M_w \approx 15$ kDa) at a concentration of 2 mg ml⁻¹ were dissolved in the aforementioned buffer. Subsequently, EDC and NHS at a concentration of 5 and 3 mg ml⁻¹, respectively were added for 30 min at RT to the GAG solutions (Hermanson, 1996). Thereafter, the EDC/NHS-activated GAG solutions were immobilized on the NH₂-terminated surfaces for 24 hr with light protection. Afterward, an inactivation of the remaining reactive carboxyl species of the EDC linker was achieved by immersing the samples in 1 M ethylene diamine solution for 10 min. The slides were rinsed with ethanol and washed with double-distilled water (6 × 5 min) then dried under nitrogen flow (Köwitsch et al., 2011).

2.1.3 | Labelling of GAG

The fluorescein isothiocyanate (FITC)-labeled GAG were prepared to determine the localization of stained HA and Hep within the cells according to a protocol published recently (Kowitsch et al., 2014). HA and Hep at a concentration of 2 mg ml⁻¹ were dissolved in a 50 mM MES-buffer (pH adjusted to 4.75). Thereafter, ×2 mmol of EDC and ×2 mmol of NHS were added to the GAG solutions under continuous stirring for 1 hr with further pH adjustment to 7.0. The concentrations were adjusted to obtain 10% labeled carboxylic groups with fluorescein. Subsequently, a solution of 1 mg ml⁻¹ of 6-aminofluorescein in dimethyl sulfoxide was added overnight. Eventually, the solutions were dialyzed against double-distilled water for 3 days with a subsequent freeze drying step. All steps were performed under light protection.

2.2 | Characterization of surfaces

2.2.1 | Atomic force microscopy (AFM)

Surface topography of NH₂ and GAG-modified silicon wafers (Si) was investigated using AFM (Nano-R, Pacific Nanotechnology, Santa Clara, CA). The Si wafers (10 × 10 mm²) were probed in contact mode under ambient (air) laboratory conditions of temperature and humidity. AFM tips with 125 μm length, 35 μm width, 14–16 μm height, and tip radius of <10 nm were used for imaging. The used scan area was 10 × 10 μm² per image with a scan rate of 0.2 Hz and a resolution of (512 × 512 pixel²). Image processing was done using the Gwiddyon software (version 2.40).

2.2.2 | Water contact angle measurements

The sessile drop method was used for static water contact angle (WCA) measurements using OCA 15+ device from Dataphysics (Filderstadt, Germany). Here, five droplets of 2 μl ultrapure water were applied to each sample at RT. Consequently, the experimental values were used to calculate the mean and standard deviation of two independent experiments.

2.2.3 | Streaming potential measurements

Streaming potential measurements were performed with a SurPASS device (Anton Paar, Graz, Austria). Two identically modified glass slides were mounted oppositely into the adjustable measurement chamber. The flow of electrolyte (1 mM KCl in water) was adjusted to a distance to maintain 300 mbar as a maximum pressure. Hydrochloric acid (HCl) at concentration 0.1 M was used for pH titration. In addition, the pH value was adjusted to pH 10.5 using 1 M sodium hydroxide (NaOH) before starting a measurement. Finally, the measurements were carried out with an automated titration ranged from pH 10.5 to pH 2.25, which was adjusted by two titration steps: 0.03 ml from pH 10.5 to pH 5.0 and 0.25 ml from pH 5.0 to pH 3.0.

2.3 | Studies with THP-1 derived macrophages

2.3.1 | Cell culture

The THP-1 human monocytic cells (DSMZ, Braunschweig, Germany) were cultured in RPMI-1640 medium (Lonza, Wuppertal, Germany) supplemented with 10% (v/v) fetal bovine serum (FBS, Biochrom AG, Berlin, Germany) and 1% (v/v) antibiotic-antimycotic solution (AAS, Lonza, Wuppertal, Germany) at 37°C in a humidified 5% CO₂/95% air atmosphere using a NUAIRE® DH Autoflow incubator (NuAire, Plymouth, MN). Every second day the nonadherent cells were passaged to maintain a cell density of 1 × 10⁶ cells ml⁻¹. THP-1 derived macrophages were obtained by incubation of floating monocytes with 200 nM phorbol-12-myristate-13-acetate (PMA, Sigma Aldrich, Darmstadt, Germany) in T75 cell culture

flasks (Greiner Bio-One GmbH & Co. KG, Frickenhausen, Germany) for 48 hr, as reported in literature (Zhou et al., 2010). Thereafter, macrophages were detached using 0.25% trypsin/0.02% EDTA (Biochrom AG, Berlin, Germany) with further addition of serum-containing RPMI-1640 medium to stop the activity of trypsin. Eventually, the harvested cells were used for seeding on the different modified surfaces.

2.3.2 | Cell adhesion studies

The modified substrates were sterilized with 70% ethanol for 15 min and rinsed twice with phosphate buffer saline (PBS). Macrophages were seeded on either NH₂-terminated and HA- or Hep-modified surfaces at a cell density of 2.5×10^4 cells ml⁻¹ in serum-containing RPMI-1640 medium (10% FBS). Samples were incubated for 24 hr at 37°C in a humidified 5% CO₂/95% air atmosphere. Thereafter, the nonadherent cells were gently washed twice with PBS. Attached cells were fixed with cold methanol (Roth, Karlsruhe, Germany) for 10 min and stained with 10% (v/v) Giemsa (Merck KGaA, Darmstadt, Germany) in ultrapure water for another 10 min. The cells were photographed with a transmitted light microscope (Nikon ECLIPSE Ti2, Tokyo, Japan) equipped with a CCD camera (DCIN, 12 V, EXT1/0, Tokyo, Japan) to evaluate cell count and morphology using the ImageJ software (version 1.46r).

2.3.3 | Multinucleated giant cells (MNGCs) characterization

The MNGCs formation was evaluated after 10 days culture of macrophages seeded as described in the previous section using a cell density of 2.5×10^5 cells ml⁻¹. The higher cell density compared to cell adhesion experiments was chosen to permit aggregation of macrophages as prerequisite for their fusion. The modified surfaces with cells were gently washed twice with PBS. Attached cells were fixed with cold methanol and stained with 10% (v/v) Giemsa in ultrapure water as described in the adhesion studies. Micrographs of macrophages were taken by a transmitted light microscope equipped with a CCD camera (Axiovert 100, Carl Zeiss, Oberkochen, Germany) and the area percentage of MNGCs was calculated by the ImageJ software as described in our previous articles (Zhou, Al-Khoury, & Groth, 2016; Zhou, Niepel, et al., 2016).

2.3.4 | IL-1 β production measurement

Macrophages were seeded at a cell density of 5.0×10^5 cells ml⁻¹ on the modified surfaces and incubated for 24 hr in presence or absence of 1 μ g ml⁻¹ lipopolysaccharide (LPS, Sigma Aldrich, Darmstadt, Germany). The cytokine containing supernatants, both with LPS treatment and without LPS, were collected and stored at -20°C until needed for investigation. The IL-1 β production was measured using an ELISA kit following the manufacturers' instructions (Thermo Scientific, Bonn, Germany).

2.3.5 | Immunofluorescence (IF) staining of NF- κ B

The translocation of p65 subunit of NF- κ B to the nuclear area was evaluated by immunostaining according to the method developed by Noursadeghi et al. (2008). FITC-labeled HA and Hep were immobilized on NH₂-modified slides. Macrophages were seeded on modified surfaces at a density of 2.5×10^5 cells ml⁻¹ in serum-containing RPMI 1640 medium and incubated for 48 hr at 37°C in a humidified 5% CO₂/95% air atmosphere. Two sets of samples were analyzed to compare between the absence and presence of 1 μ g ml⁻¹ LPS (Sigma Aldrich). Thereafter, cells cultured on modified surfaces were fixed with 4% paraformaldehyde (Sigma Aldrich, Darmstadt, Germany) for 15 min, permeabilized with 0.1% (v/v) Triton[®] X-100 (Sigma-Aldrich, Taufkirchen, Germany) for 10 min at RT, and rinsed twice with PBS. The nonspecific binding sites were blocked with a 1% (w/v) bovine serum albumin \geq 98% (BSA, Carl Roth GmbH, Halle (Saale), Germany) in PBS for 30 min. Subsequently, cells were incubated with monoclonal p65 subunit of NF- κ B antibody (1:100, Santa Cruz Biotechnology, Dallas, TX) at 4°C overnight. After washing with PBS for 5 min on a shaker, a secondary monoclonal anti-rabbit IgG antibody conjugated with Cy2 (1:200, Jackson Immunoresearch, Ely, UK) was applied for another 30 min at RT. The nuclei were stained with TO-PRO-3 (1:500, Invitrogen) for 40 min at RT. Finally, the samples were mounted on glass slides with polyvinyl alcohol (PVA, Sigma Aldrich, Darmstadt, Germany) and examined on confocal microscope LSM 710 (Carl Zeiss) using a 40-fold oil immersion objective. Image processing was done with ImageJ (v.1.52i). The TO-PRO-3 channel was used to mask a region of interest (ROI) representing the nucleus, while the Cy2 channel was used to mask a cellular ROI. Then the nuclear ROI was subtracted from the cellular ROI to obtain a cytosolic ROI. Finally, the fluorescence intensity was evaluated in the nuclear and cytosolic ROI and a ratio calculated. The principle of the method is visualized in Figure S1.

2.3.6 | Cell lysis for immunoblotting (IB)

Macrophages differentiated from THP-1 monocytic cell line as described above were seeded at cell density of 52×10^5 cells ml⁻¹ for 48 hr on NH₂ as well as GAG-modified samples (glass slides with a total area of 19.76 cm², Menzel GmbH, Bielefeld, Germany). The four-well plates (Greiner Bio-one, Leipzig, Germany) were placed on ice and the cells were washed twice with ice-cold PBS. Thereafter, cell lysate buffer (RIPA buffer) with protease and phosphatase inhibitors (ThermoFisher Scientific, Waltham, MA) was added and the macrophages were scraped using a cold plastic cell scraper. Subsequently, the cell lysates were gently transferred to precooled tubes and a constant agitation at 4°C for 30 min was maintained. In addition, the cell lysates were centrifuged at 4°C and 13,000 rpm for 20 min with subsequent storage of the supernatants at -80°C up to 1 month before performance of IB.

2.3.7 | Bicinchoninic acid protein assay

The bicinchoninic acid (BCA) test was performed according to the manual of the Pierce BCA Protein Assay Kit (Thermo Scientific, Bonn, Germany). A working solution was prepared by mixing 50 parts of BCA Reagent A with 1 part of BCA Reagent B. Thereafter, 25 μl of cell lysates were pipetted in a 96-well plate and 200 μl working solution was added. The samples were incubated for 30 min at 37°C. Then, the absorbance was measured at 562 nm with a plate reader (Fluostar Optima, BMG LABTECH, Offenburg, Germany).

2.3.8 | SDS-PAGE and Western blotting

Twenty-five micro liter of cell lysates were separated by PAGE using 15% SDS-polyacrylamide gels. Then, immunoblotting was done using nitrocellulose membranes (Schleicher & Schuell). Membranes were blocked in 3% (w/v) milk powder in TBS-T, probed with monoclonal antibodies against phospho-NF- κB (CST, #3033), NF- κB (Santa Cruz Biotechnology, sc-8008), and β -actin (MERCK, A1978), followed by incubation with HRP-labeled secondary antibodies and visualized with the enhanced chemiluminescence reaction (ThermoFisher Scientific) in a ChemiDoc Imaging System (Biorad). Obtained grayscale images were densitometrically analyzed by the Li-Cor Image Studio software using automatic background determination and subtraction function. Results of two samples were used to calculate means.

2.3.9 | Association of FITC-GAG with macrophages studied by confocal laser scanning microscopy

Macrophages were seeded on the NH_2 -terminated and FITC-labeled HA and Hep modified surfaces at a concentration of 2.5×10^5 cells ml^{-1} for 24 hr, then fixed for 10 min with 4% paraformaldehyde (Sigma Aldrich, Darmstadt, Germany). Afterward, the red fluorescent carbocyanine solution, a cytoplasmic membrane dye (DID, Biotium, Fremont, CA), was prepared at a ratio of 5 μl to 1 ml PBS, 0.5 ml, added to each sample and incubated for 10 min to stain macrophages. Eventually, all samples were washed twice with PBS, mounted on objective slides using polyvinyl alcohol (PVA, Sigma Aldrich, Darmstadt, Germany) and examined with confocal laser scanning microscopy (CLSM) using $\times 63$ oil immersion objective (LSM 710, Carl Zeiss). Images were processed using the ZEN2011 software (Carl Zeiss).

2.3.10 | Uptake of FITC-GAG by macrophages studied with flow cytometry

Macrophages were seeded for 48 hr as described above preparing two sets of samples with presence and absence of LPS. Thereafter,

the modified surfaces were transferred to new well plates, gently washed with PBS, Then, 300 μl of 0.25% Trypsin was added for 3 min with further addition of serum-containing RPMI 1640 medium to stop the trypsin effect. The cells were scraped-off, centrifuged, washed once with PBS and re-suspended in 200 μl PBS. Finally, 100 μl cell suspension was transferred to 96-well plate and measured with a flow cytometry device (LSR Fortessa II, BD Bioscience, Germany). The data were analyzed with the FACS-Diva software (version 6.2).

2.4 | Statistics

Kruskal-Wallis and one-way analysis of variance (ANOVA) followed by posthoc Tukey's test using the Origin 8 Pro software (Origin Lab, Northampton, MA) were used for statistical calculations. Data are presented as mean values \pm standard deviations (SD) or medians with box plots. The number of samples has been indicated in the respective figure captions. Statistical significance was considered for $p \leq .05$ and is indicated by asterisks in the figures.

3 | RESULTS

3.1 | Characterization of surface properties

The modified surfaces were investigated toward surface topography with AFM. It can be seen in Figure 1a that the immobilization of HA and heparin (Hep) resulted in slight changes of the topography in comparison to NH_2 -modified control surfaces. In addition, smoother surfaces were achieved after the immobilization of both GAG, which was considered as an evidence of complete coating of the substratum with HA and Hep.

The wetting properties of plain NH_2 -terminated surfaces and those modified by covalent immobilization of either HA or Hep were determined by static WCA measurements. Figure 1b demonstrates a significant increase in the hydrophilicity of GAG-modified samples compared to NH_2 -terminated surfaces. In addition, a significant difference between the HA and Hep was found with Hep being the most hydrophilic surface. Furthermore, Figure 1c shows the zeta-potentials of samples in dependence on the pH of electrolyte solution (1 mM KCl). It shows a clear difference between all surfaces with a sequence of NH_2 , HA, and Hep, which corresponded well with the chemical composition of substrata.

3.2 | Adhesion and fusion of macrophages

In Figure 2a, the micrographs of macrophages cultured for 24 hr on modified surfaces are shown, representing the adhesion and shape of cells. Macrophages showed highest adherence on the NH_2 -terminated surfaces with a spread and elongated shape, while a lower quantity of cells with more round shape were seen on HA, while cells on Hep

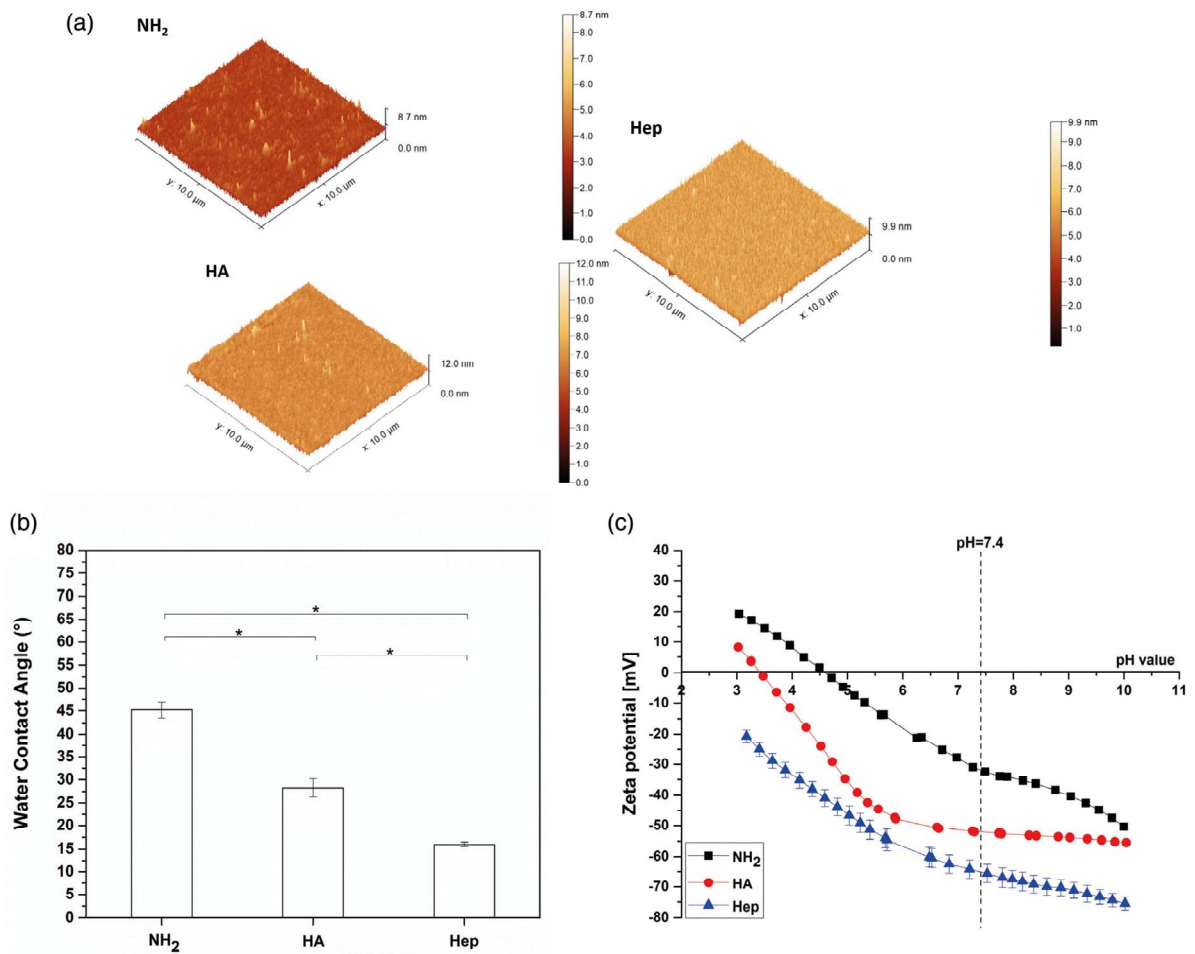


FIGURE 1 (a) Atomic force microscopy (AFM) images to visualize surface topography of the aminoterminated (NH₂) and NH₂ modified with covalent immobilization of either hyaluronic acid (HA) or heparin (Hep). (b) Static water contact angle measurements using the sessile drop method to characterize surface wettability of amino-terminated surfaces (NH₂) and covalent immobilization of either hyaluronic acid (HA) or heparin (Hep). Results are presented as means ± SD, **p* < .05, *n* = 5. (c) Zeta potentials of aminoterminated surfaces (NH₂) and covalent immobilization of either HA or Hep, abbreviated as (NH₂ [■], HA [●], and Hep [▲]), respectively. Results are presented as means ± SD in the pH range 10–3.0

were fewer and had a more elongated phenotype. The number of adherent macrophages per area shown in Figure 2b displays the highest cell adhesion on NH₂-terminated surfaces, followed by Hep, while the lowest adhesion of macrophages was found on HA-coated samples. In addition, Figure 2c shows the aspect ratio of adherent macrophages with a clear trend of enhanced cell polarization on the NH₂-terminated samples. By contrast, the mean and median values of aspect ratio illustrated a significant decrease on HA-modified samples and higher again on Hep-coated surface in accordance with the micrographs.

Figure 3a shows the micrographs of the MNGCs formation obtained after 10 days culture of cells in serum-containing medium. Evaluation of macrophage fusion showed that the significantly highest was observed on the NH₂ surfaces in terms of number of nuclei (≥2)

per cell body and size of MNGC. In contrast, the GAG-modified surfaces lowered significantly the fusion extent. Subsequently, image analysis software was used to evaluate the area percentage of the MNGC, which is illustrated in Figure 3b. The GAG-modified surfaces showed a significant reduced percentage of MNGC in comparison to the NH₂-coated samples

3.2.1 | IL-1β pro-inflammatory cytokine release

The IL-1β production was analyzed after 24 hr of cultivation of cells with (black bars) or without (white bars) LPS stimulation as shown in Figure 4. A higher release of IL-1β was noticed in cell culture supernatants of macrophages cultured on NH₂ samples both in presence or absence of LPS.

FIGURE 2 (a) Transmitted light microscopic images of adherent macrophages stained with 10% (v/v) Giemsa after 24 hr cultivation on the amino-terminated surfaces (NH₂) and covalent immobilization of either hyaluronic acid (HA) or heparin (Hep). (Scale bar: 100 μm). (b) Number of adherent macrophages per surface area after 24 hr of incubation. Data represent means ± SD, n = 5, *p ≤ .05. (c) Aspect ratio of adherent macrophages. The box plot indicates the 25th and 75th percentile, the lowest and highest values are represented by the whiskers, whereas the median (horizontal line) and mean value (black square) are shown as well

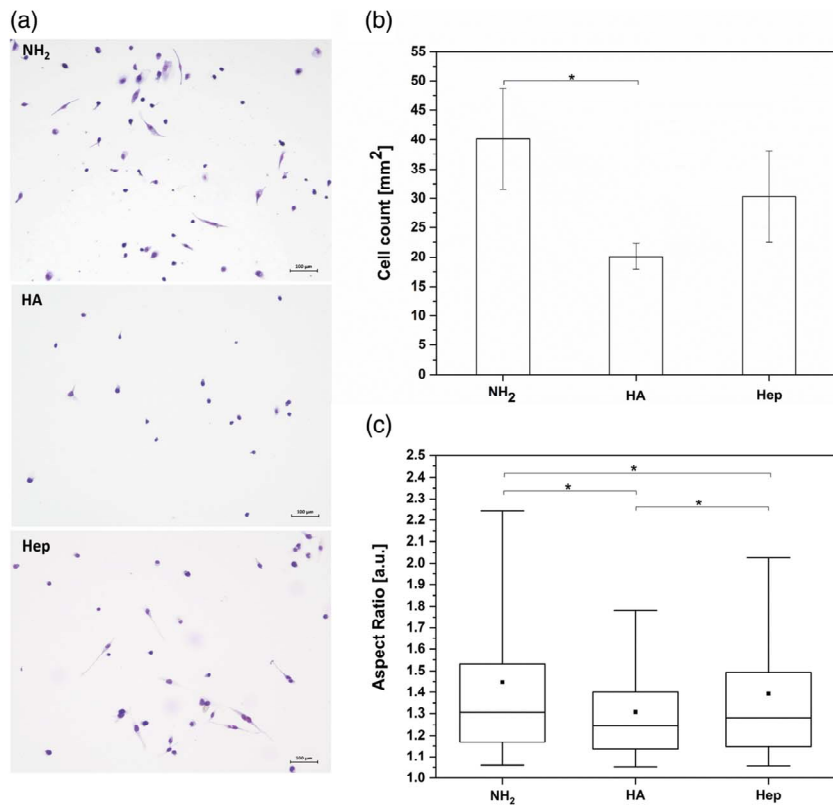
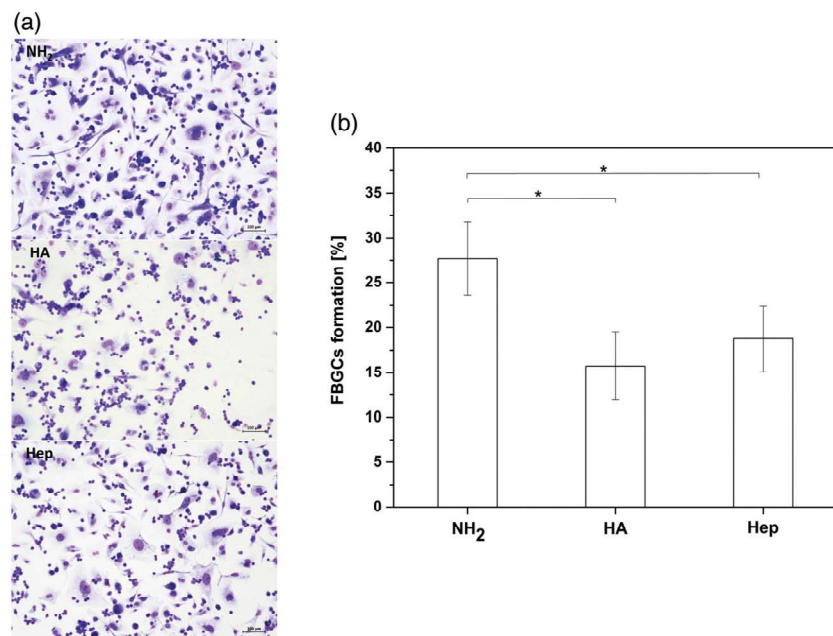


FIGURE 3 (a) Transmitted light microscopic images of multinucleated giant cells (MNGCs) stained with 10% (v/v) Giemsa after 10 days incubation on the amino-terminated surfaces (NH₂) and NH₂ modified with covalent immobilization of either hyaluronic acid (HA) or heparin (Hep). (Scale bar: 100 μm). (b) The area percentage of formed MNGCs on NH₂, HA and Hep surfaces by quantitative evaluation of micrographs. Results are the means ± SD, *p < .05, n = 10



On the other hand, the GAG-modified surfaces significantly lowered the IL-1β release, which was observed under both conditions. In addition, it can be noticed that IL-1β secretion by THP-1 derived macrophages was

upregulated in all samples when stimulated with LPS, which indicates their responsiveness and functional activity of THP-1-derived macrophages during the studies.

3.2.2 | IF staining of NF-κB in macrophages

Figure 5a shows TO-PRO-3 staining (blue) of macrophage nuclei and staining of nonphosphorylated p65 subunit of NF-κB (green) that was found both in cell cytoplasm and nuclei. The quantitative evaluation of the ratio of nuclear to cytoplasmic was used as an indicator for translocation of NF-κB and is shown in Figure 5b. It was highest in macrophages on the control NH₂ surfaces; both in the presence and absence of LPS. A significant reduction of the nuclear to cytoplasmic

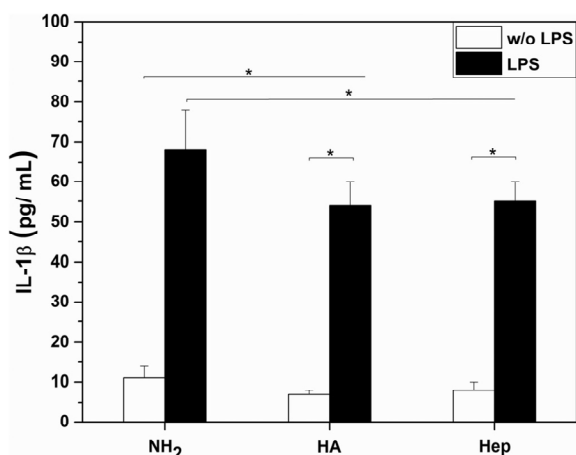


FIGURE 4 IL-1β production by macrophages after 24 hr of cultivation in the absence (white bars) and presence (black bars) of lipopolysaccharide (LPS) on the amino-terminated surface (NH₂) and NH₂ modified by covalent immobilization of either hyaluronic acid (HA) or heparin (Hep). Data represent mean ± SD, n = 6, *p ≤ .05

ratio was found comparing NH₂ surfaces with that of GAG immobilization. Hep shows the highest suppression of translocation of p65 into the nucleus both in absence and presence of LPS

3.2.3 | Western blotting

Figure 6a shows the blots from macrophage cell lysates showing both the bands for phosphorylated p65 of NF-κB (pNF-κB) and actin with the latter used for normalization of densitometry data. The bands of two cell lysates from duplicate samples illustrate higher phosphorylation of NF-κB on NH₂-terminated surfaces in comparison to GAG-modified. It was also observed that the LPS stimulation upregulated the phosphorylation of pNF-κB. Furthermore, Figure 6b shows the quantitative values of pNF-κB in macrophages plated on GAG compared to the NH₂ samples evaluated by densitometry. Similar effects were found for both HA and Hep in terms of a reduced intensity of pNF-κB in the blots

3.2.4 | Association of GAG with macrophages studied by CLSM

Figure 7 shows selected images of DID-stained macrophages cultured on FITC-labeled GAG. The confocal images of macrophages on NH₂ terminated surfaces show the red staining of the cell membrane by DID. On the other hand, macrophages cultured on FITC-GAG-modified samples clearly show an association of FITC-labeled HA and Hep with DID stained cells. The 3D images in Figure 7 show that FITC-labeled HA seems to be mainly co-localized with the cell surface. By contrast, FITC-labeled Hep is seen rather intracellularly, with some apparent presence in the nuclear area. Higher amounts of FITC-labeled HA can

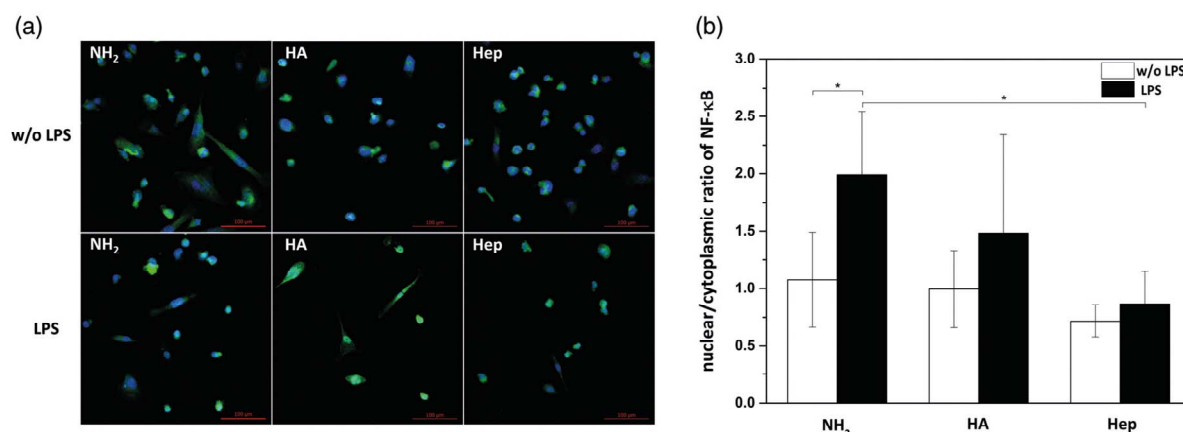


FIGURE 5 (a) TO-PRO-3 (blue color) and p65 followed by CY2 staining (green color) of the nucleus and the cytoplasm are shown for unstimulated (upper row) and of 1 μg ml⁻¹ Lipopolysaccharide (LPS) stimulated macrophages (lower row). The cells were seeded for 48 hr on the amino-terminated surfaces (NH₂) and NH₂ modified with covalent immobilization of either hyaluronic acid (HA) or heparin (Hep). The sequential processing using the ImageJ software is shown to produce binary masks of nuclear and cytoplasmic regions of interest (ROI). (Scale bar: 100 μm). (b) Quantification of nuclear to cytoplasmic ratio in the absence (white bars) and the presence (black bars) of LPS on the NH₂, HA and Hep surfaces, which can be translated as amount of p65 in the nucleus compared to the cytosol. Data represent mean ± SD, n = 10, *p ≤ .05

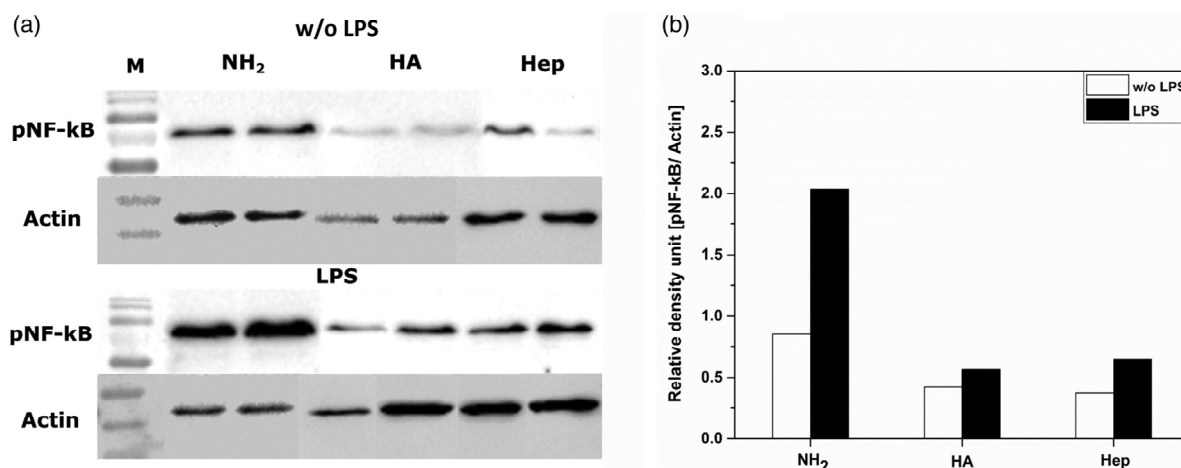


FIGURE 6 (a) Lysates from macrophages cultured on amino-terminated surfaces (NH₂) and NH₂ modified with covalent immobilization of either hyaluronic acid (HA) or heparin (Hep) in the absence and presence of lipopolysaccharide (LPS). The two cell lysates from duplicates of samples were collected after 48 hr and were blotted toward phosphorylated p65 subunit of NF-κB (pNF-κB). The blot was stripped and re-probed with anti-actin antibody (b) The immunoblotting bands were analyzed densitometrically and normalized to the actin content. The relative density of pNF-κB was evaluated in the absence (white bars) and the presence (black bars) of LPS. Data represent mean ± SD, n = 2

be seen on the surface of macrophages compared to smaller quantities of Hep inside the cells. Additional cell images are visualized in Figure S3 and S4.

3.2.5 | Association of FITC-labeled GAG with macrophages studied by flow cytometry

Two sets of samples were investigated in the absence (left column) and presence (right column) of 1 μg ml⁻¹ LPS. Figure 8a shows the flow cytometry histograms with side scatter (SSC). The raw data were obtained after setting the negative controls to a baseline by determining a threshold, beyond which, any signal was considered as a positive signal indicating association of FITC-labeled GAG with macrophages.

Here, the number of cells with fluorescence was measured, which represents the quantity of macrophages that are able to take up or associate with FITC-labeled-GAG. Figure 8b demonstrates that a significant difference between HA-coated and Hep-coated samples was found. The FITC-labeled HA showed a higher affinity to be associated with macrophages in comparison to FITC-labeled Hep. These findings are in accordance to the 3D images in Figure 7 obtained by CLSM.

4 | DISCUSSION

In this study, we tried to shed a light on the potential mechanism of anti-inflammatory action of HA or Hep regarding the signaling pathway of NF-κB, when these GAG were used to modify model biomaterials in a covalent manner. We confirmed here findings of previous studies that immobilization of these GAG diminishes activation of macrophages (Köwitsch, Zhou, & Groth, 2018). The observed effects

are related to a lowered translocation of NF-κB subunit p65 to the nuclear area and reduced phosphorylation of NF-κB on GAG-modified surfaces compared to a NH₂-terminated “pro-inflammatory” control surface.

Physical characterization of the surfaces showed that NH₂-terminated control surfaces were less hydrophilic and negatively charged than GAG-modified, which is related to the presence of amino groups (Fauchoux, Schweiss, Lützw, Werner, & Groth, 2004). HA and Hep-modified surfaces were more hydrophilic and negatively charged indicated by lower WCA and zeta potentials, which is related to presence of carboxylic and sulfate groups. These findings correspond also well to our previous studies immobilizing oxidized GAG on NH₂-terminated surfaces (Yang et al., 2016). The different adhesion of macrophages might be related to differences adsorption of adhesion-mediating proteins like fibronectin from serum. NH₂-terminated surfaces bind significantly more than hydrophilic carboxyl or hydroxyl-terminated surfaces that promote adhesion and spreading of cells by integrin-mediated mechanisms (Fauchoux et al., 2004). Also other authors stated that highly hydrophilic and negatively charged surfaces lead to lower adhesion of cells when compared moderately wetttable materials (Bacakova, Filova, Parizek, Ruml, & Svorcik, 2011). Hence, coating of substrata with GAGs like HA and Hep may reduce adhesion of macrophages, which by itself diminishes propensity of inflammatory reactions. Indeed, this is not the only mechanism by which these GAGs are acting.

Studies on NF-κB signaling pathway were performed in an attempt to investigate the mechanism of anti-inflammatory action of GAG-modified surfaces that goes beyond making surfaces more hydrophilic and negatively charged. Based on IF staining of nonphosphorylated form of p65 subunit of NF-κB (Figure 5) lowest translocation of p65 to the nuclear region occurred in macrophages cultured on Hep-, followed

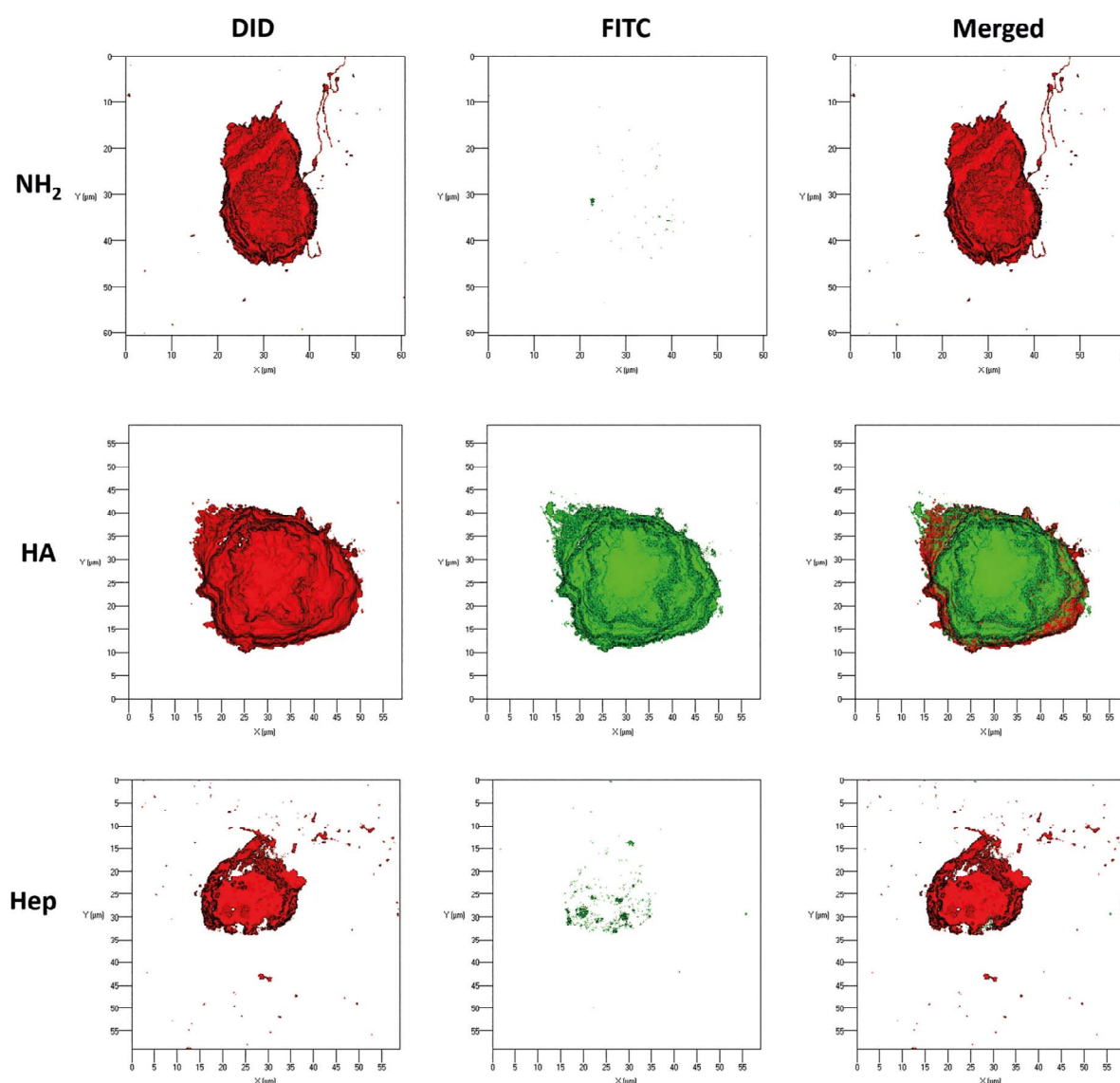


FIGURE 7 Representative 3D view of a z-stack in surface projection with confocal laser scanning microscopy (CLSM). Macrophages were cultured for 24 hr on amino-terminated surfaces (NH_2) and NH_2 modified with covalent immobilization of either hyaluronic acid (HA) or heparin (Hep). The cells were stained for DID (red, membrane staining) and the FITC-labeled GAG (green). (63-fold oil immersion objective, scale: 20 μm). In this mode, pixel values are computed as solids, which allows no transparency

by HA-modified surfaces, which corresponds to the findings of others with soluble forms of heparin and related compounds (Young, 2008). In parallel, the immunoblotting of phosphorylated NF- κ B illustrated a lower intensity of bands in whole cell lysates from macrophages cultured on GAG-modified surfaces in comparison to NH_2 -modified surfaces. This was considered as an additional evidence of the inhibitory effects of immobilized GAG on NF- κ B signaling pathways. These results are supported by reports from other groups indicating that Hep has two different mechanism of action on NF- κ B signaling pathway. One is through partial inhibition of NF- κ B translocation inside the nucleus

through the electrostatic binding of the positively charged transcription factor to the anionic Hep, taken up by endocytosis (Young, 2008; Young et al., 1999). The second is that Hep can activate the NF- κ B pathway through the phosphorylation of p65 allowing its translocation to the nucleus which further inhibits the binding of NF- κ B to DNA sequences (Lee et al., 2007). By contrast, HA possesses anti-inflammatory effects through its interactions to the cell surface receptor CD44, but also by suppression of toll-like receptors (TLR) signaling (Ruppert et al., 2014). The confocal images of DID stained macrophages demonstrated an association of FITC-labeled HA with the surface of

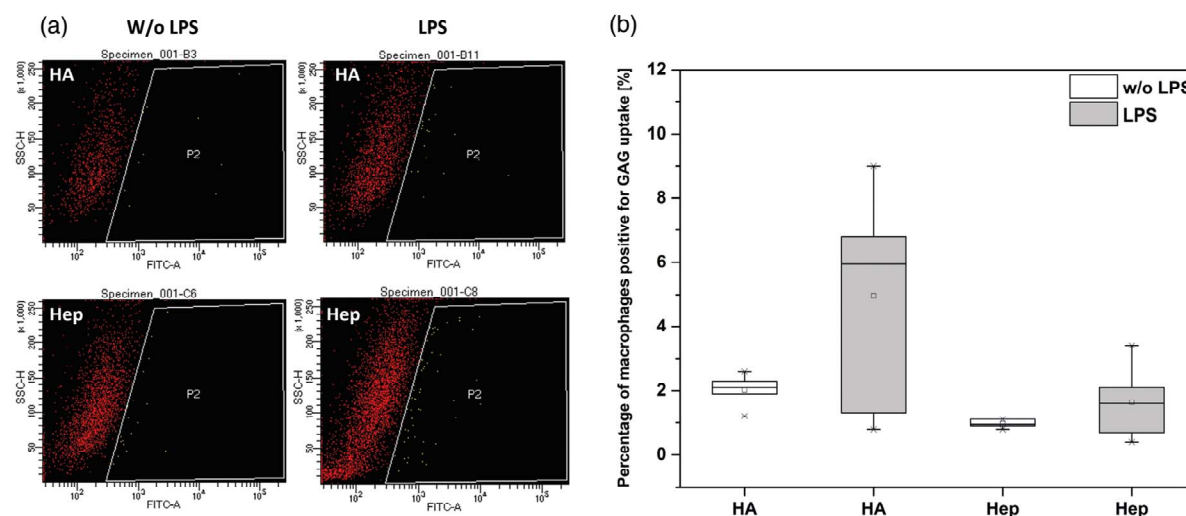


FIGURE 8 (a) Illustrative images of the flow cytometry measurements of macrophages cultured with either FITC-labeled hyaluronic acid (HA) or heparin (Hep) in the absence (left column) and presence (right column) of lipopolysaccharide (LPS). (b) The percentage of macrophages positive for GAG uptake after 48 hr cultivation on amino-terminated (NH₂) and NH₂ modified with covalent immobilization of either FITC-labeled hyaluronic acid (HA) or heparin (Hep), in the absence (white bars) and the presence (black bars) of LPS. Data represent mean \pm SD, $n = 6$, $*p \leq .05$

macrophages while on the other side an internalization of Hep in macrophages was found. The reason beyond the presence of anionic Hep inside macrophages might be due to either endocytosis or anionic transporters (Young, 2008). Indeed, the preparation of samples was based on covalent binding, which should provide a stable bond formation due to the chemical cross-linking process of GAG to amino groups on the substratum (Hermanson, 1996; Köwitsch et al., 2011). This was also observed here as we found no release of FITC-labeled GAG after covalent immobilization on NH₂-modified surfaces (see Figure S2). Thus, we assume a partial release of GAG molecules from the samples through the activity of secreted reactive oxygen species (ROS), hyaluronidases and heparinases by macrophages that could be responsible for the mobilisation of HA and Hep (Li & Vlodayvsky, 2009; Puissant & Boonen, 2016). In conclusion, Hep showed less translocation of the p65 into the cell nucleus as well as less intensity of pNF- κ B in whole cell lysates indicating the suppressive effect of Hep toward the NF- κ B signaling pathway, which was addressed recently by Young (Young, 2008). On the other hand, HA exerts its anti-inflammatory properties most likely through its association with the cell membrane by binding to CD44 as we did not find any evidence for an intracellular presence of HA and its way of action (Altman, Manjoo, Fierlinger, Niazi, & Nicholls, 2015).

5 | CONCLUSION

It can be concluded that HA and Hep possess a high potential to be used for making anti-inflammatory surface coatings based on the suppression of the canonical NF- κ B signaling pathway. This effect supports the idea of making hydrophilic coatings on biomaterial surfaces that reduce opsonisation (protein adsorption) and thus inflammatory response after implantation, but can be also combined directly with pharmaceutical effects by the anti-inflammatory activity of GAG like

hyaluronan and heparin. Hence, we conclude that coating of biomaterials with HA and Hep may have a significant impact in reducing the inflammatory response after implantation, which may increase functionality and lifetime of sensors and other implanted medical devices.

ACKNOWLEDGMENT

This work was financially supported through a PhD grant to Hala by the German Academic Exchange Service (DAAD). The study was also part of the project of bilateral cooperation funded by DAAD and Ministry of Education, Science and Technological Development of the Republic of Serbia (period 2019–2020). The kind support by Dr. rer.nat. Alexander Navarrete Santos from University Hospital of Martin Luther University Halle-Wittenberg doing flow cytometry is greatly appreciated.

CONFLICT OF INTEREST

There are no conflicts to declare.

ORCID

Thomas Groth  <https://orcid.org/0000-0001-6647-9657>

REFERENCES

- Al-Khoury, H., Espinosa-Cano, E., Rosa Aguilar, M., San Román, J., Syrowatka, F., Schmidt, G., & Groth, T. (2019). Anti-inflammatory surface coatings based on polyelectrolyte multilayers of heparin and polycationic nanoparticles of naproxen-bearing polymeric drugs. *Biomacromolecules*, 20(10), 4015–4025.
- Altman, R., Bedi, A., Manjoo, A., Niazi, F., Shaw, P., & Mease, P. (2019). Anti-inflammatory effects of intra-articular hyaluronic acid: A systematic review. *Cartilage*, 10(1), 43–52.
- Altman, R. D., Manjoo, A., Fierlinger, A., Niazi, F., & Nicholls, M. (2015). The mechanism of action for hyaluronic acid treatment in the osteoarthritic knee: A systematic review. *BMC Musculoskeletal Disorders*, 16(1), 321.

- Avenoso, A., D'Ascola, A., Scuruchi, M., Mandraffino, G., Calatroni, A., Saitta, A., ... Campo, G. M. (2018). Hyaluronan in the experimental injury of the cartilage: Biochemical action and protective effects. *Inflammation Research*, 67(1), 5–20.
- Bacakova, L., Filova, E., Parizek, M., Ruml, T., & Svorcik, V. (2011). Modulation of cell adhesion, proliferation and differentiation on materials designed for body implants. *Biotechnology Advances*, 29(6), 739–767.
- Brovold, M., Almeida, J. I., Pla-Palacin, I., Sainz-Arnal, P., Sánchez-Romero, N., Rivas, J. J., & Baptista, P. M. (2018). Naturally-derived biomaterials for tissue engineering applications. In *Novel Biomaterials for Regenerative Medicine* (pp. 421–449). USA: Springer.
- Caughman, G. B., Boackle, R. J., & Vesely, J. (1982). A postulated mechanism for heparin's potentiation of C1 inhibitor function. *Molecular Immunology*, 19(2), 287–295.
- Chanput, W., Mes, J. J., & Wichers, H. J. (2014). THP-1 cell line: an in vitro cell model for immune modulation approach. *International Immunopharmacology*, 23(1), 37–45.
- Chen, M., Li, L., Wang, Z., Li, P., Feng, F., & Zheng, X. (2019). High molecular weight hyaluronic acid regulates P. gingivalis-induced inflammation and migration in human gingival fibroblasts via MAPK and NF- κ B signaling pathway. *Archives of Oral Biology*, 98, 75–80.
- Fauchoux, N., Schweiss, R., Lützwang, K., Werner, C., & Groth, T. (2004). Self-assembled monolayers with different terminating groups as model substrates for cell adhesion studies. *Biomaterials*, 25(14), 2721–2730.
- Franz, S., Rammelt, S., Scharnweber, D., & Simon, J. C. (2011). Immune responses to implants—a review of the implications for the design of immunomodulatory biomaterials. *Biomaterials*, 32(28), 6692–6709.
- Golan, M., Burger, R., & Loos, M. (1982). Conformational changes in C1q after binding to immune complexes: Detection of neoantigens with monoclonal antibodies. *The Journal of Immunology*, 129(2), 445–447.
- Hayden, M. S., & Ghosh, S. (2004). Signaling to NF- κ B. *Genes & Development*, 18(18), 2195–2224.
- Hayden, M. S., & Ghosh, S. (2008). Shared principles in NF- κ B signaling. *Cell*, 132(3), 344–362.
- Hermanson, G. (1996). *Bioconjugate techniques* (pp. 185–186). USA: Academic Press.
- Kastellorizios, M., Tipnis, N., & Burgess, D. J. (2015). Foreign body reaction to subcutaneous implants. In *Immune Responses to Biosurfaces* (pp. 93–108). USA: Springer.
- Köwitsch, A., Yang, Y., Ma, N., Kuntsche, J., Mäder, K., & Groth, T. (2011). Bioactivity of immobilized hyaluronic acid derivatives regarding protein adsorption and cell adhesion. *Biotechnology and Applied Biochemistry*, 58(5), 376–389.
- Köwitsch, A., Zhou, G., & Groth, T. (2018). Medical application of glycosaminoglycans: A review. *Journal of Tissue Engineering and Regenerative Medicine*, 12(1), e23–e41.
- Köwitsch, A., Abreu, M. J., Chhalotre, A., Hielscher, M., Fischer, S., Mäder, K., & Groth, T. (2014). Synthesis of thiolated glycosaminoglycans and grafting to solid surfaces. *Carbohydrate Polymers*, 114, 344–351.
- Lawrence, T. (2009). The nuclear factor NF- κ B pathway in inflammation. *Cold Spring Harbor Perspectives in Biology*, 1(6), a001651.
- Lee, J. H., Lee, J., Seo, G. H., Kim, C. H., & Ahn, Y. S. (2007). Heparin inhibits NF- κ B activation and increases cell death in cerebral endothelial cells after oxygen-glucose deprivation. *Journal of Molecular Neuroscience*, 32(2), 145–154.
- Li, J.-p., & Vlodavsky, I. (2009). Heparin, heparan sulfate and heparanase in inflammatory reactions. *Thrombosis and Haemostasis*, 102(11), 823–828.
- Loos, M., Volanakis, J. E., & Stroud, R. M. (1976). Mode of interaction of different polyanions with the first (C1, C1), the second (C2) and the fourth (C4) component of complement-III: Inhibition of C4 and C2 binding site(s) on C1s by polyanions. *Immunochimistry*, 13(9), 789–791.
- Macek, M. (1993). A review of advanced wet cleaning. *Informacije MIDE M*, 23(4), 275–283.
- Moore, L. B., & Kyriakides, T. R. (2015). Molecular characterization of macrophage-biomaterial interactions. In *Immune Responses to Biosurfaces* (pp. 109–122). USA: Springer.
- Noursadeghi, M., Tsang, J., Hausteiner, T., Miller, R. F., Chain, B. M., & Katz, D. R. (2008). Quantitative imaging assay for NF- κ B nuclear translocation in primary human macrophages. *Journal of Immunological Methods*, 329(1–2), 194–200.
- Oishi, Y., & Manabe, I. (2018). Macrophages in inflammation, repair and regeneration. *International Immunology*, 30(11), 511–528.
- Paschoa, A. F. (2016). Heparin: 100 years of pleiotropic effects. *Journal of Thrombosis and Thrombolysis*, 41(4), 636–643.
- Poterucha, T. J., Libby, P., & Goldhaber, S. Z. (2017). More than an anticoagulant: Do heparins have direct anti-inflammatory effects? *Thrombosis and Haemostasis*, 117(03), 437–444.
- Puissant, E., & Boonen, M. (2016). Monocytes/macrophages upregulate the hyaluronidase HYAL1 and adapt its subcellular trafficking to promote extracellular residency upon differentiation into osteoclasts. *PLoS One*, 11(10), e0165004.
- Qi, L., Zhang, X., & Wang, X. (2016). Heparin inhibits the inflammation and proliferation of human rheumatoid arthritis fibroblast-like synoviocytes through the NF- κ B pathway. *Molecular Medicine Reports*, 14(4), 3743–3748.
- Rent, R., Ertel, N., Eisenstein, R., & Gewurz, H. (1975). Complement activation by interaction of polyanions and polycations: I. Heparin-protamine induced consumption of complement. *The Journal of Immunology*, 114 (1 Part 1), 120–124.
- Ruppert, S. M., Hawn, T. R., Arrigoni, A., Wight, T. N., & Bollyky, P. L. (2014). Tissue integrity signals communicated by high molecular weight hyaluronan and the resolution of inflammation. *Immunologic Research*, 58(2–3), 186–192.
- Shastri, M. D., Peterson, G. M., & Patel, R. P. (2017). Redefining approaches to asthma: Bridging the gap between heparin and its anti-inflammatory activities. *Current Allergy and Asthma Reports*, 17(10), 70.
- Suarez, P., Rojo, L., González-Gómez, A., & San Román, J. (2013). Self-assembling gradient copolymers of vinylimidazol and (acrylic)ibuprofen with anti-inflammatory and zinc chelating properties. *Macromolecular Bioscience*, 13(9), 1174–1184.
- Thourani, V. H., Brar, S. S., Kennedy, T. P., Thornton, L. R., Watts, J. A., Ronson, R. S., & Vinten-Johansen, J. (2000). Nonanticoagulant heparin inhibits NF- κ B activation and attenuates myocardial reperfusion injury. *American Journal of Physiology-Heart and Circulatory Physiology*, 278(6), H2084–H2093.
- Vasconcelos, D. P., Águas, A. P., Barbosa, M. A., Pelegrin, P., & Barbosa, J. N. (2019). The inflammasome in host response to biomaterials: Bridging inflammation and tissue regeneration. *Acta Biomaterialia*, 83, 1–12.
- Velnar, T., Bunc, G., Klobucar, R., & Gradisnik, L. (2016). Biomaterials and host versus graft response: A short review. *Bosnian Journal of Basic Medical Sciences*, 16(2), 82–90.
- Vroman, L., Adams, A. L., Fischer, G. C., & Munoz, P. C. (1980). Interaction of high molecular weight kininogen, factor XII, and fibrinogen in plasma at interfaces. *Blood*, 55(1), 156–159.
- Wan, F., & Lenardo, M. J. (2009). Specification of DNA binding activity of NF- κ B proteins. *Cold Spring Harbor Perspectives in Biology*, 1(4), a000067.
- Weiler, J. M., Edens, R. E., Linhardt, R. J., & Kapelanski, D. P. (1992). Heparin and modified heparin inhibit complement activation in vivo. *The Journal of Immunology*, 148(10), 3210–3215.
- Wu, F., Li, J., Zhang, K., He, Z., Yang, P., Zou, D., & Huang, N. (2015). Multifunctional coating based on hyaluronic acid and dopamine conjugate for potential application on surface modification of cardiovascular implanted devices. *ACS Applied Materials & Interfaces*, 8(1), 109–121.
- Wynn, T. A., & Vannella, K. M. (2016). Macrophages in tissue repair, regeneration, and fibrosis. *Immunity*, 44(3), 450–462.

- Yang, Y., Köwitsch, A., Ma, N., Mäder, K., Pashkuleva, I., Reis, R. L., & Groth, T. (2016). Functionality of surface-coupled oxidised glycosaminoglycans towards fibroblast adhesion. *Journal of Bioactive and Compatible Polymers*, 31(2), 191–207.
- Young, E. (2008). The anti-inflammatory effects of heparin and related compounds. *Thrombosis Research*, 122(6), 743–752.
- Young, E., Venner, T., Ribau, J., Shaughnessy, S., Hirsh, J., & Podor, T. J. (1999). The binding of unfractionated heparin and low molecular weight heparin to thrombin-activated human endothelial cells. *Thrombosis Research*, 96(5), 373–381.
- Zhang, X., Zhang, G., Zhang, H., Li, J., Yao, X., & Tang, B. (2018). Surface immobilization of heparin and chitosan on titanium to improve hemocompatibility and antibacterial activities. *Colloids and Surfaces B: Biointerfaces*, 172, 338–345.
- Zhou, G., Al-Khoury, H., & Groth, T. (2016). Covalent immobilization of glycosaminoglycans to reduce the inflammatory effects of biomaterials. *The International Journal of Artificial Organs*, 39, 37–44.
- Zhou, G., Niepel, M. S., Saretia, S., & Groth, T. (2016). Reducing the inflammatory responses of biomaterials by surface modification with glycosaminoglycan multilayers. *Journal of Biomedical Materials Research. Part A*, 104(2), 493–502.
- Zhou, L., Shen, L. H., Hu, L. H., Ge, H., Pu, J., Chai, D. J., ... He, B. (2010). Retinoid X receptor agonists inhibit phorbol-12-myristate-13-acetate (PMA)-induced differentiation of monocytic THP-1 cells into macrophages. *Molecular and Cellular Biochemistry*, 335(1–2), 283–289.

SUPPORTING INFORMATION

Additional supporting information may be found online in the Supporting Information section at the end of this article.

How to cite this article: AlKhoury H, Hautmann A, Erdmann F, et al. Study on the potential mechanism of anti-inflammatory activity of covalently immobilized hyaluronan and heparin. *J Biomed Mater Res*. 2020;108A:1099–1111. <https://doi.org/10.1002/jbm.a.36885>

Reprinted with permission from Journal of Biomedical Materials Research (JBMR) part A,

Hala Alkhoury, Adrian Hautmann, Frank Erdmann, Guoying Zhou, Sanja Stojanovic, Stevo Najman and Thomas Groth (2020), Study on the potential mechanism of anti-inflammatory activity of covalently immobilized hyaluronan and heparin, *J Biomed Mater Res*. 108A:1099–1111.

© 2020 Wiley Periodicals, Inc. DOI: 10.1002/jbm.a.36885

Chapter 3 - Studies on the Mechanisms of Anti-Inflammatory Activity of Heparin- and Hyaluronan-Containing Multilayer Coatings—Targeting NF- κ B Signalling Pathway

In this chapter, the focus lays on the potential increase of anti-inflammatory properties by using the LbL technique instead of covalent attachment to the surface. We hypothesized that the concentration and availability of GAGs to interact with macrophages is increased. The PEMs were created by alternately adsorbing polyanions of either HA or Hep in conjunction with the polycation CHI on top of a primary layer of poly(ethylene imine) (PEI). As a result, we suspected a higher amount of GAGs present, which are also not as strongly bonded as the SAM-based covalent approach described in the previous chapter. Again, the macrophage response and potential mechanism of anti-inflammatory effects of HA and Hep on the NF- κ B signaling pathway was of interest. To assess the surface properties associated with the physical adsorption of GAGs, we performed physicochemical studies on wettability, thickness, and topography of the PEM. The results indicated a significant increase in thickness and hydrophilicity upon multilayer formation compared to the control PEI and the covalent-bound monolayer samples of previous chapter. Scanning electron microscopy (SEM) and AFM analysis revealed complete surface coverage by the PEMs. THP-1 derived macrophages adhesion, fusion, and IL-1 β production on GAG-modified samples were used to study the inflammatory reaction to the surface coatings. The results show a substantial reduction in macrophage inflammatory responses compared to the control samples. Most importantly, we observed an inhibitory effect on the translocation of p65 into the nucleus and lower expression profiles of NF- κ B western blots in macrophages on the GAG-PEMs in comparison to the control PEI samples. Moreover, the macrophages exhibit the ability to associate with and uptake FITC-labeled GAGs. Interestingly, the Hep-based PEM demonstrates the most significant inhibitory effects on both macrophage inflammatory responses and the NF- κ B pathway. Indeed, the GAG multilayers display a higher anti-inflammatory activity than the covalent-bound monolayers. Especially, IL-1 β release was significantly reduced compared to the covalent monolayers. This is not only rooted in the more hydrophilic nature of the multilayers. From the quantification of the flow cytometry data, it is evident that macrophages can take up higher GAG amounts from the multilayer as the macrophages with verifiable uptake of GAGs was more than threefold. The multilayers provide more amounts of GAGs which can be uptaken by cell surface receptors by the macrophages.



Article

Studies on the Mechanisms of Anti-Inflammatory Activity of Heparin- and Hyaluronan-Containing Multilayer Coatings—Targeting NF- κ B Signalling Pathway

Hala Alkhoury ^{1,2}, Adrian Hautmann ¹, Bodo Fuhrmann ², Frank Syrowatka ², Frank Erdmann ³, Guoying Zhou ¹, Sanja Stojanović ^{4,5}, Stevo Najman ^{4,5}  and Thomas Groth ^{1,2,6,*} 

- ¹ Department Biomedical Materials, Institute of Pharmacy, Martin Luther University Halle Wittenberg, Heinrich Damerow Strasse 4, 06120 Halle (Saale), Germany; hala.al-khoury@student.uni-halle.de (H.A.); adrian.hautmann@pharmazie.uni-halle.de (A.H.); guoying.zhou@pharmazie.uni-halle.de (G.Z.)
 - ² Interdisciplinary Center of Materials Science, Martin Luther University Halle-Wittenberg, 06120 Halle (Saale), Germany; bodo.fuhrmann@cmat.uni-halle.de (B.F.); frank.syrowatka@cmat.uni-halle.de (F.S.)
 - ³ Pharmaceutical Biology and Pharmacology Department, Institute of Pharmacy, Martin Luther University Halle Wittenberg, Wolfgang-Langenbeck-Str. 4, 06120 Halle (Saale), Germany; frank.erdmann@pharmazie.uni-halle.de
 - ⁴ Department of Biology and Human Genetics, Faculty of Medicine, University of Niš, 18000 Niš, Serbia; s.sanja88@gmail.com (S.S.); stevo.najman@gmail.com (S.N.)
 - ⁵ Department for Cell and Tissue Engineering, Scientific Research Center for Biomedicine, Faculty of Medicine, University of Niš, 18000 Niš, Serbia
 - ⁶ Laboratory of Biomedical Nanotechnologies, Institute of Bionic Technologies and Engineering, I.M. Sechenov First Moscow State University, Trubetskaya street 8, 119991 Moscow, Russia
- * Correspondence: thomas.groth@pharmazie.uni-halle.de

Received: 22 April 2020; Accepted: 22 May 2020; Published: 25 May 2020



Abstract: The use of implants can be hampered by chronic inflammatory reactions, which may result in failure of the implanted device. To prevent such an outcome, the present study examines the anti-inflammatory properties of surface coatings made of either hyaluronic acid (HA) or heparin (Hep) in combination with chitosan (Chi) prepared as multilayers through the layer-by-layer (LbL) technique. The properties of glycosaminoglycan (GAG)-modified surfaces were characterized in terms of surface topography, thickness and wettability. Results showed a higher thickness and hydrophilicity after multilayer formation compared to poly (ethylene imine) control samples. Moreover, multilayers containing either HA or Hep dampened the inflammatory response visible by reduced adhesion, formation of multinucleated giant cells (MNGCs) and IL-1 β release, which was studied using THP-1 derived macrophages. Furthermore, investigations regarding the mechanism of anti-inflammatory activity of GAG were focused on nuclear transcription factor- κ B (NF- κ B)-related signal transduction. Immunofluorescence staining of the p65 subunit of NF- κ B and immunoblotting were performed that showed a significant decrease in NF- κ B level in macrophages on GAG-based multilayers. Additionally, the association of FITC-labelled GAG was evaluated by confocal laser scanning microscopy and flow cytometry showing that macrophages were able to associate with and take up HA and Hep. Overall, the Hep-based multilayers demonstrated the most suppressive effect making this system most promising to control macrophage activation after implantation of medical devices. The results provide an insight on the anti-inflammatory effects of GAG not only based on their physicochemical properties, but also related to their mechanism of action toward NF- κ B signal transduction.

Keywords: inflammation; glycosaminoglycans; LbL technique; macrophages adhesion; multinucleated giant cell (MNGCs) formation; NF- κ B; immunoblotting; endocytosis

1. Introduction

Biomaterial implants can trigger an undesired host response upon surgical insertion in the human body leading to limited functionality, longevity and eventually to failure of the biomedical device [1,2]. Therefore, it is desirable to design biomaterials that will guide the inflammation process to achieve the desired function of the device. The series of events that will determine implant fate is initiated by adsorption of blood proteins and the recruitment of leukocytes. Monocytes represent key players at the implantation site, where they differentiate to macrophages [3,4] that secrete pro-inflammatory cytokines such as IL-1 β and tumour necrosis factor- α (TNF α), chemokines and growth factors [5,6]. Furthermore, the surrounding tissue may also be damaged by the biocide activity of reactive oxygen and nitrogen species secreted by macrophages [7]. The persistent stimulation of the immune system may shift acute to chronic inflammation, which is characterized by the formation of multinucleated giant cells (MNGCs) as a result of macrophage fusion in an attempt to phagocytose biomaterials larger in size than a single cell [8,9]. Eventually, fibroblasts are recruited upon the prolonged inflammatory phase, which may finally result in encapsulation of the biomedical device causing its failure [10,11].

A passive mechanism to control inflammation after implantation is based on making biomaterial surfaces hydrophilic or to exploit steric repulsion to reduce the opsonization of the implant by plasma proteins, which is achieved for example by covalent immobilisation of polyethylene glycol [12]. This requires often an activation of the biomaterial surface by chemical or plasma treatment [13]. However, the effect is often limited due to the lack of the ability to inhibit protein adsorption completely and for longer periods of time [14,15]. Another approach is the development of controlled-release systems of nonsteroidal anti-inflammatory drugs (NSAIDs) to reduce the inflammatory response, which can be achieved by blending polymers with NSAID or immobilisation of NSAID nanoparticles on biomaterial surfaces [16,17]. A non-covalent modification of implant materials can be achieved by building up multilayer systems using the layer-by-layer (LbL) method [18]. The LbL method is based on the alternating deposition of oppositely charged polyelectrolytes among them also biopolymers like chitosan (Chi), hyaluronan (HA), heparin (Hep) and others [19,20]. The obvious advantage of LbL is that no chemical or plasma activation of implants is required and that a broad range of molecules is available. Moreover, physical surface properties like wettability can be tuned to achieve hydrophilic surfaces like those based on Chi as polycation and Hep and HA as polyanions that adsorb lower quantities of proteins [21,22]. It is interesting to note that beside their hydrophilic nature the glycosaminoglycans (GAG) HA and Hep possess anti-inflammatory properties through their effect on the nuclear transcription factor- κ B (NF- κ B) signalling pathway, which makes them interesting candidates for regulation of inflammatory processes [23,24].

The NF- κ B transcription factor family consists of a variety of homodimers and heterodimers that regulate and play a crucial role in apoptosis, cell proliferation, differentiation, cell migration, inflammation as well as angiogenesis and metastasis [25,26]. The activation of NF- κ B involves two major signalling pathways, the canonical (classic) and non-canonical (alternative) that depends on different stimuli and responding proteins [27]. The NF- κ B transcription factor is a key factor in inflammation having a direct influence on the regulation of cytokine release as well as inflammatory-related gene activation and gene expression [26,28]. The anti-inflammatory properties of high molecular weight HA (HMW-HA) is achieved by its binding to cell receptor CD44 leading to down regulation of toll-like-receptor (TLR) signalling, which mediates NF- κ B activation [29,30]. In addition, the binding of HA to CD44 promotes the release of anti-inflammatory cytokines like IL-2 and IL-10 [24,31]. On the other hand, Hep has two different mechanisms of inhibition on the NF- κ B signalling pathway in which one is focused on inhibiting the translocation of the transcription factor into the nucleus. The second

is explained as the ability of Hep to interfere non-specifically with the binding of NF- κ B to DNA in the nucleus [32]. Hence, leukocyte adhesion and activation as well as pro-inflammatory cytokine production is downregulated as a result of the inhibitory effect of Hep toward the NF- κ B signalling [33].

In previous studies, we could show that covalent or adsorptive binding of HA and Hep make surface coatings that reduce macrophage adhesion and activation [21,34]. Here, we extend our findings shedding light on the underlying mechanism of action of multilayers made of Chi and HA or Hep focussing on the inhibition of the p65 subunit of NF- κ B protein family as a target of canonical NF- κ B pathway in THP-1 monocyte-derived macrophages. A survey on the general structure of polyelectrolyte multilayers (PEMs) and their effect on macrophages investigated by different biological studies are shown in Figure 1.

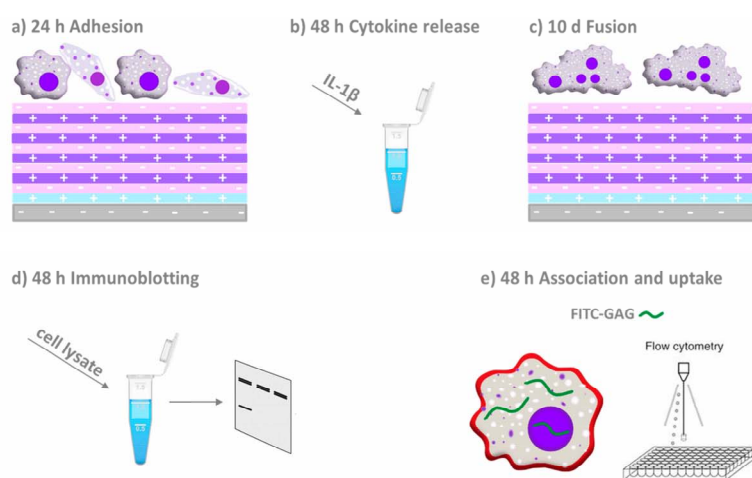


Figure 1. Schematic overview on the material system and design of the biological studies. Polyelectrolyte multilayers were assembled on model substrata glass or silicone (grey base layer with negative charge) on which a priming layer of poly (ethylene imine; blue layer with positive charge) was adsorbed first. Then alternately the polyanions heparin or hyaluronan (pink layer with negative charge) and chitosan as polycation (purple layer with positive charge) were adsorbed until 10 layers in total were assembled. Macrophages derived from the THP-1 monocytic cell line were seeded on these multilayers to study (a) adhesion and spreading of cells after 24 h, (b) evaluation of the pro-inflammatory (IL-1 β) cytokine release, (c) multinucleated giant cells formation, (d) immunoblotting and confocal laser scanning microscopy (CLSM) to study the p65 subunit of NF- κ B and (e) association and uptake of fluorescein isothiocyanate (FITC)-labelled GAG through macrophages by CLSM and flow cytometry.

2. Results

2.1. Characterization of Physical Properties of Coatings

The thickness of surface coatings prepared on silicon wafers was studied by ellipsometry in the dry state to verify the deposition of polyelectrolytes. The measurements were performed for the primary poly (ethylene imine) (PEI) layer that was used to provide a positive surface charge for binding the polyanions HA and Hep and formation of PEMs. The PEMs made of hyaluronan and chitosan were then designated as PEI(HA/Chi)₄HA. The PEMs made of heparin and chitosan were abbreviated as PEI(Hep/Chi)₄Hep. Altogether, 10 single layers were absorbed subsequently as described in the Materials and Methods Section. In Figure 2A a significantly higher thickness of PEMs was visible in comparison to PEI-modified silicon wafers. Static water contact angle (WCA) measurements were done to identify the wetting properties of the surface coatings. Figure 2B depicted a significantly lower WCA of PEMs compared to PEI surfaces. In addition, a significant difference between the two glycosaminoglycans was observed, showing the lowest WCA for multilayers composed of PEI(Hep/Chi)₄Hep.

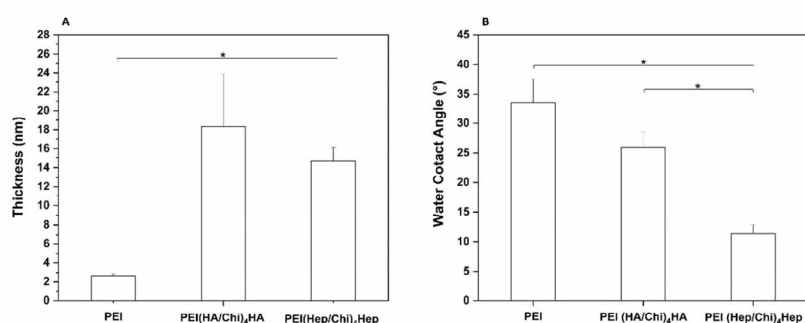


Figure 2. (A) Ellipsometry measurements to obtain the average thickness of poly (ethylene imine) (PEI) coating and multilayers made of either hyaluronic acid (HA) or heparin Hep as polyanions and chitosan (Chi) as a polycation, abbreviated as (PEI, PEI(HA/Chi)₄HA and PEI(Hep/Chi)₄Hep), respectively. Results represent means \pm SD, $n = 6$, * $p < 0.05$. (B) Static water contact angle measurements using the sessile drop method to characterize surface wettability of the same surface coatings. Results represent means \pm SD, $n = 10$, * $p < 0.05$.

A deposition of a 15 nm Cr layer to achieve a sufficient conductivity of samples was performed prior to surface topography visualization with scanning electron microscopy shown in Figure 3A. PEMs containing HA demonstrated island-like structures while PEMs containing Hep expressed a more homogenous, smooth surface coverage. On the other hand, atomic force microscopy studies of surface topography shown in Figure 3B indicated smaller differences between both PEM, since the observed surface features had a similar range of 40–60 nm in the z scale though PEMs with HA as a terminal layer looked more homogenous here than those with Hep as a polyanion.

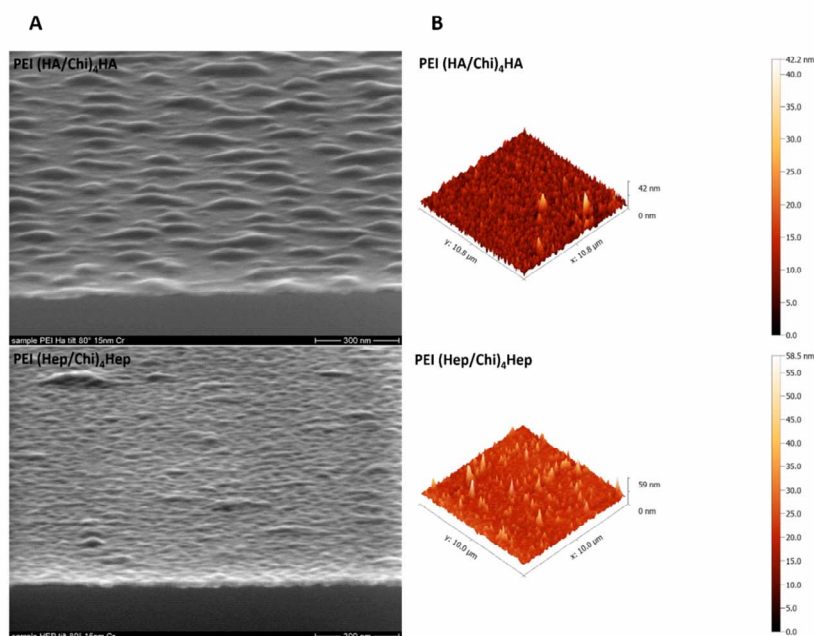


Figure 3. (A) Scanning electron microscopy (SEM), Scale bar: 300 nm and (B) atomic force microscopy (AFM) for studying topography of samples poly (ethylene imine) (PEI) and terminal layers of polyelectrolyte multilayers (PEMs) composed of either hyaluronic acid (HA) or heparin (Hep) as polyanions and chitosan (Chi) as polycation abbreviated as (PEI(HA/Chi)₄HA, PEI(Hep/Chi)₄Hep), respectively.

2.2. Adhesion of Macrophages and Multinucleated Giant Cell Formation

Micrographs visualizing the adhesion and shape of macrophages after 24 h of culture are shown in Figure 4A. Cells showed the highest adherence on PEI with a spread and elongated phenotype. On the other hand, a smaller number of predominantly round, less elongated macrophages were observed on PEMs. Quantitative data based on image analysis shown in Figure 4B displayed that the number of adherent macrophages was highest on the control substratum PEI, while the number of cells was significantly lower on PEMs with the smallest number on PEI(Hep/Chi)₄Hep.

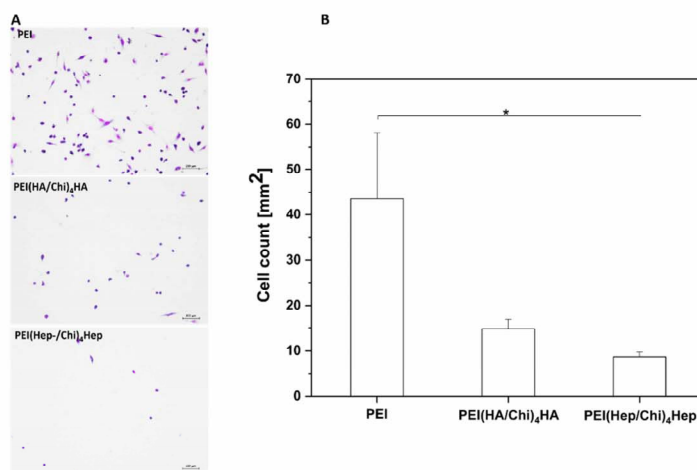


Figure 4. (A) Transmitted light microscopy images of adherent macrophages stained with 10% (v/v) Giemsa after 24 h on poly (ethylene imine) (PEI) and terminal layers of PEMs composed of either hyaluronic acid (HA) or heparin (Hep) as polyanions and chitosan (Chi) as polycation abbreviated as (PEI(HA/Chi)₄)HA, PEI(Hep/Chi)₄Hep, respectively. Scale: 100 μm . (B) Number of adherent macrophages per surface area after 24 h of cultivation. Data represent means \pm SD, $n = 5$, $* p \leq 0.05$.

Image analysis was also used to quantify the size and shape of adherent macrophages. Figure 5A shows that the aspect ratio of adherent macrophages was higher related to an enhanced polarization of macrophages on PEI samples compared to cells on PEMs, where it was significantly lower. Figure 5B shows that also spreading of macrophages was significantly lower on PEMs in comparison to PEI.

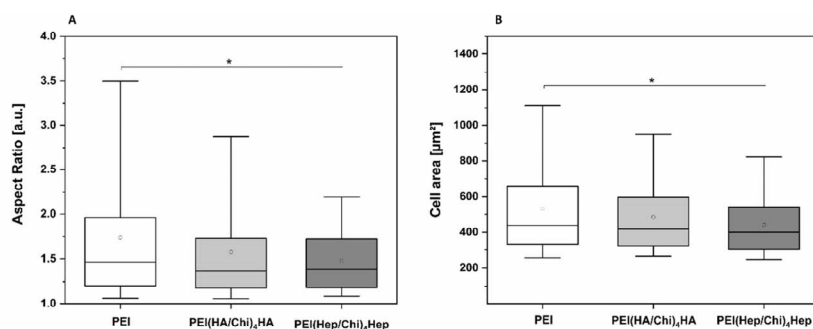


Figure 5. (A) Aspect ratio of adherent macrophages on poly (ethylene imine) (PEI) and terminal layers of PEMs composed of either hyaluronic acid (HA) or heparin (Hep) as polyanions and chitosan (Chi) as polycation abbreviated as (PEI(HA/Chi)₄)HA, PEI(Hep/Chi)₄Hep, respectively. (B) Cell area of adherent macrophages per surface area after 24 h of cultivation. The box plot indicates the 25th and 75th percentile; the lowest and highest values are represented by the whiskers, whereas the median (dash) and mean value (white circle) are shown as well. $n = 15$, $* p \leq 0.05$.

Furthermore, micrographs presented in Figure 6A visualized significantly higher numbers of multinucleated giant cells (MNGCs) on PEI samples, which can be identified by the number of nuclei (≥ 2) per cell body as well as the larger cell size. By contrast, on PEMs a lower number of MNGCs was seen. The quantitative analysis of area percentage of MNGCs presented in Figure 6B shows that fusion of macrophages was significantly lower on PEMs in comparison to PEI. In addition, the formation of MNGCs was also significantly lower on PEI(Hep/Chi)₄Hep in comparison to PEI(HA/Chi)₄HA.

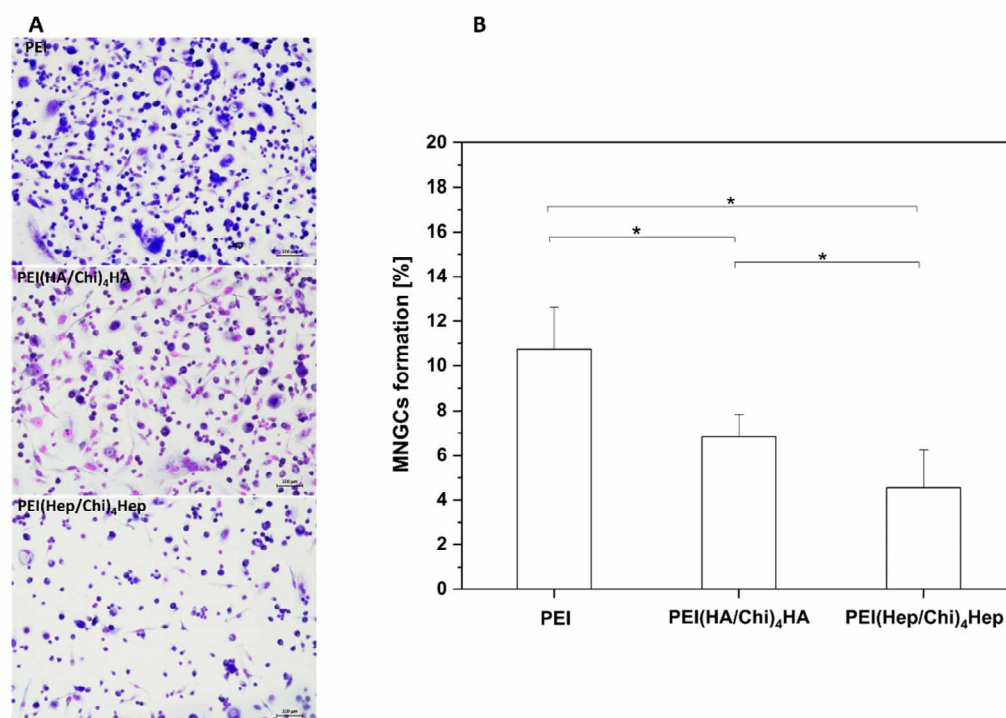


Figure 6. (A) Images of multinucleated giant cells (MNGCs) stained with 10% (v/v) Giemsa after 10 days cultivation on poly (ethylene imine) (PEI) and terminal layers of PEMs composed of either hyaluronic acid (HA) or heparin (Hep) as polyanions and chitosan (Chi) as polycation abbreviated as PEI(HA/Chi)₄HA, PEI(Hep/Chi)₄Hep, respectively. Scale bar: 100 μ m. (B) The area percentage of MNGCs on PEI, PEI(HA/Chi)₄HA and PEI(Hep/Chi)₄Hep surfaces based on quantitative image analysis of micrographs. Results represent means \pm SD, * $p < 0.05$, $n = 15$.

2.3. IL-1 β Pro-Inflammatory Cytokine Release

Results of studies on the release of Interleukin-1 β are shown in Figure 7. Two sets of samples were studied with the absence (white bars) and presence (black bars) of lipopolysaccharide (LPS). LPS stimulation leads to an up regulation of IL-1 β in THP-1 derived macrophages, which is also an indicator of the functionality of these cells. Macrophages adhering on PEI-coated surfaces produced the highest quantity of IL-1 β under both conditions (with or without LPS). By contrast macrophages cultured on both PEMs had a significantly reduced release of this cytokine in the presence and absence of LPS. In addition, IL-1 β release from macrophages cultured on PEI(Hep/Chi)₄Hep was significantly lower in comparison to PEI(HA/Chi)₄HA.

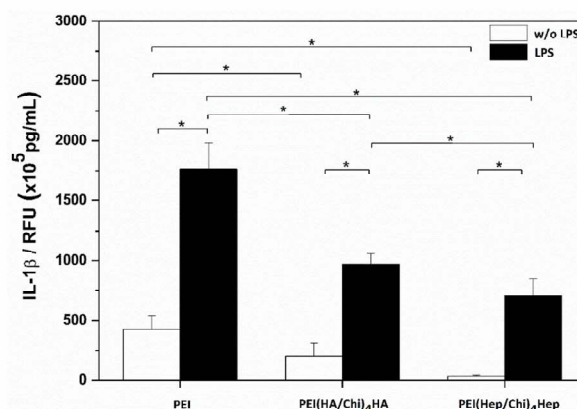


Figure 7. IL-1 β release from macrophages after 24 h incubation in absence (white bars) and presence (black bars) of lipopolysaccharide (LPS) on poly (ethylene imine) (PEI) and terminal layers of PEMs composed of either hyaluronic acid (HA) or heparin (Hep) as polyanions and chitosan (Chi) as polycation abbreviated as PEI(HA/Chi)₄HA and PEI(Hep/Chi)₄Hep, respectively. Data represent means \pm SD, $n = 6$, * $p \leq 0.05$.

2.4. Immunofluorescence Staining of NF- κ B in Macrophages

In Figure 8A the cell nuclei have been stained with the nuclear stain TO-PRO-3 (blue colour) and the non-phosphorylated p65 subunit of NF- κ B with a monoclonal antibody (green colour). It is visible that the p65 subunit of NF- κ B can be found both in the cell cytoplasm and nuclei. The nuclear to cytoplasmic ratio of NF- κ B was quantitatively evaluated and used as an indicator for the translocation of the transcription factor into the nuclear area. The highest extent of p65 translocation was observed in macrophages on PEI; both in the presence and absence of LPS (Figure 8B). By contrast, a significantly lower nuclear to cytoplasmic ratio was found in macrophages cultured on PEMs. Indeed, the lowest quantity of p65 translocation into the nuclear area both in the absence and presence of LPS was found in cells cultured on PEI(Hep/Chi)₄Hep (Figure 8B).

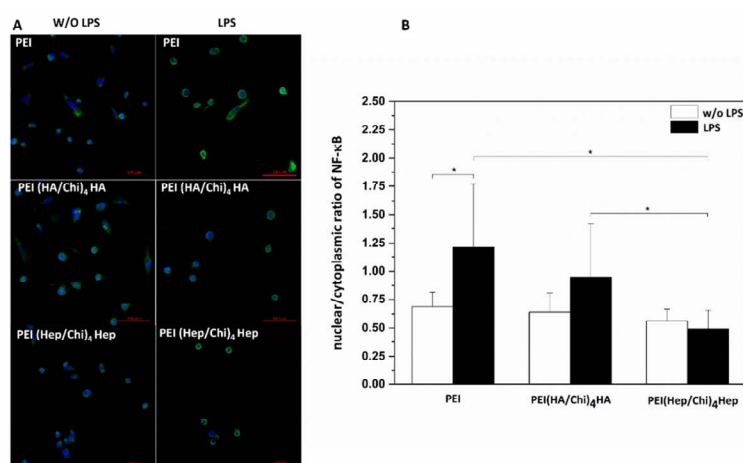


Figure 8. (A) TO-PRO-3 (blue colour) staining of nuclei and monoclonal antibody detection (green colour) of NF- κ B p65 subunit shown for non-stimulated (left row) and stimulated ($1 \mu\text{g}\cdot\text{mL}^{-1}$ LPS) macrophages (right row). The cells were cultured for 48 h on poly (ethylene imine) (PEI) and terminal layers of PEMs composed of either hyaluronic acid (HA) or heparin (Hep) as polyanions and chitosan (Chi) as polycation abbreviated as PEI(HA/Chi)₄HA, PEI(Hep/Chi)₄Hep, respectively. Scale bar: 100 μm . (B) Quantification of nuclear/cytoplasmic ratio in absence (white bars) and presence (black bars) of LPS in cells cultured on PEI and PEMs. Data represent means \pm SD, $n = 10$, * $p \leq 0.05$.

2.5. Western Blotting

Figure 9A depicts the bands for the non-phosphorylated p65 subunit of NF- κ B (named here as NF- κ B only) and actin, in which the latter was used for normalization of data in the quantitative evaluation by densitometry. It is visible that a higher expression of NF- κ B was observed in cell lysates from macrophages cultured on PEI samples compared to cells on PEMs. Figure 9B shows the quantitative evaluation of band intensities of NF- κ B expression in macrophages cultured on PEI and PEMs, quantified by densitometry. The lowest intensity of NF- κ B in cell lysates was observed in macrophages cultured on PEI(Hep/Chi)₄Hep. The original blots from different gels can be found in Figures S2 and S3.

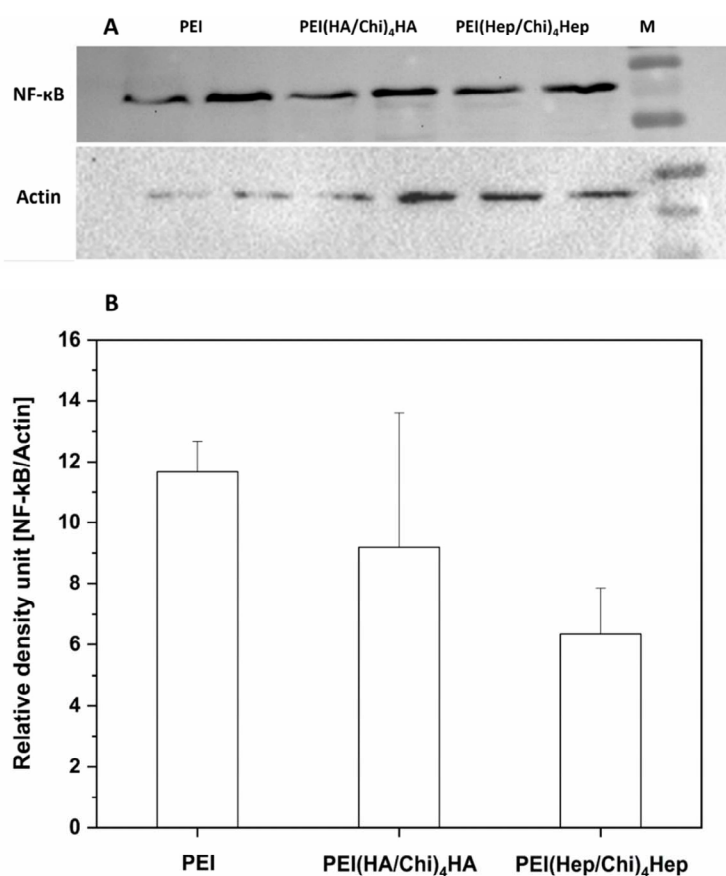


Figure 9. (A) Western blots with bands of p65 of NF- κ B and actin from two samples of lysates of macrophages cultured on poly (ethylene imine) (PEI) and terminal layers of PEMs composed of either hyaluronic acid (HA) or heparin (Hep) as polyanions and chitosan (Chi) as a polycation abbreviated as PEI(HA/Chi)₄HA, PEI(Hep/Chi)₄Hep, respectively. The lysates, collected after 48 h, were blotted toward (NF- κ B) and actin. (B) The immunoblotting bands were analysed by densitometry. Bands of p65 subunit of NF- κ B were normalized to expression of actin. The ratio was named as relative density units. Data represent means, $n = 2$.

2.6. Association of GAG with Macrophages Studied by Confocal Laser Scanning Microscopy (CLSM)

DID-stained macrophages cultured on terminal layers of PEMs containing fluorescent FITC-labelled glycosaminoglycans (GAG, green colour) visualized by CLSM are shown in Figure 10. Here, the macrophages cultured on PEI expressed a red staining of DID of the cell membrane, only because no FITC-labelled GAG were present on this surface (Figure 10A). The macrophages cultured on PEMs with FITC-labelled GAG show an association of FITC-labelled HA or Hep (green in

confocal images) with DID-stained (red) cells. 3D images of FITC-labelled HA and Hep are shown in Figure 10B. Here, it is visible that HA or Hep were either co-localized with the cell surface or found intracellularly. Figure 10A,B shows the ability of macrophages to associate with and the uptake of the immobilized FITC-GAG. Additional cell images are provided in Figures S4 and S5.

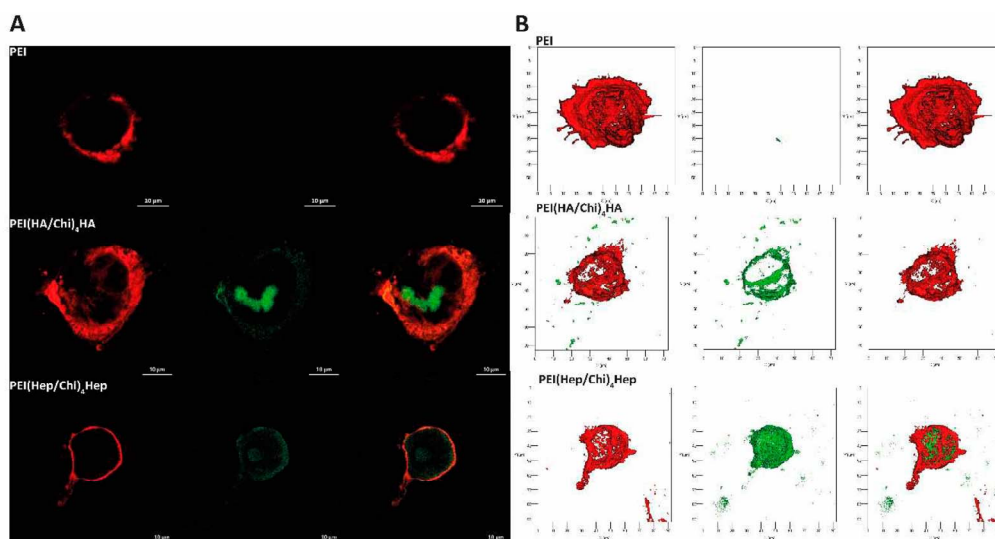


Figure 10. (A) Representative confocal laser microscopy (CLSM) images of adherent macrophages stained with the membrane stain DID (red colour) after 24 h cultivation on poly (ethylene imine) (PEI) and terminal layers of PEMs composed of either hyaluronic acid (HA) or heparin (Hep) as polyanions (stained with FITC, green colour) and chitosan (Chi) as a polycation abbreviated as (PEI(HA/Chi)₄HA, PEI(Hep/Chi)₄Hep), respectively (63-fold oil immersion objective, Scale bar: 10 μ m). (B) Representative 3D view of a z-stacks in surface projection with CLSM (63-fold oil immersion objective, scale: 20 μ m). In this mode, pixel values are computed as solids, which allows no transparency.

2.7. Association of FITC-Labelled GAG with Macrophages Studied by Flow Cytometry

The results of flow cytometry with dot blots of the side scatter (SSC, y axis) versus the FITC fluorescence (x axis) are shown in Figure 11A. Macrophages located in the P4 region were considered to be negative for GAG-FITC due to cell auto-fluorescence. An uptake of FITC-labelled-GAG by macrophages is denoted by an increase of the cellular fluorescence related to the emission of fluorescein (FITC). Hence, the P5 region shows the number of macrophages positive for FITC-labelled-GAG. Figure 11B shows the quantitative evaluation of macrophages positive for FITC-GAG demonstrating that cells cultured on multilayers containing HA expressed a significantly lower uptake of FITC-labelled GAG in comparison to the cell cultured on PEM with FITC-heparin.

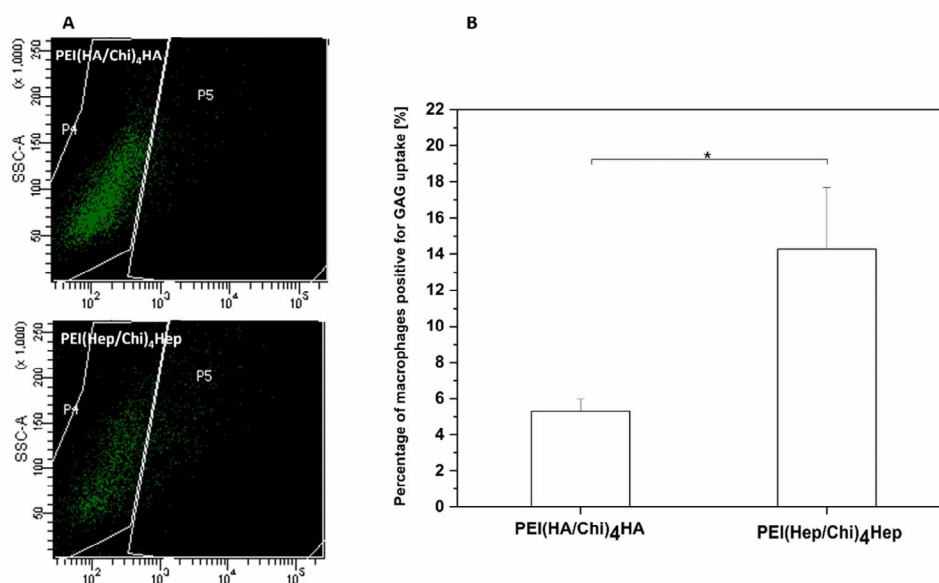


Figure 11. (A) Illustrative images of the flow cytometry measurements of GAG association and uptake by macrophages cultured on either FITC-labelled hyaluronic acid or FITC-heparin multilayers abbreviated as $(\text{PEI}(\text{HA}/\text{Chi})_4\text{HA})$, $(\text{PEI}(\text{Hep}/\text{Chi})_4\text{Hep})$, respectively. (B) The percentage of macrophages positive for GAG uptake after 48 h cultivation on $(\text{PEI}(\text{HA}/\text{Chi})_4\text{HA})$ and $(\text{PEI}(\text{Hep}/\text{Chi})_4\text{Hep})$. Data represent means \pm SD, $n = 4$, * $p \leq 0.05$.

3. Discussion

This study aimed to investigate the mechanism of the anti-inflammatory action of PEMs systems based on either HA or Hep as polyanions in combination with Chi as polycation fabricated by the LbL technique to explore their potential for making implantable biomedical devices more immune compatible to avoid chronic inflammation and subsequent fibrosis. The polyethylene imine (PEI) that serves often as an anchoring layer in the LbL technique [35] was used here for comparison because it is known that amino-terminated surfaces provoke an activation of macrophages [36], which is also known for PEI-modified substrata [34].

Physicochemical studies were performed to characterize surface properties like wettability and topography that have an impact on protein adsorption and cell adhesion [37]. Studies of the topography and thickness showed that the LbL technique was able to achieve a complete coating of substrata (glass or silicone) with PEMs of a dry thickness in the range of 15–20 nm with a rather smooth surface topography in the micrometre scale with differences between HA and Hep multilayer systems. Indeed, multilayers with HA showed a more island-like structure when studied with SEM, which might be related to the much larger molecular weight of hyaluronan compared to heparin used as polyanions in multilayer formation. Wettability studies showed that both glycosaminoglycans HA and Hep formed multilayer coatings of more hydrophilic character despite the presence of chitosan as found also in previous studies [38,39]. By contrast, highest WCA was found for the PEI modified surface, which also corresponds typically to increased protein adsorption, adhesion, and spreading of cells in comparison to more hydrophilic substrata [34].

Accordingly, the result of macrophage adhesion and spreading corresponded to the wetting properties of surfaces showing that it was highest on PEI, while PEMs with GAG reduced their adhesion and spreading with lowest on $(\text{PEI}(\text{Hep}/\text{Chi})_4\text{Hep})$. However, macrophage adhesion was not statistically different between HA and Hep-terminated PEMs. In contrast to that MNGC formation was significantly decreasing from PEI to HA and then Hep. Although, MNGC formation is related to the number of adhering macrophages that are required to aggregate before their fusion, other factors like cytokine release play a more dominant role [40]. Therefore, studies on the release of IL-1 β were

performed that demonstrated a significant reduction of release of this pro-inflammatory cytokine from macrophages cultured on PEMs. It should be noted that IL-1 β release was normalized to the number of viable cells. Hence, the reduced adhesion of macrophages due to higher wettability of PEM alone as a physical effect was not sufficient to explain the suppressive effect of multilayer coatings based on HA and Hep on macrophage activation.

Since, wetting properties of HA and Hep-based PEMs were quite similar, pharmaceutical effects of both GAG might play an important role for the observed inhibition on macrophage fusion and release of pro-inflammatory cytokines. It is known that reduced secretion of pro-inflammatory cytokines like IL-1 β is related to the inhibition of NF- κ B signalling pathway [41,42]. Hence, the focus was set on the study of the NF- κ B signalling pathway, which plays a pivotal role during the activation of macrophages and other cells [26]. As it could be expected from the studies on macrophage adhesion, fusion and cytokine release, translocation of the p65 subunit of NF- κ B to the nuclear area and its concentration were highest in macrophages on the control surface PEI. On the other hand, all parameters were lower in macrophages cultured on PEMs based on either HA or Hep. However, most effective in this regard was the multilayer system PEI(Hep/Chi)₄Hep. A question how both GAG can control the activation of macrophages was related to the fact that both GAGs were physically bound to chitosan in multilayers. Indeed, we have shown previously that such multilayer systems made of biogenic polyelectrolytes represent a living interface, in which polyelectrolytes can interact with and be translocated by cells [43]. Hence, we studied association and potential internalization of FITC-labelled GAG by macrophages using CLSM showing that both association as well as internalization of these GAG can occur. Moreover, studies with flow cytometry confirmed such an association and showed also that a larger quantity of FITC-Hep was found to be associated with macrophages in comparison to FITC-HA.

Indeed, heparin can be internalized by cells either through anionic membrane transporters or by endocytosis [44]. It is known that heparin, taken up by endocytosis, may bind to the positively charged p50–p65 subunits of NF- κ B, leading to a partial inhibition of the phosphorylation process and a reduced translocation of the transcription factor to the nucleus [44,45]. A further mechanism is that intracellular heparin can interfere non-specifically with DNA binding of NF- κ B in the nucleus [32]. On the other hand, the high molecular weight form of hyaluronan (HMW-HA) used here for fabrication of PEMs possesses an anti-inflammatory potential through cross-linking the surface receptor CD44 on cells like macrophages, which suppresses the pro-inflammatory signaling by toll-like receptors (TLR), resulting in down-regulation the phosphorylation cascade of NF- κ B pathway [46]. In addition, CD44 is thought to play an important role in the reduction of pro-inflammatory cytokines release by other pathways [13,47]. The intracellular presence of FITC-HA shown by CLSM may be related to CD44 by receptor endocytosis with the bound ligand [48], but probably not affecting intracellular signal transduction. Since, NF- κ B signalling is one of the important pathways of the regulation of cytokine gene expression, an inhibition by both hyaluronan and heparin, may eventually decrease the potential inflammatory response of macrophages [49,50], which is obviously the case for both multilayer systems that have been presented in this study.

4. Materials and Methods

4.1. Chemicals for Surface Modification

Glass cover slips, \varnothing 12 mm and 15 mm, were provided from Menzel GmbH (Bielefeld, Germany). Silicon wafers of 10 \times 10 mm² surface were obtained from LG Siltron Inc. (Gumi, Korea). Poly (ethylene imine) (PEI, $M_w \approx 750$ kDa) was purchased from Polysciences Inc. (Warrington, PA, USA). Heparin (Hep, $M_w \approx 15$ kDa) and hyaluronic acid (HA, $M_w \approx 1.3$ MDa) were provided from Serva (Heidelberg, Germany) and Innovent e.V. (Jena, Germany), respectively. Labelling of GAG was done with fluorescein isothiocyanate (FITC) according to the protocol published recently to obtain 10% labelled carboxylic groups of either HA or Hep with FITC [51]. Chitosan 85/500 with a deacetylation degree of 85% (Chi, $M_w \approx 500$ kDa) was delivered from Heppe Medical Chitosan GmbH (Halle, Germany). Sodium

chloride (NaCl) was obtained from Roth (Karlsruhe, Germany), while acetic acid was provided from Applichem (Darmstadt, Germany). Ammonia (25%) and hydrogen peroxide (30%) were purchased from TH-Geyer GmbH and Co. KG and Roth (Renningen, Karlsruhe, Germany), respectively. AFM tips were provided from AppNano (Applied Nanostructures Inc., Santa Clara, CA, USA).

4.2. Substrates and Polyelectrolyte (PEL) Preparation

The physicochemical and biological properties of multilayers were investigated by using model substrates, such as silicon wafers and glass cover slips. A solution of ammonia, hydrogen peroxide and water (1:1:5, v/v/v) at 75 °C for 10 min was used for cleaning of substrata. Thereafter, the wafers as well as the glass cover slips were washed with ultrapure water (6×5 min), and dried with a stream of nitrogen [52]. Hyaluronic acid, heparin and chitosan solutions were prepared at a concentration of ($2 \text{ mg}\cdot\text{mL}^{-1}$) by dissolution in 150 mM NaCl at pH 4.0. Poly (ethylene imine) was dissolved at a concentration of $5 \text{ mg}\cdot\text{mL}^{-1}$ in 150 mM NaCl at pH 7.0 as in previous studies [17]. Poly (ether sulfone) filters of 0.2 μm pore size was used for sterilization of solutions.

4.3. Polyelectrolyte Multilayers (PEMs) Formation

An anchoring base layer of poly (ethylene imine) was applied to obtain a positive surface net charge on silicon and glass substrates for subsequent adsorption of polysaccharides as done in previous studies [17]. In addition, this substrate was used as a control for comparison with multilayers. PEI was adsorbed for 30 min on glass or silicone slides and rinsed with 150 mM NaCl at pH 7.0, three times for 5 min each. Subsequently, multilayers of HA or Hep as polyanions, followed by washing with PBS and subsequent adsorption of Chi for 15 min each until 4 double layers and a final GAG layer were obtained. The control surface was always abbreviated as PEI, while the multilayer systems were always abbreviated as either (PEI, PEI(HA-Chi)₄HA or PEI(Hep-Chi)₄Hep). In studies on association and uptake of FITC-GAG, the last two GAG layers consisted of either FITC-HA or FITC-Hep [17].

4.4. Characterization of Surface Properties and Multilayer Formation

4.4.1. Scanning Electron Microscopy (SEM)

The coated silicon wafers with PEMs were analysed by Philips ESEM XL 30 FEG (Eindhoven, Netherlands) in high vacuum ($p = 10^{-6}$ mbar) to visualize the surface topography. A conductive layer of 15 nm thick chromium (Cr) was deposited by sputtering.

4.4.2. Atomic Force Microscopy (AFM)

AFM (Nano-R, Pacific Nanotechnology, Santa Clara, CA, USA) was also used to study surface topography of PEI- and GAG-modified silicon wafers (Si) in a three-dimensional view. A contact mode under ambient (air) laboratory conditions of temperature and humidity was selected in order to probe the coated Si wafers ($10 \times 10 \text{ mm}^2$). Images were taken by using AFM tips with 125 μm length, 35 μm width, 14–16 μm height and a tip radius of <10 nm. A resolution of ($512 \times 512 \text{ pixel}^2$) as well as a scan area of $10 \times 10 \text{ }\mu\text{m}^2$ per image was applied with a scan rate of 0.2 Hz. Gwiddyon software (Nano-R, Pacific Nanotechnology, Santa Clara, CA, USA) (version 2.40) was used for image processing [17].

4.4.3. Water Contact Angle (WCA)

The wettability of the samples was determined with static water contact angle (WCA). An OCA 15+ device from Dataphysics (Filderstadt, Germany) using the sessile drop method was applied here. Ultrapure water of 2 μL with a minimum of five droplets was investigated to each sample (2 for each material) at room temperature. The obtained values were used to calculate the means and standard deviations [38].

4.4.4. Measurement of Multilayer Thickness by Ellipsometry

The average thickness of the PEMs was determined by the spectroscopic ellipsometry (M-2000 V, J.A. Woollam Company, Lincoln, NE, USA). The used reference substrate was a cleaned Si wafer with a SiO₂ layer thickness of 2.5 nm. A Cauchy model was used to extract the optical constants of the multilayers, which was previously described in the literature [51].

4.5. Studies with THP-1 Derived Macrophages

4.5.1. Cell Culture

RPMI-1640 medium (Lonza, Wuppertal, Germany) supplemented with 10% (v/v) foetal bovine serum (FBS, Biochrom AG, Berlin, Germany) and 1% (v/v) antibiotic-antimycotic solution (AAS, Lonza, Wuppertal, Germany) was used for culturing THP-1 human monocytic cells (DSMZ, Braunschweig, Germany) at 37 °C in a humidified 5% CO₂/95% air atmosphere in a NUAIRE® DH Autoflow incubator (NuAire, Plymouth, MN, USA). Cells were passaged every second day to maintain a cell density of 1×10^6 cells mL⁻¹. Macrophages were differentiated from floating THP-1 cells by incubation with 200 nM phorbol-12-myristate-13-acetate (PMA, Sigma Aldrich, Darmstadt, Germany) in T75 cell culture flasks (Greiner Bio-One GmbH and Co.KG, Frickenhausen, Germany) for 48 h. Afterwards, 0.25% trypsin/0.02% EDTA (Biochrom AG, Berlin, Germany) was used to detach the adherent macrophages with further addition of serum-containing RPMI-1640 medium to stop the trypsin effect. Finally, the harvested cells were used for seeding on the different PEMs-modified surfaces [34].

4.5.2. Cell Adhesion Studies

An ultraviolet light chamber (Bio-Link BLX, LTF Labortechnik GmbH and Co. KG, Wasserburg, Germany) set at 254 nm ($50 \text{ J}\cdot\text{cm}^{-2}$) was used for sterilization of PEM modified samples and PEI coated control surfaces (samples were placed in 24-well tissue culture plates, Greiner Bio-One GmbH and Co.KG, Frickenhausen, Germany). Sterilization by UV light was done for 60 min prior to cell studies. Macrophages were seeded at a cell density of 2.5×10^4 cells·mL⁻¹ in serum-containing RPMI-1640 medium. Cells were cultured on the samples for 24 h at 37 °C in a humidified 5% CO₂/95% air atmosphere. Thereafter, gentle washing with phosphate buffer saline (PBS) was done twice to remove non-adherent cells. The attached cells were fixed with cold methanol (Roth, (Karlsruhe, Germany)) for 10 min and stained with 10% (v/v) Giemsa (Merck KGaA, Darmstadt, Germany) in ultrapure water for another 10 min. Micrographs were taken by a light microscope (Nikon ECLIPSE Ti2, Tokyo, Japan) equipped with a CMOS camera (Nikon DS-Fi3, Tokyo, Japan). ImageJ software (version 1.52p, <https://imagej.nih.gov>) was used to quantify the number of adhering cells of the images [21].

4.5.3. Analysis of Multinucleated Giant Cells (MNGCs) Formation

The formation of MNGCs was evaluated through MNGCs area percentage after culturing macrophages, initially seeded at density of 2.5×10^5 cells·mL⁻¹, on the PEMs and PEI surfaces for 10 days. Samples were gently washed twice with PBS followed by fixation of attached cells with cold methanol and staining with 10% (v/v) Giemsa in ultrapure water. Cells were imaged using light microscopy. The area percentage of MNGCs was calculated by ImageJ software [38].

4.5.4. IL-1 β Production Measurement

The pro-inflammatory cytokine release was investigated using an enzyme linked immunosorbent assay (ELISA). The measurements were performed according to the manufacturer's instructions (Thermo Scientific, Germany) for the medium supernatants of samples. Two sets of samples were collected after 24 h of incubation in the absence and presence of LPS and stored at -20 °C until needed for investigation. A QBlue® cell viability assay (BioChain, California, USA) was used to estimate the

cell viability in attempt to normalize the cytokine production to the quantity of metabolic active cells on the different PEMs surfaces.

Therefore, the attached cells of the different surfaces were washed carefully with sterile PBS after supernatant collection. Then, a pre-warmed, colourless Dulbecco's modified Eagle's medium (DMEM) with QBlue[®] assay reagent (10:1) were added and incubated for 2 h at 37 °C in humidified 5% CO₂/95% air atmosphere. Eventually, the relative fluorescence unit (RFU) values were measured after transferring 100 µL of the supernatant from each well to a black 96-well plate. The values were measured at an excitation wavelength of 544 nm and emission wavelength of 590 nm with plate reader [34].

4.5.5. Immunofluorescence (IF) Staining of NF-κB

Immunostaining was performed to study the translocation of the p65 subunit of NF-κB according to the method developed by Noursadeghi et al. [53]. Macrophages were seeded like in the aforementioned section and cultured for 48 h. Samples were analysed in two sets in the absence and presence of 1 µg·mL⁻¹ lipopolysaccharide (LPS, Sigma Aldrich, Darmstadt, Germany). Thereafter, fixation of the cultured cells on PEI and PEMs surfaces was performed with 4% paraformaldehyde (Sigma Aldrich, Darmstadt, Germany) for 15 min, permeabilized with 0.1% (v/v) Triton[®] X-100 (Sigma-Aldrich, Taufkirchen, Germany) for 10 min at RT, and rinsed twice with PBS. The non-specific binding sites were blocked by using bovine serum albumin (BSA, ≥98%, Carl Roth GmbH, Halle (Saale), Germany; 1%, w/v) in PBS for 30 min. Afterwards, cells were incubated with a monoclonal p65 subunit of the NF-κB antibody (1:100, Santa Cruz Biotechnology, Dallas, TX, USA) at 4 °C overnight. A secondary monoclonal anti-rabbit IgG antibody conjugated with CY2 (1:200, Jackson ImmunoResearch, Ely, UK) was applied for another 30 min at RT after washing with PBS for 5 min on a shaker. TO-PRO-3 (1:500, Invitrogen, CA, USA) for 40 min at RT was used for the nuclei staining. Eventually, confocal microscope LSM 710 (Carl Zeiss, Oberkochen, Germany) applying a 40-fold oil immersion objective was utilized to examine the samples that were mounted on glass slides with polyvinyl alcohol (PVA, Sigma Aldrich, Darmstadt, Germany). ImageJ (v.1.52i) software was used for image processing. The TO-PRO-3 channel was used to mask a region of interest (ROI). Then the nuclear ROI was subtracted from the cellular ROI to obtain a cytosolic ROI. Finally, the fluorescence intensity was evaluated in the nuclear and cytosolic ROI and a ratio calculated [21]. The principle of the method is visualized in Figure S1.

4.5.6. Cell Lysis for Immunoblotting (IB)

THP-1 derived macrophages were differentiated as described above and cultured for 48 h at a cell density of 52 × 10⁵ cells·mL⁻¹ on the prepared PEMs and PEI on objective glass slides with a total area of 19.76 cm² (Menzel GmbH, Bielefeld, Germany) in the four well plates (Greiner Bio-one, Leipzig, Germany). Thereafter, plates were placed on ice and the cells were washed twice with ice-cold PBS. Afterwards, the macrophages were scraped using a cold plastic cell scraper after adding a cell lysate buffer (RIPA buffer) with protease and phosphatase inhibitors (Thermo Fisher scientific, Waltham, MA, USA). Then, a constant agitation at 4 °C for 30 min was maintained beyond the gentle transfer of cell lysates into pre-cooled tubes. Subsequently, the cell lysates were centrifuged at 4 °C and 13,000 rpm for 20 min then the supernatants were stored at -80 °C up to one month before performance of IB [21].

4.5.7. SDS-PAGE and Western Blotting

The same amount of proteins from each samples cell lysate were separated in 15% SDS-polyacrylamide gels and transferred onto nitrocellulose membranes (Schleicher and Schuell GmbH, Munich, Germany). In TBS-T, 3% (w/v) milk powder was used to block membranes, probed with monoclonal antibodies against phospho-NF-κB (CST, #3033), NF-κB (Santa Cruz Biotechnology, sc-8008) and β-actin (MERCK, A1978), followed by incubation with HRP-labelled secondary antibodies and visualized with the enhanced chemiluminescence reaction (Thermo Fisher Scientific, Waltham, MA, USA) in a ChemiDoc Imaging System (Bio-Rad, CA, USA). Obtained grayscale images were

densitometrically analysed by Li-Cor Image Studio software using automatic background determination and subtraction function [21].

4.5.8. Association of FITC-GAG with Macrophages Studied by Confocal Laser Scanning Microscopy

The same density as in the MNGCs formation analysis was used for culturing macrophages for 24 h on PEI and PEMs with terminal layers of FITC-labelled GAG. Cell fixation was performed by adding 4% paraformaldehyde (Sigma Aldrich, Darmstadt, Germany) for 10 min. Thereafter, each sample and incubated for 10 min after adding 0.5 mL of membrane dye carbocyanine (DID, Biotium, Fremont, CA, USA) solution (5 μ L of dye in 1 mL PBS). Eventually, CLSM using 63-fold oil immersion objective (LSM 710, Carl Zeiss, Oberkochen, Germany) was used to examine all samples that were washed twice with PBS, mounted on objective slides using polyvinyl alcohol (PVA, Sigma Aldrich, Darmstadt, Germany). ZEN2011 software (Carl Zeiss, Oberkochen, Germany) was utilized for image processing [21].

4.5.9. Uptake of FITC-GAG by Macrophages Studied with Flow Cytometry

Cells were seeded on PEI and PEMs with the terminal two single layers of FITC-labelled GAG and cultured for 48 h as described in the aforementioned section of CLSM. The cells were scraped after trypsinization, centrifuged, washed once with PBS and resuspended in 200 μ L PBS. Then, a flow cytometry device (LSR Fortessa II, BD Bioscience, Germany) was used to measure the 100 μ L cell suspension, which was transferred to 96-well plate. FACS-Diva software (LSR Fortessa II, BD Bioscience, Germany) (version 6.2) was used for data analysis [21].

4.6. Statistics

An origin 8 Pro software (Origin Lab, Northampton, MA, USA) was used here for the statistical calculations. The one-way analysis of variance (ANOVA) followed by post-hoc Tukey's test was applied. The mean values \pm standard deviations (SD) represented all used data. It is indicated in the respective figure captions, the samples' number. Statistical significance was considered for $p \leq 0.05$ and is visualized by asterisks in the figures.

5. Conclusions

In this study, it was shown that the anti-inflammatory effect of PEMs made of either heparin or hyaluronan with chitosan as a polycation were related to reduced adhesion, interleukin I- β release and macrophage fusion, when compared to a pro-inflammatory model surface based on the highly cationic polyethylene imine. It was evident that the observed effects are not solely based on the hydrophilic character of these PEMs when compared to PEI. Indeed, it was shown that the pharmaceutical effects of heparin and hyaluronan known from other studies came into play when macrophages adhering on PEMs associated with and took up these molecules through different membrane receptors that may lead to the suppression of the canonical NF- κ B signalling pathway. Hence, such multilayer systems may be of great interest and potential to modulate inflammatory responses of biomaterials improving function and lifetime of implantable biomedical devices.

Supplementary Materials: Supplementary materials can be found at <http://www.mdpi.com/1422-0067/21/10/3724/s1>.

Author Contributions: Conceptualization, T.G. and H.A.; methodology, H.A.; formal analysis, H.A. and A.H.; investigation, H.A., A.H., B.F., F.S., F.E. and G.Z.; data curation, H.A. and A.H.; writing—original draft preparation, H.A.; writing—review and editing, S.S., S.N. and T.G.; supervision, T.G.; project administration, T.G. All authors have read and agreed to the published version of the manuscript.

Funding: This research was funded by German Academic Exchange Service (DAAD) as well as by a bilateral cooperation between DAAD and Ministry of Education, Science and Technological Development of the Republic of Serbia (period 2019–2020).

Acknowledgments: This work was financially supported by the German Academic Exchange service (DAAD) through a PhD grant to Hala Alkhoury. The study was also part of the project of bilateral cooperation funded by DAAD and Ministry of Education, Science and Technological Development of the Republic of Serbia (period 2019–2020). The kind support by Alexander Navarrete Santos from the university hospital, in the core facility of cell analysis and cell sorting at Martin Luther University Halle-Wittenberg, in the flow cytometry is greatly appreciated.

Conflicts of Interest: The authors declare no conflict of interest.

References

1. Tang, L.; Eaton, J.W. Inflammatory responses to biomaterials. *Am. J. Clin. Pathol.* **1995**, *103*, 466–471. [[CrossRef](#)]
2. Anderson, J.M. In vitro and in vivo monocyte, macrophage, foreign body giant cell, and lymphocyte interactions with biomaterials. In *Biological Interactions on Materials Surfaces*; Springer: Berlin, Germany, 2009; pp. 225–244.
3. Mariani, E.; Lisignoli, G.; Borzì, R.M.; Pulsatelli, L. Biomaterials: Foreign bodies or tuners for the immune response? *Int. J. Mol. Sci.* **2019**, *20*, 636. [[CrossRef](#)]
4. Murray, P.J.; Wynn, T.A. Protective and pathogenic functions of macrophage subsets. *Nat. Rev. Immunol.* **2011**, *11*, 723. [[CrossRef](#)]
5. Schutte, R.J.; Parisi-Amon, A.; Reichert, W.M. Cytokine profiling using monocytes/macrophages cultured on common biomaterials with a range of surface chemistries. *J. Biomed. Mater. Res.* **2009**, *88*, 128–139. [[CrossRef](#)]
6. Wynn, T.A.; Barron, L. Macrophages: Master regulators of inflammation and fibrosis. *Semin. Liver Dis.* **2010**, *30*, 245–257. [[CrossRef](#)]
7. Fialkow, L.; Wang, Y.; Downey, G.P. Reactive oxygen and nitrogen species as signaling molecules regulating neutrophil function. *Free Radic. Biol. Med.* **2007**, *42*, 153–164. [[CrossRef](#)]
8. Underhill, D.M.; Goodridge, H.S. Information processing during phagocytosis. *Nat. Rev. Immunol.* **2012**, *12*, 492. [[CrossRef](#)]
9. Xia, Z.; Triffitt, J.T. A review on macrophage responses to biomaterials. *Biomed. Mater.* **2006**, *1*, R1. [[CrossRef](#)]
10. Serini, G.; Bochaton-Piallat, M.-L.; Ropraz, P.; Geinoz, A.; Borsi, L.; Zardi, L.; Gabbiani, G. The fibronectin domain ED-A is crucial for myofibroblastic phenotype induction by transforming growth factor- β 1. *J. Cell Biol.* **1998**, *142*, 873–881. [[CrossRef](#)]
11. Barron, L.; Wynn, T.A. Fibrosis is regulated by Th2 and Th17 responses and by dynamic interactions between fibroblasts and macrophages. *Am. J. Physiol. -Gastrointest. Liver Physiol.* **2011**, *300*, G723. [[CrossRef](#)]
12. Ratner, B.D.; Bryant, S.J. Biomaterials: Where we have been and where we are going. *Annu. Rev. Biomed. Eng.* **2004**, *6*, 41–75. [[CrossRef](#)]
13. Altman, R.D.; Manjoo, A.; Fierlinger, A.; Niazi, F.; Nicholls, M. The mechanism of action for hyaluronic acid treatment in the osteoarthritic knee: A systematic review. *Bmc Musculoskelet. Disord.* **2015**, *16*, 321. [[CrossRef](#)]
14. Franz, S.; Rammelt, S.; Scharnweber, D.; Simon, J.C. Immune responses to implants—a review of the implications for the design of immunomodulatory biomaterials. *Biomaterials* **2011**, *32*, 6692–6709. [[CrossRef](#)]
15. Vroman, L.; Adams, A.; Fischer, G.; Munoz, P. Interaction of high molecular weight kininogen, factor XII, and fibrinogen in plasma at interfaces. *Blood* **1980**, *55*, 156–159. [[CrossRef](#)]
16. Suarez, P.; Rojo, L.; Gonzalez-Gomez, A.; Roman, J.S. Self-assembling gradient copolymers of vinylimidazol and (acrylic)ibuprofen with anti-inflammatory and zinc chelating properties. *Macromol. Biosci.* **2013**, *13*, 1174–1184. [[CrossRef](#)]
17. Al-Khoury, H.; Espinosa-Cano, E.; Aguilar, M.a.R.; Román, J.S.; Syrowatka, F.; Schmidt, G.; Groth, T. Anti-inflammatory Surface Coatings Based on Polyelectrolyte Multilayers of Heparin and Polycationic Nanoparticles of Naproxen-Bearing Polymeric Drugs. *Biomacromolecules* **2019**, *20*, 10. [[CrossRef](#)]
18. Borges, J.; Mano, J.F. Molecular interactions driving the layer-by-layer assembly of multilayers. *Chem. Rev.* **2014**, *114*, 8883–8942. [[CrossRef](#)]
19. Benkirane-Jessel, N.; Schwinte, P.; Falvey, P.; Darcy, R.; Haïkel, Y.; Schaaf, P.; Voegel, J.C.; Ogier, J. Build-up of polypeptide multilayer coatings with anti-inflammatory properties based on the embedding of piroxicam-cyclodextrin complexes. *Adv. Funct. Mater.* **2004**, *14*, 174–182. [[CrossRef](#)]
20. Shao, J.; Wen, C.; Xuan, M.; Zhang, H.; Frueh, J.; Wan, M.; Gao, L.; He, Q. Polyelectrolyte multilayer-cushioned fluid lipid bilayers: A parachute model. *Phys. Chem. Chem. Phys.* **2017**, *19*, 2008–2016. [[CrossRef](#)]

21. AlKhoury, H.; Hautmann, A.; Erdmann, F.; Zhou, G.; Stojanovic, S.; Najman, S.; Groth, T. Study on the potential mechanism of anti-inflammatory activity of covalently immobilized hyaluronan and heparin. *J. Biomed. Mater. Res.* **2020**. [[CrossRef](#)]
22. Aggarwal, N.; Altgärde, N.; Svedhem, S.; Michanetzi, G.; Missirlis, Y.; Groth, T. Tuning Cell Adhesion and Growth on Biomimetic Polyelectrolyte Multilayers by Variation of p H During Layer-by-L ayer Assembly. *Macromol. Biosci.* **2013**, *13*, 1327–1338. [[CrossRef](#)]
23. Mehta, V.B.; Besner, G.E. Inhibition of NF- κ B activation and its target genes by heparin-binding epidermal growth factor-like growth factor. *J. Immunol.* **2003**, *171*, 6014–6022. [[CrossRef](#)]
24. Neumann, A.; Schinzel, R.; Palm, D.; Riederer, P.; Münch, G. High molecular weight hyaluronic acid inhibits advanced glycation endproduct-induced NF- κ B activation and cytokine expression. *FEBS Lett.* **1999**, *453*, 283–287. [[CrossRef](#)]
25. Karin, M.; Greten, F.R. NF- κ B: Linking inflammation and immunity to cancer development and progression. *Nat. Rev. Immunol.* **2005**, *5*, 749. [[CrossRef](#)]
26. Lawrence, T. The nuclear factor NF-kappaB pathway in inflammation. *Cold Spring Harb. Perspect Biol.* **2009**, *1*, a001651. [[CrossRef](#)]
27. Liu, T.; Zhang, L.; Joo, D.; Sun, S.-C. NF- κ B signaling in inflammation. *Signal Transduct. Target. Ther.* **2017**, *2*, 17023. [[CrossRef](#)]
28. Ghosh, S.; Hayden, M.S. New regulators of NF- κ B in inflammation. *Nat. Rev. Immunol.* **2008**, *8*, 837. [[CrossRef](#)]
29. Avenoso, A.; D'Ascola, A.; Scuruchi, M.; Mandraffino, G.; Calatroni, A.; Saitta, A.; Campo, S.; Campo, G.M. Hyaluronan in the experimental injury of the cartilage: Biochemical action and protective effects. *Inflamm. Res.* **2018**, *67*, 5–20. [[CrossRef](#)]
30. Altman, R.; Bedi, A.; Manjoo, A.; Niazi, F.; Shaw, P.; Mease, P. Anti-inflammatory effects of intra-articular hyaluronic acid: A systematic review. *Cartilage* **2019**, *10*, 43–52. [[CrossRef](#)]
31. Naor, D.; Nedvetzki, S.; Walmsley, M.; Yayon, A.; Turley, E.A.; Golan, I.; Caspi, D.; Sebban, L.E.; Zick, Y.; Garin, T. CD44 involvement in autoimmune inflammations. *Ann. N. Y. Acad. Sci.* **2007**, *1110*, 233–247. [[CrossRef](#)]
32. Lee, J.H.; Lee, J.; Seo, G.H.; Kim, C.H.; Ahn, Y.S. Heparin inhibits NF- κ B activation and increases cell death in cerebral endothelial cells after oxygen-glucose deprivation. *J. Mol. Neurosci.* **2007**, *32*, 145–154. [[CrossRef](#)] [[PubMed](#)]
33. Köwitsch, A.; Zhou, G.; Groth, T. Medical application of glycosaminoglycans: A review. *J. Tissue Eng. Regen. Med.* **2018**, *12*, e23–e41. [[CrossRef](#)]
34. Zhou, G.; Niepel, M.S.; Saretia, S.; Groth, T. Reducing the inflammatory responses of biomaterials by surface modification with glycosaminoglycan multilayers. *J. Biomed. Mater. Res.* **2016**, *104*, 493–502. [[CrossRef](#)] [[PubMed](#)]
35. Kolasinska, M.; Krastev, R.; Warszynski, P. Characteristics of polyelectrolyte multilayers: Effect of PEI anchoring layer and posttreatment after deposition. *J. Colloid Interface Sci.* **2007**, *305*, 46–56. [[CrossRef](#)] [[PubMed](#)]
36. Zhou, G.; Loppnow, H.; Groth, T. A macrophage/fibroblast co-culture system using a cell migration chamber to study inflammatory effects of biomaterials. *Acta Biomater* **2015**, *26*, 54–63. [[CrossRef](#)]
37. Bacakova, L.; Filova, E.; Parizek, M.; Ruml, T.; Svorcik, V. Modulation of cell adhesion, proliferation and differentiation on materials designed for body implants. *Biotechnol. Adv.* **2011**, *29*, 739–767. [[CrossRef](#)]
38. Zhou, G.; Al-Khoury, H.; Groth, T. Covalent immobilization of glycosaminoglycans to reduce the inflammatory effects of biomaterials. *Int. J. Artif. Organs* **2016**, *39*, 37–44. [[CrossRef](#)]
39. Hernández-Montelongo, J.; Nascimento, V.F.; Murillo, D.; Taketa, T.B.; Sahoo, P.; de Souza, A.A.; Beppu, M.M.; Cotta, M.A. Nanofilms of hyaluronan/chitosan assembled layer-by-layer: An antibacterial surface for *Xylella fastidiosa*. *Carbohydr. Polym.* **2016**, *136*, 1–11. [[CrossRef](#)]
40. Sheikh, Z.; Brooks, P.; Barzilay, O.; Fine, N.; Glogauer, M. Macrophages, foreign body giant cells and their response to implantable biomaterials. *Materials* **2015**, *8*, 5671–5701. [[CrossRef](#)]
41. Min, Y.-D.; Choi, C.-H.; Bark, H.; Son, H.-Y.; Park, H.-H.; Lee, S.; Park, J.-W.; Park, E.-K.; Shin, H.-I.; Kim, S.-H. Quercetin inhibits expression of inflammatory cytokines through attenuation of NF- κ B and p38 MAPK in HMC-1 human mast cell line. *Inflamm. Res.* **2007**, *56*, 210–215. [[CrossRef](#)]

42. Blackwell, T.S.; Blackwell, T.R.; Christman, J.W. Impaired activation of nuclear factor-kappaB in endotoxin-tolerant rats is associated with down-regulation of chemokine gene expression and inhibition of neutrophilic lung inflammation. *J. Immunol.* **1997**, *158*, 5934–5940. [PubMed]
43. Zhao, M.; Altankov, G.; Grabiec, U.; Bennett, M.; Salmeron-Sanchez, M.; Dehghani, F.; Groth, T. Molecular composition of GAG-collagen I multilayers affects remodeling of terminal layers and osteogenic differentiation of adipose-derived stem cells. *Acta Biomater.* **2016**, *41*, 86–99. [CrossRef] [PubMed]
44. Young, E. The anti-inflammatory effects of heparin and related compounds. *Thromb. Res.* **2008**, *122*, 743–752. [CrossRef]
45. Young, E.; Venner, T.; Ribau, J.; Shaughnessy, S.; Hirsh, J.; Podor, T.J. The binding of unfractionated heparin and low molecular weight heparin to thrombin-activated human endothelial cells. *Thromb. Res.* **1999**, *96*, 373–381. [CrossRef]
46. Ruppert, S.M.; Hawn, T.R.; Arrigoni, A.; Wight, T.N.; Bollyky, P.L. Tissue integrity signals communicated by high-molecular weight hyaluronan and the resolution of inflammation. *Immunol. Res.* **2014**, *58*, 186–192. [CrossRef]
47. Neuman, M.G.; Nanau, R.M.; Oruña, L.; Coto, G. In vitro anti-inflammatory effects of hyaluronic acid in ethanol-induced damage in skin cells. *J. Pharm. Pharm. Sci.* **2011**, *14*, 425–437. [CrossRef]
48. Knudson, W.; Chow, G.; Knudson, C.B. CD44-mediated uptake and degradation of hyaluronan. *Matrix Biol.* **2002**, *21*, 15–23. [CrossRef]
49. Yamamoto, Y.; Gaynor, R.B. Therapeutic potential of inhibition of the NF- κ B pathway in the treatment of inflammation and cancer. *J. Clin. Investig.* **2001**, *107*, 135–142. [CrossRef]
50. Zang, Y.C.; Halder, J.B.; Hong, J.; Rivera, V.M.; Zhang, J.Z. Regulatory effects of estriol on T cell migration and cytokine profile: Inhibition of transcription factor NF- κ B. *J. Neuroimmunol.* **2002**, *124*, 106–114. [CrossRef]
51. Köwitsch, A.; Abreu, M.J.; Chhalotre, A.; Hielscher, M.; Fischer, S.; Mäder, K.; Groth, T. Synthesis of thiolated glycosaminoglycans and grafting to solid surfaces. *Carbohydr. Polym.* **2014**, *114*, 344–351. [CrossRef]
52. Macek, M. A review of advanced wet cleaning. *Inf. Midem* **1993**, *23*, 275–283.
53. Noursadeghi, M.; Tsang, J.; Hausteiner, T.; Miller, R.F.; Chain, B.M.; Katz, D.R. Quantitative imaging assay for NF- κ B nuclear translocation in primary human macrophages. *J. Immunol. Methods* **2008**, *329*, 194–200. [CrossRef]



© 2020 by the authors. Licensee MDPI, Basel, Switzerland. This article is an open access article distributed under the terms and conditions of the Creative Commons Attribution (CC BY) license (<http://creativecommons.org/licenses/by/4.0/>).

Reprinted under the open access CC BY 4.0 license.

International Journal of Molecular Bioscience (IJMS),

Hala Alkhoury, Adrian Hautmann, Bodo Fuhrmann, Frank Syrowatka, Frank Erdmann, Guoying Zhou, Sanja Stojanovic, Stevo Najman and Thomas Groth (2020), Studies on the mechanisms of anti-inflammatory activity of heparin- and hyaluronan-containing multilayer coatings-Targeting NF- κ B signalling pathway,

Int. J. Mol. Sci. 2020, 21, 3724.

DOI: 10.3390/ijms21103724

Chapter 4 - Free-standing multilayer films as growth factor reservoirs for future wound dressing applications

In this study a novel application for the LbL technique was explored. Widely researched as implant coating, the development of multilayered FSFs based on the LbL-technique gained traction in recent years. Building on this expertise, we created FSFs using the LbL method with CHI and ALG as polyelectrolytes and investigated, as novelty, the suitability of free-standing multilayer films as a wound dressing for chronic wounds. To improve wound healing prowess, we explored the potential of CHI/ALG FSFs as reservoirs for growth factors (FGF2 as mitogenic model GF) with controlled release, previously only investigated for thin LbL coatings. Finally, for the first-time biocompatibility was tested *in vivo* for said films. The production of our FSFs demanded a leap in the construction technique compared to previous study. We adapted an automatic dip coating process to allow the construction of free-standing films with a hundred bilayers of CHI and ALG, which is not feasible by a manual process, which take 30 min per bilayer to produce. The result are easily detachable films of approximately 450 μm thickness, produced in about 24 h. Two chemical crosslinking techniques using either EDC/NHS (E-FSF) or genipin (G-FSF) were compared to the non-crosslinked FSF (N-FSF). Crosslinking reduces swelling and oxygen permeability for both crosslinked films compared to non-crosslinked films. However, the crosslinking allows the controlled release of FGF2 encapsulated within the film. This increases the GF efficacy *in vivo* as the application of GFs is often compromised by swift inactivation within the hostile wound microenvironment. In biocompatibility studies *in vitro* with human dermal fibroblasts cultured underneath the films we found that all films, with and without FGF2, lead to more cell growth and migration. Especially G-FSF loaded with FGF2 greatly increases cell proliferation and migration. Meanwhile, E-FSF causes an inflammatory tissue response *in vivo* after subcutaneous implantation in mice that is absent in the case of G-FSF. N-FSF is also biocompatible but shows early degradation *in vivo*. In conclusion, FSF made from a combination of ALG and CHI and crosslinked with genipin have the potential to control the release FGF2. These films are well-tolerated by fibroblasts *in vivo* and when implanted in mice. Notably, all FSFs, crosslinked or not, support cell growth and migration but also possesses antibacterial properties. This makes LbL based free-standing films a promising option for wound care applications.



Free-standing multilayer films as growth factor reservoirs for future wound dressing applications

Adrian Hautmann^a, Devaki Kedilaya^a, Sanja Stojanović^{b,c}, Milena Radenković^b, Christian K. Marx^d, Stevo Najman^{b,c}, Markus Pietzsch^d, João F. Mano^e, Thomas Groth^{a,f,*}

^a Department of Biomedical Materials, Institute of Pharmacy, Martin Luther University Halle-Wittenberg, Heinrich-Damerow-Strasse 4, 06120 Halle (Saale), Germany

^b Department for Cell and Tissue Engineering, Scientific Research Center for Biomedicine, Faculty of Medicine, University of Niš, Blvd. Dr Zorana Dindića 81, 18000, Niš, Serbia

^c Department of Biology and Human Genetics, Faculty of Medicine, University of Niš, Niš, Serbia

^d Department of Downstream Processing, Institute of Pharmacy, Martin Luther University Halle-Wittenberg, Weinbergweg 22, 06120 Halle (Saale), Germany

^e CICECO—Aveiro Institute of Materials, Department of Chemistry, University of Aveiro, 3810-193 Aveiro, Portugal

^f Interdisciplinary Center of Material Research, Martin Luther University Halle-Wittenberg, Germany

ARTICLE INFO

Keywords:

Wound dressing
Layer-by-layer technique
Free-standing films
Growth factor delivery
In vitro biocompatibility
In vivo study

ABSTRACT

Chronic skin wounds place a high burden on patients and health care systems. The use of angiogenic and mitogenic growth factors can facilitate the healing but growth factors are quickly inactivated by the wound environment if added exogenously. Here, free-standing multilayer films (FSF) are fabricated from chitosan and alginate as opposing polyelectrolytes in an alternating manner using layer-by-layer technique. One hundred bilayers form an about 450 μm thick, detachable free-standing film that is subsequently crosslinked by either ethyl (dimethylaminopropyl) carbodiimide combined with *N*-hydroxysuccinimide (E-FSF) or genipin (G-FSF). The characterization of swelling, oxygen permeability and crosslinking density shows reduced swelling and oxygen permeability for both crosslinked films compared to non-crosslinked films (N-FSF). Loading of fibroblast growth factor 2 (FGF2) into the films results in a sustained release from crosslinked FSF in comparison to non-crosslinked FSF. Biocompatibility studies *in vitro* with human dermal fibroblasts cultured underneath the films demonstrate increased cell growth and cell migration for all films with and without FGF2. Especially G-FSF loaded with FGF2 greatly increases cell proliferation and migration. *In vivo* biocompatibility studies by subcutaneous implantation in mice show that E-FSF causes an inflammatory tissue response that is absent in the case of G-FSF. N-FSF also represents a biocompatible film but shows early degradation. All FSF possess antibacterial properties against gram+ and gram- bacteria demonstrated by an agar diffusion disc assay. In summary, FSF made of alginate and chitosan crosslinked with genipin can act as a reservoir for the sustained release of FGF2, possessing high biocompatibility *in vitro* and *in vivo*. Moreover, G-FSF promotes growth and migration of human dermal fibroblasts and has antibacterial properties, which makes it an interesting candidate for bioactive wound.

1. Introduction

Chronic wounds represent a major problem in medical care, intensified by an ageing society. With a prevalence of about 1 % in Germany (2012) it places a high burden on the quality of life of patients as well as the health care system [1]. Chronic wounds are non-healing wounds,

which develop due to defective regulation of a tightly controlled healing process, often because of severe traumata and/or side effects from diseases, such as diabetes, age of patients and others [2]. Problems associated with chronic wounds, are extracellular matrix destruction, low amounts of oxygen (hypoxia), high amounts of reactive oxygen species and bacterial invasion. This results in a further progression of the

Abbreviations: ALG, alginate; CHI, chitosan; EDC, 1-ethyl-3-(3-dimethylaminopropyl) carbodiimide; E-FSF, EDC/NHS crosslinked free-standing film; ELISA, enzyme-linked immunosorbent assay; FGF2, fibroblast growth factor 2; FL-ALG, fluorescein labelled alginate; FSF, free-standing films; GF, growth factor; G-FSF, genipin crosslinked free-standing film; HDF, human dermal fibroblasts; LbL, layer-by-layer; N-FSF, non-crosslinked free-standing film; NHS, *N*-hydroxysuccinimide; PEM, polyelectrolyte multilayer.

* Corresponding author at: Department Biomedical Materials, Institute of Pharmacy, Martin Luther University Halle-Wittenberg, 06099 Halle (Saale), Germany.

E-mail address: thomas.groth@pharmazie.uni-halle.de (T. Groth).

<https://doi.org/10.1016/j.bioadv.2022.213166>

Received 20 July 2022; Received in revised form 12 October 2022; Accepted 16 October 2022

Available online 20 October 2022

2772-9508/© 2022 The Authors. Published by Elsevier B.V. This is an open access article under the CC BY license (<http://creativecommons.org/licenses/by/4.0/>).

wound, which can ultimately lead to sepsis and amputation of extremities associated with high mortality [2]. Very often these wounds are full thickness wounds; the epidermis, dermis and underlying structures are destroyed [3]. These kinds of wounds close by epithelial resurfacing and wound contraction. The normal wound healing process is characterized by four timely and locally orchestrated processes of hemostasis; inflammation, cell proliferation (granulation and reepithelization) and tissue remodeling [2]. The formation of granulation tissue for improved epithelial migration has been identified to be pivotal for the healing of chronic wounds [4]; The anti-inflammatory signals of macrophages shifted to an M2 state allows fibroblasts and keratinocytes to proliferate and migrate from the borders of the wound [4]. After the formation of granulation tissue, keratinocytes use this newly formed structure to migrate on top of the fibroblasts to reepithelize the wound [5].

To treat chronic wounds, a wide selection of advanced wound dressings has been developed such as semipermeable films, foam dressings, alginate (ALG) dressings, hydrogel, hydrocolloid, and hydrofiber dressings [6]. Their individual use case, advantages and disadvantages are discussed in a recent review published by Han et al. [6]. All wound dressings must be non-toxic, maintaining a moist wound environment while retaining the ability to absorb wound exudates, permitting gas exchange, and preventing bacterial invasion. Additionally, during the granulation phase, they should be non-adherent to the wound area [7]. To improve the resolution of the inflammation phase in chronic wounds, growth factor supplementation has gained particular attention since chronic wounds have been found to possess low amounts of growth factors, like platelet-derived growth factor (PDGF), epidermal growth factor (EGF), fibroblast growth factor (FGF), transforming growth factor (TGF- β) and vascular endothelial growth factor (VEGF) [8]. FGF2, also known as basic FGF (bFGF), has gained particular attention in recent years [9]. It plays an important role in the wound healing process, mainly by stimulating migration, proliferation, and differentiation of fibroblasts and keratinocytes cells, but also because of its angiogenic effects [9]. The application of FGF2 has shown positive outcomes in clinical studies of eardrum reconstruction, in periodontal regeneration, treatment of burns and diabetic ulcers [10–12]. However, FGF2 loses quickly its bioactivity in a wound due to degradation by proteases and other processes [13,14]. This requires the protection of growth factors (GF) by carrier systems for controlled release as inherent additional function of advanced wound dressings. FGF2-containing wound dressings were examined in several pre-clinical studies [15–17]. While the aforementioned FGF2 loaded wound dressings show successful application and efficacy of FGF2, these designs are hampered in either one of the following categories; they are monolithic in design and therefore limited in their choice of tuneable parameters, need demanding production requirements or possess lacking release kinetics of GF and other bioactive substances.

One technique interesting for wound healing applications is the layer-by-layer (LbL) method, based on the consecutive adsorption of oppositely charged polyelectrolytes on a substrate [18]. Biological building blocks, representing polyelectrolytes interesting for the area of wound dressings, are charged polysaccharides like ALG and chitosan (CHI), but also proteins like collagens or elastin [19]. In addition, particulate charged matter like microgels and nanoparticles, that can be loaded with bioactive substances for medical applications, represent building blocks for LbL, too [20,21]. LbL can be used for polyelectrolyte multilayer (PEM) coating of implants, scaffolds for tissue engineering applications or preparation of multilayer capsules used for cell immobilization or drug delivery applications [22]. In recent years the application of the technique was extended to the construction of detachable free-standing PEM films [23]. Such films can be prepared to a thickness in mm scale enabled by automatic dip or spray coating processes [24]. The substrate supported PEM films are freed either by dissolution of a sacrificial layer or by peeling off leading to the formation of free-standing films (FSF) [25]. Advantages of LbL technique as bottom-up process are that it is simple, cost effective and allows great

customizability [24]. PEMs possess high loading capacities for biomolecules, drugs or metal ions and enable release time spans from weeks to months [26,27]. Based on these assets, bioactive functions, like antibacterial effects or immunomodulation of multilayer films were already realized [28,29]. Compared to other types of conventional wound dressings, the most relevant advantage of PEM-based FSF lies in their potential to be built in a modular manner. It allows the combination of different polyelectrolytes, bioactive substances, or particulate matter together or in separate sections of the film. Hence, a multitude of wound dressing related functions could be realized such as control of swelling and permeability, promotion of wound healing, as well as anti-oxidative and antibacterial functions.

Here, we used negatively charged ALG and positively charged CHI as building blocks for biogenic FSF prepared by LbL technique. ALG and CHI are valued for their biological origin, availability and cost efficiency. ALG in particular for its ability to absorb water and body fluids [30] and CHI for its antibacterial, anti-inflammatory and hemostatic effect [31]. Therefore, both are commonly used as single components in wound dressings [30]. Moreover, combinations of both polysaccharides in free-standing films were researched by several groups, focussing on their potential use as membranes in tissue regeneration [23,25]. In our study we additionally performed crosslinking with either 1-ethyl-3-(3-dimethylaminopropyl) carbodiimide (EDC) and *N*-hydroxysuccinimide (NHS) or genipin and subsequent loading of FGF2, because of the positive effect of this growth factor on regeneration of wound tissue including neovascularization [9]. These FSF were comprehensively characterized regarding their physical properties, especially regarding the effect of cross-linking on uptake and release of FGF2. The anticipated application of this FSF as wound dressings was investigated concerning growth and migration of fibroblasts *in vitro*, biocompatibility in a mouse subcutaneous implantation model and antibacterial properties. Results indicate that FSF crosslinked with genipin have a delayed release of FGF2, which promotes growth and migration of fibroblasts greatly, possess excellent biocompatibility *in vivo* and potent antibacterial activity. These properties are important prerequisites for regeneration of dermis, which makes this FSF highly interesting for wound healing applications. Results are reported herein.

2. Material and methods

2.1 Chemicals

Chitosan 85/500 with a deacetylation degree of 85 % (CHI, Mw \approx 500 kDa) was delivered from Hepe Medical Chitosan GmbH (Halle, Germany) and sodium alginate acid (low viscosity) from Alfa Aesar (ThermoFisher GmbH, Schwerte, Germany). Sodium chloride, acetic acid and hydrochloric acid were obtained from Carl Roth GmbH + Co. KG (Karlsruhe, Germany),

2.1. Cell culture

DMEM (without pyruvate, with 4.5 g/L glucose) (Carl Roth) supplemented with 10 % (v/v) fetal bovine serum (FBS, Biochrom AG, Berlin, Germany) and 1 % (v/v) antibiotic-antimycotic solution (AAS, Lonza, Basel, Switzerland) was used for culturing human dermal fibroblasts (HDF, PromoCell GmbH, Heidelberg, Germany) at 37 °C in a humidified 5 % CO₂/95 % air atmosphere in a NUAIRE® DH Autoflow incubator (NuAire, Plymouth, Minnesota, USA). Cells were passaged every second day to maintain a maximum of 80 % confluence in a T75 cell culture flasks (Greiner Bio-One GmbH and Co.KG, Frickenhausen, Germany). Trypsin/EDTA solution (0.25 % /0.02 % (w/v)) (BioChrom AG) was used to detach the adherent fibroblasts.

2.2. Multilayer formation

0.15 M NaCl solution (buffer and washing solution for dip coating),

2 mg/mL CHI solution and 5 mg/mL ALG solution (polymer reservoirs for dip coating) were prepared as previously described. [30]. The multilayered films were fabricated on objective glass slides (Menzel-Gläser, 76 × 26 mm², Thermo Scientific, Germany) by alternating deposition of CHI and ALG with intermediate washing steps using NaCl solution with an automated dip coater (DR01, Riegler & Kirstein, Berlin, Germany) to obtain 100 double layers. The first layer was CHI and last layer ALG. Coating time with polysaccharide solutions was 5 min. Washing time with NaCl solution was 2.5 min. After completion of film formation, samples were washed with Milli-Q H₂O and manually detached from the slides. As a result, free-standing films with a thickness up to 500 μm were obtained as shown by us before [30]. Finally, the films were either crosslinked (E-FSF, G-FSF) or stored at 4 °C (N-FSF) for further experiments. Fig. 1 provides an overview on the preparation, detachment and the cross-linking chemistry of the free-standing films.

2.3. Film crosslinking

After detachment, films were punched into circular 12 mm diameter disks and placed inside 24-well plates. Two different crosslinking methods were applied, which mechanisms are illustrated in Fig. 1. In the first case, films were immersed inside 1 mg/mL in genipin (Wako Chemicals GmbH, Neuss, Germany) in Milli-Q water at 37 °C for 24 h. Absolute Ethanol (AppliChem Panreac ITW Companies, Darmstadt, Germany) was used to stop the reaction, followed by three 15 min washing cycles with Milli-Q water. Alternatively, crosslinking using 1-ethyl-3-(3-dimethylaminopropyl) carbodiimide hydrochloride (EDC) (Carl Roth GmbH + Co. KG) and *N*-hydroxysuccinimide (NHS) (Sigma-Aldrich Chemie GmbH, Steinheim, Germany) was applied. EDC was used at a concentration of 50 mg/mL, dissolved in 150 mM NaCl (pH 5.0) followed by the addition of NHS at 11 mg/mL in 150 mM NaCl. The

crosslinking solution was added to the films that were subsequently incubated at 4 °C for 18 h. 0.15 M NaCl solution at pH 8.0 was used to remove the crosslinkers, washing the films for 1 h, repeated three times.

2.4. Determination of crosslinking degree

The crosslinked films were dried in a desiccator for 72 h. Afterwards they were placed into the measuring module of a fourier-transform infrared spectrometer (Bruker Alpha II) in attenuated total reflection mode. The baseline was subtracted with Origin Pro 2019 (v.9.60) and the data normalized. Additionally, crosslinking of the films with genipin and EDC/NHS was evaluated by determining the quantity of free amines using trypan blue following the method by Silva et al. [18]. The films were freeze-dried for 24 h and weighed to obtain the non-hydrated weight. Afterwards the films were rehydrated in 150 mmol NaCl (pH 4) overnight. A 0.08 % trypan blue solution in 150 mmol NaCl (pH 4) was added to the films overnight at 37 °C. Afterwards the supernatants were transferred to 96 well plates and the absorbance was measured at 580 nm in a microplate reader (FLUOstar, BMG LabTech, Offenburg, Germany). A standard curve was prepared by measuring the absorbance for a series of trypan blue solutions at different concentrations. The degree of crosslinking was calculated as follows (Eq. (1)):

$$CL(\%) = \frac{(\text{NH}_3^+ \text{ non crosslinked solution}) - (\text{NH}_3^+ \text{ crosslinked solution})}{\text{NH}_3^+ \text{ non crosslinked solution}} \quad (1)$$

2.5. Oxygen permeability

Deionized water was deoxygenated by purging with N₂ under vacuum for 15 min. This water was carefully transferred to glass bottles

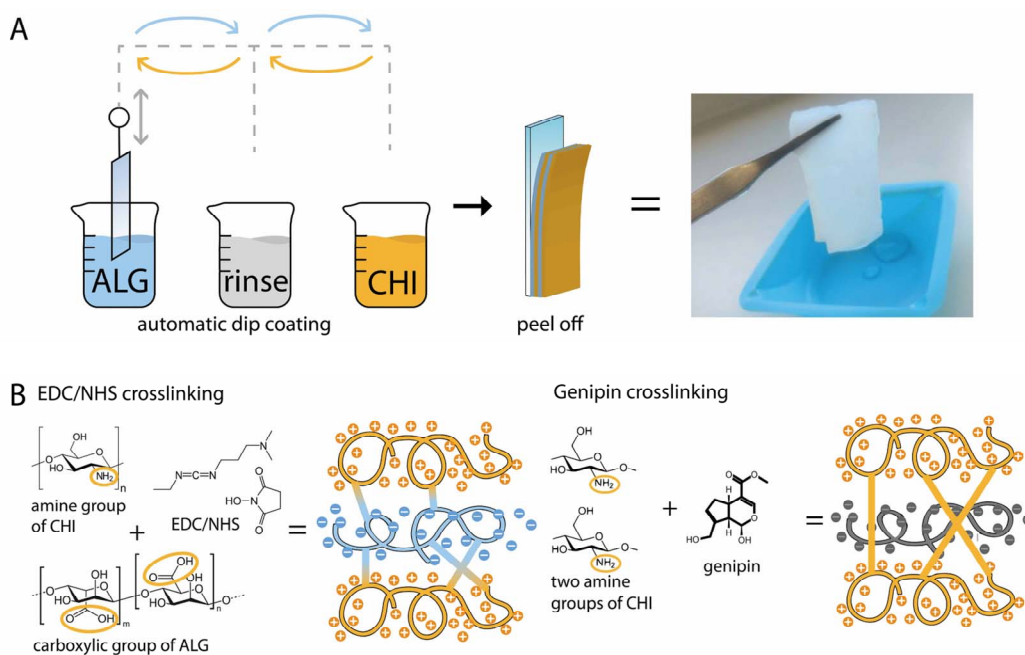


Fig. 1. A) Production of free-standing films (FSF) by automatic dip coating using chitosan (CHI) as first layer followed by rinsing with 150 mM NaCl solution and subsequent coating with alginate (ALG) with following rinsing, until 100 bilayers were deposited. The finished films were manually detached from the glass substrate. B) EDC/NHS crosslinking: the carbodiimide conjugation works via the activation of carboxyl groups for direct reaction with primary amines via amide bond formation, which leads to the crosslinking of ALG with CHI. Genipin crosslinking: The ester group of genipin reacts with amine groups of biomolecules forming an amide bond. In the case of the multilayer films, genipin crosslinks only CHI. The ALG layers are not crosslinked due to the absence of amine groups.

with a volume of 300 mL. On the bottle opening the free-standing films were fixed. Additionally, the bottles were left open (positive control) or closed with an airtight cap (blank). All bottles were constantly agitated for 24 h. Finally, the dissolved oxygen amount in the water was determined by Winkler-oximetry titration [31].

2.6. FGF2 upload and release

A solution of 5 µg/mL FGF2 (recombinant human FGF-basic, Peptidech, New Jersey, USA) containing 0.1 % BSA (albumin fraction V (Carl Roth GmbH + Co. KG) was prepared in PBS. The sterile films (12 mm diameter discs) were incubated in 300 µL FGF2 solution overnight (18 h was maintained for all the experiments) at 4 °C in a 24 well plate [32]. After washing the FGF2-loaded films once with PBS, 1 mL release medium (PBS, pH 7.4) was added to the film. 0.5 mL of the supernatant was collected at various time points and replaced with fresh 0.5 mL of PBS. All the supernatants were evaluated by using a human FGF-basic standard ABTS enzyme-linked immunosorbent assay (ELISA) development kit and ABTS ELISA buffer kit (both Peptidech).

2.7. Localization of FGF2 distribution in films

The localization of the FGF2 distribution in the film was determined by recording z-stacks of the whole thickness of the film using a Zeiss LSM 710 (Zeiss, Jena, Germany) loosely based on a method by Picart et al. [33] and Uhlig et al. [34]. Therefore, alginate was labelled with 6-amino-fluorescein (Sigma-Aldrich Chemie GmbH) by EDC/NHS chemistry to obtain 10 % labelled carboxylic groups, according to the protocol published by our group [35]. As a second component, FGF2 was labelled with ATTO 514 NHS-Ester according to the protocol of the producer (ATTO-TEC GmbH, Siegen, Germany). Briefly, 20 µg of FGF2 was dissolved in 100 µL of a labelling buffer, consisting of 20 parts PBS and 1 part 0.2 M sodium bicarbonate solution adjusted to pH 8.3. Afterwards, 10 µL of 5 mg/mL ATTO 514 in DMSO (Carl Roth GmbH + Co. KG) was added and the solution incubated under light protection for 1 h at RT. The resulting product was filtered with ROTI Spin MINI columns (Carl Roth GmbH + Co. KG) at 12.000 g for 10 min. The precipitate was then reconstituted in PBS and stored in Protein LoBind® Tubes (Eppendorf, Hamburg, Germany) at -20 °C. FSF preparation with FL-ALG and loading with ATTO-FGF2 was done according to the procedure described above. Films were transferred in 24-well cell imaging plates (Eppendorf) and a z-stack of each film with consistent settings over all samples recorded. The fluorescence intensity of each individual z-layer was quantified with ImageJ (1.53c). The thickness of the films was determined based on the intensities of FL-ALG, as a uniform distribution of alginate in the films was assumed. This was done by the use of the 3D Objects Counter plug-in (2.01) of ImageJ, which identified all connected voxels of the FL-ALG channel.

2.8. Cell culture

Normal Human Dermal Fibroblasts were used in this study to investigate the metabolic activity, cytotoxicity, growth, and migration in combination with different multilayers coatings. Cryoconserved cells were thawed and cultured in Dulbecco's modified Eagle medium supplemented with 10 % fetal bovine serum 1 % penicillin, streptomycin and Fungizone. HDF cells were harvested with 0.25 % trypsin/0.02 % EDTA solution at 37 °C for 3–5 min. The trypsin reaction was stopped by adding DMEM with 10 % FBS. Subsequently, the cells were re-suspended and seeded at a desired density on the well plate.

2.9. In vitro biocompatibility studies

The metabolic activity of HDF cells cultured exposed to the films was analyzed using a resazurin assay (Deep Blue Cell Viability Kit (BioLegend, San Diego, USA)). All films were sterilized by immersion in 70 %

ethanol, with subsequent threefold washing with PBS for 5 min each. 1 mL cell suspension with a density of 25,000 cells per well was seeded in a 24 well plate and incubated for 12 h (DMEM +10 % FBS + 1 % AB). Films were added on top of the cells after the latter were attached on the well and the medium was changed to DMEM with 1 % FBS and 1 % AB. After 24 h the films were temporarily transferred to a new well plate. The films were removed before each measurement, to remove effects of cell adhesion to the films. Deep Blue was prepared at a ratio of 1:10 with colourless DMEM (without pyruvate, with 4.5 g/L glucose (Lonza)) and was added to each existing well and incubated at 37 °C for 3 h. After incubation, duplicates of 100 µL of the supernatant were transferred to a black 96-well-plate (Greiner Bio-One GmbH). The converted fluorescent products were photometrically quantified at an excitation wavelength of 544 nm and an emission wavelength of 590 nm using a plate reader (FLUOstar). Cells without films were used as negative control. After measurements were conducted, the Deep Blue medium was aspirated from the wells and was replaced by DMEM medium supplemented with 1 % FBS and 1 % AB pen/strep/fungi. The films, which were stored in a different well plate, were added back to the respective wells. The same procedure was repeated on day 3 and day 7.

2.10. Cell migration studies

Autoclaved migration fences (Aix Scientifics CRO, Aachen, Germany) were inserted into the 24 well plate and incubated for 30 min at 37 °C, to increase the attachment of the silicone sealing of the fence to the bottom of well plates. 150 µL of cell suspension containing 50,000 cells per well were seeded at the center of the migration chamber. The outer chamber was filled only with medium. This assembly was incubated for 12 h at 37 °C, 5 % CO₂. Following this, the migration chambers were removed carefully, and the wells were washed once with DPBS (with Ca and Mg (Lonza)). Following the removal of the migration chamber, the films were added on top of the cells and incubated for 48 h. The test medium used was DMEM + 1 % FBS + 1 % AB with the addition of 5 µg/mL of mitomycin C (abcr GmbH, Karlsruhe, Germany) to inhibit cell proliferation. After incubation for 24 h, the cells were washed once with PBS and fixed with 1 mL methanol (Carl Roth GmbH + Co. KG) for 10 min. Then the methanol was removed, and the cells washed with PBS. For visualization, the cells were stained with 1 mL 10 % Giemsa's azur eosin methylene blue solution (Merck KGaA, Darmstadt, Germany) in milli-Q water for 10 min. Subsequently the cells were washed once with PBS followed by ultrapure water. Series of microscopic images using 4× objective (Nikon Eclipse Ti2) were taken along the length of the diameter. These images were then stitched by using the image stitching plugin by Preibisch et al. [36] (v. 1.2) which is provided as part of the Fiji project (v. 1.53c) and the length of the diameter was measured.

In an additional scratch assay the cells were seeded directly on the 24 well plate at a density of 50,000 cells per well. After incubation for 24 h, the cells were washed once with DPBS and subjected to 24 h serum starvation (DMEM without FBS). A 100 µL sterile pipette tip was used to make a uniform scratch on the well plate. The detached and floating cells were removed by washing the wells once with DPBS. 5 µM Cell-Tracker Green CMFDA (ThermoFisher GmbH) was added and was incubated for 45 min to stain all living cells. After washing with DPBS, medium (DMEM with 1 % FBS, 1 % AB and 5 µg/mL of mitomycin C) was added to the cells. At regular time points pictures were taken for 24 h with a Zeiss LSM 710 with an incubator XL S1 (Zeiss). The wound area was assessed with the help of the segmentation ImageJ plug-in Scratch Assay Analyzer developed by Glaß et al. [37]. At $t = 0$ the wound area was set as 100 %. To determine the *in vitro* wound closure rate a linear fit was applied.

2.11. In vivo biocompatibility studies

Free-standing films were implanted subcutaneously into mice to

examine the tissue reaction related to the different crosslinking methods. Experimental groups were formed based on the crosslinking method used as follows: 1) non-crosslinked films (N-FSF); 2) films crosslinked with EDC/NHS (E-FSF) and 3) films crosslinked with genipin (G-FSF). Prior to implantation of samples, animals were anesthetized by intraperitoneal administration of the ketamine/xylazine mixture according to the guidelines for mouse anesthesia. The skin on the back was shaved, washed with povidone iodine and incision was made. One film, 13 mm in diameter, was implanted per animal, subcutaneously, just below the interscapular region as previously published [38–40]. Each experimental group consisted of 15 animals carrying the same sample type. Implants were extracted and analyzed after 3, 10 and 30 days (five animals from each group were sacrificed per each experimental period). Extracted films with surrounding tissue were further used for histological analysis and were fixed in 10 % neutral buffered formalin (NBF) until further tissue processing.

After fixation in 10 % NBF, tissue samples were dehydrated by ascending concentrations of ethanol, cleared in xylene, embedded in paraffin and then sliced on a microtome Leica RM2125 RT (Leica Biosystems, Germany). The haematoxylin and eosin (H&E) and Azan trichrome (AT) staining were performed on tissue sections from five different animals per group for each experimental period and sample type. Histomorphometrical measurements were performed in NIS-Elements software version 3.2 (Nikon, Tokyo, Japan) on imaged tissue slides. The images were obtained on a microscope Leica DMLS equipped with the camera CMEX-10 Pro (Euromex Microscopen BV, Netherlands) at various magnifications. Film thickness after explantation and zone of cell migration into the material on tissue sections were measured. Results are presented as mean free-standing film thickness (μm) and cell migration zone (μm) \pm standard deviation (SD), for each group and time point.

2.12. Antibacterial activity

Disc diffusion test was used to study the antibacterial activity. *E. coli* (DH5 α) and *B. subtilis* DSM 10 (wild type) were the two bacteria strains used for the study. A single colony of the bacteria was inoculated in 5 mL LB liquid medium (Carl Roth GmbH + Co. KG) separately. This was then incubated overnight at 37 °C with constant agitation (160 rpm). The following day, the optical density (OD at 600 nm) was measured. The culture was diluted with sterile LB medium to obtain an OD₆₀₀ of 1 and 200 μL of this was spread on the LB plate (using a spreader). Then, films were placed on separate quadrants of the plate. 25 μL of kanamycin (0.5 $\mu\text{g}/\mu\text{L}$) (Carl Roth GmbH + Co. KG) was added on sterile cellulose acetate filter paper and was used as the positive control. The negative control was sterile filter paper with autoclaved water. The plates were then incubated at 37 °C for 24 h. Later, images of the plates were taken, and the inhibition zone was measured using ImageJ (v.1.53c). Finally, the disc diameter was subtracted from the inhibition zone diameter.

2.13. Statistical analysis

All quantitative data were statistically processed using OriginPro 2019 (v.9.6.0.172, OriginLab Corporation, Northampton, USA). For normal distributed data (tested with Shapiro-Wilk) one-way analysis of variance (ANOVA) with a post-hoc Tukey test were used. Nonparametric data were tested with a Kruskal-Wallis test. The results of histomorphometry were statistically analyzed by (ANOVA) in SPSS software 20.0. Data are represented as mean values \pm standard deviations (SD). The statistical significance is shown by asterisks in the figures ($p \leq 0.05$).

3. Results and discussion

3.1 Physical characterization of free-standing films

3.1.1 Studies on effects of crosslinking

The crosslinking density of FSF crosslinked by either EDC/NHS or genipin was evaluated using FTIR spectroscopy and trypan blue assay (Fig. 2A). The FTIR spectrum of CHI (Fig. S1) shows characteristic, overlapping absorption bands at 1647 cm^{-1} (amide-I) and 1587 cm^{-1} (amide-II), which are the result of the 85 % *N*-deacetylation degree of the chitin [41]. ALG is characterized by the presence of carboxylic groups, which can be found in the spectrum as carbonyl bond (C=O) at 1591 cm^{-1} [42]. In the recorded spectrum of N-FSF the overlapping absorption bands of amide-I and amide-II of CHI disappear through the electrostatic interaction with carboxylic groups of ALG [42,43]. By crosslinking with EDC/NHS and genipin, in both cases, a band shifting of the amide II band to a lower wavelength can be observed (from 1606 cm^{-1} (N-FSF) to 1602.77 cm^{-1} (E-FSF) and 1587.34 cm^{-1} (G-FSF)) (arrows in Fig. 2A) [44]. This band shifting is characteristic for the formation of a secondary amine and indicates a higher crosslinking degree of amine groups by genipin. In the case of both crosslinked films, the N—H peak that occurred at 3293 cm^{-1} was weak and almost absent, which can be attributed to N—H being crosslinked by either genipin or EDC/NHS.

Due to the electrostatic attraction of trypan blue to free amino groups, the number of amide bonds can be assessed [45]. The calculated crosslinking degree of G-FSF of $40.6 \pm 4\%$ is in accordance with the results of other groups employing a similar genipin crosslinking strategy for free-standing PEM films [23]. In comparison to G-FSF, the crosslinking density in the E-FSF sample was found to be significantly lower ($6.9 \pm 1\%$). This can be explained by the different crosslinking chemistry of EDC/NHS compared to genipin (Fig. 1). EDC/NHS forms covalent amide bonds between amino groups of CHI and carboxylic groups of ALG. Through this, all sterically accessible CHI and ALGs, are crosslinked. Genipin on the other hand crosslinks amino groups only and therefore is only capable of crosslinking CHI molecules. Then, ALG is only connected to CHI by ion pairing with the remaining amino groups of CHI. Indeed, the presence of genipin was validated by the very broad fluorescence of G-FSF [46], which was used to ensure batch-to-batch reproducibility (Fig. S2).

3.1.1. Oxygen permeability

The oxygen permeability of FSF is of interest due to their anticipated application as wound dressing that should enable a sufficient oxygen supply to the damaged tissue [47]. Moreover, oxygen permeability is linked to angiogenesis and cell proliferation, inhibits growth of anaerobic bacteria and enhances leukocyte bacterial killing capacity [48,49]. E-FSF possessed the least oxygen permeability compared to G-FSF and N-FSF (Fig. 2B). Although none of the films reaches an oxygen permeation like the open control, the N-FSF and G-FSF showed a non-significant reduction, which in case of the G-FSF was similar to results of other studies [23]. The degree of swelling shown in Fig. 2B is related positively with the oxygen permeability. This might be caused by the swelling of the polymer chains, which increases the O₂ penetration and the increased transport of O₂ through the water present in the films [50].

3.1.2. FGF2 uptake and release

Bioactive wound dressings should support neovascularization and promote regeneration of skin. This can be promoted by growth factors like FGF2, which represents a strong mitogen, promoting growth of fibroblasts, endothelial and other cells [8]. The amount and distribution of uploaded fluorescence labelled FGF2 (ATTO-FGF2) was studied by CLSM z-stack quantification. In all films ATTO-FGF2 was present in the core of the film, confirming diffusion throughout the layers (Fig. 3A and S3). FGF2 is known to interact with the amino groups of CHI which protects the growth factor against denaturation by heat, acidic pH, and proteolysis [51]. At the same time the basic epitopes of FGF2 can bind to negatively charged carboxylic groups of ALG [52]. The total uptake of

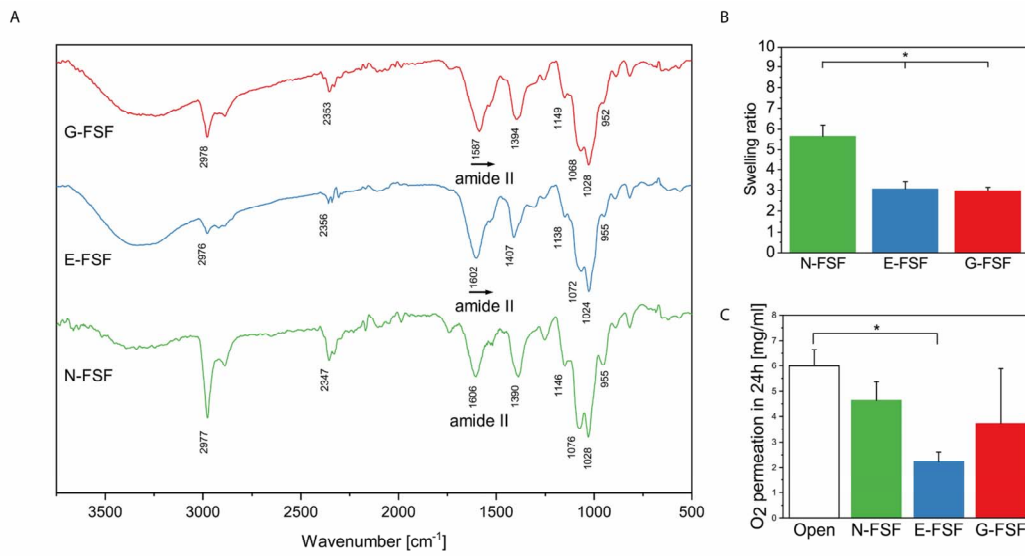


Fig. 2. A) FTIR spectra of free-standing films. After crosslinking a band shift of the secondary amine groups to a lower wavelength can be observed (from 1606 cm⁻¹ (N-FSF) to 1602.77 cm⁻¹ (E-FSF) and 1587.34 cm⁻¹ (G-FSF)). B) Swelling ratio determined by gravimetric method in PBS after 48 h. *n* = 5 **p* ≤ 0.05 C) Oxygen permeation through the FSFs during 24 h. *n* = 3 **p* ≤ 0.05.

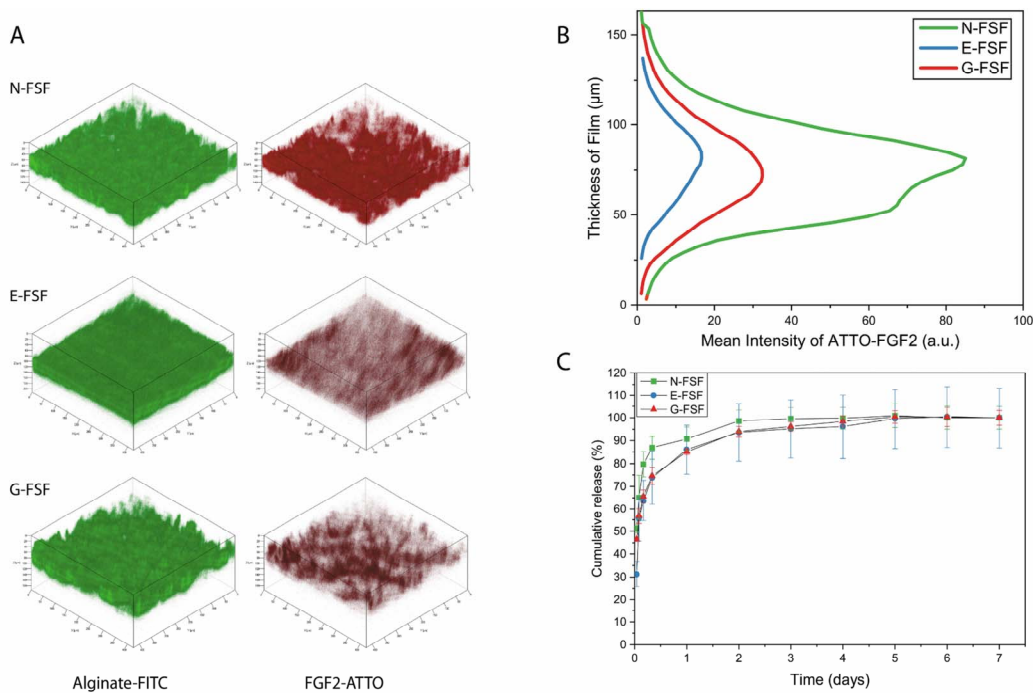


Fig. 3. A) 3D-volume renderings based on z-stacks of films recorded by CLSM to determine the distribution of FGF2 in the films. Green is FL-ALG. Red is FGF2-ATTO. B) Mean Intensity of FGF2 in each z-layer throughout the thickness of the fluorescent-labelled film. Area under Curve of each condition is significantly different. (*n* = 6, **p* ≤ 0.05) C) Cumulative release of FGF2 from the films over the duration of 7 days. Half of the release medium was discarded, to emulate sink conditions in part. The release was quantified by ELISA. (*n* = 3, **p* ≤ 0.05). (For interpretation of the references to colour in this figure legend, the reader is referred to the web version of this article.)

FGF2 into the N-FSF was higher than in G-FSF, which was higher compared to E-FSF. This is indicated by the distribution of the ATTO-FGF2 z-stacks in the FSF (Fig. 3B). Accordingly, a higher cumulative release of FGF2 from N-FSF (97 ± 5 ng/mL) was measured after 7 days in comparison to the crosslinked films (E-FSF: 19 ± 3 ng/mL and G-FSF: 39 ± 1 ng/mL) by ELISA (Fig. 3C). The high uptake of N-FSF can be accounted to the higher swelling ratio, which increases absorption of FGF2. Additionally, the release from N-FSF is faster, caused by the easier diffusion of FGF2 through the films probably because of the looser packing of the polyelectrolytes and comparable weaker electrostatic interactions between CHI and ALG at pH 7.4.

It is important to note that the initial burst from N-FSF (49.7 ± 2 ng/mL) was significantly higher than from the crosslinked films (E-FSF: 6.0 ± 1 ng/mL and G-FSF: 17.9 ± 0.11 ng/mL). The release slopes were statistically significant from each other (N-FSF: 6.2 ng/d, E-FSF: 1.9 ng/d and G-FSF: 3.9 ng/d) and were fitted to different models of release shown in the (Table S4). For both crosslinked and non-crosslinked films the correlation coefficient (r^2) for the Higuchi model was the highest, indicating that the release is determined by the diffusion through polymers [53]. These findings are similar to studies of FGF2 released from poly (methacrylic acid)/poly-l-histidine polyelectrolyte multilayers [54]. In the case of crosslinked FSF, a dense network created by crosslinking is known to decrease and delay the release [55,56]. However, even though the crosslinking density of G-FSF is higher than of E-FSF it was able to take up more FGF2 with higher cumulative release. This might be related to the presence of non-crosslinked carboxylic groups of ALG, which can undergo ionic interactions with the basic epitopes of FGF2 [56]. Additionally, the presence of genipin with its indol alkaloid backbone might lead to the association of aromatic amino acids [57]. This may explain the occurrence of high amounts of bound FGF2.

3.2 Biological characterization

3.2.1 *In vitro* biocompatibility studies

To assess the biocompatibility and the mitogenic effect of the films, with and without FGF2 loading, a growth assay with HDF cells was conducted. The number of cells directly attached to the films was found to be very low (Fig. S5), which can be regarded as a positive property of a wound dressing [2]. Therefore, in all further experiments cells cultured on tissue culture plastic (TCP) were evaluated, excluding cells adhering to the films. As seen from Fig. 4, the cell viability for G-FSF on day 1 was lower compared to that of the control (cells without films). G-FSF on day 1 caused a lower cell growth compared to all other FSF (N-

FSF and E-FSF). However, on day 3 and day 7 the same G-FSF samples stimulated the growth of cells compared to the control and E-FSF. This statement can be extended to all films as the cell viability of cells subjected to the different FSF was significantly higher compared to the respective controls on day 3 and 7. The cultured fibroblast can interact with the highly deacetylated CHI (85 %), which is known to enhance the proliferation, by interaction with serum proteins [58]. This effect might be supported by the ability of G-FSF to delay the FGF2 release, leading to higher levels of active FGF2 from day 3 of the experiment on. Overall, N-FSF and the crosslinked films (E-FSF and G-FSF) did not exhibit any cytotoxicity and an increase in cell proliferation was verified for all tested films.

The effect of FGF2 loading on fibroblasts growth was studied in the same manner. It was found that the presence of FGF2 in the films stimulates the growth of the cells significantly. After day 3 all FGF2 loaded films showed significantly more cell growth than the control. After day 7 G-FSF promoted the highest cell growth closely followed by E-FSF and with a certain distance N-FSF. The stronger promotion of fibroblast growth by crosslinked films is related to the differences in the concentration and kinetics of FGF2 release. The proliferative effect of FGF2 is concentration dependent; Low concentrations of FGF2 (<1 ng/mL) and high concentrations of FGF2 (100 ng/mL) are known to trigger survival and differentiation while delaying or inhibiting proliferation. Intermediate concentrations (1–10 ng/mL) are stimulating cell proliferation [59]. Another important aspect is the low stability of FGF2 in solution, particularly in presence of cells where it is proteolytically degraded within 24 as shown previously [14]. Hence, a fast release of larger quantities of FGF2 at early stages of cell growth will be less effective than a slower release over time. We suggest that the FGF2 loaded crosslinked films (E-FSF and G-FSF), kept the concentration of FGF2 in cell growth promoting range (1–10 ng/mL) [56,59]. FGF2 loaded N-FSF showed a comparatively high burst release (97.01 ng/mL), which was in the growth inhibitory range of FGF2. Additionally, FGF2, being positively charged at pH 7.4, can bind to the ALG layer and be presented to the cells as matrix-bound FGF2, which allows prolonged presentation of the growth factor to the cells [56]. This possibly allows G-FSF, with its non-crosslinked ALG, to increase the cell growth further. Overall, it can be stated that FGF2 loaded crosslinked FSF significantly increased the cell growth of fibroblasts compared to N-FSF, while utilizing lower amounts of FGF2.

Migration of fibroblasts and other cells plays an important role in wound healing to restore the damaged tissue. Hence, we studied here migration of fibroblast with two different methods. In both assays Mitomycin C, a mitotic inhibitor, was added to inhibit changes in the

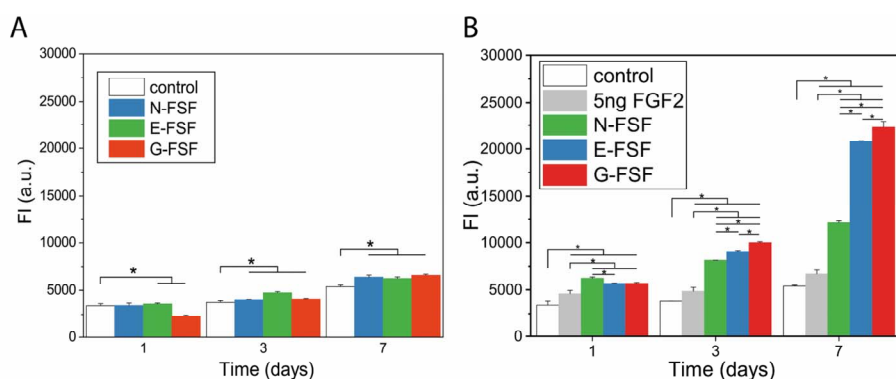


Fig. 4. A) Biocompatibility testing of films towards fibroblasts (HDF) determined by Deep blue assay. The intensity values are a measure of the metabolic activity. Cells were grown on tissue culture plastic (TCP) with the films above. DMEM Medium was changed on day 1 and 3. ($n = 6$, $*p \leq 0.05$). B) Cell growth assay with FGF2 loaded FSF. Experimental setup as described in A. (For interpretation of the references to colour in this figure legend, the reader is referred to the web version of this article.)

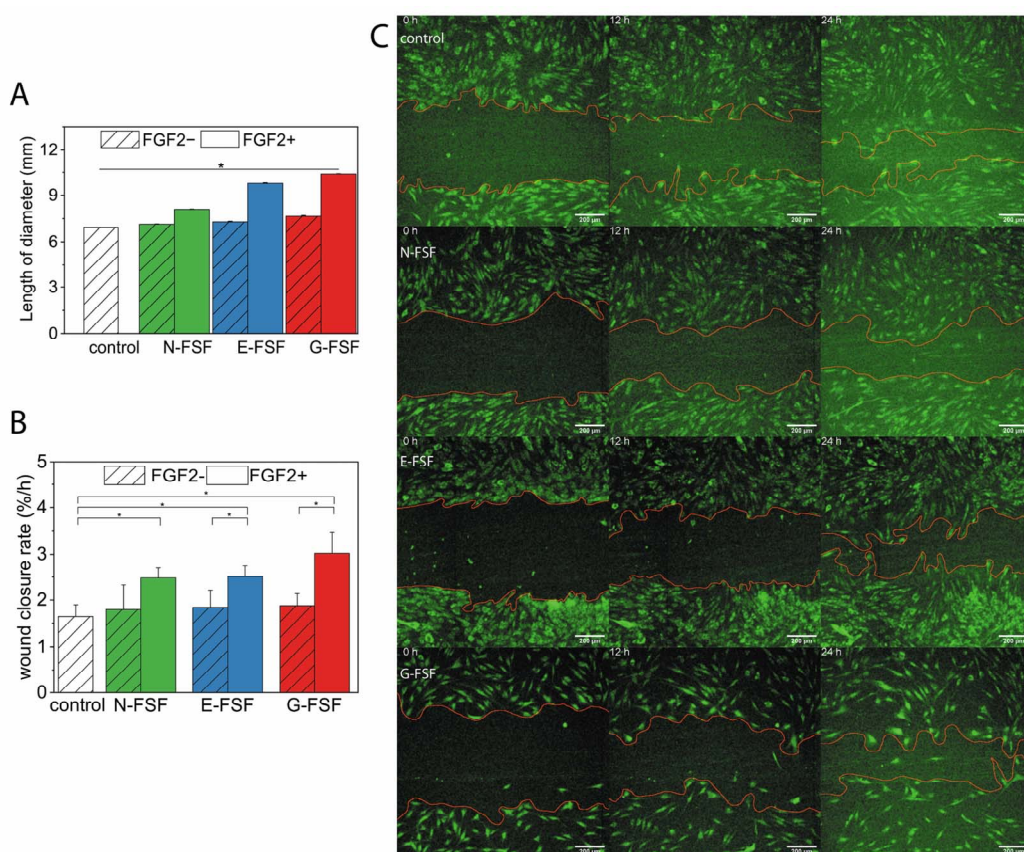


Fig. 5.

positioning of cells due to expansion of the growing cell layer. As seen in Fig. 5A, the films loaded with FGF2 showed a significantly larger diameter than all non-loaded films. FGF2 loaded G-FSF showed the highest cell migration, followed by E-FSF, while N-FSF exhibited the lowest migration of fibroblasts. A comparable behavior was observed in an *in vitro* scratch assay, which mimics cell migration during wound healing *in vivo* more closely.

Here, the cell-free area was determined over 24 h and subsequently the *in vitro* wound area closure rate calculated (Fig. 5B). The G-FSF loaded with FGF2 showed the fastest *in vitro* wound closure (Fig. 5C). Followed by E-FSF and N-FSF. Remarkable is the similarity in the initial decrease of wound area for all conditions. However, G-FSF and E-FSF permitted a faster *in vitro* wound closure over the whole duration of 24 h. These results confirm the positive effects of FGF2 as stimulator of migration in a possible wound environment [9]. The incorporation of FGF2 into the films leads to a faster migration and *in vitro* wound closure. The crosslinking with genipin seems to modulate the burst release of FGF2 in a way, which is beneficial for the migration of cells. The higher concentration of FGF2 in the medium, released in 24 h by N-FSF (88 ± 5 ng/mL) seem to be inferior to the medium concentration of G-FSF (33 ± 1 ng/mL) or E-FSF (16 ± 2 ng/mL). As reported in the literature around 25 ng/mL FGF2 concentration is an optimum for migration and *in vitro* wound healing [60,61].

3.1.3. *In vivo* biocompatibility

To extend the biocompatibility study to living organisms, soft tissue

reaction to FSF was examined in a subcutaneous implantation model in mice. Samples were taken at 3, 10 and 30 days after implantation. Macroscopic analysis revealed that there was difference in reaction of surrounding tissue to the films (Fig. 6). For N-FSF a significant change in shape can be seen from the 3rd to the 30th day of implantation in terms of degradation and loss of integrity (Fig. 6-a, d, g). No noticeable adverse tissue reaction was observed. E-FSF induced a notable surrounding tissue reaction directly from the onset of implantation. A very pronounced surrounding tissue vascularization, swelling and granulation could be observed, which are signs of inflammatory tissue reaction to the foreign material (Fig. 6-b, e, h). On the other hand, G-FSF was the most stable over time and did not induce visible macroscopic signs of adverse reactions after longer time post implantation (Fig. 6-c, f, i).

Histological analysis was undertaken to further study the host reaction to implantation of FSF (Fig. 7). After 3 days, an intense cell infiltration was observed in all groups. However, the presence and arrangement of cell populations differed. In the N-FSF group connective tissue cells from surrounding tissue could be seen, which aligned onto the films, went inside the films and started degradation. Additionally, signs of stratification as well as induction of collagen synthesis were observed. In the E-FSF and G-FSF group, infiltration of inflammation-related cells, such as neutrophils and macrophages, appeared in the surrounding tissue. Further, increased vascularization of surrounding tissue was noticed for both E-FSF and G-FSF. This suggests the initiation of an inflammatory reaction to the implanted films, which is an expected reaction to implanted biomaterials at that time point.

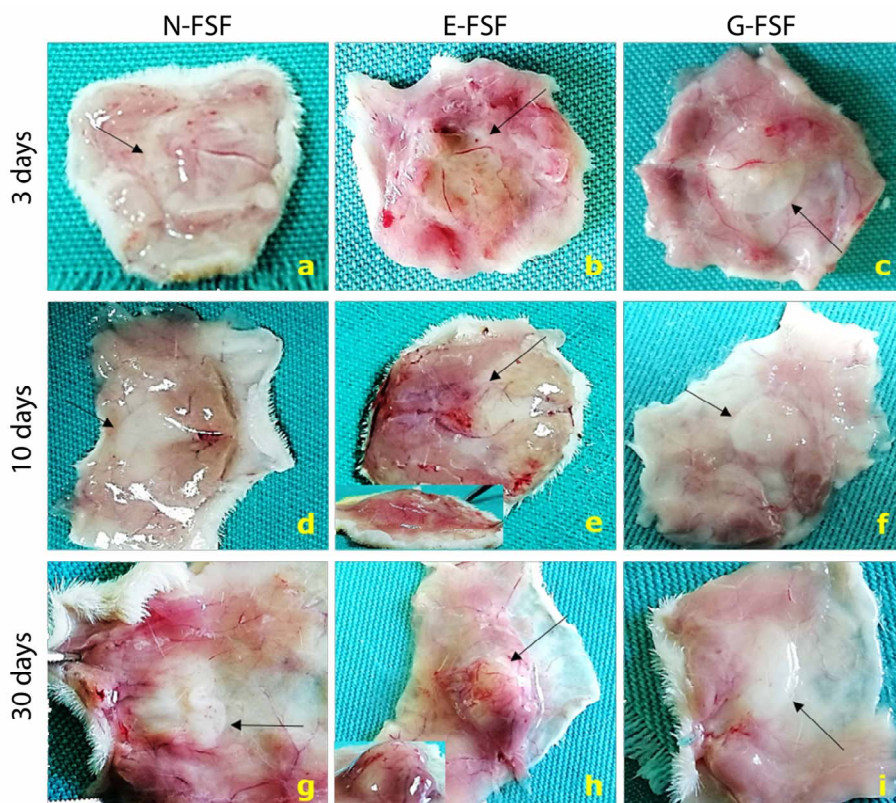


Fig. 6. Macroscopic appearance of explanted free-standing films and surrounding tissue reaction 3, 10 and 30 days after implantation; arrows points to free-standing films.

After 10 days, the inflammatory tissue reaction was reduced for N-FSF and G-FSF-groups, but not in the E-FSF group, which exhibited a strong inflammatory response. In the E-FSF group large infiltrates of inflammatory cells and connective tissue cells, which are lined onto the films and started migrating inside the film could be found. Additionally, in the surrounding tissue blood vessels were found in greater number, compared to the N-FSF and G-FSF group. EDC/NHS has shown toxic effects in *in-vivo* studies, where it was used in comparable concentrations [62]. While the EDC/NHS crosslinking method usually yields biocompatible systems, at higher concentrations cytotoxic EDC and reaction by-products cannot be fully removed via simple rinsing [63]. N-FSF seemed to be loosely packed, with great number of connective tissue infiltrates, but without visible signs of inflammatory reaction at this time point.

At day 30, in the N-FSF group, single cells migrating even deeper into the pores of the partially degraded N-FSF as well as newly formed collagen fibers and blood vessels surrounding the films could be observed. The inflammatory reaction seen in the E-FSF group at day 10 seemed to be reduced at day 30, possibly showing the elimination of cytotoxic compounds in the E-FSF group. A lot of cells migrated into the films and deposited collagen, but also blood vessels surrounding and inside the films can be observed. This could be the consequence of a strong inflammatory tissue reaction in earlier time points of the E-FSF group. In the G-FSF group no signs of inflammatory reaction of the surrounding tissue could be observed. The connective tissue cells were well integrated in the films depositing collagen fibers onto the films.

Histomorphometric measurements indicated that indeed the thickness of the N-FSF (Fig. 7B) gradually decreased from day 3 to day 30,

which suggests *in vivo* degradation. Crosslinked FSF were significantly more stable against degradation compared to N-FSF. Significant difference in cell infiltration and migration into implanted films from day 3 to day 30 was noticed for N-FSF and E-FSF group (Fig. 7C). N-FSF-groups cell migration zones decreased over time, while showing initially the thickest migration zone. An increase in cell infiltration and migration at day 10 was observed in E-FSF and G-FSF group with a slight decrease at day 30. Overall, N-FSF and G-FSF lead to a controlled tissue response towards their implantation, while N-FSF was showing degradation after 10 days compared to the more stable G-FSF but both FSF represent obviously biocompatible materials *in vivo*. By contrast, E-FSF showed a pro-inflammatory effect towards the surrounding tissue which makes this crosslinking method less suitable for making of FSF in wound dressing applications.

3.1.4. Antibacterial activity

Wound dressings should have also an anti-bacterial activity because infection is a common occurrence in chronic wounds [6]. Here, the antibacterial activity of FSF was studied with *E. coli* DSM 6897 as Gram-negative (G-) and *B. subtilis* DSM 10 as Gram-positive (G+) germs using the disc diffusion method (Fig. 8A). These bacteria are widely used to study the antibacterial activity of wound dressings [64]. The positive control (12 mm filter paper disc impregnated with kanamycin) produced a large zone of inhibition for both *E. coli* and *B. subtilis* as visible in Fig. 8B. In general, the inhibitory effect of all FSF (cut in 12 mm discs) is lower compared to the aminoglycoside antibiotic kanamycin used as a positive control. It is visible that the N-FSF shows a comparable effect on

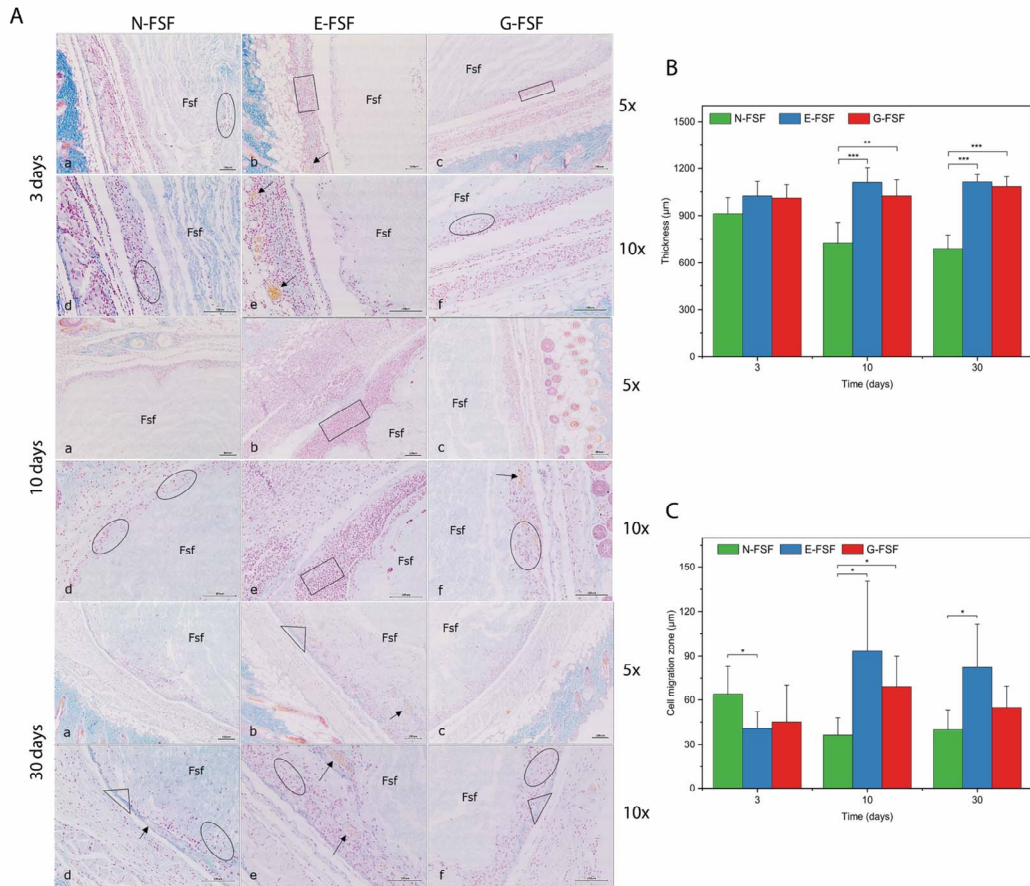


Fig. 7. A) Histologic sections of explanted free-standing films with surrounding tissue 3, 10 and 30 days after implantation; AT staining; brightfield; objective magnification 5x (a-c) and 10x (d-f); blue colour on the images indicates collagen staining; Fsf – free-standing films; blood vessels (arrows); inflammatory-like cell infiltrates (rectangles); connective tissue cell infiltrates (ellipses); scale bar = 100 µm. B) Histomorphometric measurements; thickness (µm) of explanted free-standing films 3, 10 and 30 days after implantation and C cell migration zone (µm) in explanted free-standing films 3, 10 and 30 days after implantation. (*) $p \leq 0.05$, (**) $p \leq 0.01$, (***) $p \leq 0.001$; $n = 5$ for each group. (For interpretation of the references to colour in this figure legend, the reader is referred to the web version of this article.)

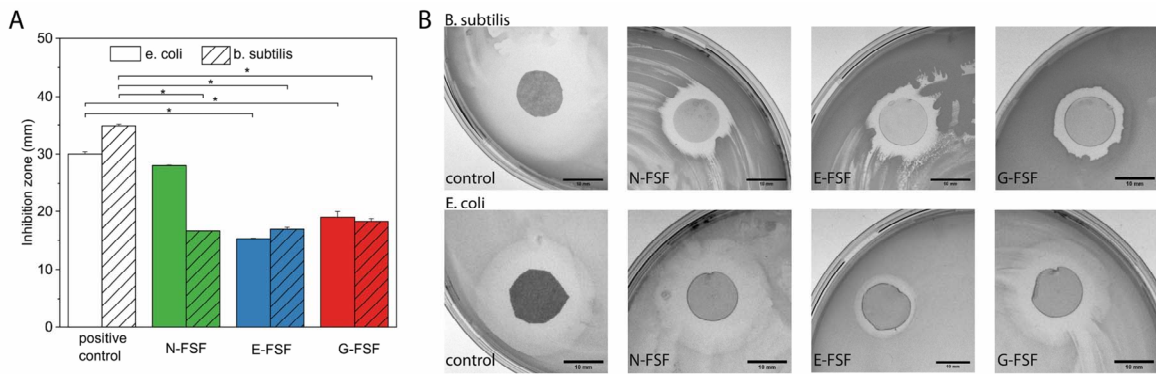


Fig. 8. A) Antibacterial activity of films towards *E. coli* DSM 6897 (G-) and *B. subtilis* DSM 10 (G+). Positive control is kanamycin (0.5 g/L). ($n = 4$, * $p \leq 0.05$). B) Micrographs of antibacterial test. Scale bar = 10 mm.

E. coli like kanamycin but lower for *B. subtilis*. Both crosslinked films show a decreased antibacterial effect indicating that a lowered release/mobility of CHI is probably responsible for that. Indeed, CHI is most probably responsible for the antibacterial effect as shown in other studies [65,66]. In summary, all FSF possess antibacterial activity which is an important finding that further qualifies the FSF developed here for a future application as wound dressing.

4. Conclusions

Here, we could demonstrate that the use of LbL- based dip coating enables the design of FSF, based on the cost effective combination of chitosan, as an antibacterial agent and alginate, which provides swelling capabilities useful for uptake of wound exudates. The most interesting finding are as follows: Additional crosslinking with genipin increases the stability of films *in vivo* and allows the control of FGF2 release, and, in notable contrast to N-FSF, it also improves the general biocompatibility *in vitro* and *in vivo* with a promoting effect on migration and growth of fibroblasts. Hence, free-standing films prepared by LbL-process have a great potential to serve as wound dressing materials that may support regeneration of dermis as a prerequisite for the re-epithelization of wounds. All together the proposed FSF made of alginate and chitosan, crosslinked with genipin and loaded with FGF2 may hold great promises for use as wound dressings which will be studied in future investigations.

Supplementary data to this article can be found online at <https://doi.org/10.1016/j.bioadv.2022.213166>.

CRedit authorship contribution statement

Adrian Hautmann: Conceptualization, Methodology, Software, Investigation, Writing - Original draft, Visualization; Devaki Kedilaya: Conceptualization, Methodology, Investigation; Sanja Stojanović: Methodology, Investigation, Writing - Review & Editing; Milena Radenković: Methodology, Investigation; Christian K. Marx: Methodology, Investigation; Stevo Najman: Resources, Writing - Review & Editing, Supervision; Markus Pietzsch: Resources, Writing - Review & Editing, Supervision; João F. Mano: Conceptualization, Writing - Review & Editing; Thomas Groth: Conceptualization, Methodology, Resources, Writing - Reviewing and Editing, Supervision, Project administration, Funding acquisition.

Declaration of competing interest

The authors declare that they have no known competing financial interests or personal relationships that could have appeared to influence the work reported in this paper.

Data availability

Data will be made available on request.

Acknowledgments

The International Graduate School AGRIPOLY funded by the European Regional Development Fund (ERDF) and the Federal State Saxony-Anhalt supported this work. Additionally, this project was supported by a Project-Related Personal Exchange program funded by the Ministry of Education, Science and Technological Development of the Republic of Serbia and the German Academic Exchange Service (DAAD). Finally, parts of this work were developed within the scope of the project CICECO- Aveiro Institute of Materials, UIDB/50011/2020, UIDP/50011/2020, and LA/P/0006/2020, financed by national funds through the FCT/MEC (PIDDAC).

References

- [1] K. Heyer, K. Herberger, K. Protz, G. Glaeske, M. Augustin, Epidemiology of chronic wounds in Germany: analysis of statutory health insurance data, *Wound Repair Regen.* 24 (2016) 434–442, <https://doi.org/10.1111/wrr.12387>.
- [2] L. Cañedo-Dorantes, M. Cañedo-Ayala, Skin acute wound healing: a comprehensive review, *Int. J. Inflamm.* 2019 (2019), 3706315, <https://doi.org/10.1155/2019/3706315>.
- [3] H. Sorg, D.J. Tilkorn, S. Hager, J. Hauser, U. Mirastschijski, Skin wound healing: an update on the current knowledge and concepts, *Eur. Surg. Res.* 58 (2017) 81–94, <https://doi.org/10.1159/000454919>.
- [4] L. Rittié, Cellular mechanisms of skin repair in humans and other mammals, *J. Cell Commun. Signal.* 10 (2016) 103–120, <https://doi.org/10.1007/s12079-016-0330-1>.
- [5] P. Rousselle, F. Braye, G. Dayan, Re-epithelialization of adult skin wounds: cellular mechanisms and therapeutic strategies, *Adv. Drug Deliv. Rev.* 146 (2019) 344–365, <https://doi.org/10.1016/j.addr.2018.06.019>.
- [6] G. Han, R. Ceilley, Chronic wound healing: a review of current management and treatments, *Adv. Ther.* 34 (2017) 599–610, <https://doi.org/10.1007/s12325-017-0478-y>.
- [7] J. Boateng, O. Catanzano, Advanced therapeutic dressings for effective wound healing—a review, *J. Pharm. Sci.* 104 (2015) 3653–3680, <https://doi.org/10.1002/jps.24610>.
- [8] S. Barrientos, H. Brem, O. Stojadinovic, M. Tomic-Canic, Clinical application of growth factors and cytokines in wound healing, *Wound Repair Regen.* 22 (2014) 569–578, <https://doi.org/10.1111/wrr.12205>.
- [9] Q.M. Nunes, Y. Li, C. Sun, T.K. Kinnunen, D.G. Fernig, Fibroblast growth factors as tissue repair and regeneration therapeutics, *PeerJ* 4 (2016), e1535, <https://doi.org/10.7717/peerj.1535>.
- [10] Z.-H. Jin, Y.-H. Dong, Z.-H. Lou, The effects of fibroblast growth factor-2 delivered via a Gelfoam patch on the regeneration of myringosclerotic traumatic eardrum perforations lying close to the malleus, *Am. J. Otolaryngol.* 38 (2017) 582–587, <https://doi.org/10.1016/j.amjoto.2017.06.005>.
- [11] M. Kitamura, M. Akamatsu, M. Machigashira, Y. Hara, R. Sakagami, T. Hirofujii, T. Hamachi, K. Maeda, M. Yokota, J. Kido, T. Nagata, H. Kurihara, S. Takashiba, T. Sibutani, M. Fukuda, T. Noguchi, K. Yamazaki, H. Yoshie, K. Iroji, T. Arai, T. Nakagawa, K. Ito, S. Oda, Y. Izumi, Y. Ogata, S. Yamada, H. Shimauchi, K. Kunimatsu, M. Kawanami, T. Fujii, Y. Furuichi, T. Furuuchi, T. Sasano, E. Imai, M. Omae, M. Watanuki, S. Murakami, FGF-2 stimulates periodontal regeneration: results of a multi-center randomized clinical trial, *J. Dent. Res.* 90 (2011) 35–40, <https://doi.org/10.1177/0022034510384616>.
- [12] S. Akita, K. Akino, T. Imaizumi, A. Hirano, Basic fibroblast growth factor accelerates and improves second-degree burn wound healing, *Wound Repair Regen.* 16 (2008) 635–641, <https://doi.org/10.1111/j.1524-475X.2008.00414.x>.
- [13] G. Gainza, S. Villullas, J.L. Pedraz, R.M. Hernandez, M. Igartua, Advances in drug delivery systems (DDSs) to release growth factors for wound healing and skin regeneration, *nanomedicine: nanotechnology, Biol. Med.* 11 (2015) 1551–1573, <https://doi.org/10.1016/j.nano.2015.03.002>.
- [14] A. Weltrowski, M.-L. da Silva Almeida, D. Peschel, K. Zhang, S. Fischer, T. Groth, Mitogenic activity of sulfated chitosan and cellulose derivatives is related to protection of FGF-2 from proteolytic cleavage, *Macromol. Biosci.* 12 (2012) 740–750, <https://doi.org/10.1002/mabi.201100518>.
- [15] K. Mizuno, K. Yamamura, K. Yano, T. Osada, S. Saeki, N. Takimoto, T. Sakurai, Y. Nimura, Effect of chitosan film containing basic fibroblast growth factor on wound healing in genetically diabetic mice, *J. Biomed. Mater. Res. A* 64 (2003) 177–181, <https://doi.org/10.1002/jbm.a.10396>.
- [16] X. Zhang, X. Kang, L. Jin, J. Bai, W. Liu, Z. Wang, Stimulation of wound healing using bioinspired hydrogels with basic fibroblast growth factor (bFGF), *IJN* 13 (2018) 3897–3906, <https://doi.org/10.2147/IJN.S168998>.
- [17] X. Sun, L. Cheng, J. Zhao, R. Jin, B. Sun, Y. Shi, L. Zhang, Y. Zhang, W. Cui, bFGF-grafted electrospun fibrous scaffolds via poly(dopamine) for skin wound healing, *J. Mater. Chem. B* 2 (2014) 3636–3645, <https://doi.org/10.1039/C3TB21814G>.
- [18] J.M. Silva, S.G. Caridade, R.R. Costa, N.M. Alves, T. Groth, C. Picart, R.L. Reis, J. F. Mano, pH responsiveness of multilayered films and membranes made of polysaccharides, *Langmuir* 31 (2015) 11318–11328, <https://doi.org/10.1021/acs.langmuir.5b02478>.
- [19] B.A. Aderibigbe, B. Buyana, Alginate in wound dressings, *Pharmaceutics* 10 (2018) 42, <https://doi.org/10.3390/pharmaceutics10020042>.
- [20] R.R. Costa, M. Alatorre-Meda, J.F. Mano, Drug nano-reservoirs synthesized using layer-by-layer technologies, *Biotechnol. Adv.* 33 (2015) 1310–1326, <https://doi.org/10.1016/j.biotechadv.2015.04.005>.
- [21] C. Husteden, F. Doberenz, N. Goergen, S.R. Pinnapreddy, C. Janich, A. Langner, F. Syrowatka, A. Repanas, F. Erdmann, J. Jedelská, U. Bakowsky, T. Groth, C. Wölk, Contact-triggered lipofection from multilayer films designed as surfaces for in situ transfection strategies in tissue engineering, *ACS Appl. Mater. Interfaces* 12 (2020) 8963–8977, <https://doi.org/10.1021/acsami.9b18968>.
- [22] R. Kurapati, T.W. Groth, A.M. Raichur, Recent developments in layer-by-layer technique for drug delivery applications, *ACS Appl. Bio Mater.* 2 (2019) 5512–5527, <https://doi.org/10.1021/acsabm.9b00703>.
- [23] J.M. Silva, A.R.C. Duarte, S.G. Caridade, C. Picart, R.L. Reis, J.F. Mano, Tailored freestanding multilayered membranes based on chitosan and alginate, *Biomacromolecules* 15 (2014) 3817–3826, <https://doi.org/10.1021/bm501156v>.
- [24] A.S. Ivanov, L.V. Pershina, K.G. Nikolaev, E.V. Skorb, Recent progress of layer-by-layer assembly, free-standing film and hydrogel based on polyelectrolytes, *Macromol. Biosci.* 21 (2021), e2100117, <https://doi.org/10.1002/mabi.202100117>.

Chapter 5 - Design of a composite wound dressing: Combining an electrospun fleece with a free-standing multilayer film

This chapter builds on the cumulative insights gained from the previous studies. Previous we concluded that FSFs can be used as reservoirs for growth factors and have generally very suitable characteristics for the use as wound dressings. Additionally, LbL assemblies can modulate inflammation using HA and Hep. However, cell adhesion directly on multilayered FSFs is rather poor, due to their very hydrophilic and soft nature. This time we hypothesized that a combination of a FSF with an electrospun fleece could improve cell adhesion and cell growth facilitated by the electrospun scaffold and modulate inflammation by the addition of HA to the multilayers. However, this novel approach introduces a fresh set of technical challenges, specifically the preservation of the (nano)-structure of the electrospun fleece while ensuring that the multilayer film covers only one side. To overcome this challenge, we adopted a spray coating technique to enable the asymmetric construction of the composite, allowing us to successfully integrate the two components. The spray coating also allowed the utilization of HA as building block, since HA leads to thin and poorly detachable films in the dipping process. Nonetheless, for the bulk of the layers ALG was used to harness the fast buildup of CHI/ALG layers, which are intended to function as a swelling and protection layer. Finally, the layer buildup time was reduced to 4 hours for 150 bilayers compared to 24 hours for 100 bilayers in the prior dip coating study through optimization of the process. The resulting composite has a final thickness of approximately 1 mm. The gelatin fleece, used as the substrate, underwent partial crosslinking through exposure to formaldehyde vapor before spray coating, as uncrosslinked gelatin fleece is not stable enough to allow the water-based layer-by-layer process on top. Validated through electron scanning microscopy, confocal microscopy, profilometry, and nano-tomography the nano-topography of the fleece was successfully preserved. To assess biocompatibility, we conducted cell proliferation experiments using human dermal fibroblasts and THP-1 derived macrophages. These experiments, supported by immunohistochemical staining and a pro/anti-inflammatory cytokine assay, demonstrate the non-cytotoxic nature and *in vitro* biocompatibility of the composite. The electrospun fleece fibers serve as a robust scaffold, notably enhancing cell adhesion and proliferation. Meanwhile, the modular architecture of the multilayered FSF, coupled with genipin crosslinking, offers the ability to finely modulate the anti-inflammatory response through HA. In summary, these findings position the composite as a promising cornerstone for the development of an innovative wound dressing solution.



Contents lists available at ScienceDirect

Next Materials

journal homepage: www.sciencedirect.com/journal/next-materials

Research article

Design of a composite wound dressing: Combining an electrospun fleece with a free-standing multilayer film

Adrian Hautmann^a, Tobias Hedtke^b, Sonia Sislema-Muñoz^a, Juliana Martins-Schalinski^b, Christian E.H. Schmelzer^b, Thomas Groth^{a,c,*}

^a Department Biomedical Materials, Institute of Pharmacy, Martin Luther University Halle-Wittenberg, Germany

^b Fraunhofer Institute for Microstructure of Materials and Systems IMWS Halle (Saale), Germany

^c Interdisciplinary Center for Materials Science, Martin Luther University Halle-Wittenberg, Germany



ARTICLE INFO

Keywords:

Layer-by-Layer
Electrospinning
Wound Dressing
Free-standing Film
Freestanding Membranes

ABSTRACT

Chronic skin wounds place a heavy burden on patients and healthcare systems. To address this problem, we have developed a novel composite material consisting of an electrospun fleece and a free-standing multilayer film that combines the wound healing benefits of both materials. In detail a combination of spray coating and electrospinning is used to create a layer-by-layer film on top of a gelatin fleece, with a final thickness of about 1 mm. A gelatin fleece is partially crosslinked in formaldehyde vapor and 30 pH-sensitive bonding bilayers of partially oxidized hyaluronic acid (HIA) and chitosan, followed by 120 bilayers of alginate and chitosan are sprayed on top. The resulting composite is crosslinked with genipin. Uncrosslinked and genipin crosslinked composites are compared to the unprocessed fleece and free-standing multilayer film. The spray coating method produces a stable composite, allows a fast growth of the film part and most importantly retains the nano-topography of the fleece side as confirmed by electron microscopy, profilometry, nano-tomography and dynamic mechanical analysis. To test biocompatibility, cell proliferation experiments with human dermal fibroblasts and THP-1 derived macrophages are performed, proliferative assays are accompanied by immunohistochemical staining and a pro/anti-inflammatory cytokine assay. The composite shows no cytotoxicity and is biocompatible in vitro. Furthermore, the electrospun fibers of the fleece act as a scaffold to highly promote cell adhesion and proliferation, while the modular design of the multilayer free-standing film, in combination with genipin crosslinking, allows the tuning of the anti-inflammatory effect by HA. Overall, the composite seems to be a promising starting point for the design of a novel wound dressing.

1. Introduction

Chronic wounds pose a significant challenge to healthcare systems worldwide, affecting patients' well-being and incurring substantial economic costs. These wounds, which encompass conditions such as diabetic foot ulcers, venous ulcers, and pressure ulcers create a substantial burden on both patients and healthcare providers [1]. Currently, the therapy is characterized by frequent medical interventions, long healing times and long-term continuous treatment with a variety of wound dressings [2]. Acute skin wound healing is characterized by the four dynamic, timely and locally orchestrated processes of hemostasis, inflammation, cell proliferation and tissue remodeling [3]. In contrast, chronic wounds deviate from this normal progression and remain stuck in the inflammatory stage, which does not allow the initiation of the

proliferation phase. This chronic inflammation is characterized by elevated protease activity, increased pro-inflammatory cytokines, and reduced levels of growth factors [4]. The impaired angiogenesis leads to insufficient blood supply and therefore lowered oxygenation of the wound bed, perpetuating the inflammation. Similarly, lymphatic vessels are affected in chronic wounds, leading to inadequate drainage of interstitial fluid and a reduced immune response [5]. Furthermore, surveys in the US show that nearly 60% of chronic wounds are associated with microbial infections [6].

Key cell types involved in wound healing are macrophages and fibroblasts. Macrophages, as immune cells, act as 'clean-up' cells, removing debris and bacteria from the wound site in the inflammation phase [7]. In this phase, monocytes are recruited to the wound site, differentiate to macrophages and adopt an activated M1-like phenotype,

* Correspondence to: Department Biomedical Materials, Institute of Pharmacy, Martin Luther University Halle-Wittenberg, 06099 Halle (Saale), Germany.
E-mail address: thomas.groth@pharmazie.uni-halle.de (T. Groth).

<https://doi.org/10.1016/j.nxmate.2023.100060>

Received 1 July 2023; Received in revised form 9 October 2023; Accepted 31 October 2023

Available online 8 February 2024

2949-8228/© 2023 The Authors. Published by Elsevier Ltd. This is an open access article under the CC BY-NC-ND license (<http://creativecommons.org/licenses/by-nc-nd/4.0/>).

driven by pro-inflammatory cytokines, DAMPs (damage-associated molecular patterns) and PAMPs (pathogen-associated molecular patterns) [8]. M1 macrophages exhibit enhanced microbicidal activity by producing reactive oxygen species (ROS) and antimicrobial peptides that contribute to pathogen clearance [4]. They are also capable of engulfing and eliminating foreign particles, debris and apoptotic cells present in the wound area, as well as capturing and displaying foreign antigens, thereby activating the adaptive immune response [9]. Over time, in normal wound healing, external stimuli, for example cytokines secreted by Th2 lymphocytes, contribute to a shift in macrophage activation towards the M2 phenotype [10]. The transition from M1 to M2 macrophages is a dynamic process in wound healing where control of inflammation and tissue repair promotion is essential for the resolution of inflammation and the subsequent phases of wound healing [10]. The M2 activation states include a number of different phenotypes that are associated with regenerative functions. Through their different activation states, macrophages exert regulatory effects on fibroblasts, angiogenesis and wound healing by producing a range of growth factors and cytokines [7]. For example, M1-like macrophages secrete pro-inflammatory interleukin-6 (IL-6), while M2-like macrophages produce interleukin-10 (IL-10), which suppresses the inflammatory response while stimulating fibroblast proliferation and collagen synthesis [7,10]. Fibroblasts migrate to the wound site and secrete collagens, GAGs (glycosaminoglycans), proteoglycans and glycoproteins to form the extracellular matrix that is critical for wound closure [11]. The combined efforts of fibroblasts and macrophages are essential for the regeneration of injured tissue and are the basis for wound contraction and the reepithelization by keratinocytes [7].

To alleviate chronic wounds, conventional wound dressings aim to provide an optimal wound healing environment. Their purposes include the maintenance of a moist healing environment (e.g., films, foams, hydrocolloids, hydrogels), reduction of bacterial load and infection (e.g., dressings containing silver or iodine) or the support of the healing process by collagen, cellulose and other factors [12]. Wound dressings can be produced by a variety of techniques, such as fibrous sheets or fleeces prepared using conventional textile technologies but also electrospinning. Moreover, there are membranes and films prepared by solvent-based techniques or foams by thermal phase inversion techniques [13–15]. A review by Han and Ceilley highlights the limitations of current wound dressing materials, which often address only some of the challenges of chronic wounds and lack active components that promote wound healing through increased activity of tissue cells and neovascularization [16]. Therefore, the complexity of the healing process and the phase dependent requirements of wound dressings have led to the research of active biodegradable scaffolds, which mimic the skin microenvironment [17]. The optimal resolution of chronic wounds requires an integrated approach addressing both the resolution of inflammation and the facilitation of fibroblast migration. One promising strategy might be the combination of composite electrospun scaffolds and free-standing multilayer films prepared by layer-by-layer (LbL) technique to create a controlled microenvironment for wound healing.

Electrospun fibers have gained significant attention as a material for wound dressing applications due to their unique microstructure and mechanical properties [18]. Their small diameter and large surface area provide a suitable environment for cell attachment, proliferation and differentiation, while their high porosity and mechanical strength supports wound healing by providing a supportive scaffold for tissue regeneration [18]. The promoting effect of proteins like collagen, fibrinogen and others implemented into nanofiber matrices on cell attachment and proliferation was proven in several studies [19,20]. Gelatin is a popular biomaterial for electrospinning due to its inherent bioactivity, cytocompatibility, low immunogenicity and ease of processing [21]. Gelatin has been shown to contain functional peptide sequences associated with cell surface receptor integrin binding, the best known being the arginine-glycine-aspartic acid RGD sequence [22]. Electrospun gelatin fleece can serve as a scaffold for fibroblasts, which

are responsible for the production of collagen thereby enhancing the formation of granulation tissue and wound closure [23]. A drawback of gelatin is its weak mechanical properties and poor stability in aqueous conditions and against proteolytic enzymes which necessitates a cross-linking step [24].

The LbL technique, based on the complexation of polyelectrolytes on solid surfaces allows the formation of nanometer sized surface coatings but also free-standing films in millimeter scale by the automation of layer deposition [25–27]. Since polysaccharides like alginate, GAGs (e.g. Hyaluronan), and chitosan represent polyelectrolytes they can be used in the LbL process to generate biogenic, biocompatible and even bioactive polyelectrolyte multilayers (PEMs). Such multilayers can have anti-inflammatory, bioactive and anti-bacterial properties dependent on the use of specific polysaccharides [28–31]. Recently, we have demonstrated that such multilayer films can be prepared as free-standing films with a thickness of around 500 μm combined with the incorporation of bioactive factors for controlled release of growth factors, offering potential benefits in chronic wound healing [30]. With the substantial increase of the number of layers, the construction methods of LbL systems becomes increasingly important. Spray coating offers distinctive advantages, as the complexation of the polyelectrolytes is accelerated by the impact of the charged species on the previous layer, instead of relying only on diffusion [32]. Despite yielding thinner free-standing films compared to dip coating, spray coating allows therefore faster complexation and eliminates the need for a rinsing step [32,33]. Alginate (ALG), chitosan (CHI), and hyaluronic acid (HA) have been extensively studied for their wound healing properties and were therefore selected as polyelectrolytes in this study [34,35]. HA and ALG represent polyanions, while CHI, in aqueous solutions with a pH below 6, is a polycation to form PEMs that can control cell adhesion and differentiation [36,37]. ALG, derived from brown seaweed, is a common constituent of hydrogels and can absorb large amounts of wound exudates, creating a moist environment that promotes wound healing [38]. CHI, has a positive charge and can form electrostatic interactions with negatively charged bacteria, helping to prevent infection [39]. HA, a naturally occurring glycosaminoglycan in the body, has a high water-holding capacity which helps to establish a moist wound environment, promoting fibroblasts growth, migration and collagen synthesis, which is important for granulation tissue formation [40]. Most importantly, high molecular weight HA has also anti-inflammatory properties that rely on the binding to the cell receptor CD44, which leads to downregulation of toll-like receptor (TLR) signaling, which in turn mediates NF- κB activation [41,42]. As a result, HA binding to CD44 promotes the release of anti-inflammatory cytokines such as IL-2 and IL-10, switching macrophages to a M2-like state [43]. Due to the presence of ROS (reactive oxygen species) and hyaluronidases in the wound bed, high molecular weight-HA (HMW-HA) gets degraded to low molecular weight HA (LMW-HA) [5]. Low-HA has been found to promote angiogenesis and lymphangiogenesis, mediated by the LYVE-signaling pathway, contributing to the formation of new blood and lymphatic vessels, which are crucial for wound healing [44]. Due to chemical modifications, it is also used as a popular polymer in controlled drug release systems by retaining its bioactivity [44].

Here, for the first time, PEMs were constructed on an electrospun fleece, by spray coating. The resulting composites attempt to incorporate both biophysical and biochemical cues that should increase cell adhesion, proliferation and anti-inflammatory properties. In particular, we created a composite film consisting of a gelatin-based nanofiber fleece as the basal layer and a thicker multilayer film of HA, CHI and ALG on top. The preserved nano-topography on the cell-facing side is intended to provide topographical cues, while the spray-coated multilayer film with HA provides anti-inflammatory biological cues, has the potential to absorb wound fluid and has antibacterial properties due to the inclusion of CHI and ALG.

2. Methods

2.1. Preparation of composites

2.1.1. Oxidation of hyaluronic acid

Oxidation of HA was conducted according to a protocol published previously [45]. The process is illustrated in Fig. 1. Briefly, 1 g of HA was added slowly into 200 ml dH₂O and stirred overnight. An equivalent of 1 of NaIO₃ was then added (0.530 g) and incubated for 24 h in the dark. The product was dialyzed for 3 days against water and lastly freeze dried. The final product was stored at 4 °C for further usage. The oxidation degree was measured by titration and Schiff's test protocols found in above mentioned publication [45].

2.1.2. Fluorescence labelling of chitosan

For an estimated labelling of 20% 100 ml CHI 2 mg/ml solution was mixed with 46 mg fluorescein isothiocyanate (FITC) dissolved in 9 ml of dehydrated methanol and stirred for 3 h in the dark at room temperature. The mixture was precipitated by adding 0.2 M of NaOH until it reached pH 10. The next step was centrifugation at 3500 g for 10 min. Then, the precipitate was washed with methanol three times till there was no fluorescence detected in supernatant. After re-dissolving the precipitate in 30 ml 0.1 M acetic acid the mixture was dialyzed in the dark against distilled water at 4 °C for 3 days. Finally, the mixture was freeze dried for 24 h in the dark.

2.1.3. 6-aminofluorescence labelling of hyaluronic acid

An amount of 200 mg of HA was dissolved in 100 ml 2-(N-morpholino)ethanesulfonic acid (MES) buffer (50 mmol/L, pH 4.75) overnight. Followed by the addition 0.996 mmol of 1-Ethyl-3-(3-dimethylamino-propyl) carbodiimide (EDC) as well as 0.996 mmol of NHS to the solution and a pH adjustment to 7 with sodium hydroxide. For 10% of labelling 17.296 ml of 6-Aminofluorescence (1 mg/ml) solution in dimethyl sulfoxide (DMSO) was added and stirred for 18 h in the dark at room temperature. The product was dialyzed for at least three days until there was no fluorescence detected in the dialysis water. Freeze drying was performed to obtain the final product.

2.1.4. Rhodamine labelling of chitosan

To prepare rhodamine-labelled CHI (CHI-rho), 100 mg of CHI was dissolved in 10 ml of 0.1 M acetic acid, then, 10 ml of methanol and 3.25 ml of 2 mg/ml rhodamine B isothiocyanate (RITC) in methanol were added. The mixture was stirred for 18 h in the dark, followed by purification of the rhodamine-labelled CHI through dialysis. The solution was freeze dried and stored at 4 °C.

2.1.5. Electrospinning

Gelatin was dissolved in acetic acid aqueous solution (50%, v/v) to a final concentration of 20% (w/v). Stirring was necessary to obtain a homogeneous mixture. Electrospinning was performed on a LE-50 electrospinning device (Fluidnatek, Valencia, Spain) equipped with a drum collector and a moving emitter stage. The spinning distance was 180 mm, emitter and collector voltages were set to + 20 kV and - 6 kV, respectively. Fibers were collected on a polypropylene substrate that was fixed to the drum collector. The drum collector was set to 300 rpm. Electrospun gelatin fiber mats with an approximate area of 15 × 30 cm²

were obtained.

2.1.6. Crosslinking of fleece

A container filled with a volume of 25 ml of a 37% formaldehyde aqueous solution was placed inside a glass desiccator (15.5 cm of diameter and 20 cm height) following an already published protocol [46]. The electrospun gelatin mats were cut to pieces of 5 × 5 cm² and incubated in the closed desiccator over a formaldehyde reservoir for 90 min

2.1.7. Spray coating

A 2 mg/ml of CHI solution was prepared by dissolving CHI in 150 mM NaCl solution at 50 °C for 3 h, pH was adjusted to 4 using a 30% acetic acid solution. ALG (5 mg/ml) oxidized hyaluronic acid (oxHA) and HA solution (2 mg/ml) were dissolved in 150 mM NaCl solution, and pH adjusted to 4 using HCl. Afterwards, all solutions were sterilized by filtration using 0.22 μm pore size filters and stored at 4 °C. A vertical spray coater (ND-SP Precision Spray Coater, Nadetech, Spain) was modified to spray horizontally, allowing drainage of excessive poly-electrolyte solution and avoidance of washing steps during layer-by-layer build up. Additionally, a script was written to allow unlimited deposition loops, which was previously limited to 4 bilayers by the proprietary ND-SP spray coater software (2.0.1.0). The electrospun fleece was fixed to the vertical spraying area by a custom 3d printed clamp and for the preparation of free-standing films, a polypropylene substrate was used instead of the fleece. All four syringes were fixed and filled with polyelectrolytes. The first and third syringes with the CHI solution, and the second and forth syringes with the respective poly-anion solutions. The first 10 sprayed bilayers contained oxHA and CHI, while the following 20 bilayers, HA and CHI. The subsequent 120 bilayers were made up of ALG and CHI. Regarding the free-standing film, samples were peeled from the polypropylene substrate. The final samples with 150 bilayers were cut into a round shape of 1 cm diameter each, employing a toggle press.

2.1.8. Crosslinking of composites

The cut composites were placed in a 24 well plate and crosslinking started by adding to each well 1 ml of 1 mg/ml Genipin solution prepared in distilled water. The crosslinking reaction took place at 37 °C for 18 h. To stop the reaction the genipin solution was removed, followed by the addition of 70% ethanol for 15 min, which was useful to maintain sterility of the samples. The films were then washed 3 times with sterile PBS for 15 min each under a laminar flow hood.

2.2. Physical studies

2.2.1. Amino acid analysis

To determine the crosslinking degree of fleece, amino acid analysis was performed. Gelatin granulate, formaldehyde-crosslinked and uncrosslinked electrospun gelatin nanofiber fleeces were hydrolyzed in 6 N HCl at 110 °C for 24 h. Free amino acids were subsequently analyzed on a Biochrom 30 amino acid analyzer (Biochrom, UK) according to the standard protocol provided by the manufacturer. For detection and quantification, post-column ninhydrin derivatization was applied with leucine as an external standard.

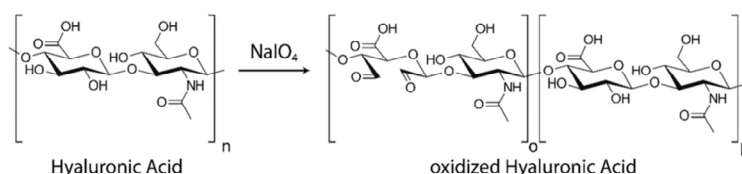


Fig. 1. Introduction of an aldehyde group into HA by sodium-periodate.

2.2.2. Film growth measurements

Confocal laser scanning microscopy (CLSM) was performed with a Carl Zeiss 710 LSM microscope to investigate the film's thickness, swelling and the location of HA-FITC. The samples were prepared according to the described protocol with fluorescence labelled polyelectrolyte solutions and dried in desiccator before observation. The FITC and rhodamine fluorescence was detected using z-stack mode. As for the swelling studies, the dried samples were immersed in PBS after the first observation for 24 h. The microscopy pictures were then extracted with ImageJ (ver. 1.53p), using the 3D object plugin to detect the volume in μm^3 [47]. The volume was divided by the image area to calculate the thickness of respective fluorescent labelled polyelectrolyte.

2.2.3. Profilometry

Optical profilometric analyses were performed using a laser-scanning microscope (VK-X1050, Keyence) to determine the thickness. The wet samples were placed on a slide and a part of the sample was cut with a razor blade to obtain a smooth edge for height measurement. The analysis was performed with a red laser at 661 nm in reflection mode.

2.2.4. Environmental scanning electron microscope

The samples were cut from each specimen into smaller pieces of approximately $2 \times 2 \text{ mm}^2$ and placed on self-adhesive conductive carbon tape (Plano GmbH, Wetzlar, Germany) on microscope stubs. Afterwards the samples were then coated with a thin layer of platinum (2–3 nm) and analyzed on a Quanta 3D Field-Emission Gun Scanning Electron Microscope (FEG-SEM) (FEI, Hillsboro, OR, USA) at an acceleration voltage of 5 kV.

2.2.5. Nano-computed tomography

Imaging experiments were performed on dried samples of the composite materials in a Carl Zeiss Xradia 810 Ultra X-ray microscope (XRM) equipped with a chromium source (5.4 keV). A small piece of each sample was glued onto the tip of a metallic pin that was inserted in the sample holder of the microscope. The imaging experiments were performed using Zernike phase-contrast, a field-of-view of $64 \mu\text{m}^2$ and a total of 1001 projection images were acquired by rotating the sample over 180° . The exposure time for each projection was 20 s and a detector binning of 2×2 was used, resulting in an isotropic voxel size of 128 nm in the final image. Image reconstruction was performed by a filtered back-projection algorithm using the XMReconstructor software integrated into the microscope. The tomograms obtained were then exported as a stack of 16-bit TIFF images and visualized in 3D using Avizo (Thermo Fischer, version 3D 2022.2). Image processing and segmentation were done in the same program, by first applying a median filter followed by segmenting the sample using an interactive threshold. Fiber tracing was done using an auto skeleton module, porosity was estimated by the volume fraction module, and fiber diameter by the spatial graph statistics module. Considering resolution, only values larger than 3 pixels were considered in the fiber diameter distribution.

2.2.6. Dynamic mechanical analysis

A TA.XTplusC from Stable Micro Systems (Godalming, UK) was used to determine mechanical properties using the penetrating ball method. Samples were fixed over a perforated metal plate. A 5 mm diameter spherical ball probe was pressed into the surface at a constant speed of 1 mm/s and the force-displacement relationship was recorded after reaching a trigger force of 0.005 N. The sampling rate was set to 200 measurements per second and the test was terminated when the material failed. The ultimate tensile strength was calculated by dividing the force applied at the failure point by the area in contact with the sample. For determination of the Young's modulus the initial linear slope between 1% and 4% of the stress/strain curve was used.

2.3. Biological studies

2.3.1. Cell culture

In this study human dermal fibroblast (HDF) and THP-1 human monocytes were used. The HDF were grown in Dulbecco's modified Eagle medium (DMEM without pyruvate, with 4.5 g/L glucose) (Carl Roth) and THP-1 in RPMI1640 (with L-Glutamine) (Lonza), both supplemented with 10% fetal bovine serum (FBS, Biochrom AG, Berlin, Germany) and antibiotic-antimycotic solution (AAS, Lonza, Wuppertal, Germany) at 37°C in a humidified 5% CO_2 using a NUAIRE DH Auto-flow incubator (NuAire Corp, Plymouth, MN, USA). Cells were cultured in T75 cell culture flasks and media was changed every second day; cell subculturing was performed to maintain cell density from 5×10^5 to 5×10^6 cell per ml. HDF cells were harvested with 0.25% trypsin/0.02% ethylenediaminetetraacetic acid (EDTA) solution at 37°C for 3–5 min. The trypsin reaction was stopped by adding DMEM with 10% FBS. Subsequently, the cells were re-suspended and seeded at a desired density on the well plate. The THP-1 cells were differentiated with 200 nM phorbol-12-myristate-13-acetate (PMA) to M0-like macrophages following a published procedure [42]. Afterwards cells were harvested with 0.25% trypsin/0.02% EDTA solution at 37°C for 3 min and the help of a cell scraper.

2.3.2. Biocompatibility studies

All samples were sterilized by immersion in 70% ethanol, with subsequent threefold washing with PBS for 5 min each. A cell suspension with a density of 25,000 cells per well was seeded in a 24 well plate and incubated for 12 h. After a media change composites and films were carefully added on top of the cells after the latter were attached to the well bottom following a previous published protocol [30]. Cell damage was avoided as the films float over the cell layer. After 24 h the films were temporarily transferred to a new well plate. Then samples were removed before each measurement, to avoid effects of cell adhesion to the samples. The metabolic activity of NHDF cells cultured exposed to the composites and films were analyzed using a resazurin based assay (Deep Blue Cell Viability Kit (BioLegend, San Diego, USA)). Deep Blue was prepared at a ratio of 1:10 with colorless DMEM (without pyruvate, with 4.5 g/L glucose (Lonza, Basel, Switzerland)), added to each well and incubated at 37°C for 3 h. After incubation, duplicates of 100 μl of the supernatant were transferred to a black 96-well-plate (Greiner Bio-One International GmbH). The converted fluorescent products were photometrically quantified at an excitation wavelength of 544 nm and an emission wavelength of 590 nm using a plate reader (FLUOstar, BMG LabTech, Offenburg, Germany). Cells without samples were used as negative control. After measurements were conducted, the DeepBlue medium was aspirated from the wells and was replaced by DMEM medium. The films, which were stored in a different well plate, were added back to the initial wells plate. The same procedure was repeated on day 3 and day 7.

2.3.3. Live/Dead cell assay

HDF Cells (50,000 cells/well) were incubated for 7 days on top of the samples. Medium change was undertaken every 3 days. Z-Stacks of Samples were recording using a Carl Zeiss ZEN 710 LSM after day 7. Z-stacks were necessary since the samples possess a macroscopically rough surface. A max-intensity projection process was undertaken with ZEN 2012 (v.8.1) to add up all signals present on all slices of the z-stack. Topro3 (Thermo Fisher Scientific, Germany) was used to stain any present DNA content, which allows the location of nuclei. CellTracker Green CMFDA (Thermo Fisher Scientific, Germany), which is only contained in the cell by metabolically active cells, was used to stain living cells. With ImageJ (ver. 1.53p) the number of nuclei was determined by thresholding and particle analysis. Afterwards a cell mask was created using the thresholded CellTracker Green CMFDA channel. Finally, the ImageJ image calculator was used to subtract the cell mask from the nucleus mask. Any remaining particles (stained DNA without Co-

Localization of a living cell) were considered dead cells.

2.3.4. Pro- and anti-inflammatory cytokine production assay

To assess the potential anti-inflammatory activity of the composites, the concentration of Interleukin 6 and 10 secreted by THP-1 derived macrophages was assessed by the enzyme-linked immunosorbent assay (ELISA). Previously sterilized, native composites, genipin crosslinked composites and fleece were placed into two 24-well tissue culture plates and fixed in place by glass cloning rings. Then, 250,000 THP-1 derived macrophages were seeded on top of each sample, and in empty wells as control sample. After 24 h incubation at 37 °C, 5% CO₂ in humidified air, the supernatant was collected from each well and kept in low protein binding tubes (Protein LoBind, Eppendorf, Germany) at -80 °C for further analysis. Both plates with samples were threefold washed with PBS. To one plate 500 µl of fresh media was added, while to the second plate 500 µl media containing lipopolysaccharides (LPS) at a concentration of 1 µg/ml, similarly, to above mentioned conditions after 24 h incubation the supernatant was collected and kept at -80 °C. Afterwards, plates were washed with PBS and samples were transferred to fresh well plates for cell viability assay, as previously described, by resazurin based DeepBlue Assay. Collected supernatant from first and second day of culturing were analyzed to detect the pro-inflammatory cytokine IL-6 and anti-inflammatory cytokine IL-10. Assays were conducted according to manufacturer instructions for Human IL-6 and Human IL-10 with the standard ABTS ELISA development kit (Peprotech, USA). Color development was monitored each 5 min with an ELISA plate reader at 405 nm and wavelength correction at 620 nm, during 30 and 40 min respectively.

2.3.5. Statistical testing

Quantitative data was statistically processed using OriginPro 2019 (v.9.6.0.172, OriginLab Corporation, Northampton, USA). Normally distribution was verified by Shapiro-Wilk. Subsequently, one-way analysis of variance (ANOVA) with a post-hoc Tukey test was used. Nonparametric data were tested with a Kruskal-Wallis test. The data is represented as mean values ± standard deviations (SD). Statistical significance is shown by asterisks in the figures ($p \leq 0.05$).

3. Results and discussion

3.1. Physical studies

3.1.1. Fleece characterization

Electrospun nanofiber fleeces can provide nano-topography that greatly improves cell adhesion and growth. However, gelatin-based fleeces lack stability in aqueous media and face proteolytic degradation in a physiological environment [21]. Since the subsequent spray coating process relies on polyelectrolytes dissolved in water, the fleeces were crosslinked with formaldehyde vapor before further processing. Formaldehyde introduces covalent crosslinks in the protein fleece that stabilize the fibrous structure. Crosslinking in liquid phase would alter the microstructure due to fiber swelling. An amino acid analysis confirmed a reduced amount of the amino acids lysine and tyrosine, which are involved in formaldehyde-mediated crosslinking (Fig. 2A). The detectable amount of free lysine after crosslinking decreased by 10%. No free tyrosine was detectable after formaldehyde treatment. The topography of the crosslinked electrospun elastin/gelatin nanofibrous fleece was analyzed by nanoscale X-ray computed tomography (nano-CT) using Zernike phase contrast. A smooth fiber structure can be confirmed throughout the whole fleece (Fig. 2B). The mean fiber diameter after crosslinking was $0.28 \mu\text{m} \pm 0.08 \mu\text{m}$ as shown in Fig. 2C, a representation of the microstructure. The porosity was calculated from the nano-CT data to be 75%. Both fiber diameter and porosity are known to stimulate fibroblast growth in this range [48].

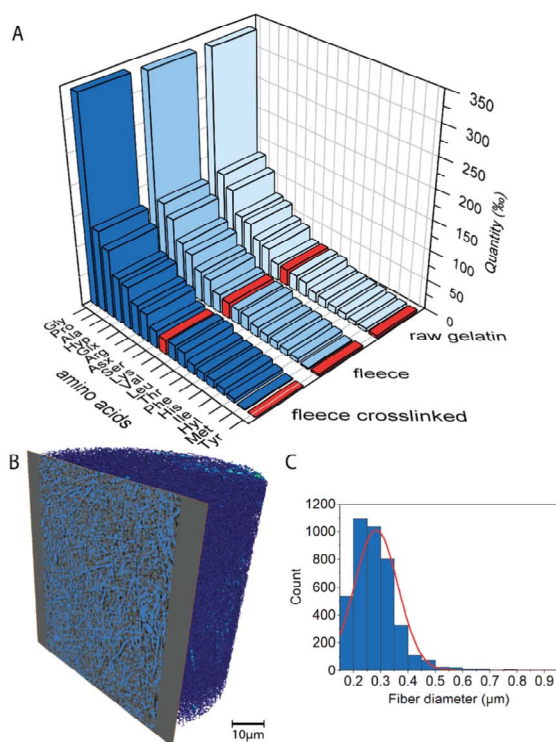


Fig. 2. A) Amino acid analysis. In red are the quantities of the primary amine-containing amino acids lysine and tyrosine marked. These are noticeably decreased between the uncrosslinked and crosslinked fleece. B) Nano-CT image of fleece representing the microstructure of the electrospun formaldehyde crosslinked gelatin fleece. C) Fiber diameter distribution of the electrospun elastin/gelatin fleece after chemical crosslinking with formaldehyde vapor.

3.1.2. Composite architecture

Spray coating has been shown to be a superior method compared to dip coating in LbL assembly, as it allows for faster deposition of the polyelectrolytes, and eliminates the need for washing, provided sufficient drainage is achieved [32]. By modifying the spray coater to spray horizontally, we could reduce the time for the preparation of one layer on an area of $15 \times 15 \text{ cm}$ to 1.6 mins. Additionally, the crosslinking of the electrospun fleece was important to guarantee stability of this substrate during the full duration of the spray coating process, where large quantities of aqueous solutions were used. To functionalize the composite and improve its stability, a complex film architecture was selected; The first 10 bilayers were comprised of alternating oxHA and CHI, while the next 20 bilayers of HA/CHI, the final 120 bilayers consisted of ALG/CHI (as shown in Fig. 3).

The purpose of the first 10 bilayers was to enhance the bonding between the layers and the electrospun fleece, by utilizing oxHA, which allows crosslinking of amine groups by imine bond formation [48,49]. The successful oxidation was confirmed by Schiff reaction. A degree of substitution of $20.85 \pm 1.1\%$ was measured, indicating a comparable degree of substitution to earlier studies employing oxHA for PEMs. [49]. The next 20 bilayers were made up of native HA and CHI to exploit the anti-inflammatory effects of HA [12]. The final 120 bilayers of ALG/CHI were added because the layer thickness increases much faster than with HA/CHI. Furthermore, the excellent swelling properties of alginate could be exploited for wound dressing applications.

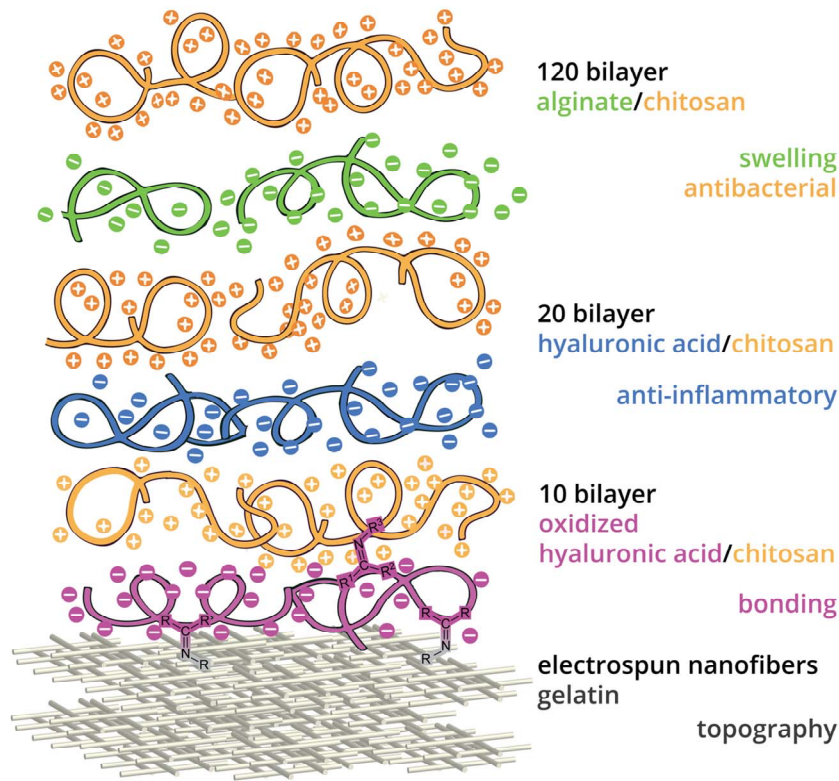


Fig. 3. Composite architecture with a total number of 150 bilayers. Polymer pairs represent bilayer combination with their respective number. Right justified their intended function is given.

3.1.3. Film growth on fleece

To determine the thickness of the film at various time points during deposition, we used fluorescence-labeled CHI and quantified it using z-stacks recorded by confocal laser scanning microscopy (CLSM).

The results (Fig. 4A) show that the first 30 bilayers, composed of oxHA/CHI and HA/CHI, exhibited a moderate increase in thickness, suggesting a linear deposition process in which the polyelectrolytes interact only with polyelectrolytes of opposite charge to form the next

layer of the film. The addition of ALG/CHI as layer pair, resulted in an exponential increase in thickness. This exponential growth is attributed to the diffusion of at least one of the polyelectrolytes throughout the multilayers/film, leading to the restructuring of the film with more hydrogel-like properties [50]. In particular for CHI/ALG bilayers a fast thickness growth is reported, caused by the high charge density of ALG [51]. However, after around 100 bilayers, the rate of thickness growth slowed down again. As previously described in the literature, there

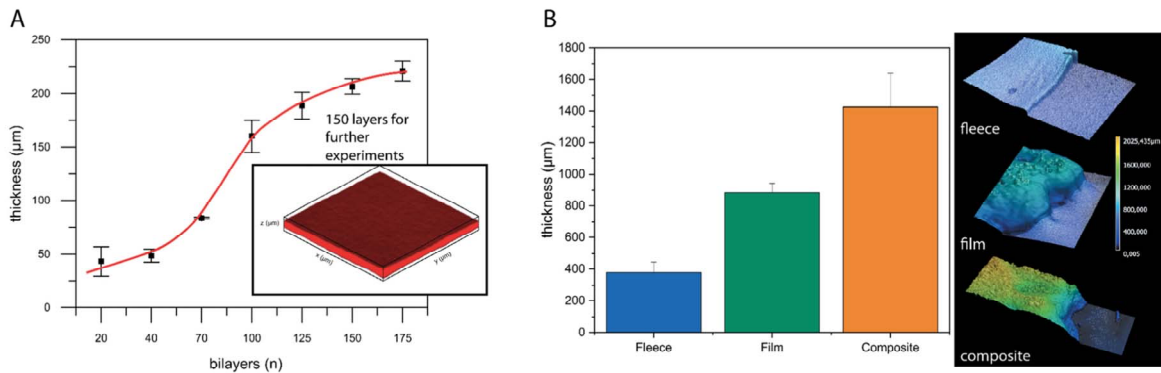


Fig. 4. A) Thickness growth of the free-standing film (without fleece), CHI-rhodamine was used in layer build up. The thickness was derived from the volume of apparent fluorescence found in CLSM z-stacks. The films showed a linear-exponential-linear growth (sigmoidal fitting (Boltzmann) adj. $R^2 = 0.997 \pm 0.01$). 150 bilayers were chosen for further experiments. $n \geq 5$ B) Optical Profilometry images of wet fleece, film, and composites. Differences between the sum of the thickness of fleece + film on one hand and the composite on the other, indicate a partly diffusion of components. $n \geq 5$, all sig. to each other $^*p \leq 0.05$.

comes a point during the formation of PEMs where exponential growth switches back to linear growth [51]. Triggered by decreased effect of ion pairing and coulomb forces towards multilayer formation [52]. However, the combined use of different polyelectrolytes limits a comprehensive understanding of the growth mechanism. Nonetheless, the partly exponential growth of the ALG/CHI allows for the efficient and cost-effective production of the free-standing film/film part of the composite to achieve a thickness required for a potential application as wound dressing. 150 bilayers were selected as the optimal balance between preparation time and resulting thickness.

3.1.4. Structural characterization of composite

Fig. 4B depicts the thickness of the wet composites measured by

profilometry. It is evident that most of the composite is comprised of the film, with only about a third being constituted by the fleece. Since the total thickness of the composite is smaller than the sum of the thickness of each individual component, penetration, and successful bonding of bilayers into the fleece is presumable. Although the polyelectrolyte solution is sprayed with a droplet size of well below $1\ \mu\text{m}$, the LbL-system can bridge $5\text{--}10\ \mu\text{m}$ gaps between the fibers (Fig. 5). Here the fiber network might function as an electrostatic barrier through its interfacial interactions, as a result fiber spanning occurs across the larger pores as the LbL cycle is repeated [53]. However, the film does not penetrate or diffuse through the whole composite as the penetration is limited to less than $100\ \mu\text{m}$ inside of the fleece (Fig. 4B). Therefore, the topography of the bottom side is still intact, which was also confirmed by nano-CT

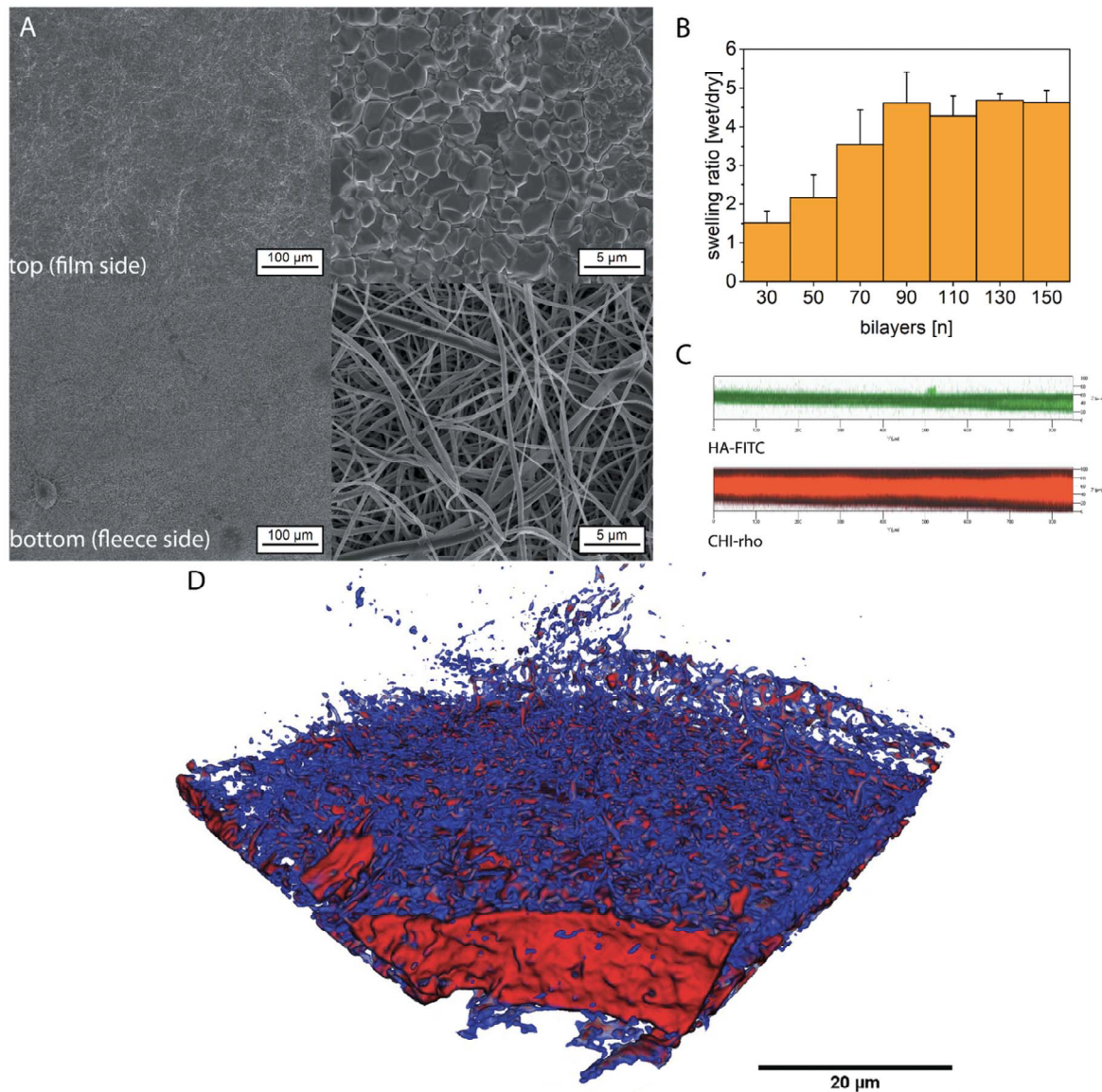


Fig. 5. A) ESEM images of dry composites. B) Swelling ratio of the film at several layer numbers determined by CLSM based on the fluorescence distribution of CHI-FITC, constitutes the polycation for all bilayers. $n = 5$ C) Location of HA determined by fluorescent HA-FITC inside the CHI-rho detected by CLSM-based z-stacks. HA-FITC appears to diffuse to a certain degree throughout the multilayer film D) Nano-CT image of the native composite (flipped; fibers on top (blue), film below (red)).

image in Fig. 5D, where the different densities of the two components are identifiable. In this way polyelectrolyte multilayers form an effective barrier against the environment to prevent for example penetration of bacteria from the outer environment, demonstrating the unique asymmetric properties of this composite. Fig. 5C depicts a cross section of the film as CLSM z-stack (CHI-rho channel). HA-FITC used as a polyelectrolyte in the PEMs remained mostly at the bottom of the film part, indicating a limited diffusion.

3.1.5. Swelling, dynamic mechanical analysis and hydrophilicity

Swelling of the composite was determined by CLSM using CHI-FITC as a fluorescence tracer in the film (Fig. 5B). The samples were dried for 3 days, measured and re-submerged prior to the second measurement. The first 30 bilayers are composed of CHI/(ox)HA, while the consecutive 110 bilayers are made of CHI/ALG, which is known to have superior swelling properties. The swelling ratio increases with the number of bilayers and plateaued at 90 bilayers. The first 30 bilayers are composed of CHI/(ox)HA, while the consecutive 110 bilayers are made of CHI/ALG. ALG/CHI are known to have superior swelling properties [30]. With increasing number of layers, the percentage share of the ALG/CHI bilayers increases, while the influence of the CHI/oxHA layers decreases. These show less swelling ability rooted in the effect of oxHA crosslinking by imine bonds between HA and CHI, which reduces the amount of hydrophilic amine groups and the mobility of the polyelectrolytes [54].

The Young's modulus and tensile strength of composites used in wound healing is of particular interest, as sufficient mechanical stability is key for covering a wound and protect it from the environment, while allowing flexibility for the user. To estimate the Young's modulus, the samples were studied with a texture analyzer using a ball penetration test to measure the elongation of the material at an increasing force. As shown in Fig. 6, there is no significant increase in tensile strength or Young's modulus when the film was fabricated on top of the fleece to form the composite. The composite, with the fleece below and the free-standing film on top, can be considered a two-component system. The fleece is the less elastic, more rigid component in this system. Therefore, the Young's modulus is also a result of the two-component system. Here, the Young's modulus is representative for the properties of the film rather than the fleece since it is the first to contact the probe due to the penetrating ball method. As the Young's modulus is calculated from the initial elastic deformation, it is characterizing the elastic properties of the film in this assay. As a result, the Young's modulus is lower for the composite. In a comparable manner, the tensile strength is also dependent mainly on the fleece. Hence the free-standing film, which is more hydrogel-like in the wet state, has no significant influence. The additional genipin crosslinking of the composite did not lead to a significant increase in either of the two properties. Probably, the crosslinking degree could be increased, or a more sensitive test method used. For an application as a wound dressing, the tensile strength must be improved. However, the composites show comparable tensile strength as alginate dressings (e.g., Kaltostat® 1.3 ± 0.2 MPa), which are usually combined with a secondary wound dressing [55].

However, the crosslinking of the composite by genipin results in a slight modification of the fleece surface. This can be seen in the captive bubble contact angle measurement, where the drop shape of an air bubble which is in contact with the surface of the fleece is analyzed (Fig. 6C). The result indicates a less hydrophilic state, as genipin crosslinks free amine groups, providing aromatic heterocyclic ring systems, which decrease the hydration of the polymer [26]. Although it must be noted that the contact angle cannot be compared to flat surfaces, since it is an apparent contact angle, dependent on the roughness of the surface.

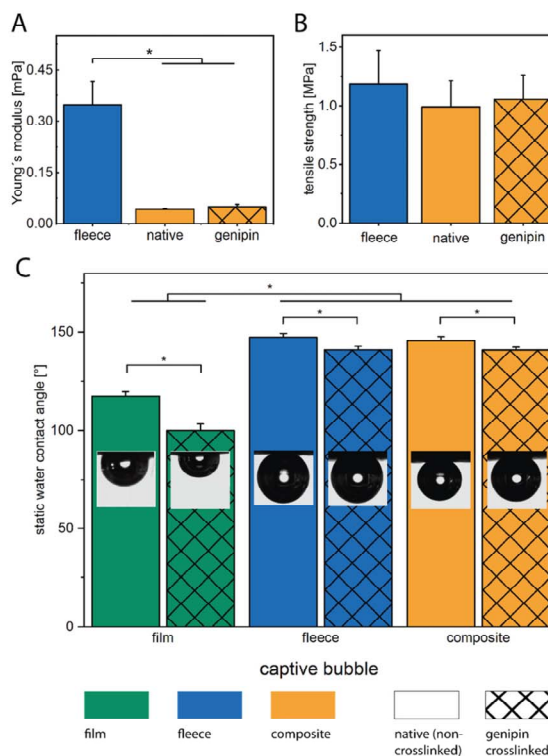


Fig. 6. A) Young's modulus and B) Tensile strength of wetted samples, determined by using a ball penetration test. Original stress/strain curves can be found in S1. $n \geq 3$ C) Contact angle measurement by the captive bubble method. Higher values indicate a less hydrophilic nature. $n \geq 5$.

3.2. Biological characterization

3.2.1. Cytotoxicity and cell growth of fibroblasts

The cytotoxicity of the individual components and the composite was analyzed by evaluating the cell growth of human dermal fibroblasts underneath the samples (Fig. 7A). After 1, 3 and 7 days the cell viability was tested using the resazurin based DeepBlue assay to test if any cytotoxic components diffuse out of the samples and negatively influence cell growth on the well bottom. As shown in Fig. 7, after day 1 and day 3 neither film, fleece nor the composite showed any toxic effect towards the cells or any significant differences in cell viability. After day 7, measured cell viability is significantly higher in the composite and film samples, regardless of crosslinking. Most probably this is a result of an increase of cell growth by the effect of HA [40]. Additionally, there could be a buffering effect of the swollen films, which are able to store mitogenic serum components or growth factors released from cells. These components could be released afterwards, increasing cell growth [30].

Another cell growth and live/dead assay was performed by seeding cells on top of the samples (Fig. 7B and Fig. 8). The composite samples were therefore flipped so that the fleece side was facing upwards. The genipin crosslinked composite allowed significantly more cell growth from day 1 to day 3 compared to the control and the films. While the fleece samples showed comparable cell growth, with prolonged contact with the media, the fleece began to shrink and collapse, resulting in a

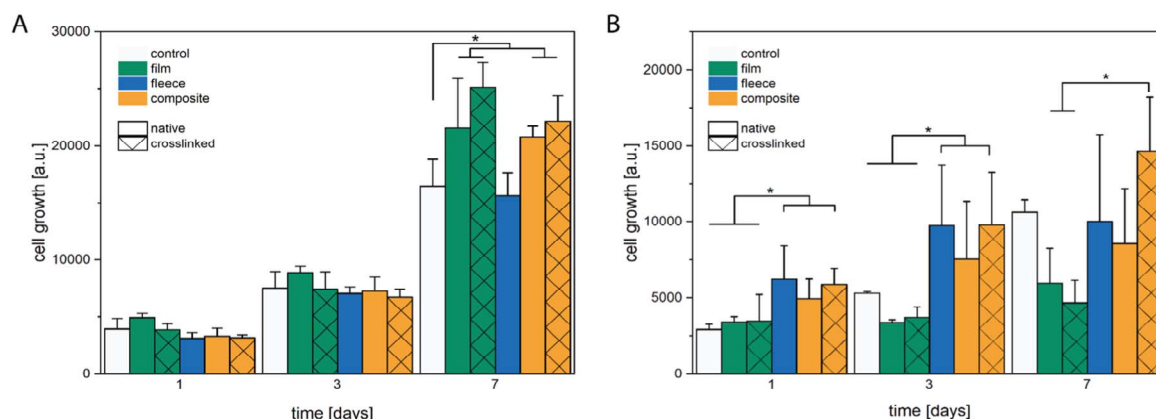


Fig. 7. A) Cell growth assay of with HDF cells seeded on the well plate's bottom underneath the samples. All samples show no significant difference to the control (cells cultured on TCPS). B) Cell growth assay with HDF cells cultured on top of the samples. Both assays based on DeepBlue assay. (n = 5).

decreased cell growth and increased standard deviation at day 7 compared to day 3. The native and crosslinked composite remained stable throughout the 7-day period. However, cell growth was not significantly higher after 7 days compared to the TCPS control. The film samples demonstrated low cell growth due to the low stiffness of the surface of free-standing multilayer films and high hydrophilicity of the surface, resulting in marginal cell adhesion and only small increases in cell growth on days 3 and 7 as shown previously in a comparable study [26].

Films and fleece were excluded from further HDF studies due to poor cell growth. Live/dead cell ratios after 7 days were assessed using a CLSM-based assay recording cell area and nuclei (Fig. 8). Z-stacks of the 3d topography and incorporated cells were recorded and flattened with maximum intensity projection. Nuclei, without association of a cytoplasm were counted as dead cells, cytoplasm without associated nuclei were not considered as adherent cells. Genipin crosslinked samples had the highest cell counts, followed by the native composite and the control. However, the genipin composite had a slightly higher percentage of dead cells. The results indicate that cells can adhere to the gelatin scaffolds, regardless of genipin crosslinking. The increased cell number in the genipin crosslinked samples may be attributed to the reduced hydrophilicity (Fig. 6), which is known to enhance protein adsorption [56]. As a result of the adsorption of proteins like cell secreted fibronectin, cell adhesion is increased [57]. Altogether, the fleece increased cell growth by providing a larger attachment area and possibly by the presentation of RGD sequences in gelatin for integrin-mediated cell binding [22].

3.2.2. Inflammatory response of macrophages

Macrophages play a crucial role in induction and resolution of inflammation, key processes in wound healing [8]. In this study, M0 activated macrophages derived from THP-1 cells were used. Cell viability assays were performed after seeding macrophages onto the fleece side of the composite for 48 h (Fig. 9). Compared to the TCPS control, macrophage viability and corresponding quantity of cells on the samples was significantly lower, although the fleece part of the composite should provide necessary cues for macrophage adhesion. The genipin crosslinking did increase cell adhesion comparable to the effect seen at the cell growth assay with HDF cells.

Production of pro- and anti-inflammatory cytokines (IL-6 and IL-10) by macrophages was studied with and without stimulation of cells by LPS as done in a previous study of our group [58]. IL-6 is a

pro-inflammatory cytokine produced mainly by M1 activated macrophages and acts in an autocrine and paracrine manner to modulate various cellular processes, including inflammation, immune response and cell proliferation [59]. IL-10 on the other hand is commonly associated with M2 polarized macrophages, characterized as a mostly anti-inflammatory phenotype [10]. As a result, the IL-6 and IL-10 secretion can be used as a marker for macrophage differentiation [60]. Biomaterials are able to modulate these activation modes of macrophages by a number of direct and indirect factors like topography, hydrophobicity and surface chemistry [61]. According to the data presented in Fig. 9B, non LPS stimulated macrophages cultured on both native and genipin crosslinked composites for 48 h show a higher release of IL-10 compared to the fleece, indicating an M2-like state. This observation suggests that the topographical adhesion cues may play a role, which are known to nudge cells to an M2 pro healing phenotype [59]. Furthermore, HMW-HA, as used in this study, is known to have the ability to increase IL-10 secretion. This effect is attributed to the ability of HMW-HA to counteract the effects of LMW-HA on TLR mediated activation by inhibiting the NF- κ B pathway [9,41,62]. As a result, HMW-HA can promote macrophage differentiation from M1 to M2 [63].

IL-6 production can be stimulated by a variety of factors, including microbial components and damage-associated molecules, like LPS, via the NF- κ B pathway [64]. Our results show a decrease in the M1-relevant IL-6 expression in LPS-stimulated cells seeded on all composites in comparison to the fleece. Our findings suggest that HA modulates the IL-6 production, by downregulating NF- κ B activation through ligation of CD44 [65]. Since the fleece part of the composites is not coated by the PEMs (Fig. 5) we expect no direct surface mediation of CD44-receptor by HA. More likely is the diffusion of HA molecules through the fleece to the macrophages where they can associate with the cell receptors. We hypothesize that the high release of IL-6 by the cells seeded on the fleece is caused by the crosslinking of the fleece by formaldehyde vapor before the spray coating. This effect could be counteracted by the influence of HA in the composite samples or by use of another crosslinking method in future studies. Overall, the combination of topographical cues provided by the composite materials and the influence of HMW-HA on the activation state of macrophages likely contributes to the promotion of an M2-like phenotype and enhanced secretion of IL-10 as well as down-regulating the IL-6 secretion in macrophages cultured on the native and genipin crosslinked composites. As a result, the composite could have a significant effect on resolving inflammation and promoting tissue repair.

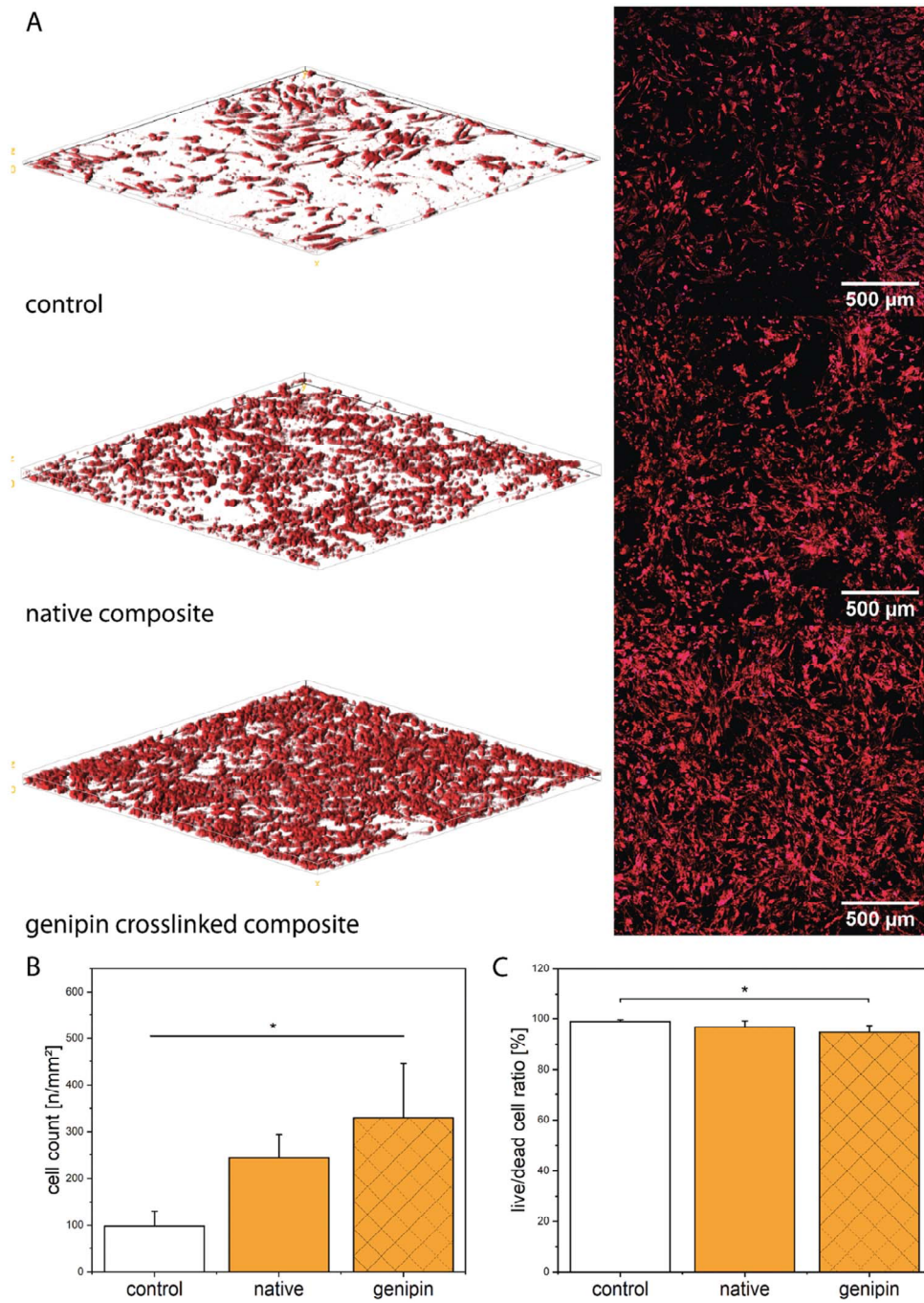


Fig. 8. A) NHDF cells cultured for 7 days on top of the samples. Control on TCPS. In S2 the original live/dead images can be found. B) Quantitative data, determined by z-stack maximum intensity projection and automated counting. The number of cells in each sample are significant to each other. $n \geq 6$ C) Live/dead cell ratio, all nuclei without associated cell body were considered as dead. Genipin crosslinked composites lead to a significant lower live/dead cell ratio compared to the control. $n \geq 6$.

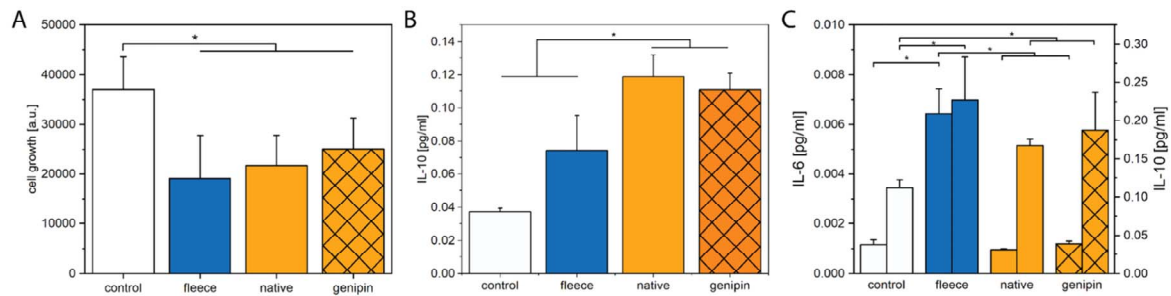


Fig. 9. A) cell growth of THP-1 derived macrophages without LPS stimulation. $n \geq 5$ B) IL-10 secretion of THP-1 derived macrophages normalized to cell growth without LPS after 48 h. IL-6 secretion was not detectable without LPS stimulation $n \geq 3$ C) Interleukin ratio IL-6 (left) and IL-10 (right) normalized to cell growth with LPS after 48 h. $n \geq 3$.

4. Conclusion

The presented modified spray coating process is able to add a multilayer system efficiently on top of the fleece part. The result is a novel composite which provides nano-topography, while the free-standing multilayer film part shows excellent swelling properties and incorporates HA for anti-inflammatory effect. Moreover, it greatly improves cell adhesion and growth of fibroblasts, which is novel for free-standing multilayer films, as they usually lack topography, have low stiffness and high hydrophilicity. The nano fleece counteracts this by acting as a scaffold to enable fibroblast migration and adhesion, while the modular design of the free-standing multilayer film allows control and tuning of key properties, specially, stability and swelling, which are necessary for the design of wound dressings. The use of HA and CHI as bioactive components of the film part introduces anti-inflammatory, anti-bacterial and wound healing capabilities. Genipin crosslinking of the composite enhances the composites bioactive properties while there is no difference in the inflammatory response. In the future this composite can be tailored to different sizes and shapes and produced by continuous spray coating processes. In addition, due to the layered nature of the system, this composite has the potential to incorporate a wide range of other polyelectrolytes, drugs, growth factors or carriers, such as charged nanoparticles or lipoplexes, and can be designed asymmetrically to control cell adhesion for other medical applications. In conclusion our study presents for the first time a successful combination of a nano fleece with a free-standing multilayer film for wound healing applications. Overall, this composite shows great promise as a platform for the development of novel bioactive wound dressings.

Declaration of Competing Interest

The authors declare that they have no known competing financial interests or personal relationships that could have appeared to influence the work reported in this paper.

Acknowledgements

Prof. Jürgen Brickmann and Heiko Steenbock (University of Lübeck) are thanked for assistance with amino acid analysis. Zahra Damayanti (Martin Luther University Halle-Wittenberg) is thanked for conducting experiments on oxidation, spray coating and film growth measurements. Marko Stäter (Fraunhofer IMWS) is thanked for assistance with mechanical testing and electron microscopy. Maria Morawietz and Sandra Saremba (Fraunhofer IMWS) are thanked for assistance with optical profilometry. The work was supported by the European Regional Development Fund in Saxony-Anhalt (project ProTect), by the Fraunhofer Internal programs under Grant No.: Attract 069-608203 (CEHS) and the Federal Ministry of Education and Research under the GO-Bio initial project "Active Layers" (16LW0046).

Appendix A. Supporting information

Supplementary data associated with this article can be found in the online version at [doi:10.1016/j.nxmate.2023.100060](https://doi.org/10.1016/j.nxmate.2023.100060).

References

- [1] G.S. Lazarus, D.M. Cooper, D.R. Knighton, R.E. Percoraro, G. Rodeheaver, M. C. Robson, Definitions and guidelines for assessment of wounds and evaluation of healing. *Wound Repair Regen. Off. Publ. Wound Heal. Soc. Eur. Tissue Repair Soc.* 2 (1994) 165–170, <https://doi.org/10.1046/j.1524-475x.1994.20305.x>.
- [2] E. Eriksson, P.Y. Liu, G.S. Schultz, M.M. Martins-Green, R. Tanaka, D. Weir, L. J. Gould, D.G. Armstrong, G.W. Gibbons, R. Wolcott, O.O. Olotuyo, R.S. Kirsner, G. C. Gurtner, Chronic wounds: Treatment consensus, *Wound Repair Regen. Off. Publ. Wound Heal. Soc. and Eur. Tissue Repair Soc.* 30 (2022) 156–171, <https://doi.org/10.1111/wrr.12994>.
- [3] C.K. Sen, Human wound and its burden: updated 2020 compendium of estimates, *Adv. Wound care* 10 (2021) 281–292, <https://doi.org/10.1089/wound.2021.0026>.
- [4] L. Cañedo-Dorantes, M. Cañedo-Ayala, Skin acute wound healing: a comprehensive review, *Int. J. Inflamm.* 2019 (2019) 3706315, <https://doi.org/10.1155/2019/3706315>.
- [5] A.P. Veith, K. Henderson, A. Spencer, A.D. Sligar, A.B. Baker, Therapeutic strategies for enhancing angiogenesis in wound healing, *Adv. Drug Deliv. Rev.* 146 (2019) 97–125, <https://doi.org/10.1016/j.addr.2018.09.010>.
- [6] G.A. James, E. Swogger, R. Wolcott, Ed Pulcini, P. Secor, J. Sestrich, J. W. Costerton, P.S. Stewart, Biofilms in chronic wounds, *Wound Repair Regen. Off. Publ. Wound Heal. Soc. Eur. Tissue Repair Soc.* 16 (2008) 37–44, <https://doi.org/10.1111/j.1524-475x.2007.00321.x>.
- [7] P. Krzyszczak, R. Schloss, A. Palmer, F. Berthiaume, The role of macrophages in acute and chronic wound healing and interventions to promote pro-wound healing phenotypes, *Front. Physiol.* 9 (2018) 419, <https://doi.org/10.3389/fphys.2018.00419>.
- [8] L. Parisi, E. Gini, D. Baci, M. Tremolati, M. Fanuli, B. Bassani, G. Farronato, A. Bruno, L. Mortara, Macrophage polarization in chronic inflammatory diseases: killers or builders? *J. Immunol. Res.* 2018 (2018) 8917804 <https://doi.org/10.1155/2018/8917804>.
- [9] H. Alkhoury, A. Hautmann, F. Erdmann, G. Zhou, S. Stojanović, S. Najman, T. Groth, Study on the potential mechanism of anti-inflammatory activity of covalently immobilized hyaluronan and heparin, *J. Biomed. Mater. Res. Part A* 108 (2020) 1099–1111, <https://doi.org/10.1002/jbm.a.36885>.
- [10] F.O. Martinez, S. Gordon, The M1 and M2 paradigm of macrophage activation, *F1000prime Rep.* 6 (2014) 13, <https://doi.org/10.12703/P6-13>.
- [11] H. Sorg, D.J. Tilkorn, S. Hager, J. Hauser, U. Mirastschijski, Skin wound healing: an update on the current knowledge and concepts, *European surgical research. Europäische chirurgische Forschung, Rech. Chir. Eur.* 58 (2017) 81–94, <https://doi.org/10.1159/000454919>.
- [12] H. Roehrs, J.G.D. Stocco, F. Pott, G. Blanc, K. Crozeta, M.J. Meier, F.A.L. Dias, Dressings and topical agents containing hyaluronic acid for chronic wound healing, *Cochrane Database of Systematic Reviews.* <https://doi.org/10.1002/14651858.CD012215>.
- [13] A.S. Asran, K. Razghandi, N. Aggarwal, G.H. Michler, T. Groth, Nanofibers from blends of polyvinyl alcohol and polyhydroxy butyrate as potential scaffold material for tissue engineering of skin, *Biomacromolecules* 11 (2010) 3413–3421, <https://doi.org/10.1021/bm100912v>.
- [14] L.E. Tracy, R.A. Minasian, E.J. Catterson, Extracellular Matrix and Dermal Fibroblast Function in the Healing Wound, *Adv. Wound care* 5 (2016) 119–136, <https://doi.org/10.1089/wound.2014.0561>.
- [15] S. Dhivya, V.V. Padma, E. Santhini, Wound dressings - a review, *BioMedicine* 5 (2015) 22, <https://doi.org/10.7603/s40681-015-0022-9>.
- [16] G. Ihan, R. Ceilley, Chronic wound healing: a review of current management and treatments, *Adv. Ther.* 34 (2017) 599–610, <https://doi.org/10.1007/s12325-017-0478-y>.

- [17] M. Hosseini, A. Shafiee, *Engineering Bioactive Scaffolds for Skin Regeneration*, Small 17 (2021) e2101384, <https://doi.org/10.1002/smll.202101384>.
- [18] Y. Liu, T. Li, Y. Han, F. Li, Y. Liu, *Recent development of electrospun wound dressing*, Curr. Opin. Biomed. Eng. 17 (2021) 100247, <https://doi.org/10.1016/j.cobme.2020.100247>.
- [19] C.-Y. Huang, K.-H. Hu, Z.-H. Wei, *Comparison of cell behavior on pva/pva-gelatin electrospun nanofibers with random and aligned configuration*, Sci. Rep. 6 (2016) 37960, <https://doi.org/10.1038/srep37960>.
- [20] J. Shi, L. Wang, F. Zhang, H. Li, L. Lei, L. Liu, Y. Chen, *Incorporating protein gradient into electrospun nanofibers as scaffolds for tissue engineering*, ACS Appl. Mater. Interfaces 2 (2010) 1025–1030, <https://doi.org/10.1021/am9007962>.
- [21] I. Lukin, I. Erezuma, L. Maeso, J. Zarate, M.F. Desimone, T.H. Al-Tel, A. Dolatshahi-Pirouz, G. Orive, *Progress in Gelatin as Biomaterial for Tissue Engineering*, Pharmaceutics 14 (2022), <https://doi.org/10.3390/pharmaceutics14061177>.
- [22] N. Davidenko, C.F. Schuster, D.V. Bax, R.W. Farndale, S. Hamaia, S.M. Best, R. E. Cameron, *Evaluation of cell binding to collagen and gelatin: a study of the effect of 2D and 3D architecture and surface chemistry*, J. Mater. Sci. Mater. Med. 27 (2016) 148, <https://doi.org/10.1007/s10856-016-5763-9>.
- [23] S. Zhang, Y. Huang, X. Yang, F. Mei, Q. Ma, G. Chen, S. Ryu, X. Deng, *Gelatin nanofibrous membrane fabricated by electrospinning of aqueous gelatin solution for guided tissue regeneration*, J. Biomed. Mater. Res. Part A 90 (2009) 671–679, <https://doi.org/10.1002/jbm.a.32136>.
- [24] A. Ehrmann, *Non-toxic crosslinking of electrospun gelatin nanofibers for tissue engineering and biomedicine—a review*, Polymers 13 (2021), <https://doi.org/10.3390/polym13121973>.
- [25] G. Decher, *Fuzzy nanoassemblies: toward layered polymeric multicomposites*, Science 277 (1997) 1232–1237, <https://doi.org/10.1126/science.277.5330.1232>.
- [26] G. Apte, A. Repanas, C. Willems, A. Mujtaba, C.E.H. Schmelzer, A. Raichur, F. Syrowatka, T. Groth, *Effect of different crosslinking strategies on physical properties and biocompatibility of freestanding multilayer films made of alginate and chitosan*, Macromol. Biosci. 19 (2019) e1900181, <https://doi.org/10.1002/mabi.201900181>.
- [27] A.S. Ivanov, L.V. Pershina, K.G. Nikolaev, E.V. Skorb, *Recent progress of layer-by-layer assembly, free-standing film and hydrogel based on polyelectrolytes*, Macromol. Biosci. 21 (2021) e2100117, <https://doi.org/10.1002/mabi.202100117>.
- [28] C. Correia, R.O. Sousa, A.C. Vale, D. Peixoto, T.H. Silva, R.L. Reis, I. Pashkuleva, N. M. Alves, *Adhesive and biodegradable membranes made of sustainable catechol-functionalized marine collagen and chitosan*, Colloids Surf. B, Biointerfaces 213 (2022) 112409, <https://doi.org/10.1016/j.colsurfb.2022.112409>.
- [29] J.M. Silva, A.R.C. Duarte, S.G. Caridade, C. Picart, R.L. Reis, J.F. Mano, *Tailored freestanding multilayered membranes based on chitosan and alginate*, Biomacromolecules 15 (2014) 3817–3826, <https://doi.org/10.1021/bm501156v>.
- [30] A. Hautmann, D. Kedilaya, S. Stojanović, M. Radenković, C.K. Marx, S. Najman, M. Pietzsch, J.F. Mano, T. Groth, *Free-standing multilayer films as growth factor reservoirs for future wound dressing applications*, Biomater. Adv. 142 (2022) 213166, <https://doi.org/10.1016/j.bioadv.2022.213166>.
- [31] S. Amorim, I. Pashkuleva, C.A. Reis, R.L. Reis, R.A. Pires, *Tunable layer-by-layer films containing hyaluronic acid and their interactions with CD44*, J. Mater. Chem. B 8 (2020) 3880–3885, <https://doi.org/10.1039/D0TB00407C>.
- [32] A. Izquierdo, S.S. Ono, J.-C. Voegel, P. Schaaf, G. Decher, *Dipping versus spraying: exploring the deposition conditions for speeding up layer-by-layer assembly*, Langmuir 21 (2005) 7558–7567, <https://doi.org/10.1021/la047407s>.
- [33] G. Cado, H. Kerdjoudj, A. Chassepot, M. Lefort, K. Benmlih, J. Hemmerlé, J.-C. Voegel, L. Jiery, P. Schaaf, Y. Frère, F. Boulmedais, *Polysaccharide films built by simultaneous or alternate spray: a rapid way to engineer biomaterial surfaces*, Langmuir ACS J. Surf. Colloids 28 (2012) 8470–8478, <https://doi.org/10.1021/la300563s>.
- [34] I.P. Monteiro, A. Shukla, A.P. Marques, R.L. Reis, P.T. Hammond, *Spray-assisted layer-by-layer assembly on hyaluronic acid scaffolds for skin tissue engineering*, J. Biomed. Mater. Res. Part A 103 (2015) 330–340, <https://doi.org/10.1002/jbm.a.35178>.
- [35] S.G. Caridade, C. Monge, F. Gilde, T. Boudou, J.F. Mano, C. Picart, *Free-standing polyelectrolyte membranes made of chitosan and alginate*, Biomacromolecules 14 (2013) 1653–1660, <https://doi.org/10.1021/bm400314s>.
- [36] K. Cai, A. Rechtenbach, J. Hao, J. Bossert, K.D. Jandt, *Polysaccharide-protein surface modification of titanium via a layer-by-layer technique: characterization and cell behaviour aspects*, Biomaterials 26 (2005) 5960–5971, <https://doi.org/10.1016/j.biomaterials.2005.03.020>.
- [37] S. Zankovych, J. Bossert, M. Faucon, U. Finger, K.D. Jandt, *Selectively promoting or preventing osteoblast growth on titanium functionalized with polyelectrolyte multilayers*, Adv. Eng. Mater. 13 (2011) B454–B461, <https://doi.org/10.1002/adem.201180020>.
- [38] B.A. Aderibigbe, B. Buyana, *Alginate in Wound Dressings*, Pharmaceutics 10 (2018) 42, <https://doi.org/10.3390/pharmaceutics10020042>.
- [39] S. Ahmed, S. Ikram, *Chitosan based scaffolds and their applications in wound healing*, Achiev. Life Sci. 10 (2016) 27–37, <https://doi.org/10.1016/j.als.2016.04.001>.
- [40] J.S. Frenkel, *The role of hyaluronan in wound healing*, Int. Wound J. 11 (2014) 159–163, <https://doi.org/10.1111/j.1742-481X.2012.01057.x>.
- [41] A. Köwitsch, G. Zhou, T. Groth, *Medical application of glycosaminoglycans: a review*, J. Tissue Eng. Regen. Med. 12 (2018) e23–e41, <https://doi.org/10.1002/term.2398>.
- [42] H. Alkhoury, A. Hautmann, B. Fuhrmann, F. Syrowatka, F. Erdmann, G. Zhou, S. Stojanović, S. Najman, T. Groth, *Studies on the mechanisms of anti-inflammatory activity of heparin- and hyaluronan-containing multilayer coatings-targeting NF- κ B signalling pathway*, Int. J. Mol. Sci. 21 (2020), <https://doi.org/10.3390/ijms21103724>.
- [43] R. Altman, A. Bedi, A. Manjoo, F. Niazi, P. Shaw, P. Mease, *Anti-inflammatory effects of intra-articular hyaluronate: a systematic review*, Cartilage 10 (2019) 43–52, <https://doi.org/10.1177/1947603517749919>.
- [44] M. Wu, Y. Du, Y. Liu, Y. He, C. Yang, W. Wang, F. Gao, *Low molecular weight hyaluronan induces lymphangiogenesis through LYVE-1-mediated signaling pathways*, PloS One 9 (2014) e92857, <https://doi.org/10.1371/journal.pone.0092857>.
- [45] M. Muhammad, C. Willems, J. Rodríguez-Fernández, G. Gallego-Ferrer, T. Groth, *Synthesis and Characterization of Oxidized Polysaccharides for In Situ Forming Hydrogels*, Biomolecules 10 (2020), <https://doi.org/10.3390/biom10081185>.
- [46] C. Santos de Oliveira, A.T. González, T. Hedtko, T. Kürbitz, A. Heilmann, C.E. H. Schmelzer, J. Martins de, S.E. Silva, *Direct three-dimensional imaging for morphological analysis of electrospun fibers with laboratory-based Zernike X-ray phase-contrast computed tomography*, Mater. Sci. Eng. C, Mater. Biol. Appl. 115 (2020) 111045, <https://doi.org/10.1016/j.msec.2020.111045>.
- [47] S. Bolte, F.P. Cordelières, *A guided tour into subcellular colocalization analysis in light microscopy*, J. Microsc. 224 (2006) 213–232, <https://doi.org/10.1111/j.1365-2818.2006.01706.x>.
- [48] Y. Jia, J. Li, *Molecular assembly of Schiff Base interactions: construction and application*, Chem. Rev. 115 (2015) 1597–1621, <https://doi.org/10.1021/cr400559g>.
- [49] M. Zhao, L. Li, C. Zhou, F. Heyroth, B. Fuhrmann, K. Maeder, T. Groth, *Improved stability and cell response by intrinsic cross-linking of multilayers from collagen I and oxidized glycosaminoglycans*, Biomacromolecules 15 (2014) 4272–4280, <https://doi.org/10.1021/bm501286f>.
- [50] C. Porcel, P. Lavalle, G. Decher, B. Senger, J.-C. Voegel, P. Schaaf, *Influence of the polyelectrolyte molecular weight on exponentially growing multilayer films in the linear regime*, Langmuir ACS J. Surf. Colloids 23 (2007) 1898–1904, <https://doi.org/10.1021/la062728k>.
- [51] J. Campbell, A.S. Vikulina, *Layer-By-Layer Assemblies of Biopolymers: Build-Up, Mechanical Stability and Molecular Dynamics*, Polymers 12 (2020), <https://doi.org/10.3390/polym12091949>.
- [52] C. Porcel, P. Lavalle, V. Ball, G. Decher, B. Senger, J.-C. Voegel, P. Schaaf, *From exponential to linear growth in polyelectrolyte multilayers*, Langmuir ACS J. Surf. Colloids 22 (2006) 4376–4383, <https://doi.org/10.1021/la053218d>.
- [53] K.C. Krogman, J.L. Lowery, N.S. Zacharia, G.C. Rutledge, P.T. Hammond, *Spraying asymmetry into functional membranes layer-by-layer*, Nat. Mater. 8 (2009) 512–518, <https://doi.org/10.1038/nmat2430>.
- [54] D. Volodkin, R. von Klitzing, *Competing mechanisms in polyelectrolyte multilayer formation and swelling: Polycation–polyanion pairing vs. polyelectrolyte–ion pairing*, Curr. Opin. Colloid Interface Sci. 19 (2014) 25–31, <https://doi.org/10.1016/j.cocis.2014.01.001>.
- [55] J.J. Elmsler, A. Shefy-Peleg, M. Zilberman, *Novel biodegradable composite wound dressings with controlled release of antibiotics: microstructure, mechanical and physical properties*, J. Biomed. Mater. Res. Part B, Appl. Biomater. 93 (2010) 425–435, <https://doi.org/10.1002/jbm.b.31599>.
- [56] J. Kuchinka, C. Willems, D.V. Telyshev, T. Groth, *Control of Blood Coagulation by Hemocompatible Material Surfaces—A Review*, Bioeng. (Basel, Switz.) 8 (2021), <https://doi.org/10.3390/bioengineering8120215>.
- [57] M. Zhao, G. Altankov, U. Grabiec, M. Bennett, M. Salmeron-Sanchez, F. Delghani, T. Groth, *Molecular composition of GAG-collagen I multilayers affects remodeling of terminal layers and osteogenic differentiation of adipose-derived stem cells*, Acta Biomater. 41 (2016) 86–99, <https://doi.org/10.1016/j.actbio.2016.05.023>.
- [58] G. Zhou, H. Loppnow, T. Groth, *A macrophage/fibroblast co-culture system using a cell migration chamber to study inflammatory effects of biomaterials*, Acta Biomater. 26 (2015) 54–63, <https://doi.org/10.1016/j.actbio.2015.08.020>.
- [59] R. Sridharan, A.R. Cameron, D.J. Kelly, C.J. Kearney, F.J. O'Brien, *Biomaterial based modulation of macrophage polarization: a review and suggested design principles*, Mater. Today 18 (2015) 313–325, <https://doi.org/10.1016/j.mattod.2015.01.019>.
- [60] G. Zhou, A. Liedmann, C. Chatterjee, T. Groth, *In vitro study of the host responses to model biomaterials via a fibroblast/macrophage co-culture system*, Biomater. Sci. 5 (2016) 141–152, <https://doi.org/10.1039/c6bm00247a>.
- [61] J.E. Rayahin, R.A. Gemeinhart, *Activation of Macrophages in Response to Biomaterials*, in: M. Kloc (Ed.), *Macrophages: Origin, Functions and Biointervention*, Springer International Publishing, Cham, 2017, pp. 317–351.
- [62] M. Saraiva, A. O'Garra, *The regulation of IL-10 production by immune cells*, Nature reviews, in: Immunology, 10, 2010, pp. 170–181, <https://doi.org/10.1038/nri2711>.
- [63] H. He, S. Zhang, S. Tighe, J. Son, S.C.G. Tseng, *Immobilized heavy chain-hyaluronic acid polarizes lipopolysaccharide-activated macrophages toward M2 phenotype*, J. Biol. Chem. 288 (2013) 25792–25803, <https://doi.org/10.1074/jbc.M113.479584>.
- [64] K.V. Eaton, H.L. Yang, C.M. Giachelli, M. Scatena, *Engineering macrophages to control the inflammatory response and angiogenesis*, Exp. Cell Res. 339 (2015) 300–309, <https://doi.org/10.1016/j.yexcr.2015.11.021>.
- [65] J.E. Rayahin, J.S. Buhrman, Y. Zhang, T.J. Koh, R.A. Gemeinhart, *High and low molecular weight hyaluronan differentially influence macrophage activation*, ACS Biomater. Sci. Eng. 1 (2015) 481–493, <https://doi.org/10.1021/acsbomaterials.5b00181>.

Reprinted under the open access CC BY 4.0 license.

Adrian Hautmann, Tobias Hedtke, Sonia Sislema-Muñoz, Juliana Martins-Schalinski, Christian E.H. Schmelzer, Thomas Groth (2024), Design of a composite wound dressing: Combining an electrospun fleece with a free-standing multilayer film, Next Materials, Volume 2, 100060

DOI: [10.1016/j.nxmte.2023.100060](https://doi.org/10.1016/j.nxmte.2023.100060)

Chapter 6 - Conclusion and Outlook

In this thesis, different techniques of surface modification, preparation of FSFs, and composites were investigated with the common aim of immune modulation and wound healing. The results show that the anti-inflammatory properties of GAGs are not only based on making GAG modified samples more hydrophilic and anionic, HA and Hep have a direct anti-inflammatory effect by their ability to act on the NF- κ B pathway, mitigating the inflammation and modulating macrophages. By establishing novel LbL-based biomaterials, it was demonstrated that the anti-inflammatory properties of GAGs and the mitogenic effect of FGF2 can be exploited to control the inflammatory process and accelerate wound closure *in vitro*. Finally, the combination of electrospun nanofibers and a FSF further enhanced the wound healing ability by providing a scaffold for cell adhesion and cell growth.

In detail, in the first and second study, different immobilization techniques were used to coat surfaces with GAGs: covalent binding to SAMs and the LbL technique. Both GAG surface coatings modulate macrophage activation, not only due their surface characteristics, but by the direct interaction of GAG-molecules with the macrophages. Especially, heparin multilayers allow a high uptake of Hep molecules into the cells; cell fusion, IL-1 β -release and NF- κ B activation was at a minimum. Covalent Hep surfaces control foreign body giant cell (FBGC)-formation, inhibit NF- κ B and allow endocytosis at an inferior level compared to the Hep multilayers. Both findings affirm various studies on the NF- κ B inhibition by Hep after endocytosis and extend its validity to the proposed Hep surface modifications (92). Interestingly, covalently attached HA is superior regarding anti-inflammatory activity in comparison to HA multilayers and covalent bound Hep, while being lower to the Hep multilayers. Covalent HA surfaces reduce macrophage adhesion, most likely due to their highest hydrophilicity, but lack control over fusion and NF- κ B activation. The pathway of NF- κ B inhibition by CD44 crosslinking with soluble HMW-HA does not directly apply to HA surfaces due to endocytosis of HA found in the cells, regardless of immobilization technique. This endocytosis cannot be distinguished to take place by the mediation of CD44 after crosslinking or TLR-receptors in this study, due to limitations of used method. When comparing both immobilization techniques, it is noteworthy that LbL surfaces exhibit a higher uptake of GAGs by macrophages. This enhanced uptake is attributed to the reorganization of layers and the limited diffusion out of the layers, making GAGs more accessible to macrophages (208). However, it is essential to recognize that each immobilization method offers unique advantages. Covalent immobilization stands out for its stability in long-term *in vivo* applications, while the LbL-technique, is more versatile and does not necessitate prior surface activation.

The versatility/modularity of the LbL-technique was further utilized in the third study to prepare

CHI/ALG FSF based on automatic dip coating, measuring about 500 μm in thickness. These films were tested with application as a wound dressing for chronic wounds in scope. In some regards they showed similarities to hydrogel based wound dressings, e.g. they exhibited excellent oxygen permeability and swelling capabilities to uptake wound exudate. With the incorporation of CHI as building block of the film, antibacterial properties against both gram-positive and gram-negative bacteria were achieved, making the addition of silver or antibiotics superfluous. *In vitro* and *in vivo* investigations, revealed the excellent biocompatibility of these CHI/ALG multilayer films, highlighting their ability to stimulate fibroblast migration and growth – a critical aspect of wound healing. With the two crosslinking methods tested (EDC/NHS and genipin) the stability increases and the FSFs can be turned in a FGF2 controlled release system, further increasing cell proliferation and migration. Although, FGF2-loaded genipin crosslinked FSF show superior cell proliferation and migration the uncrosslinked and EDC/NHS-crosslinked films were not far behind in most assays. However, the *in vivo* subcutaneous implantation in mice, revealed N-FSF, while biocompatible, displays early degradation. Although, the degradation mode is different in wounds than in subcutaneous implantation it underlines the necessity to crosslink such ALG/CHI FSF to ensure the function as a wound dressing and to allow controlled release of FGF2. Meanwhile, E-FSF, although considered a zero-length crosslinker, triggers a pro-inflammatory response *in vivo*. This was not apparent *in vitro*. Possibly degradation processes *in vivo* lead to this divergent result. Here further investigations could be fruitful. Nonetheless, genipin crosslinked FSF provide swelling capabilities useful for uptake of wound exudate, control of the release of mitogenic FGF2, show high biocompatibility both *in vitro* and *in vivo*, stimulate fibroblast growth and migration, while incorporating an anti-bacterial effect. In short, they possess properties which could boost the regeneration of chronic wounds, making them a compelling concept for bioactive wound management.

For the last study, the LbL technique was extended even further by going from an automatic dip coating to a custom spray coating process significantly reducing production time, while efficiently adding a multilayer system on top of an electrospun fleece. This innovation resulted in a novel composite which provides nano-topography, while the FSF part shows excellent swelling properties. Using HA and CHI as bioactive components in the film part, anti-inflammatory, anti-bacterial, and wound healing capabilities are introduced. Moreover, the composite greatly improves cell adhesion and growth of fibroblasts, which is novel for FSFs, as they typically lack topography, have low stiffness and high hydrophilicity. The fleece part serves as a scaffold to enable fibroblast migration and adhesion, while the modular design of the FSF part allows control and tuning of key properties, specially, stability and swelling, which are necessary for the design of chronic wound dressings. Genipin crosslinking of the composite further enhances the

composites bioactive properties, while there is no significant difference in the inflammatory response. In conclusion our study presents for the first time a successful combination of a nano fleece with a free-standing multilayer film for wound healing applications. This composite could be the starting point of a novel wound dressing, combining advantages of foam, film and hydrogel wound dressings. In the future, the FSF part could be used to incorporate a controlled release system, similar to the one in chapter 4, while keeping its properties to allow gaseous exchange, protect against bacterial colonization and allow the uptake of wound exudate.

Based on the findings of above studies we can conclude that LbL based FSFs can address the multimodal requirements to foster wound healing; controlling the inflammation, fight bacterial colonization and stimulating proliferation. This can be achieved by macrophage modulation through GAGs, the antibacterial effect of CHI and the supplementation of mitogenic GFs like FGF2. LbL based FSFs or derived composites are a completely innovative approach for the development of novel bioactive wound dressings that support regeneration of dermis as a prerequisite for the promotion of granulation tissue and re-epithelization of wounds. While these results already show great promise, the system can be further enhanced. Optimizing the release profile could be achieved by incorporating the growth factor during layer assembly, allowing it to function as a layer-building polyelectrolyte itself. This method could also enable the combination of multiple cytokines, released sequentially. However, for cargo lacking polyelectrolyte properties or non-water-soluble drugs, a drug carrier is required. Encapsulation in microgels, charged nanoparticles, or liposomes, followed by their addition to an LbL assembly, could be a promising approach. To finetune the release profile, the close simulation of chronic wounds would be of high value. Unfortunately, no established *in vitro* simulation of degradation in context of chronic wounds is available.

The future development of multilayered FSFs holds significant potential. Here several technologies wait to be combined and applied to fine-tune these constructs for a wide range of clinical needs. Nevertheless, while the advantages of FSFs are well-established at the laboratory scale, their economic viability remains limited due to high production costs, challenging storage conditions, and stringent regulatory requirements. In a recent GoBio-Initial translation project we explored the feasibility of producing larger FSFs or composites (209). By using a novel semi-continuous spray coating assembly some shortcomings of conventional spray processes could be addressed (Figure 17).

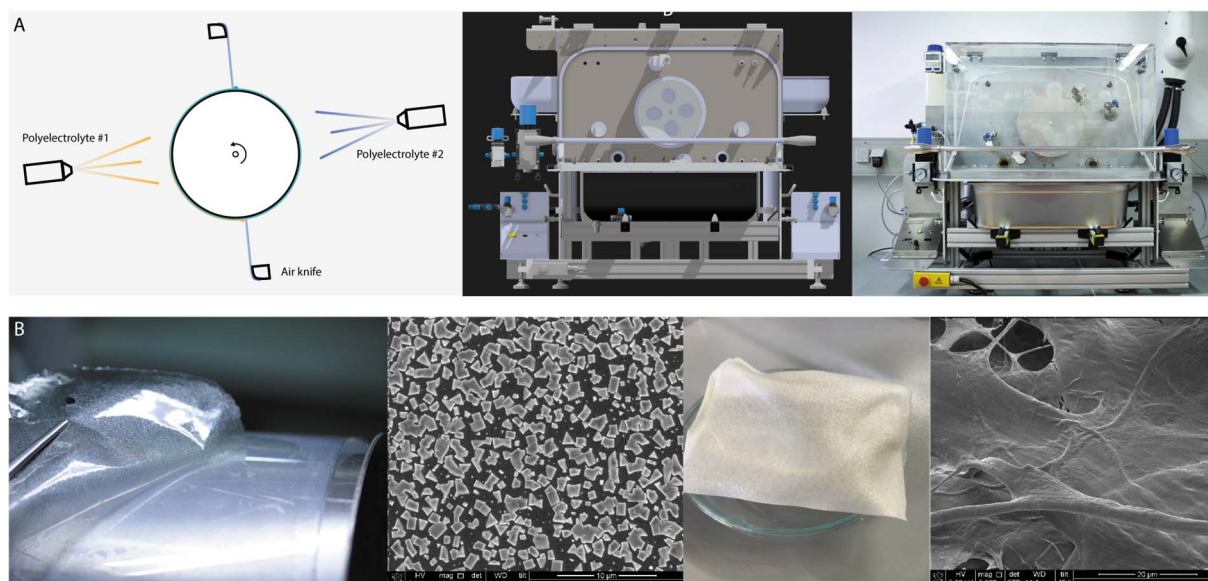


Figure 17 - A) from left to right: 1) Concept of an automatic semi-continuous spray coater, using air knives to separate the polyelectrolyte deposition. 2) CAD drawing of a spray coater based on this concept. 3) Realized spray coater B) 1) HA/CHI 100 bilayer free-standing multilayer film peeled from polypropylene substrate after air drying. 2) SEM image, showing salt deposition on an otherwise smooth surface of said film. Scale bar 10 μ m 4) HA/CHI 100 bilayer free-standing multilayer film deposited on a collagen membrane. 5) SEM image of film on top decellularized collagen membrane, showing bridging of the fibers scale bar= 20 μ m

This process utilizes air knives to expedite the drying phase and more accurately control the layer buildup of FSFs by removing undesirable bulk formation. It can produce smooth 80 cm x 20 cm > 100 bilayer FSFs in a matter of minutes. The continuous production can help multilayer FSFs to overcome their reputation of uneconomical production costs, opening new perspectives for research and medical applications. For instance, continuous production could lead to the construction of an inline high-throughput system for analyzing optimal layer build-up parameters to better understand layer growth processes. This could lead in the short term to an optimization of the process technology, allowing the verification of simulation models and in the long term lay the basis for quality control in a regulatory environment (210). In combination with masked plasma discharge, which renders a hydrophobic substrate locally hydrophilic, the x/y dimensions of subsequent LbL buildup could be highly controlled (211). In that way, FSF in different shapes for wound dressing application could be produced in line, or micrometer sized FSFs as drug carriers in bulk rapidly produced. Given that spray coating can be costly for low-volume drugs with high material costs, the combination of spray coating with inkjet-based LbL deposition or inkjet-based drug loading is also of significant interest. It offers precise control over the x/y axis of FSFs, with inkjet technology allowing exact deposition at a picoliter scale. Some inkjet LbL assemblies have been proposed but not in combination with multilayered FSFs (212, 213). Newer wide format inkjet arrangements could allow the combination with continuous spray coating, further increasing the economic potential of FSFs (214).

In conclusion, this thesis highlights the potent anti-inflammatory properties of HA and Hep based PEM and SAM-based coatings. Furthermore, it underscores the immense opportunities free-standing multilayer films provide, especially for wound dressing design. These go beyond merely covering wounds; they have the potential to actively participate in tissue regeneration, facilitating complete skin regeneration while reducing scar formation. These unique advantages make them appealing platforms for the future treatment of chronic wounds. Their adaptability to combine controlled delivery of growth factors, antibacterial properties of the building blocks and the introduction of nanostructures can significantly contribute to improving human health.

References

1. Robert Koch-Institut. Gesundheit in Deutschland **2016**. DOI: 10.17886/RKI-GBE-2016-021.2.
2. Raeder, K.; Jachan, D. E.; Müller-Werdan, U.; Lahmann, N. A. Prevalence and risk factors of chronic wounds in nursing homes in Germany: A Cross-Sectional Study. *International Wound Journal* **2020**, *17* (5), 1128–1134. DOI: 10.1111/iwj.13486.
3. Robert Koch-Institut. 12-Monats-Prävalenz des bekannten Diabetes mellitus in Deutschland **2017**. DOI: 10.17886/RKI-GBE-2017-008.
4. Eriksson, E.; Liu, P. Y.; Schultz, G. S.; Martins-Green, M. M.; Tanaka, R.; Weir, D.; Gould, L. J.; Armstrong, D. G.; Gibbons, G. W.; Wolcott, R.; Olutoye, O. O.; Kirsner, R. S.; Gurtner, G. C. Chronic wounds: Treatment consensus. *Wound repair and regeneration : official publication of the Wound Healing Society [and] the European Tissue Repair Society* **2022**, *30* (2), 156–171. DOI: 10.1111/wrr.12994.
5. Arbeitsgemeinschaft der Wissenschaftlichen Medizinischen Fachgesellschaften (AWMF). S3 Lokalthherapie chronischer Wunden **2012**.
6. Schreml, S.; Szeimies, R.-M.; Prantl, L.; Landthaler, M.; Babilas, P. Wound healing in the 21st century. *Journal of the American Academy of Dermatology* **2010**, *63* (5), 866–881. DOI: 10.1016/j.jaad.2009.10.048.
7. Falanga, V.; Isseroff, R. R.; Soulika, A. M.; Romanelli, M.; Margolis, D.; Kapp, S.; Granick, M.; Harding, K. Chronic wounds. *Nature reviews. Disease primers* **2022**, *8* (1), 50. DOI: 10.1038/s41572-022-00377-3.
8. Sorg, H.; Tilkorn, D. J.; Hager, S.; Hauser, J.; Mirastschijski, U. Skin Wound Healing: An Update on the Current Knowledge and Concepts. *European surgical research. Europäische chirurgische Forschung. Recherches chirurgicales europeennes* **2017**, *58* (1-2), 81–94. DOI: 10.1159/000454919.
9. Young, A.; McNaught, C.-E. The physiology of wound healing. *Surgery (Oxford)* **2011**, *29* (10), 475–479. DOI: 10.1016/j.mpsur.2011.06.011.
10. Rodrigues, M.; Kosaric, N.; Bonham, C. A.; Gurtner, G. C. Wound Healing: A Cellular Perspective. *Physiological reviews* **2019**, *99* (1), 665–706. DOI: 10.1152/physrev.00067.2017.
11. Probst, W.; Vassel-Biergans, A. *Wundmanagement: Ein illustrierter Leitfaden für Ärzte und Apotheker ; mit 133 Tabellen, 2., völlig neu bearb. und erw. Aufl.;* Wiss. Verl.-Ges, 2010.
12. Landén, N. X.; Li, D.; Stähle, M. Transition from inflammation to proliferation: a critical step during wound healing. *Cellular and molecular life sciences : CMLS* **2016**, *73* (20), 3861–3885. DOI: 10.1007/s00018-016-2268-0.
13. Versteeg, H. H.; Heemskerk, J. W. M.; Levi, M.; Reitsma, P. H. New fundamentals in hemostasis. *Physiological reviews* **2013**, *93* (1), 327–358. DOI: 10.1152/physrev.00016.2011.
14. MacLeod, A. S.; Kwock, J. T. Inflammation in Wound Repair: Role and Function of Inflammation in Wound Repair. In *Wound Healing*; Turksen, K., Ed.; Wiley, 2018, pp 177–194. DOI: 10.1002/9781119282518.ch14.
15. Cañedo-Dorantes, L.; Cañedo-Ayala, M. Skin Acute Wound Healing: A Comprehensive Review. *International journal of inflammation* **2019**, *2019*, 3706315. DOI: 10.1155/2019/3706315.

16. Rittié, L. Cellular mechanisms of skin repair in humans and other mammals. *Journal of cell communication and signaling* **2016**, *10* (2), 103–120. DOI: 10.1007/s12079-016-0330-1.
17. Han, G.; Ceilley, R. Chronic Wound Healing: A Review of Current Management and Treatments. *Advances in Therapy* **2017**, *34* (3), 599–610. DOI: 10.1007/s12325-017-0478-y.
18. Parisi, L.; Gini, E.; Baci, D.; Tremolati, M.; Fanuli, M.; Bassani, B.; Farronato, G.; Bruno, A.; Mortara, L. Macrophage Polarization in Chronic Inflammatory Diseases: Killers or Builders? *Journal of immunology research* **2018**, *2018*, 8917804. DOI: 10.1155/2018/8917804.
19. Rodero, M. P.; Khosrotehrani, K. Skin wound healing modulation by macrophages. *International Journal of Clinical and Experimental Pathology* **2010**, *3* (7), 643–653.
20. Saharinen, P.; Tammela, T.; Karkkainen, M. J.; Alitalo, K. Lymphatic vasculature: development, molecular regulation and role in tumor metastasis and inflammation. *Trends in Immunology* **2004**, *25* (7), 387–395. DOI: 10.1016/j.it.2004.05.003.
21. Klingberg, F.; Hinz, B.; White, E. S. The myofibroblast matrix: implications for tissue repair and fibrosis. *The Journal of pathology* **2013**, *229* (2), 298–309. DOI: 10.1002/path.4104.
22. Galligan, C. L.; Fish, E. N. The role of circulating fibrocytes in inflammation and autoimmunity. *Journal of leukocyte biology* **2013**, *93* (1), 45–50. DOI: 10.1189/jlb.0712365.
23. Rousselle, P.; Braye, F.; Dayan, G. Re-epithelialization of adult skin wounds: Cellular mechanisms and therapeutic strategies. *Advanced Drug Delivery Reviews* **2019**, *146*, 344–365. DOI: 10.1016/j.addr.2018.06.019.
24. Larson, B. J.; Longaker, M. T.; Lorenz, H. P. Scarless fetal wound healing: a basic science review. *Plastic and reconstructive surgery* **2010**, *126* (4), 1172–1180. DOI: 10.1097/PRS.0b013e3181eae781.
25. Tracy, L. E.; Minasian, R. A.; Catterson, E. J. Extracellular Matrix and Dermal Fibroblast Function in the Healing Wound. *Advances in wound care* **2016**, *5* (3), 119–136. DOI: 10.1089/wound.2014.0561.
26. Shirakami, E.; Yamakawa, S.; Hayashida, K. Strategies to prevent hypertrophic scar formation: a review of therapeutic interventions based on molecular evidence. *Burns & trauma* **2020**, *8*, tkz003. DOI: 10.1093/burnst/tkz003.
27. Walmsley, G. G.; Maan, Z. N.; Wong, V. W.; Duscher, D.; Hu, M. S.; Zielins, E. R.; Wearda, T.; Muhonen, E.; McArdle, A.; Tevlin, R.; Atashroo, D. A.; Senarath-Yapa, K.; Lorenz, H. P.; Gurtner, G. C.; Longaker, M. T. Scarless wound healing: chasing the holy grail. *Plastic and reconstructive surgery* **2015**, *135* (3), 907–917. DOI: 10.1097/PRS.0000000000000972.
28. Prey, S.; Ezzedine, K.; Doussau, A.; Grandoulier, A.-S.; Barcat, D.; Chatelus, E.; Diot, E.; Durant, C.; Hachulla, E.; Korwin-Krokowski, J.-D. de; Kostrzewa, E.; Quemeneur, T.; Paul, C.; Schaefferbeke, T.; Seneschal, J.; Solanilla, A.; Sparsa, A.; Bouchet, S.; Lepreux, S.; Mahon, F.-X.; Chene, G.; Taïeb, A. Imatinib mesylate in scleroderma-associated diffuse skin fibrosis: a phase II multicentre randomized double-blinded controlled trial. *The British journal of dermatology* **2012**, *167* (5), 1138–1144. DOI: 10.1111/j.1365-2133.2012.11186.x.
29. Denton, C. P.; Merkel, P. A.; Furst, D. E.; Khanna, D.; Emery, P.; Hsu, V. M.; Silliman, N.; Streisand, J.; Powell, J.; Akesson, A.; Coppock, J.; van Hoogen, F. den; Herrick, A.; Mayes, M. D.; Veale, D.; Haas, J.; Ledbetter, S.; Korn, J. H.; Black, C. M.; Seibold, J. R. Recombinant human anti-transforming

- growth factor beta1 antibody therapy in systemic sclerosis: a multicenter, randomized, placebo-controlled phase I/II trial of CAT-192. *Arthritis and rheumatism* **2007**, *56* (1), 323–333. DOI: 10.1002/art.22289.
30. Moura, L. I. F.; Dias, A. M. A.; Carvalho, E.; Sousa, H. C. de. Recent advances on the development of wound dressings for diabetic foot ulcer treatment—a review. *Acta Biomaterialia* **2013**, *9* (7), 7093–7114. DOI: 10.1016/j.actbio.2013.03.033.
 31. Zhang, J.; Li, Y. Therapeutic uses of FGFs. *Seminars in Cell & Developmental Biology* **2016**, *53*, 144–154. DOI: 10.1016/j.semcdb.2015.09.007.
 32. Araújo, R. de; Lôbo, M.; Trindade, K.; Silva, D. F.; Pereira, N. Fibroblast Growth Factors: A Controlling Mechanism of Skin Aging. *Skin pharmacology and physiology* **2019**, *32* (5), 275–282. DOI: 10.1159/000501145.
 33. Coentro, J. Q.; Pugliese, E.; Hanley, G.; Raghunath, M.; Zeugolis, D. I. Current and upcoming therapies to modulate skin scarring and fibrosis. *Advanced Drug Delivery Reviews* **2019**, *146*, 37–59. DOI: 10.1016/j.addr.2018.08.009.
 34. Schilrreff, P.; Alexiev, U. Chronic Inflammation in Non-Healing Skin Wounds and Promising Natural Bioactive Compounds Treatment. *International journal of molecular sciences* **2022**, *23* (9). DOI: 10.3390/ijms23094928.
 35. Kandhwal, M.; Behl, T.; Singh, S.; Sharma, N.; Arora, S.; Bhatia, S.; Al-Harrasi, A.; Sachdeva, M.; Bungau, S. Role of matrix metalloproteinase in wound healing. *American journal of translational research* **2022**, *14* (7), 4391–4405.
 36. Chen, L.; Mehta, N. D.; Zhao, Y.; DiPietro, L. A. Absence of CD4 or CD8 lymphocytes changes infiltration of inflammatory cells and profiles of cytokine expression in skin wounds, but does not impair healing. *Experimental dermatology* **2014**, *23* (3), 189–194. DOI: 10.1111/exd.12346.
 37. Barrientos, S.; Brem, H.; Stojadinovic, O.; Tomic-Canic, M. Clinical application of growth factors and cytokines in wound healing. *Wound repair and regeneration : official publication of the Wound Healing Society [and] the European Tissue Repair Society* **2014**, *22* (5), 569–578. DOI: 10.1111/wrr.12205.
 38. Boateng, J.; Catanzano, O. Advanced Therapeutic Dressings for Effective Wound Healing—A Review. *Journal of pharmaceutical sciences* **2015**, *104* (11), 3653–3680. DOI: 10.1002/jps.24610.
 39. Ridiandries, A.; Tan, J. T. M.; Bursill, C. A. The Role of Chemokines in Wound Healing. *International journal of molecular sciences* **2018**, *19* (10). DOI: 10.3390/ijms19103217.
 40. Salmon-Ehr, V.; Ramont, L.; Godeau, G.; Birembaut, P.; Guenounou, M.; Bernard, P.; Maquart, F. X. Implication of interleukin-4 in wound healing. *Laboratory investigation; a journal of technical methods and pathology* **2000**, *80* (8), 1337–1343. DOI: 10.1038/labinvest.3780141.
 41. Kanno, E.; Tanno, H.; Masaki, A.; Sasaki, A.; Sato, N.; Goto, M.; Shisai, M.; Yamaguchi, K.; Takagi, N.; Shoji, M.; Kitai, Y.; Sato, K.; Kasamatsu, J.; Ishii, K.; Miyasaka, T.; Kawakami, K.; Imai, Y.; Iwakura, Y.; Maruyama, R.; Tachi, M.; Kawakami, K. Defect of Interferon γ Leads to Impaired Wound Healing through Prolonged Neutrophilic Inflammatory Response and Enhanced MMP-2 Activation. *International journal of molecular sciences* **2019**, *20* (22). DOI: 10.3390/ijms20225657.
 42. Ashcroft, G. S.; Jeong, M.-J.; Ashworth, J. J.; Hardman, M.; Jin, W.; Moutsopoulos, N.; Wild, T.; McCartney-Francis, N.; Sim, D.; McGrady, G.; Song, X.-Y.; Wahl, S. M. Tumor necrosis factor-alpha

- (TNF- α) is a therapeutic target for impaired cutaneous wound healing. *Wound repair and regeneration : official publication of the Wound Healing Society [and] the European Tissue Repair Society* **2012**, *20* (1), 38–49. DOI: 10.1111/j.1524-475X.2011.00748.x.
43. Konop, M.; Rybka, M.; Drapała, A. Keratin Biomaterials in Skin Wound Healing, an Old Player in Modern Medicine: A Mini Review. *Pharmaceutics* **2021**, *13* (12). DOI: 10.3390/pharmaceutics13122029.
 44. Duplantier, A. J.; van Hoek, M. L. The Human Cathelicidin Antimicrobial Peptide LL-37 as a Potential Treatment for Polymicrobial Infected Wounds. *Front. Immunol.* **2013**, *4*, 143. DOI: 10.3389/fimmu.2013.00143.
 45. Ramshaw, H. S.; Kular, J.; Samuel, M. S. Wound Healing and the Non-cellular Microenvironment. In *Wound Healing*; Turksen, K., Ed.; Wiley, 2018, pp 79–87. DOI: 10.1002/9781119282518.ch6.
 46. Sridharan, R.; Cameron, A. R.; Kelly, D. J.; Kearney, C. J.; O’Brien, F. J. Biomaterial based modulation of macrophage polarization: A review and suggested design principles. *Materials Today* **2015**, *18* (6), 313–325. DOI: 10.1016/j.mattod.2015.01.019.
 47. Martinez, F. O.; Gordon, S. The M1 and M2 paradigm of macrophage activation: Time for reassessment. *F1000prime reports* **2014**, *6*, 13. DOI: 10.12703/P6-13.
 48. Shi, C.; Pamer, E. G. Monocyte recruitment during infection and inflammation. *Nature Reviews Immunology* **2011**, *11* (11), 762. DOI: 10.1038/nri3070.
 49. Brown, B. N.; Ratner, B. D.; Goodman, S. B.; Amar, S.; Badylak, S. F. Macrophage polarization: An opportunity for improved outcomes in biomaterials and regenerative medicine. *Biomaterials* **2012**, *33* (15), 3792–3802. DOI: 10.1016/j.biomaterials.2012.02.034.
 50. Sheikh, Z.; Brooks, P. J.; Barzilay, O.; Fine, N.; Glogauer, M. Macrophages, Foreign Body Giant Cells and Their Response to Implantable Biomaterials. *Materials* **2015**, *8* (9), 5671–5701. DOI: 10.3390/ma8095269.
 51. Mantovani, A.; Sica, A.; Sozzani, S.; Allavena, P.; Vecchi, A.; Locati, M. The chemokine system in diverse forms of macrophage activation and polarization. *Trends in Immunology* **2004**, *25* (12), 677–686. DOI: 10.1016/j.it.2004.09.015.
 52. Lawrence, T.; Natoli, G. Transcriptional regulation of macrophage polarization: Enabling diversity with identity. *Nature Reviews Immunology* **2011**, *11* (11), 750. DOI: 10.1038/nri3088.
 53. Mackaness, G. B. Cellular resistance to infection. *The Journal of experimental medicine* **1962**, *116*, 381–406.
 54. Murray, P. J.; Wynn, T. A. Protective and pathogenic functions of macrophage subsets. *Nature Reviews Immunology* **2011**, *11*, 723 EP -. DOI: 10.1038/nri3073.
 55. Franz, S.; Rammelt, S.; Scharnweber, D.; Simon, J. C. Immune responses to implants - a review of the implications for the design of immunomodulatory biomaterials. *Biomaterials* **2011**, *32* (28), 6692–6709. DOI: 10.1016/j.biomaterials.2011.05.078.
 56. Reinke, J. M.; Sorg, H. Wound Repair and Regeneration. *ESR* **2012**, *49* (1), 35–43. DOI: 10.1159/000339613.
 57. Murray, P. J.; Allen, J. E.; Biswas, S. K.; Fisher, E. A.; Gilroy, D. W.; Goerdts, S.; Gordon, S.; Hamilton, J. A.; Ivashkiv, L. B.; Lawrence, T.; Locati, M.; Mantovani, A.; Martinez, F. O.; Mege, J.-L.; Mosser, B.; Owens, C. A.; Roskelley, C. Y.; Soehnlein, O.; Stancovski, I.; Taniuchi, I.; Littman, D. R. Macrophage polarization: From conceptual models to molecular circuitry. *Nature Reviews Immunology* **2014**, *14*, 483–497. DOI: 10.1038/nri3665.

- D. M.; Natoli, G.; Saeij, J. P.; Schultze, J. L.; Shirey, K. A.; Sica, A.; Suttles, J.; Udalova, I.; van Ginderachter, J. A.; Vogel, S. N.; Wynn, T. A. Macrophage activation and polarization: Nomenclature and experimental guidelines. *Immunity* **2014**, *41* (1), 14–20. DOI: 10.1016/j.immuni.2014.06.008.
58. Liu, T.; Zhang, L.; Joo, D.; Sun, S.-C. NF- κ B signaling in inflammation. *Signal Transduction And Targeted Therapy* **2017**, *2*, 17023 EP -. DOI: 10.1038/sigtrans.2017.23.
59. Sen, R.; Baltimore, D. Inducibility of kappa immunoglobulin enhancer-binding protein Nf-kappa B by a posttranslational mechanism. *Cell* **1986**, *47* (6), 921–928. DOI: 10.1016/0092-8674(86)90807-x.
60. Gasparini, C.; Feldmann, M. NF- κ B as a Target for Modulating Inflammatory Responses. *CPD* **2012**, *18* (35), 5735–5745. DOI: 10.2174/138161212803530763.
61. Oeckinghaus, A.; Ghosh, S. The NF- κ B Family of Transcription Factors and Its Regulation. *Cold Spring Harbor Perspectives in Biology* **2009**, *1* (4). DOI: 10.1101/cshperspect.a000034.
62. Sasaki, C. Y.; Barberi, T. J.; Ghosh, P.; Longo, D. L. Phosphorylation of RelA/p65 on Serine 536 Defines an I κ B α -independent NF- κ B Pathway. *J. Biol. Chem.* **2005**, *280* (41), 34538–34547. DOI: 10.1074/jbc.M504943200.
63. Christian, F.; Smith, E. L.; Carmody, R. J. The Regulation of NF- κ B Subunits by Phosphorylation. *Cells* **2016**, *5* (1). DOI: 10.3390/cells5010012.
64. Renner, F.; Schmitz, M. L. Autoregulatory feedback loops terminating the NF- κ B response. *Trends in Biochemical Sciences* **2009**, *34* (3), 128–135. DOI: 10.1016/j.tibs.2008.12.003.
65. Lawrence, T. The Nuclear Factor NF- κ B Pathway in Inflammation. *Cold Spring Harbor Perspectives in Biology* **2009**, *1* (6). DOI: 10.1101/cshperspect.a001651.
66. Arias-Salvatierra, D.; Silbergeld, E. K.; Acosta-Saavedra, L. C.; Calderon-Aranda, E. S. Role of nitric oxide produced by iNOS through NF- κ B pathway in migration of cerebellar granule neurons induced by Lipopolysaccharide. *Cellular Signalling* **2011**, *23* (2), 425–435. DOI: 10.1016/j.cellsig.2010.10.017.
67. Aderibigbe, B. A.; Buyana, B. Alginate in Wound Dressings. *Pharmaceutics* **2018**, *10* (2), 42. DOI: 10.3390/pharmaceutics10020042.
68. Catanzano, O.; D'Esposito, V.; Acierno, S.; Ambrosio, M. R.; Caro, C. de; Avagliano, C.; Russo, P.; Russo, R.; Miro, A.; Ungaro, F.; Calignano, A.; Formisano, P.; Quaglia, F. Alginate–hyaluronan composite hydrogels accelerate wound healing process. *Carbohydrate polymers* **2015**, *131*, 407–414. DOI: 10.1016/j.carbpol.2015.05.081.
69. Yuan, N.; Shao, K.; Huang, S.; Chen, C. Chitosan, alginate, hyaluronic acid and other novel multifunctional hydrogel dressings for wound healing: A review. *International journal of biological macromolecules* **2023**, *240*, 124321. DOI: 10.1016/j.ijbiomac.2023.124321.
70. Kuchinka, J.; Willems, C.; Telyshev, D. V.; Groth, T. Control of Blood Coagulation by Hemocompatible Material Surfaces-A Review. *Bioengineering (Basel, Switzerland)* **2021**, *8* (12). DOI: 10.3390/bioengineering8120215.
71. Lukin, I.; Erezuma, I.; Maeso, L.; Zarate, J.; Desimone, M. F.; Al-Tel, T. H.; Dolatshahi-Pirouz, A.; Orive, G. Progress in Gelatin as Biomaterial for Tissue Engineering. *Pharmaceutics* **2022**, *14* (6).

DOI: 10.3390/ pharmaceuticals14061177.

72. Toole, B. P. Hyaluronan: From extracellular glue to pericellular cue. *Nature Reviews Cancer* **2004**, *4* (7), 528. DOI: 10.1038/nrc1391.
73. Laurent, T. C.; Laurent, U. B.; Fraser, R. E. J. The structure and function of hyaluronan: An overview. *Immunology and Cell Biology* **1996**, *74* (2), a1-a7. DOI: 10.1038/icb.1996.32.
74. Lee-Sayer, S. S. M.; Dong, Y.; Arif, A. A.; Olsson, M.; Brown, K. L.; Johnson, P. The Where, When, How, and Why of Hyaluronan Binding by Immune Cells. *Front. Immunol.* **2015**, *6*, 150. DOI: 10.3389/fimmu.2015.00150.
75. Ruppert, S. M.; Hawn, T. R.; Arrigoni, A.; Wight, T. N.; Bollyky, P. L. Tissue integrity signals communicated by high-molecular weight hyaluronan and the resolution of inflammation. *Immunologic research* **2014**, *58* (0), 186–192. DOI: 10.1007/s12026-014-8495-2.
76. Liu, Y.; Li, L.; Wang, L.; Lu, L.; Li, Y.; Huang, G.; Song, J. ‘Two-faces’ of hyaluronan, a dynamic barometer of disease progression in tumor microenvironment. *Discover. Oncology* **2023**, *14* (1), 11. DOI: 10.1007/s12672-023-00618-1.
77. Frenkel, J. S. The role of hyaluronan in wound healing. *International Wound Journal* **2014**, *11* (2), 159–163. DOI: 10.1111/j.1742-481X.2012.01057.x.
78. Köwitsch, A.; Zhou, G.; Groth, T. Medical application of glycosaminoglycans: A review. *Journal of tissue engineering and regenerative medicine* **2017** (12), 1–17. DOI: 10.1002/term.2398.
79. Rayahin, J. E.; Buhman, J. S.; Zhang, Y.; Koh, T. J.; Gemeinhart, R. A. High and low molecular weight hyaluronic acid differentially influence macrophage activation. *ACS biomaterials science & engineering* **2015**, *1* (7), 481–493. DOI: 10.1021/acsbomaterials.5b00181.
80. Wu, M.; Du, Y.; Liu, Y.; He, Y.; Yang, C.; Wang, W.; Gao, F. Low molecular weight hyaluronan induces lymphangiogenesis through LYVE-1-mediated signaling pathways. *PloS one* **2014**, *9* (3), e92857. DOI: 10.1371/journal.pone.0092857.
81. Köwitsch, A.; Zhou, G.; Groth, T. Medical application of glycosaminoglycans: a review. *Journal of tissue engineering and regenerative medicine* **2018**, *12* (1), e23-e41. DOI: 10.1002/term.2398.
82. Knudson, W.; Chow, G.; Knudson, C. B. CD44-mediated uptake and degradation of hyaluronan. *Matrix Biology* **2002**, *21* (1), 15–23. DOI: 10.1016/S0945-053X(01)00186-X.
83. Orecchioni, M.; Ghosheh, Y.; Pramod, A. B.; Ley, K. Macrophage Polarization: Different Gene Signatures in M1(LPS+) vs. Classically and M2(LPS-) vs. Alternatively Activated Macrophages. *Front. Immunol.* **2019**, *10*, 1084. DOI: 10.3389/fimmu.2019.01084.
84. Banerji, S.; Wright, A. J.; Noble, M.; Mahoney, D. J.; Campbell, I. D.; Day, A. J.; Jackson, D. G. Structures of the Cd44–hyaluronan complex provide insight into a fundamental carbohydrate-protein interaction. *Nature Structural & Molecular Biology* **2007**, *14* (3), 234. DOI: 10.1038/nsmb1201.
85. Yasuda, T. Hyaluronan Inhibits Akt, Leading to Nuclear Factor- κ B Down-Regulation in Lipopolysaccharide-Stimulated U937 Macrophages. *Journal of Pharmacological Sciences* **2011**, *115* (4), 509–515. DOI: 10.1254/jphs.10244FP.
86. Liang, J.; Jiang, D.; Griffith, J.; Yu, S.; Fan, J.; Zhao, X.; Bucala, R.; Noble, P. W. CD44 Is a Negative Regulator of Acute Pulmonary Inflammation and Lipopolysaccharide-TLR Signaling in Mouse

- Macrophages. *The Journal of Immunology* **2007**, *178* (4), 2469. DOI: 10.4049/jimmunol.178.4.2469.
87. Casu, B. Structure and Biological Activity of Heparin. *Advances in Carbohydrate Chemistry and Biochemistry* **1985**, *43*, 51–134. DOI: 10.1016/S0065-2318(08)60067-0.
88. Mikami, T.; Kitagawa, H. Glycosaminoglycans: Their Modes of Action for a Possible New Avenue for Therapeutic Intervention. In *Glycoscience: Biology and Medicine*; Endo, T., Seeberger, P. H., Hart, G. W., Wong, C.-H., Taniguchi, N., Eds.; Springer Japan, 2014, pp 1–7. DOI: 10.1007/978-4-431-54836-2_116-1.
89. Lima, M.; Rudd, T.; Yates, E. New Applications of Heparin and Other Glycosaminoglycans. *Molecules* **2017**, *22* (5). DOI: 10.3390/molecules22050749.
90. Rabenstein, D. L. Heparin and heparan sulfate: Structure and function. *Natural Product Reports* **2002**, *19* (3), 312–331. DOI: 10.1039/B100916H.
91. Shriver, Z.; Capila, I.; Venkataraman, G.; Sasisekharan, R. Heparin and Heparan Sulfate: Analyzing Structure and Microheterogeneity. *Handbook of experimental pharmacology* **2012** (207), 159–176. DOI: 10.1007/978-3-642-23056-1_8.
92. Young, E. The anti-inflammatory effects of heparin and related compounds. *Thrombosis Research* **2008**, *122* (6), 743–752. DOI: 10.1016/j.thromres.2006.10.026.
93. Hochart, H.; Jenkins, P. V.; Smith, O. P.; White, B. Low-molecular weight and unfractionated heparins induce a downregulation of inflammation: Decreased levels of proinflammatory cytokines and nuclear factor- κ B in LPS-stimulated human monocytes. *British Journal of Haematology* **2005**, *133* (1), 62–67. DOI: 10.1111/j.1365-2141.2006.05959.x.
94. Lee, J. H.; Lee, J.; Seo, G. H.; Kim, C. H.; Ahn, Y. S. Heparin inhibits NF-kappaB activation and increases cell death in cerebral endothelial cells after oxygen-glucose deprivation. *Journal of molecular neuroscience : MN* **2007**, *32* (2), 145–154.
95. Stewart, M. D.; Sanderson, R. D. Heparan sulfate in the nucleus and its control of cellular functions. *Matrix Biology* **2014**, *35*, 56–59. DOI: 10.1016/j.matbio.2013.10.009.
96. Croisier, F.; Jérôme, C. Chitosan-based biomaterials for tissue engineering. *European Polymer Journal* **2013**, *49* (4), 780–792. DOI: 10.1016/j.eurpolymj.2012.12.009.
97. Ahmed, S.; Ikram, S. Chitosan Based Scaffolds and Their Applications in Wound Healing. *Achievements in the Life Sciences* **2016**, *10* (1), 27–37. DOI: 10.1016/j.als.2016.04.001.
98. Caridade, S. G.; Monge, C.; Gilde, F.; Boudou, T.; Mano, J. F.; Picart, C. Free-standing polyelectrolyte membranes made of chitosan and alginate. *Biomacromolecules* **2013**, *14* (5), 1653–1660. DOI: 10.1021/bm400314s.
99. Jayakumar, R.; Prabakaran, M.; Sudheesh Kumar, P. T.; Nair, S. V.; Tamura, H. Biomaterials based on chitin and chitosan in wound dressing applications. *Biotechnology Advances* **2011**, *29* (3), 322–337. DOI: 10.1016/j.biotechadv.2011.01.005.
100. Caetano, G. F.; Frade, M. A. C.; Andrade, T. A. M.; Leite, M. N.; Bueno, C. Z.; Moraes, Â. M.; Ribeiro-Paes, J. T. Chitosan-alginate membranes accelerate wound healing. *Journal of biomedical materials research. Part B, Applied biomaterials* **2015**, *103* (5), 1013–1022. DOI: 10.1002/jbm.b.33277.

101. Archana, D.; Singh, B. K.; Dutta, J.; Dutta, P. K. Chitosan-PVP-nano silver oxide wound dressing: In vitro and in vivo evaluation. *International journal of biological macromolecules* **2015**, *73*, 49–57. DOI: 10.1016/j.ijbiomac.2014.10.055.
102. Pogorielov, M. V.; Sikora, V. Z. Chitosan as a Hemostatic Agent: Current State. *European Journal of Medicine. Series B* **2015**, *2* (1), 24–33. DOI: 10.13187/ejm.s.b.2015.2.24.
103. Jennings, J. A. Controlling chitosan degradation properties in vitro and in vivo. In: *Chitosan Based Biomaterials Volume 1*; Elsevier, 2017, pp 159–182. DOI: 10.1016/B978-0-08-100230-8.00007-8.
104. Szekalska, M.; Puciłowska, A.; Szymańska, E.; Ciosek, P.; Winnicka, K. Alginate: Current Use and Future Perspectives in Pharmaceutical and Biomedical Applications. *International Journal of Polymer Science* **2016**, *2016*, 1–17. DOI: 10.1155/2016/7697031.
105. Lee, K. Y.; Mooney, D. J. Alginate: properties and biomedical applications. *Progress in polymer science* **2012**, *37* (1), 106–126. DOI: 10.1016/j.progpolymsci.2011.06.003.
106. Gilchrist, T.; Martin, A. M. Wound treatment with Sorbsan — an alginate fibre dressing. *Biomaterials* **1983**, *4* (4), 317–320. DOI: 10.1016/0142-9612(83)90036-4.
107. Kumar, A.; Sah, D. K.; Khanna, K.; Rai, Y.; Yadav, A. K.; Ansari, M. S.; Bhatt, A. N. A calcium and zinc composite alginate hydrogel for pre-hospital hemostasis and wound care. *Carbohydrate polymers* **2023**, *299*, 120186. DOI: 10.1016/j.carbpol.2022.120186.
108. Son, E. H.; Moon, E. Y.; Rhee, D. K.; Pyo, S. Stimulation of various functions in murine peritoneal macrophages by high mannuronic acid-containing alginate (HMA) exposure in vivo. *International immunopharmacology* **2001**, *1* (1), 147–154. DOI: 10.1016/S1567-5769(00)00012-6.
109. Ullm, S.; Krüger, A.; Tondera, C.; Gebauer, T. P.; Neffe, A. T.; Lendlein, A.; Jung, F.; Pietzsch, J. Biocompatibility and inflammatory response in vitro and in vivo to gelatin-based biomaterials with tailorable elastic properties. *Biomaterials* **2014**, *35* (37), 9755–9766. DOI: 10.1016/j.biomaterials.2014.08.023.
110. Zhang, S.; Huang, Y.; Yang, X.; Mei, F.; Ma, Q.; Chen, G.; Ryu, S.; Deng, X. Gelatin nanofibrous membrane fabricated by electrospinning of aqueous gelatin solution for guided tissue regeneration. *Journal of biomedical materials research. Part A* **2009**, *90* (3), 671–679. DOI: 10.1002/jbm.a.32136.
111. Ehrmann, A. Non-Toxic Crosslinking of Electrospun Gelatin Nanofibers for Tissue Engineering and Biomedicine-A Review. *Polymers* **2021**, *13* (12). DOI: 10.3390/polym13121973.
112. Santos de Oliveira, C.; González, A. T.; Hedtke, T.; Kürbitz, T.; Heilmann, A.; Schmelzer, C. E. H.; Martins de S E Silva, J. Direct three-dimensional imaging for morphological analysis of electrospun fibers with laboratory-based Zernike X-ray phase-contrast computed tomography. *Materials science & engineering. C, Materials for biological applications* **2020**, *115*, 111045. DOI: 10.1016/j.msec.2020.111045.
113. Fee, T.; Surianarayanan, S.; Downs, C.; Zhou, Y.; Berry, J. Nanofiber Alignment Regulates NIH3T3 Cell Orientation and Cytoskeletal Gene Expression on Electrospun PCL+Gelatin Nanofibers. *PLoS one* **2016**, *11* (5), e0154806. DOI: 10.1371/journal.pone.0154806.
114. Liu, Y.; Li, T.; Han, Y.; Li, F.; Liu, Y. Recent development of electrospun wound dressing. *Current Opinion in Biomedical Engineering* **2021**, *17*, 100247. DOI: 10.1016/j.cobme.2020.100247.

115. Forrest, R. D. Early history of wound treatment. *Journal of the Royal Society of Medicine* **1982**, *75* (3), 198–205. DOI: 10.1177/014107688207500310.
116. Dyson, M.; Young, S.; Pendle, C. L.; Webster, D. F.; Lang, S. M. Comparison of the effects of moist and dry conditions on dermal repair. *The Journal of investigative dermatology* **1988**, *91* (5), 434–439. DOI: 10.1111/1523-1747.ep12476467.
117. Dhivya, S.; Padma, V. V.; Santhini, E. Wound dressings - a review. *BioMedicine* **2015**, *5* (4), 22. DOI: 10.7603/s40681-015-0022-9.
118. Piaggese, A.; Läubli, S.; Bassetto, F.; Biedermann, T.; Marques, A.; Najafi, B.; Palla, I.; Scarpa, C.; Seimetz, D.; Triulzi, I.; Turchetti, G.; Vaggelas, A. Advanced therapies in wound management: cell and tissue based therapies, physical and bio-physical therapies smart and IT based technologies. *Journal of wound care* **2018**, *27* (Sup6a), S1-S137. DOI: 10.12968/jowc.2018.27.sup6a.s1.
119. Lee, S. M.; Park, I. K.; Kim, Y. S.; Kim, H. J.; Moon, H.; Mueller, S.; Jeong, Y.-I. Physical, morphological, and wound healing properties of a polyurethane foam-film dressing. *Biomaterials research* **2016**, *20*, 15. DOI: 10.1186/s40824-016-0063-5.
120. Madden, M. R.; Nolan, E.; Finkelstein, J. L.; Yurt, R. W.; Smeland, J.; Goodwin, C. W.; Hefton, J.; Staiano-Coico, L. Comparison of an occlusive and a semi-occlusive dressing and the effect of the wound exudate upon keratinocyte proliferation. *The Journal of trauma* **1989**, *29* (7), 924-30; discussion 930-1. DOI: 10.1097/00005373-198907000-00004.
121. Broussard, K. C.; Powers, J. G. Wound dressings: selecting the most appropriate type. *American journal of clinical dermatology* **2013**, *14* (6), 449–459. DOI: 10.1007/s40257-013-0046-4.
122. Hoffman, A. S. Hydrogels for biomedical applications. *Advanced Drug Delivery Reviews* **2012**, *64*, 18–23. DOI: 10.1016/j.addr.2012.09.010.
123. Liang, Y.; He, J.; Guo, B. Functional Hydrogels as Wound Dressing to Enhance Wound Healing. *ACS nano* **2021**, *15* (8), 12687–12722. DOI: 10.1021/acsnano.1c04206.
124. Rezvani Ghomi, E.; Khalili, S.; Nouri Khorasani, S.; Esmaeely Neisiany, R.; Ramakrishna, S. Wound dressings: Current advances and future directions. *J Appl Polym Sci* **2019**, *136* (27), 47738. DOI: 10.1002/app.47738.
125. Varghese, M. C. Local Environment of Chronic Wounds Under Synthetic Dressings. *Arch Dermatol* **1986**, *122* (1), 52. DOI: 10.1001/archderm.1986.01660130056025.
126. Salloum, A.; Bazzi, N.; Squires, S.; Chu, T.; Benedetto, P.; Benedetto, A. Comparing the application of various engineered xenografts for skin defects: A systematic review. *Journal of cosmetic dermatology* **2023**, *22* (3), 921–931. DOI: 10.1111/jocd.15517.
127. Hussey, G. S.; Dziki, J. L.; Badylak, S. F. Extracellular matrix-based materials for regenerative medicine. *Nature Reviews Materials* **2018**, *3* (7), 159–173. DOI: 10.1038/s41578-018-0023-x.
128. Veith, A. P.; Henderson, K.; Spencer, A.; Sligar, A. D.; Baker, A. B. Therapeutic strategies for enhancing angiogenesis in wound healing. *Advanced Drug Delivery Reviews* **2019**, *146*, 97–125. DOI: 10.1016/j.addr.2018.09.010.
129. Margolis, D. J.; Morris, L. M.; Papadopoulos, M.; Weinberg, L.; Filip, J. C.; Lang, S. A.; Vaikunth, S. S.; Crombleholme, T. M. Phase I study of H5.020CMV.PDGF-beta to treat venous leg ulcer disease. *Molecular therapy : the journal of the American Society of Gene Therapy* **2009**, *17* (10), 1822–1829.

DOI: 10.1038/mt.2009.169.

130. Puolakkainen, P. A.; Twardzik, D. R.; Ranchalis, J. E.; Pankey, S. C.; Reed, M. J.; Gombotz, W. R. The enhancement in wound healing by transforming growth factor-beta 1 (TGF-beta 1) depends on the topical delivery system. *The Journal of surgical research* **1995**, *58* (3), 321–329. DOI: 10.1006/jsre.1995.1050.
131. Wu, L.; Xia, Y. P.; Roth, S. I.; Gruskin, E.; Mustoe, T. A. Transforming growth factor-beta1 fails to stimulate wound healing and impairs its signal transduction in an aged ischemic ulcer model: importance of oxygen and age. *The American journal of pathology* **1999**, *154* (1), 301–309. DOI: 10.1016/s0002-9440(10)65276-5.
132. Nunes, Q. M.; Li, Y.; Sun, C.; Kinnunen, T. K.; Fernig, D. G. Fibroblast growth factors as tissue repair and regeneration therapeutics. *PeerJ* **2016**, *4*, e1535. DOI: 10.7717/peerj.1535.
133. Abdelhakim, M.; Lin, X.; Ogawa, R. The Japanese Experience with Basic Fibroblast Growth Factor in Cutaneous Wound Management and Scar Prevention: A Systematic Review of Clinical and Biological Aspects. *Dermatology and therapy* **2020**, *10* (4), 569–587. DOI: 10.1007/s13555-020-00407-6.
134. Uchi, H.; Igrashi, A.; Urabe, K.; Koga, T.; Nakayama, J.; Kawamori, R.; Tamaki, K.; Hirakata, H.; Ohura, T.; Furue, M. Clinical efficacy of basic fibroblast growth factor (bFGF) for diabetic ulcer. *European journal of dermatology : EJD* **2009**, *19* (5), 461–468. DOI: 10.1684/ejd.2009.0750.
135. Matsumoto, S.; Tanaka, R.; Okada, K.; Arita, K.; Hyakusoku, H.; Miyamoto, M.; Tabata, Y.; Mizuno, H. The Effect of Control-released Basic Fibroblast Growth Factor in Wound Healing: Histological Analyses and Clinical Application. *Plastic and reconstructive surgery. Global open* **2013**, *1* (6), e44. DOI: 10.1097/GOX.0b013e3182a88787.
136. Budiraharjo, R.; Neoh, K. G.; Kang, E.-T. Enhancing bioactivity of chitosan film for osteogenesis and wound healing by covalent immobilization of BMP-2 or FGF-2. *Journal of biomaterials science. Polymer edition* **2013**, *24* (6), 645–662. DOI: 10.1080/09205063.2012.703949.
137. Kanda, N.; Morimoto, N.; Ayvazyan, A. A.; Takemoto, S.; Kawai, K.; Nakamura, Y.; Sakamoto, Y.; Taira, T.; Suzuki, S. Evaluation of a novel collagen-gelatin scaffold for achieving the sustained release of basic fibroblast growth factor in a diabetic mouse model. *Journal of tissue engineering and regenerative medicine* **2014**, *8* (1), 29–40. DOI: 10.1002/term.1492.
138. Lai, H.-J.; Kuan, C.-H.; Wu, H.-C.; Tsai, J.-C.; Chen, T.-M.; Hsieh, D.-J.; Wang, T.-W. Tailored design of electrospun composite nanofibers with staged release of multiple angiogenic growth factors for chronic wound healing. *Acta Biomaterialia* **2014**, *10* (10), 4156–4166. DOI: 10.1016/j.actbio.2014.05.001.
139. Losi, P.; Briganti, E.; Errico, C.; Lisella, A.; Sanguinetti, E.; Chiellini, F.; Soldani, G. Fibrin-based scaffold incorporating VEGF- and bFGF-loaded nanoparticles stimulates wound healing in diabetic mice. *Acta Biomaterialia* **2013**, *9* (8), 7814–7821. DOI: 10.1016/j.actbio.2013.04.019.
140. Klinkajon, W.; Supaphol, P. Novel copper (II) alginate hydrogels and their potential for use as anti-bacterial wound dressings. *Biomed. Mater.* **2014**, *9* (4), 45008. DOI: 10.1088/1748-6041/9/4/045008.
141. Ahmed, S.; Ikram, S. Chitosan Based Scaffolds and Their Applications in Wound Healing. *Achievements in the Life Sciences* **2016**, *10* (1), 27–37. DOI: 10.1016/j.als.2016.04.001.

142. Archana, D.; Singh, B. K.; Dutta, J.; Dutta, P. K. Chitosan-PVP-nano silver oxide wound dressing: In vitro and in vivo evaluation. *International journal of biological macromolecules* **2015**, *73*, 49–57. DOI: 10.1016/j.ijbiomac.2014.10.055.
143. Patrulea, V.; Ostafe, V.; Borchard, G.; Jordan, O. Chitosan as a starting material for wound healing applications. *European Journal of Pharmaceutics and Biopharmaceutics* **2015**, *97*, 417–426. DOI: 10.1016/j.ejpb.2015.08.004.
144. Ong, S.-Y.; Wu, J.; Moochhala, S. M.; Tan, M.-H.; Lu, J. Development of a chitosan-based wound dressing with improved hemostatic and antimicrobial properties. *Biomaterials* **2008**, *29* (32), 4323–4332. DOI: 10.1016/j.biomaterials.2008.07.034.
145. Murakami, K.; Ishihara, M.; Aoki, H.; Nakamura, S.; Nakamura, S.-I.; Yanagibayashi, S.; Takikawa, M.; Kishimoto, S.; Yokoe, H.; Kiyosawa, T.; Sato, Y. Enhanced healing of mitomycin C-treated healing-impaired wounds in rats with hydrosheets composed of chitin/chitosan, fucoidan, and alginate as wound dressings. *Wound repair and regeneration : official publication of the Wound Healing Society [and] the European Tissue Repair Society* **2010**, *18* (5), 478–485. DOI: 10.1111/j.1524-475X.2010.00606.x.
146. Humbert, P.; Mikosinski, J.; Benchikhi, H.; Allaert, F.-A. Efficacy and safety of a gauze pad containing hyaluronic acid in treatment of leg ulcers of venous or mixed origin: a double-blind, randomised, controlled trial. *International Wound Journal* **2013**, *10* (2), 159–166. DOI: 10.1111/j.1742-481X.2012.00957.x.
147. Fakhari, A.; Berkland, C. Applications and emerging trends of hyaluronic acid in tissue engineering, as a dermal filler and in osteoarthritis treatment. *Acta Biomaterialia* **2013**, *9* (7), 7081–7092. DOI: 10.1016/j.actbio.2013.03.005.
148. Jørgensen, B.; Karlsmark, T.; Vogensen, H.; Haase, L.; Lundquist, R. A pilot study to evaluate the safety and clinical performance of Leucopatch, an autologous, additive-free, platelet-rich fibrin for the treatment of recalcitrant chronic wounds. *The international journal of lower extremity wounds* **2011**, *10* (4), 218–223. DOI: 10.1177/1534734611426755.
149. Picheth, G. F.; Sierakowski, M. R.; Woehl, M. A.; Ono, L.; Cofré, A. R.; Vanin, L. P.; Pontarolo, R.; Freitas, R. A. de. Lysozyme-triggered epidermal growth factor release from bacterial cellulose membranes controlled by smart nanostructured films. *Journal of pharmaceutical sciences* **2014**, *103* (12), 3958–3965. DOI: 10.1002/jps.24205.
150. Tavakoli, M.; Labbaf, S.; Mirhaj, M.; Salehi, S.; Seifalian, A. M.; Firuzeh, M. Natural polymers in wound healing: From academic studies to commercial products. *J of Applied Polymer Sci* **2023**, *140* (22). DOI: 10.1002/app.53910.
151. Meinel, A. J.; Germershaus, O.; Luhmann, T.; Merkle, H. P.; Meinel, L. Electrospun matrices for localized drug delivery: current technologies and selected biomedical applications. *European journal of pharmaceutics and biopharmaceutics : official journal of Arbeitsgemeinschaft fur Pharmazeutische Verfahrenstechnik e.V* **2012**, *81* (1), 1–13. DOI: 10.1016/j.ejpb.2012.01.016.
152. Hosseini, M.; Shafiee, A. Engineering Bioactive Scaffolds for Skin Regeneration. *Small (Weinheim an der Bergstrasse, Germany)* **2021**, *17* (41), e2101384. DOI: 10.1002/sml.202101384.
153. Chen, C.-H.; Chen, S.-H.; Kuo, C.-Y.; Li, M.-L.; Chen, J.-P. Response of Dermal Fibroblasts to Biochemical and Physical Cues in Aligned Polycaprolactone/Silk Fibroin Nanofiber Scaffolds for Application in Tendon Tissue Engineering. *Nanomaterials (Basel, Switzerland)* **2017**, *7* (8). DOI:

10.3390/nano7080219.

154. Zhang, Y.; Lim, C. T.; Ramakrishna, S.; Huang, Z.-M. Recent development of polymer nanofibers for biomedical and biotechnological applications. *Journal of materials science. Materials in medicine* **2005**, *16* (10), 933–946. DOI: 10.1007/s10856-005-4428-x.
155. Liu, Y.; Zhou, S.; Gao, Y.; Zhai, Y. Electrospun nanofibers as a wound dressing for treating diabetic foot ulcer. *Asian Journal of Pharmaceutical Sciences* **2019**, *14* (2), 130–143. DOI: 10.1016/j.ajps.2018.04.004.
156. Catanzano, O.; Quaglia, F.; Boateng, J. S. Wound dressings as growth factor delivery platforms for chronic wound healing. *Expert opinion on drug delivery* **2021**, *18* (6), 737–759. DOI: 10.1080/17425247.2021.1867096.
157. Xue, M.; Zhao, R.; Lin, H.; Jackson, C. Delivery systems of current biologicals for the treatment of chronic cutaneous wounds and severe burns. *Advanced Drug Delivery Reviews* **2018**, *129*, 219–241. DOI: 10.1016/j.addr.2018.03.002.
158. Decher, G.; Hong, J. D.; Schmitt, J. Buildup of ultrathin multilayer films by a self-assembly process: III. Consecutively alternating adsorption of anionic and cationic polyelectrolytes on charged surfaces. *Thin Solid Films* **1992**, *210-211*, 831–835. DOI: 10.1016/0040-6090(92)90417-A.
159. Iler, R. K. Multilayers of colloidal particles. *Journal of Colloid and Interface Science* **1966**, *21* (6), 569–594. DOI: 10.1016/0095-8522(66)90018-3.
160. Richardson, J. J.; Cui, J.; Björnmalm, M.; Braunger, J. A.; Ejima, H.; Caruso, F. Innovation in Layer-by-Layer Assembly. *Chemical reviews* **2016**, *116* (23), 14828–14867. DOI: 10.1021/acs.chemrev.6b00627.
161. Costa, R. R.; Mano, J. F. Polyelectrolyte multilayered assemblies in biomedical technologies. *Chemical Society Reviews* **2014**, *43* (10), 3453–3479. DOI: 10.1039/C3CS60393H.
162. Campbell, J.; Vikulina, A. S. Layer-By-Layer Assemblies of Biopolymers: Build-Up, Mechanical Stability and Molecular Dynamics. *Polymers* **2020**, *12* (9). DOI: 10.3390/polym12091949.
163. Unagolla, J. M.; Jayasuriya, A. C. Drug transport mechanisms and in vitro release kinetics of vancomycin encapsulated chitosan-alginate polyelectrolyte microparticles as a controlled drug delivery system. *European journal of pharmaceutical sciences : official journal of the European Federation for Pharmaceutical Sciences* **2018**, *114*, 199–209. DOI: 10.1016/j.ejps.2017.12.012.
164. Shah, N. J.; Macdonald, M. L.; Beben, Y. M.; Padera, R. F.; Samuel, R. E.; Hammond, P. T. Tunable dual growth factor delivery from polyelectrolyte multilayer films. *Biomaterials* **2011**, *32* (26), 6183–6193. DOI: 10.1016/j.biomaterials.2011.04.036.
165. Iqbal, M. H.; Schroder, A.; Kerdjoudj, H.; Njel, C.; Senger, B.; Ball, V.; Meyer, F.; Boulmedais, F. Effect of the Buffer on the Buildup and Stability of Tannic Acid/Collagen Multilayer Films Applied as Antibacterial Coatings. *ACS applied materials & interfaces* **2020**. DOI: 10.1021/acsami.0c04475.
166. Sousa, M. P.; Arab-Tehrany, E.; Cleymand, F.; Mano, J. F. Surface Micro- and Nanoengineering: Applications of Layer-by-Layer Technology as a Versatile Tool to Control Cellular Behavior. *Small (Weinheim an der Bergstrasse, Germany)* **2019**, e1901228. DOI: 10.1002/smll.201901228.
167. Borges, J.; Mano, J. F. Molecular interactions driving the layer-by-layer assembly of multilayers. *Chemical reviews* **2014**, *114* (18), 8883–8942. DOI: 10.1021/cr400531v.

168. Lundin, M.; Solaqa, F.; Thormann, E.; Macakova, L.; Blomberg, E. Layer-by-Layer Assemblies of Chitosan and Heparin: Effect of Solution Ionic Strength and pH. *Langmuir* **2011**, *27* (12), 7537–7548. DOI: 10.1021/la200441u.
169. Boudou, T.; Crouzier, T.; Ren, K.; Blin, G.; Picart, C. Multiple functionalities of polyelectrolyte multilayer films: new biomedical applications. *Advanced materials (Deerfield Beach, Fla.)* **2010**, *22* (4), 441–467. DOI: 10.1002/adma.200901327.
170. Oliveira, M. B.; Hatami, J.; Mano, J. F. Coating Strategies Using Layer-by-layer Deposition for Cell Encapsulation. *Chemistry, an Asian journal* **2016**, *11* (12), 1753–1764. DOI: 10.1002/asia.201600145.
171. Lvov, Y.; Decher, G.; Moehwald, H. Assembly, structural characterization, and thermal behavior of layer-by-layer deposited ultrathin films of poly(vinyl sulfate) and poly(allylamine). *Langmuir* **1993**, *9* (2), 481–486. DOI: 10.1021/la00026a020.
172. Lavallo, P.; Boulmedais, F.; Ball, V.; Mutterer, J.; Schaaf, P.; Voegel, J.-C. Free standing membranes made of biocompatible polyelectrolytes using the layer by layer method. *Journal of Membrane Science* **2005**, *253* (1-2), 49–56. DOI: 10.1016/j.memsci.2004.12.033.
173. Izquierdo, A.; Ono, S. S.; Voegel, J.-C.; Schaaf, P.; Decher, G. Dipping versus spraying: exploring the deposition conditions for speeding up layer-by-layer assembly. *Langmuir* **2005**, *21* (16), 7558–7567. DOI: 10.1021/la047407s.
174. Dubas, S. T.; Farhat, T. R.; Schlenoff, J. B. Multiple membranes from “true” polyelectrolyte multilayers. *Journal of the American Chemical Society* **2001**, *123* (22), 5368–5369. DOI: 10.1021/ja015774%2B.
175. Schaaf, P.; Voegel, J.-C.; Jierry, L.; Boulmedais, F. Spray-assisted polyelectrolyte multilayer buildup: from step-by-step to single-step polyelectrolyte film constructions. *Advanced Materials* **2012**, *24* (8), 1001–1016. DOI: 10.1002/adma.201104227.
176. Lefort, M.; Popa, G.; Seyrek, E.; Szamocki, R.; Felix, O.; Hemmerlé, J.; Vidal, L.; Voegel, J.-C.; Boulmedais, F.; Decher, G.; Schaaf, P. Spray-on organic/inorganic films: a general method for the formation of functional nano- to microscale coatings. *Angewandte Chemie (International ed. in English)* **2010**, *49* (52), 10110–10113. DOI: 10.1002/anie.201002729.
177. Lefort, M.; Boulmedais, F.; Jierry, L.; Gonthier, E.; Voegel, J. C.; Hemmerlé, J.; Lavallo, P.; Ponche, A.; Schaaf, P. Simultaneous spray coating of interacting species: general rules governing the poly(styrene sulfonate)/poly(allylamine) system. *Langmuir : the ACS journal of surfaces and colloids* **2011**, *27* (8), 4653–4660. DOI: 10.1021/la104809z.
178. Kirshhof, K.; Andar, A.; Yin, H. B.; Gadegaard, N.; Riehle, M. O.; Groth, T. Polyelectrolyte multilayers generated in a microfluidic device with pH gradients direct adhesion and movement of cells. *Lab Chip* **2011**, *11* (19), 3326–3335. DOI: 10.1039/C1LC20408D.
179. Almodóvar, J.; Crouzier, T.; Selimović, Š.; Boudou, T.; Khademhosseini, A.; Picart, C. Gradients of physical and biochemical cues on polyelectrolyte multilayer films generated via microfluidics. *Lab Chip* **2013**, *13* (8), 1562–1570. DOI: 10.1039/C3LC41407H.
180. Gao, P.; Hunter, A.; Summe, M. J.; Phillip, W. A. A Method for the Efficient Fabrication of Multifunctional Mosaic Membranes by Inkjet Printing. *ACS applied materials & interfaces* **2016**, *8* (30), 19772–19779. DOI: 10.1021/acsami.6b06048.

181. Miller, E.; Phillippi, J.; Fisher, G.; Campbell, P.; Walker, L.; Weiss, L. Inkjet Printing of Growth Factor Concentration Gradients and Combinatorial Arrays Immobilized on Biologically-Relevant Substrates. *CCHTS* **2009**, *12* (6), 604–618. DOI: 10.2174/138620709788681907.
182. Lutkenhaus, J. L.; Hrabak, K. D.; McEnnis, K.; Hammond, P. T. Elastomeric flexible free-standing hydrogen-bonded nanoscale assemblies. *Journal of the American Chemical Society* **2005**, *127* (49), 17228–17234. DOI: 10.1021/ja053472s.
183. Sousa, C. F. V.; Monteiro, L. P. G.; Rodrigues, J. M. M.; Borges, J.; Mano, J. F. Marine-origin polysaccharides-based free-standing multilayered membranes as sustainable nanoreservoirs for controlled drug delivery. *Journal of materials chemistry. B* **2023**, *11* (28), 6671–6684. DOI: 10.1039/D3TB00796K.
184. Silva, J. M.; Caridade, S. G.; Reis, R. L.; Mano, J. F. Polysaccharide-based freestanding multilayered membranes exhibiting reversible switchable properties. *Soft matter* **2016**, *12* (4), 1200–1209. DOI: 10.1039/c5sm02458g.
185. Silva, J. M.; Duarte, A. R. C.; Caridade, S. G.; Picart, C.; Reis, R. L.; Mano, J. F. Tailored freestanding multilayered membranes based on chitosan and alginate. *Biomacromolecules* **2014**, *15* (10), 3817–3826. DOI: 10.1021/bm501156v.
186. Pahal, S.; Boranna, R.; Tripathy, A.; Goudar, V. S.; Veetil, V. T.; Kurapati, R.; Prashanth, G. R.; Vemula, P. K. Nanoarchitectonics for Free-Standing Polyelectrolyte Multilayers Films: Exploring the Flipped Surfaces. *ChemNanoMat* **2023**, *9* (2). DOI: 10.1002/cnma.202200462.
187. Gui, Z.; Qian, J.; Du, B.; Yin, M.; An, Q. Fabrication of free-standing polyelectrolyte multilayer films: a method using polysulfobetaine-containing films as sacrificial layers. *Journal of Colloid and Interface Science* **2009**, *340* (1), 35–41. DOI: 10.1016/j.jcis.2009.08.008.
188. Ono, S. S.; Decher, G. Preparation of ultrathin self-standing polyelectrolyte multilayer membranes at physiological conditions using pH-responsive film segments as sacrificial layers. *Nano letters* **2006**, *6* (4), 592–598. DOI: 10.1021/nl0515504.
189. Polak, R.; Crouzier, T.; Lim, R. M.; Ribbeck, K.; Beppu, M. M.; Pitombo, R. N. M.; Cohen, R. E.; Rubner, M. F. Sugar-mediated disassembly of mucin/lectin multilayers and their use as pH-Tolerant, on-demand sacrificial layers. *Biomacromolecules* **2014**, *15* (8), 3093–3098. DOI: 10.1021/bm5006905.
190. Pennakalathil, J.; Hong, J.-D. Self-standing polyelectrolyte multilayer films based on light-triggered disassembly of a sacrificial layer. *ACS nano* **2011**, *5* (11), 9232–9237. DOI: 10.1021/nn203490q.
191. Ma, Y.; Sun, J.; Shen, J. Ion-Triggered Exfoliation of Layer-by-Layer Assembled Poly(acrylic acid)/Poly(allylamine hydrochloride) Films from Substrates: A Facile Way To Prepare Free-Standing Multilayer Films. *Chem. Mater.* **2007**, *19* (21), 5058–5062. DOI: 10.1021/cm071260j.
192. Kong, Y.; Xu, R.; Darabi, M. A.; Zhong, W.; Luo, G.; Xing, M. M.; Wu, J. Fast and safe fabrication of a free-standing chitosan/alginate nanomembrane to promote stem cell delivery and wound healing. *International journal of nanomedicine* **2016**, *11*, 2543–2555. DOI: 10.2147/IJN.S102861.
193. Konnova, S. A.; Kahraman, M.; Zamaleeva, A. I.; Culha, M.; Paunov, V. N.; Fakhrullin, R. F. Functional artificial free-standing yeast biofilms. *Colloids and surfaces. B, Biointerfaces* **2011**, *88* (2), 656–663. DOI: 10.1016/j.colsurfb.2011.07.056.
194. Apte, G.; Repanas, A.; Willems, C.; Mujtaba, A.; Schmelzer, C. E. H.; Raichur, A.; Syrowatka, F.;

- Groth, T. Effect of Different Crosslinking Strategies on Physical Properties and Biocompatibility of Freestanding Multilayer Films Made of Alginate and Chitosan. *Macromolecular bioscience* **2019**, *19* (11), e1900181. DOI: 10.1002/mabi.201900181.
195. Sousa, M. P.; Neto, A. I.; Correia, T. R.; Miguel, S. P.; Matsusaki, M.; Correia, I. J.; Mano, J. F. Bioinspired multilayer membranes as potential adhesive patches for skin wound healing. *Biomaterials science* **2018**, *6* (7), 1962–1975. DOI: 10.1039/c8bm00319j.
196. Zykova, Y.; Kudryavtseva, V.; Gai, M.; Kozelskaya, A.; Frueh, J.; Sukhorukov, G.; Tverdokhlebov, S. Free-standing microchamber arrays as a biodegradable drug depot system for implant coatings. *European Polymer Journal* **2019**, *114*, 72–80. DOI: 10.1016/j.eurpolymj.2019.02.029.
197. Sousa, M. P.; Passos, C. T.; Fürsatz, M.; Lee, H.; Patrício, S. G.; Mano, J. F.; Nürnberger, S. Patterned Mussel-Inspired Freestanding Membranes as Efficient Delivery Device of Therapeutic Stem Cells for Cartilage Repair. *Advanced NanoBiomed Research* **2023**, *3* (8). DOI: 10.1002/anbr.202300005.
198. Martins, N. I.; Sousa, M. P.; Custódio, C. A.; Pinto, V. C.; Sousa, P. J.; Minas, G.; Cleymand, F.; Mano, J. F. Multilayered membranes with tuned well arrays to be used as regenerative patches. *Acta Biomaterialia* **2017**, *57*, 313–323. DOI: 10.1016/j.actbio.2017.04.021.
199. Chen, D.; Chen, J.; Wu, M.; Tian, H.; Chen, X.; Sun, J. Robust and Flexible Free-Standing Films for Unidirectional Drug Delivery. *Langmuir* **2013**, *29* (26), 8328–8334. DOI: 10.1021/la401423d.
200. Cassin, M. E.; Ford, A. J.; Orbach, S. M.; Saverot, S. E.; Rajagopalan, P. The design of antimicrobial LL37-modified collagen-hyaluronic acid detachable multilayers. *Acta Biomaterialia* **2016**, *40*, 119–129. DOI: 10.1016/j.actbio.2016.04.027.
201. Mandapalli, P. K.; Labala, S.; Jose, A.; Bhatnagar, S.; Janupally, R.; Sriram, D.; Venuganti, V. V. K. Layer-by-Layer Thin Films for Co-Delivery of TGF- β siRNA and Epidermal Growth Factor to Improve Excisional Wound Healing. *AAPS PharmSciTech* **2017**, *18* (3), 809–820. DOI: 10.1208/s12249-016-0571-6.
202. Gilde, F.; Fourel, L.; Guillot, R.; Pignot-Paintrand, I.; Okada, T.; Fitzpatrick, V.; Boudou, T.; Albiges-Rizo, C.; Picart, C. Stiffness-dependent cellular internalization of matrix-bound BMP-2 and its relation to Smad and non-Smad signaling. *Acta Biomaterialia* **2016**, *46*, 55–67. DOI: 10.1016/j.actbio.2016.09.014.
203. Joseph, N.; Ahmadiannamini, P.; Hoogenboom, R.; Vankelecom, I. F. J. Layer-by-layer preparation of polyelectrolyte multilayer membranes for separation. *Polym. Chem.* **2014**, *5* (6), 1817–1831. DOI: 10.1039/C3PY01262J.
204. Klitzing, R.; Tieke, B. Polyelectrolyte Membranes. In *Polyelectrolytes with Defined Molecular Architecture I*; Schmidt, M., Ed.; Advances in Polymer Science; Springer Berlin Heidelberg, 2004, pp 177–210. DOI: 10.1007/b11270.
205. Shen, L.; Wang, B.; Wang, J.; Fu, J.; Picart, C.; Ji, J. Asymmetric free-standing film with multifunctional anti-bacterial and self-cleaning properties. *ACS applied materials & interfaces* **2012**, *4* (9), 4476–4483. DOI: 10.1021/am301118f.
206. Song, Y.; Qin, S.; Gerringer, J.; Grunlan, J. C. Unusually fast and large actuation from multilayer polyelectrolyte thin films. *Soft matter* **2019**, *15* (11), 2311–2314. DOI: 10.1039/C8SM02465K.
207. Nikolaev, K. G.; Ulasevich, S. A.; Luneva, O.; Orlova, O. Y.; Vasileva, D.; Vasilev, S.; Novikov, A. S.; Skorb, E. V. Humidity-Driven Transparent Holographic Free-Standing Polyelectrolyte Films. *ACS*

- Appl. Polym. Mater.* **2020**, 2 (2), 105–112. DOI: 10.1021/acsapm.9b01151.
208. Zhao, M.; Altankov, G.; Grabiec, U.; Bennett, M.; Salmeron-Sanchez, M.; Dehghani, F.; Groth, T. Molecular composition of GAG-collagen I multilayers affects remodeling of terminal layers and osteogenic differentiation of adipose-derived stem cells. *Acta Biomaterialia* **2016**, 41, 86–99. DOI: 10.1016/j.actbio.2016.05.023.
209. Hautmann, A.; Anouz, R. *GBi2S: Entwicklung von Multi-Komponentfilmen als Plattform-Technologie für Anwendungen in der Wundheilung und Chirurgie (ActiveLayers): Sachbericht zum Verwendungsnachweis der BMBF-Fördermaßnahme „GO-Bio initial“ (Sondierungsphase) Skizzen-Nr.: lwgbi2s086*.
210. Gribova, V.; Navalikhina, A.; Lysenko, O.; Calligaro, C.; Lebaudy, E.; Deiber, L.; Senger, B.; Lavalle, P.; Vrana, N. E. Prediction of coating thickness for polyelectrolyte multilayers via machine learning. *Scientific reports* **2021**, 11 (1), 18702. DOI: 10.1038/s41598-021-98170-x.
211. Hautojärvi, J.; Laaksonen, S. On-Line Surface Modification of Polypropylene Fibers by Corona Treatment During Melt-Spinning. *Textile Research Journal* **2000**, 70 (5), 391–396. DOI: 10.1177/004051750007000503.
212. Andres, C. M.; Kotov, N. A. Inkjet deposition of layer-by-layer assembled films. *Journal of the American Chemical Society* **2010**, 132 (41), 14496–14502. DOI: 10.1021/ja104735a.
213. Akagi, T.; Fujiwara, T.; Akashi, M. Inkjet printing of layer-by-layer assembled poly(lactide) stereocomplex with encapsulated proteins. *Langmuir : the ACS journal of surfaces and colloids* **2014**, 30 (6), 1669–1676. DOI: 10.1021/la404162h.
214. Kia Silverbrook. Wide format pagewidth inkjet printer: US.

List of Illustrations

Figure 1 - Graphical Abstract.....	8
Figure 2 - Primary wound healing and secondary wound healing.....	15
Figure 3 - The individual duration of healing phases	17
Figure 4 - Wound healing processes in acute and chronic wounds.	21
Figure 5 - Transition into the proliferative phase of wound healing.	22
Figure 6 - Major GFs involved in wound healing and their targeted cell types.	23
Figure 7 – Transcriptional Regulation of macrophage activation.	26
Figure 8 - Representative examples of NF- κ B stimuli and target genes. Based on (61).	28
Figure 9 - Skeletal formula of HA.	29
Figure 10 - Pathway of action of different molecular weight HA.....	30
Figure 11 – Skeletal structure of heparin.....	31
Figure 12 -Skeletal structure of the chitosan.....	33
Figure 13- Skeletal structure of alginate	33
Figure 14 - Schematic representation of the various functions of the ideal wound dressing.	35
Figure 15 -Various technologies for the controlled release of GFs from advanced wound dressings.	40
Figure 16 - Most common used layer-by-layer techniques.....	43
Figure 17 - Concept of an automatic semi-continuous spray coater.	127

Acknowledgement

Nach fünf Jahren harter Arbeit ist das Ende meiner Promotionszeit in Sicht und ich möchte mich bei den vielen Menschen bedanken, die mich auf diesem Weg unterstützt haben.

Zuallererst möchte ich meinem Betreuer, **Prof. Thomas Groth**, meine aufrichtige Anerkennung aussprechen. Ihr Fachwissen und Unterstützung haben mich auf diesem Weg entscheidend begleitet. Ihr Engagement bei der Unterstützung meiner akademischen Entwicklung war unglaublich wichtig für meinen Werdegang, und ich fühle mich geehrt, Ihr Doktorand gewesen zu sein.

Ich möchte mich auch bei **Dr. Christian Wölk** und **Prof. Dehghani** bedanken, die sich die Zeit genommen haben, meine Arbeit sorgfältig zu lesen und zu bewerten.

Meine Kolleg*innen innerhalb und außerhalb der Arbeitsgruppe **AG Biomedizinische Materialien** waren ein Quell außerordentlicher Unterstützung und Freude im Alltag. Danken möchte ich hier insbesondere **M.Sc. Devaki Kedilaya**, **M.Sc. Tobias Hedtke**, **Dipl.-Ing. Johannes Marhoffer**, **Dr. Sanja Stojanovic**, **M.Sc. Sonia Sislema-Munoz**, **Dr. Reema Anouz**, **Dr. Christian Willems**, **me. Alexander Vinzelberg**, **Dr. Christian Schmelzer**, **Dr. Alexander Navarrete Santos** und **Dr. Frank Erdmann** für die vielfältige Unterstützung. Einen besonderen Dank gebührt **Dr. Hala Al Khoury** für meine praktische Einführung in die Welt der Wissenschaft und die sehr fruchtbare Zusammenarbeit am Anfang dieser Arbeit. Zudem bin ich Frau **Marlis Porobin** für ihre administrative und praktische Unterstützung dankbar, ihr Pragmatismus hat vieles erst möglich gemacht.

Meiner Familie möchte ich meine unermessliche Dankbarkeit aussprechen. Diese Arbeit ist das Ergebnis ihrer Liebe und Unterstützung, insbesondere durch meiner Lebensgefährtin Katja Schierhorn. Die Geburt unserer beiden Söhne Leander und Laurentin, hat mein Leben auf dem Kopf gestellt, erfüllt mich aber jeden Tag mit großer Freude und Zuversicht. Besonders möchte ich mich auch bei meinen Eltern und Schwiegereltern für die immerwährende Unterstützung bedanken.

Abschließend möchte ich mich bei den Organisationen bedanken welche Teile der Forschung finanziell unterstützt haben; der DAAD und das BMBF.

Vielen Dank auch an all jene, welche mich während meiner Promotionszeit unterstützt und ermutigt haben, hier aber nicht namentlich erwähnt wurden.

Publication List

with declaration of self-contribution to research articles.

- **Design of a composite wound dressing: combining an electrospun fleece with a free-standing multilayer film**

Adrian Hautmann, Tobias Hedtke, Sonia Sislema-Muñoz, Juliana Martins-Schalinski, Christian E.H. Schmelzer, Thomas Groth (2023)

Next Materials

My contribution was about 70%. I performed all experiments except nano-CT, amino acid analysis, profilometry and ESEM. The dynamic mechanical analysis was a collaborative effort involving Marco Sträter and the cytokine release assay was conducted jointly with Sonia Sislema-Munoz. The preparation of the electrospun fleece was carried out by Tobias Hedtke. The manuscript was conceptualized and written by me, while all co-authors contributed to the manuscript editing.

- **Intrinsically cross-linked ECM-like multilayers for BMP-2 delivery promote osteogenic differentiation of cells**
Reema Anouz, Tamaradobra Selekere, Adrian Hautmann, Catharina Husteden, Matthias Menzel, Christian Woelk, Christian E. H. Schmelzer, and Thomas Groth (2023)

***Advanced Materials Interfaces* [10.1002/admi.202201596](https://doi.org/10.1002/admi.202201596)**

My contribution was about 30%. I conceptualized and conducted the quantitative evaluation of fiber width, young modulus, roughness and BMP-2 concentration of the samples as well as the quantitative analysis of cell count, cell area, focal adhesion plaques and actin filament length of cells. Additionally, I co-edited the manuscript.

- **Comparative in Vitro Study on Anti-inflammatory Activity of Covalent Versus Layer-by-Layer-Bound Heparin and Hyaluronan Including Signal Transduction Through Transcription Factor NF-κB**

Guoying Zhou, Hala Al Khoury, Adrian Hautmann, Haitong Wan, Thomas Groth (2023) Book chapter in *Bioceramics, Biomimetic and Other Compatible*

***Materials Features for Medical Applications* [10.1007/978-3-031-17269-4_7](https://doi.org/10.1007/978-3-031-17269-4_7)**

My contribution was about 15%. I contributed to the writing of the manuscript and did the final editing.

- **Free-standing multilayer films as growth factor reservoirs for future wound dressing applications**
Adrian Hautmann, Devaki Kedilaya, Sanja Stojanović, Milena Radenković, Christian K. Marx, Stevo Najman, Markus Pietzsch, João F. Mano, Thomas Groth (2022)
***Biomaterials Advances* [10.1016/j.bioadv.2022.213166](https://doi.org/10.1016/j.bioadv.2022.213166)**

My contribution was about 70%. I performed all experiments except otherwise stated. Devaki Kedilaya performed in-vitro biocompatibility tests and FGF2 release studies, The *in-vivo* assays were jointly conducted with Sanja Stojanović and Milena Radenković. Christian K. Marx conducted the anti-bacterial testing. The manuscript was composited and written by me with some help of Sanja Stojanovic on the *in-vivo* result discussion. All co-authors edited the manuscripts.

- **Studies on the Mechanisms of Anti-Inflammatory Activity of Heparin- and Hyaluronan-Containing Multilayer Coatings-Targeting NF-κB Signalling Pathway**
Alkhoury, Hala; Hautmann, Adrian; Fuhrmann, Bodo; Syrowatka, Frank; Erdmann, Frank; Zhou, Guoying et al. (2020)
***International journal of molecular sciences* [10.3390/ijms21103724](https://doi.org/10.3390/ijms21103724)**

I contributed approximately 40%. I jointly conducted all the experimental tasks except for the IL-1β ELISA with Hala Alkhoury. The AFM and CLSM experiments were conducted only by me. Moreover, I only supplied the samples for the Western Blot analysis, which was conducted by Frank Erdmann. The composition and writing of the manuscript were undertaken by Hala Alkhoury, with my assistance. All co-authors reviewed and edited the manuscripts.

- **Study on the potential mechanism of anti-inflammatory activity of covalently immobilized hyaluronan and heparin**
Alkhoury, Hala; Hautmann, Adrian; Erdmann, Frank; Zhou, Guoying; Stojanović, Sanja; Najman, Stevo; Groth, Thomas (2020)
***Journal of biomedical materials research. Part A* [10.1002/jbm.a.36885](https://doi.org/10.1002/jbm.a.36885)**

My contribution was about 40%. I performed all other experimental work, except IL-1β ELISA, together with Hala Alkhoury. The AFM and CLSM experiments were conducted only by me. Additionally, I only provided the samples for Western Blot (Frank Erdmann). The concept and protocol of the optical NF-κB assay was developed by me. The manuscript was prepared and written by Hala Alkhoury, with support by me. All co-authors reviewed the manuscripts.

Oral Presentations

- Design of a composite wound dressing: combining electrospun fleece with a free-standing multilayer film | 2023 | *Termis EU-Chapter Manchester 2023* oral presentation *Thomas Groth & Adrian Hautmann*
- Towards layer-by-layer based wound dressings; exploring cross-linked chitosan/alginate free-standing multilayer films | 2020 | *World Biomaterials Congress (online)*, oral presentation
- Free-standing multilayer films made of chitosan/alginate | 2020 | *MRS Serbia (Belgrade)*, oral presentation

Posters

- Design of a composite wound dressing: combining electrospun gelatin fleece and free-standing LbL film | 2022 | *ESAO Winterschool 2023*, poster presentation credited with 🏆 Poster Prize
- Design of a composite wound dressing: combining electrospun gelatin fleece and free-standing LbL film | 2022 | *Termis EU-Chapter Krakow 2022*, poster presentation
- Free-standing multilayer films as growth factor reservoirs for wound dressing design application | 2021 | *ESAO Winterschool 2021 (online)*, poster presentation credited with 🏆 Poster Prize
- The anti-inflammatory action of physically adsorbed versus covalently bound glycosaminoglycans | 2020 | *ESAO Winterschool 2020 (Wittenberg)*, poster presentation

Curriculum Vitae

01/2019 – jetzt	Doktorand (AG Biomedizinische Materialien)
11/2021 – 01/2023	(Co-)Projektleitung und Projektingenieur BMBF GO-Bio initial: Entwicklung von Multi-Komponentfilmen als Plattform-Technologie für Anwendungen in der Wundheilung und Chirurgie (ActiveLayers)
10/2016 – 12/2018	Studium M.Eng. Biomedical Engineering MLU Halle-Wittenberg und Hochschule Anhalt Master thesis: „Glycosaminoglycans – A comparative Study“
03/2015 – 12/2018	Apotheker (in öffentlichen Apotheken)
12/2015	Approbation zum Apotheker
10/2009 - 10/2014	Studium der Pharmazie Martin-Luther-Universität Halle-Wittenberg und Julians-Maximilians-Universität Würzburg
06/2009	Allgemeine Hochschulreife Landkreis-Gymnasium St. Annen in Annaberg-Buchholz

Selbstständigkeitserklärung

Hiermit erkläre ich gemäß § 5 der Promotionsordnung der Naturwissenschaftlichen Fakultät I der Martin-Luther-Universität Halle-Wittenberg, dass ich die Ergebnisse der vorliegenden kumulativen Dissertationsarbeit

Inflammation Modulation, Growth Factor Reservoir and Chronic Wound Healing Potential:

From Nanoscale Coatings to a Free-Standing Layer-by-Layer Platform

am Institut für Pharmazie in der Arbeitsgruppe Biomedizinische Materialien unter Anleitung von Prof. Dr. rer. nat. habil. Thomas Groth selbständig erarbeitet und die Dissertation ohne fremde Hilfe verfasst habe.

Weiterhin erkläre ich, dass ich keine anderen als die von mir angegebenen Quellen und Hilfsmittel zur Erstellung meiner Dissertation verwendet habe. Den benutzen Werken wörtlich oder inhaltlich entnommene Stellen sind als solche gekennzeichnet.

Ferner erkläre ich, dass ich mich mit der vorliegenden Dissertationsarbeit erstmals um die Erlangung eines Doktorgrades bewerbe.

Halle (Saale), den 12. Dezember 2023

Adrian Hautmann